(90)

Theoretical and Experimental Investigations of Electrostatic Effects Associated with Ionic Surfactant Micelles

by

Nancy Zoeller Diggs

B.S.E., Chemical Engineering, Princeton University (1992)
M.S.C.E.P., Massachusetts Institute of Technology (1994)

Submitted to the Department of Chemical Engineering
in partial fulfillment of the requirements for the degree of

Doctor of Philosophy in Chemical Engineering

at the

MASSACHUSETTS INSTITUTE OF TECHNOLOGY

June 1998

Author .....
Department of Chemical Engineering
May 6, 1998

Certified by .....
Daniel Blankschtein
Professor
Thesis Supervisor

Accepted by .....
Robert E. Cohen
St. Laurent Professor of Chemical Engineering
Chairman, Committee for Graduate Students

Theoretical and Experimental Investigations of Electrostatic Effects Associated with Ionic Surfactant Micelles

by

Nancy Zoeller Diggs

Submitted to the Department of Chemical Engineering
on May 6, 1998, in partial fulfillment of the
requirements for the degree of
Doctor of Philosophy in Chemical Engineering

Abstract

Ionic surfactants are the most commonly used type of surfactant, yet the complex electrostatic intramicellar and intermicellar interactions involved in micelle formation and micellar solution phase behavior of these surfactants are not well understood. In this thesis, both theoretical and experimental investigations were conducted in order to develop a better molecular-level understanding of the micellar properties of aqueous ionic surfactant solutions.

The first major contribution of this thesis was to extend a molecular-thermodynamic theory of micellization and micellar solution phase behavior previously developed by our group for nonionic surfactants to describe and model the behavior of ionic surfactants. Analytical approximations to the Poisson-Boltzmann equation were used to calculate the electrostatic contribution to the free energy of micellization. To correct for the neglect of the finite size of the ions in the ion cloud, the model was modified to include a Stern layer, a region immediately surrounding the micelle surface from which the counterions are excluded. Including the Stern layer improved CMC predictions and provided some counterion specificity. In addition, a model for the fractional counterion binding was developed based on the Gibbs adsorption equation.

In an effort to make the molecular-thermodynamic theory more accessible to both academic and industrial surfactant researchers, it was incorporated into a user-friendly computer program, known as program PREDICT. Program PREDICT is capable of predicting a wide range of micellar solution properties for a variety of ionic, nonionic, and zwitterionic surfactants. Examples of many of its predictive capabilities are presented and compared with experimental data. In addition, some fundamental predicted surfactant solution properties are correlated with industrially-relevant surfactant performance characteristics.

The molecular-thermodynamic theory with a Stern layer model was found to underestimate micellar growth of typical ionic surfactants in the presence of added salt.

This underestimation of micelle size is due primarily to the neglect of electrostatic intermicellar interactions. In an effort to address intermicellar interactions using a more rigorous, systematic approach, a new statistical-thermodynamic framework for micellar solutions based on the McMillan-Mayer theory of multicomponent solutions was developed. The framework was first implemented in the case of nonionic surfactant solutions exhibiting attractive and excluded-volume intermicellar interactions. It was demonstrated that repulsive excluded-volume intermicellar interactions encourage micelle formation and growth. In addition, this framework was used to make accurate predictions of several micellar solution properties, such as the CMC, the critical concentration for phase separation, and the osmotic compressibility.

The McMillan-Mayer approach was then extended to model the behavior of ionic surfactant solutions which exhibit both excluded-volume and electrostatic intermicellar interactions. To model the electrostatic intermicellar interactions, the other micelles in solution were included as part of the diffuse ion cloud surrounding a central micelle. Two different approaches were used to calculate the electrostatic potential created by the micelle and the ion cloud. First, the Debye-Hückel approximation, which provides an analytical solution and can model both spherical and cylindrical micelles, was used to predict micellar growth. Indeed, it was found that electrostatic intermicellar interactions encourage micellar growth, yielding a significant improvement over the predictions of the simpler molecular-thermodynamic theory. The second approach involved the use of a modified Poisson-Boltzmann equation, which included the effect of the finite size of the charged solutes in the ion cloud. This approach represents a more accurate description of the electrostatic potential, but can only be used in the case of spherical micelles. Although quantitative accuracy is not yet achieved, both of these approaches represent a valuable "first step" in the development of a theory for electrostatic intermicellar interactions.

In conjunction with the theoretical work, an experimental investigation into the properties of dodecyl ethoxy sulfate micelles with 1, 2, 4, or 6 EO groups was conducted. Light scattering and viscosity techniques were used to measure micelle shape and size at various salt concentrations and temperatures. The DLVO potential was used to quantify the effect of electrostatic and attractive intermicellar interactions on the light scattering data. It was found that the resulting equilibrium micelle shape and size is determined by an interplay between steric and electrostatic interactions among the surfactant heads at the micelle surface. Specifically, the surfactants with one and two EO groups exhibited one-dimensional growth in the presence of added salt, a common behavior for typical ionic surfactants. In contrast, the surfactants with four or six EO groups formed small spherical micelles over the entire range of salt concentrations and temperatures examined. This experimental investigation provided valuable insight into the molecular-level interactions which govern the equilibrium micelle shape and size.

Thesis Supervisor: Daniel Blankschtein
Title: Professor

Acknowledgments

This thesis is dedicated to my husband, David Diggs, who provided constant love and encouragement, and rejoiced with my successes. He should really be a co-author of this thesis.

I could not have completed this work without the help and encouragement of many people. First, I would like to thank my advisor, Professor Daniel Blankschtein for his direction and advice. He spent a lot of time and effort in patiently teaching me how to conduct high quality research. Through our discussions, I have gained confidence in my own scientific abilities. I would also like to acknowledge my thesis committee, Professor Alan Hatton, Professor Sow-Hsin Chen, and Doctor Paul Berger for their advice and faithful attendance at committee meetings.

A large portion of what I learned at MIT came from the other students in the group. Teresa Carale, Chia-li Liu, Leo Lue, and especially Pak Yuet, tried to answer my many questions, and patiently taught me lab techniques and computer skills. Ginger Tse, Daniel Kamei, Peter Moore, Mike Mulqueen, Betty Yu, Isaac Reif, and Vibha Srinivasan asked me the tough questions, requiring me to understand my work on a deeper level. I would especially like to acknowledge Anat Shiloach, with whom I worked very closely; I hope that I was as much help to her as she was to me.

My fellow graduate students in the department made student life enjoyable. Jane, Anita, and Lori helped me to survive and even enjoy our first year. In addition, Jane, Colleen, Diane, and Sue were my loyal friends over the years, providing fun and laughs, in addition to scientific advice.

Finally, I would like to thank my parents and my sisters for their constant love, faith, and support.

Contents

List of Figures

List of Tables

Chapter 1

Introduction

1.1 Motivation

Ionic surfactants are the most commonly used type of surfactants in industry and research,[1] in diverse applications ranging from pharmaceuticals and personal care products to industrial uses involving coatings and lubrication. As the economic environment becomes more and more restrictive, companies which use these surfactants are decreasing research budgets and demanding more from surfactant manufacturers. In turn, surfactant manufacturers must provide their customers with complete information on their product's characteristics and behavior in order to sell. At the same time, they must continue to develop new surfactant products which possess certain desired qualities but are less expensive to produce. Consequently, surfactant manufacturers are relying increasingly on research to provide an understanding of surfactant behavior.[1] There are two ways to gain this understanding: experimentation and theory. Through a series of experiments, one can accurately probe the properties of a particular surfactant. However, this can be expensive and time-consuming, allowing the study of only one surfactant at a time. In order to understand the behavior of a broad class of surfactants, one must turn towards theory. As research budgets dwindle, comprehensive theories which quantitatively predict surfactant behavior become increasingly valuable.

In this thesis, I studied surfactant solutions, focusing on ionic surfactants, in

order to develop comprehensive theories which quantitatively model their behavior. A significant amount of theoretical work has already been done by others, but, due to the long-range nature of the electrostatic interactions involved, much of this work involves sophisticated models which require significant computational power. An important goal of this thesis was to develop a theory involving relatively simple computations that can accurately describe ionic surfactant solutions.

In addition to theoretical work, experiments were conducted in order to collect relevant information on surfactant solution behavior. Although a wealth of experimental data is available in the literature, it originates from a variety of different sources and hence is not systematic. In order to fully understand surfactant solution behavior, consistent reliable data is required for comparison with newly-developed theories. Towards this end, the effects of surfactant concentration, salt concentration, and temperature on the micellization behavior of a novel family of surfactants, the alkyl ethoxy sulfates, have been studied as part of this thesis.

In this chapter, a general background on current research on micellar solution behavior will be presented. In addition, the specific objectives of this thesis are delineated, and the organization of the remainder of the thesis is explained. First, however, a general background on surfactant solution properties is provided in the next section.

1.2 Background on Surfactant Solution Behavior

Surfactants are molecules composed of a polar hydrophilic group, the "head," attached to a nonpolar hydrophobic group, the "tail." The head can be anionic (negatively charged), cationic (positively charged), zwitterionic (dipolar), or nonionic (uncharged). The tail is typically a linear hydrocarbon chain, although branched tails and non-hydrocarbon tails are also encountered. This unique molecular structure leads to a rich spectrum of complex self-assembling phenomena when surfactants are dissolved in polar or nonpolar solvents.[2, 3] For example, when dissolved in water, surfactants form a monolayer at the water-air interface with the polar heads oriented

towards the water and the nonpolar tails oriented towards the air. As the surfactant concentration increases, the water-air interface becomes saturated, and the additional surfactant molecules self-assemble into aggregate microstructures, known as micelles, coexisting with the surfactant monomers, in which the polar heads remain exposed to water while the nonpolar tails are shielded inside the micellar core. The entropic cost of constraining the surfactant molecules in micellar form is balanced by the enthalpic gain of shielding the hydrophobic tails from water, the net effect being a minimum in the micellar solution free energy. The threshold surfactant concentration beyond which micellization occurs is known as the critical micellar concentration (CMC). The CMC is characteristic of a particular type of surfactant, and typically depends on temperature and salt concentration. Various solution properties, such as the surface tension, osmotic compressibility, and conductivity, exhibit dramatic changes at the CMC.[4]

Micelles are dynamic entities which are continually exchanging surfactant molecules with the monomeric state and with each other, a process which can generate an entire distribution of micellar sizes.[5, 6] Indeed, micelles can appear in sizes ranging from tens to thousands of monomers. Typically, the smaller micelles are spherical, while the larger ones are cylindrical or discoidal.[3, 5, 7] Micellar shape and size are not necessarily fixed. In some cases, dramatic morphological changes can be induced by varying solution conditions such as overall surfactant concentration, temperature, ionic strength, or pH.[2, 3, 6] For example, in the absence of salt, ionic surfactants typically form spherical micelles to maximize the available area per head at the micellar surface, thereby minimizing the electrostatic repulsions between the heads. At high salt concentrations, where the charged heads are shielded by salt ions, the micelles may elongate into cylinders.[8, 9] Since one dimension of the micelle is limited by the length of the fully-extended hydrocarbon tail, cylindrical micelles may grow to be quite long at high surfactant concentrations.[7] Beyond some surfactant concentration, the elongated micelles may entangle and form a mesh.[10] This concentration is known as the crossover surfactant concentration, and, in the case of ionic surfactants, typically occurs at very high salt concentrations. It is also possible that the micelles

may grow in two dimensions, forming discoidal structures. Again, in the case of ionic surfactants, this would typically occur at relatively high salt concentrations. Micelles may also form more complicated structures,[5] such as bilayers and vesicles, but these will not be considered in this thesis.

At low surfactant concentrations above the CMC, typically below 20wt%, micellar solutions often exist as homogeneous isotropic liquid phases. For many surfactants, particularly nonionic surfactants, phase separation can be induced in this concentration range by varying temperature or ionic strength.[6, 11, 12, 13, 14, 15] The corresponding coexistence or cloud-point curve, delineating the boundary between the one-phase and two-phase regions of the temperature-surfactant concentration phase diagram, usually exhibits a pronounced asymmetry between the dilute and concentrated branches, and can display lower and/or upper critical (consolute) points. Typically, the observed critical points occur at very dilute surfactant concentrations, for example, in aqueous solutions of nonionic surfactants at concentrations below 5wt%.[6, 11, 12, 13, 14, 15]

1.3 Previous Theoretical Work

In veiw of the broad variety of complex behavior exhibited by surfactant solutions discussed in the previous section, it would be valuable to develop a theoretical description of their behavior which explicitly incorporates the unique chemical structure of the surfactant molecules. In the past, the modeling of micellar solution behavior has proceeded primarily along two fronts: (i) describing the micellization process itself, and (ii) describing the overall micellar solution phase behavior. Along the first front, extensive work has been done on modeling micelle formation based on physicochemical arguments.[2, 3, 7, 8, 16, 17, 18, 19] These models calculate the free energy of micellization, which is the free-energy change per surfactant molecule associated with transferring a surfactant molecule from bulk solution into a micelle. In this description, the micelle is assumed to be at infinite dilution, and intermicellar interactions can thus be neglected. The CMC and information regarding micellar shape and size

can then be computed directly from the free energy of micellization.[3, 8, 16, 17, 18, 19] Many of these models also make use of various phenomenological parameters based on experimental data to obtain a high degree of predictive accuracy. For example, an empirical constant has been estimated based on CMC data to quantify the repulsive contributions to the free energy of micellization,[3, 8] and geometric packing constraints have been utilized to determine optimal micellar shapes.[7] Later models incorporated the unique molecular structure of the surfactant molecules into the formulation by explicitly describing the repulsive free-energy contributions associated with micellization through separate steric, interfacial, and electrostatic contributions.[8, 16, 19, 20]

The calculation of the electrostatic contribution represents a particularly challenging problem, one that has been addressed using several different approaches. For example, a diffuse ion cloud model was used to describe the distribution of counterions around an ionic micelle.[21, 22, 23] A modification of this approach used a cell model to calculate the electrostatic potential between two charged micelles surrounded by their ion clouds in a micellar solution which was divided into cells.[24, 25] An alternative approach used a lattice model to describe the location of the charges on the micellar surface.[26, 27] Finally, extensive work has been done using liquid-state theory to describe ionic micellar solutions.[28, 29, 30, 31, 32]

Along the second front, that is, describing the overall micellar solution, theoretical work has been driven by the need to fundamentally understand and quantitatively predict micellar growth and micellar solution phase behavior.[6, 11, 33, 34, 35, 36, 37, 38] At low surfactant concentrations, micelles are somewhat globular and monodisperse. As the surfactant concentration is increased, two additional micellar solution characteristics become important: (i) micelles may change shape and size, becoming more polydisperse, and (ii) intermicellar interactions may become stronger, possibly leading to phase separation. Early attempts to model micellar solution phase behavior assumed ideal solution behavior, where interactions between micelles are negligible, and concentrated mainly on the entropy of mixing polydisperse micelles in solution.[8, 39] However, intermicellar interactions must be treated in order to model certain micellar solution characteristics at higher surfactant concentrations, such as the stabilization

of particular micellar structures,[40, 41, 42] micellar diffusion coefficients,[43] the micellar size distribution,[44] and phase separation.[6, 11, 33, 35, 45] Experimentally, the importance of light and neutron scattering in elucidating micellar structures has also led to a demand for detailed descriptions of intermicellar interactions. Specifically, an accurate model of intermicellar interactions is required to interpret scattering data and obtain a clear description of the micellar size distribution and the diffusion coefficients.[43, 46, 47, 48, 49, 50, 51, 52, 53]

Clearly, there is a need for a theoretical approach capable of unifying the previously disconnected treatments of micellization and overall micellar solution phase behavior. Several theoretical approaches have examined the coupling of *intramicellar* and *intermicellar* interactions and their effects on micelle shape, average size, and size distribution,[37, 38, 40, 44, 54, 55] but these theories do not have a molecular basis. The fundamental challenges associated with developing a molecular-level understanding of the behavior of surfactant solutions, coupled with the tremendous practical importance of these complex fluids, indicates the need for developing a quantitative theoretical description of these systems capable of predicting their rich behavior. Preferably, the desired theory should incorporate explicitly the detailed molecular structures of the surfactants involved and the specified solution conditions.

With this in mind, a molecular-thermodynamic theory has been developed by our group to describe and predict micellization and micellar solution phase behavior of aqueous surfactant solutions.[16, 56] This molecular-thermodynamic theory combines a molecular model of micelle formation with a thermodynamic free-energy description of phase behavior and phase separation of micellar solutions. The molecular model of micellization accounts explicitly for the effects of surfactant molecular structure and solution conditions on the physical driving forces which control micelle formation and growth.[16, 56] The free-energy description accounts explicitly for the effects of intermicellar interactions (described at a mean-field level) and multiple chemical equilibrium on the micellar size distribution as well as on the equilibrium bulk thermodynamic properties of the solution.[6] It was found that this theory yields accurate predictions of micellar properties and micellar solution phase behavior for nonionic

surfactants.[16] However, since the model was developed primarily for nonionic surfactants, electrostatic effects were ignored.

The conceptual basis of the molecular model of micellization involves breaking down the process of micellization into a series of steps, each reflecting one of the important molecular factors responsible for micellization, and then calculating the free-energy changes associated with each of these steps separately. The sum of all these free-energy changes yields the free energy of micellization, g_{mic}, which is equal to the free-energy change associated with transferring a free monomer into a micelle at infinite dilution. Once g_{mic} is known, it can be utilized to calculate the equilibrium micelle shape and size. One contribution to g_{mic}, which is particularly relevant to this thesis, is the electrostatic free-energy change associated with bringing the charged polar heads into close proximity to each other on the micellar surface, known as g_{elec}. More specifically, g_{elec} can be described as the free-energy change required to localize a set of like charges on the surface of a micelle. For nonionic surfactants, this free-energy change is negligible. However, for ionic and zwitterionic surfactants, g_{elec}, or the free-energy cost associated with charging the micellar surface, is essential and hence must be calculated.

To calculate g_{elec}, the electrostatic potential around the micelle can be modelled using the Poisson-Boltzmann (PB) equation, which describes the distribution of ions around a charged surface.[57] Several key assumptions are made in the development of the PB equation. In particular, the ions are treated as point charges, and the solvent is treated as a continuum having a uniform dielectric constant. In addition, the PB equation is nonlinear, and therefore, tedious numerical routines are required for its solution. For the convenience of incorporating electrostatic interactions into a molecular-thermodynamic framework that can be easily rationalized and utilized, an analytical solution to the PB equation is desired. For this purpose, several analytical approximations to the Poisson-Boltzmann equation have been developed.[21, 22, 23, 58, 59, 60]

The calculation of the free energy of micellization, g_{mic}, is only one element in the overall thermodynamic framework to theoretically model micellar solutions. In addi-

tion to the formation of a single micelle, captured in g_{mic}, a description of the entropy of the entire micellar solution, as well as of the interactions between micelles, is needed to fully characterize the micellar system. In the molecular-thermodynamic theory, the Gibbs free energy is decomposed into three contributions accounting for: (i) formation of the micelles at infinite dilution, (ii) mixing of the micelles with monomers, water molecules, and other micelles, and (iii) attractive intermicellar interactions. The attractive intermicellar interactions are modeled using a mean-field interaction description. It was found that predictions made using this molecular-thermodynamic theory were in good agreement with available experimental data for a range of micellar solution properties for nonionic surfactants.[10, 16, 61]

In the next section, the specific objectives of this thesis are discussed.

1.4 Thesis Objectives

In view of the above discussion on current theoretical advances in modeling ionic micellar solutions, the objectives of this thesis were laid out. These include:

- Improve the ability of the molecular-thermodynamic theory to quantitatively predict the behavior of ionic micellar solutions. The main focus here was on developing accurate descriptions of the electrostatic interactions among the charged surfactant heads leading to an expression for the electrostatic free energy, g_{elec}. The Poisson-Boltzmann equation, a fundamental equation of electrostatics, was modified to improve on some of its inherent limitations. Specifically, the finite size of the counterions immediately surrounding the micelle was included in the model through the use of a Stern layer. In addition, a model based on the Gibbs adsorption equation was developed to estimate counterion binding, that is, the fraction of surfactant molecules which do not dissociate.

- Develop program PREDICT, a user-friendly computer program created to make the molecular-thermodynamic theory accessible to industrial and academic researchers interested in surfactant design and formulation.

- Develop a new thermodynamic framework to address issues regarding intermicellar interactions specifically related to the modeling of ionic micellar solutions. This framework, based on rigorous statistical-mechanical principles in the context of the McMillan-Mayer theory of multicomponent solutions, allows for the treatment of a variety of intermicellar interactions, including those of the excluded-volume and electrostatic variety, in addition to the mean-field type attractive interactions that were introduced in the context of the original thermodynamic framework.

- Perform experiments in order to obtain systematic, reliable data on ionic surfactant behavior. Dodecyl ethoxy sulfates ($C_{12}H_{25}$-$(OCH_2CH_2)_j$-$OSO_3^-Na^+$, with j =1, 2, 4, or 6) were used as a model system. This is an interesting class of ionic surfactants which can exhibit behavior typical of that of an ionic or a nonionic surfactant, depending on the number of ethoxy groups in the head and on the solution conditions. The effects of salt concentration and temperature on micelle shape and size were investigated using viscosity and static and dynamic light scattering methods.

1.5 Thesis Organization

The thesis is structured as follows. In Chapter 2, the molecular-thermodynamic theory of micellar solutions originally developed for nonionic surfactants is extended to include ionic surfactants. The classical Poisson-Boltzmann (PB) model is used to describe the distribution of ions around the charged micelle. Some modifications are made to the PB equation to correct for some of its inherent limitations. Specifically, a Stern layer is added to account for the finite size of the counterions at the micellar surface. In addition, a model for calculating the fractional counterion binding at the micellar surface using the Gibbs adsorption equation is developed. Several examples of predictions of CMC's and counterion binding for typical ionic surfactants are presented and compared with experimental data.

The molecular-thermodynamic theory was incorporated into a user-friendly com-

puter program, called program PREDICT, in an effort to make it accessible to industrial and academic researchers interested in surfactant design and formulation. The operation of this program is explained in Chapter 3, along with a thorough description of its predictive capabilities.

The molecular-thermodynamic theory presented in Chapters 2 and 3 is somewhat limited in its ability to predict micelle size for ionic surfactants. Indeed, it was found that this theory is unable to predict the micelle growth of some of the dodecyl ethoxy surfactants observed in the experimental study described in Chapter 7. Recall that the intermicellar interactions in the molecular-thermodynamic theory are limited to attractive mean-field interactions. This simple approach may not be appropriate for charged surfactants where the repulsive electrostatic interactions may be dominant, thus leading to significant correlations between micelles which are neglected in the mean-field description. In addition, splitting the solution nonidealities into mixing and interaction free-energy contributions without a rigorous underlying statistical-mechanical basis can sometimes lead to ambiguities. Specifically, when the theory is unable to describe some aspect of the experimentally observed micellar solution behavior, it is difficult to unambiguously determine if the source of the discrepancy lies in the mixing or the interaction contributions to the micellar solution Gibbs free energy. A thermodynamic framework based on rigorous statistical-thermodynamic principles is required to address these issues in an accurate and consistent manner. Therefore, a new thermodynamic framework for the modeling of micellar solutions was developed based on the McMillan-Mayer theory of multicomponent solutions. Chapter 4 presents the derivation of this framework.

Because electrostatic intermicellar interactions can be very difficult to model, the McMillan-Mayer approach was first applied to nonionic surfactant solutions which exhibit attractive and excluded-volume interactions. In particular, Chapter 5 includes a description of the implementation of the McMillan-Mayer theory for nonionic surfactant solutions. Note that the molecular model of micellization presented in Chapter 2 can be used in this thermodynamic framework, where $g_{elec} = 0$ for nonionic surfactants. The effect of including attractive and excluded-volume intermicellar

interactions in the new thermodynamic framework is examined through qualitative predictions of the micellar size distribution. In addition, quantitative predictions of several micellar solution properties are made and compared with experimental data.

In Chapter 6, the McMillan-Mayer theory is implemented in the case of ionic surfactant solutions which exhibit both excluded-volume and electrostatic intermicellar interactions. An approach for modeling the electrostatic intermicellar interactions whereby the charged micelles are included as part of the ion cloud is described. The molecular model of micellization presented in Chapter 2 can be used within this framework, with the exception of the calculation of g_{elec}. Specifically, the interaction between a charged micelle and its surrounding ion cloud (which includes counterions, salt ions, monomers, and other charged micelles) is included in the nonideal contribution. Therefore, in this approach, g_{elec} corresponds to the electrostatic contribution to the free energy of micellization, g_{mic}, at infinite dilution *with no surrounding ion cloud.* The reasons for modifying the calculation of g_{mic} in this manner are discussed further in Chapter 6. Two different models for the distribution of the charged solutes in the ion cloud are used and compared. One involves the use of the Debye-Hückel equation, which, although approximate, is analytical and can be used to model elongated micelles. The second approach involves the use of the full numerical Poisson-Boltzmann equation in which the ion distribution is modified to include the effect of the finite size of the charged solutes in the ion cloud. Several qualitative predictions are made to assess the impact of the electrostatic intermicellar interactions on the micellar size distribution.

In conjunction with the theoretical investigations described above, an experimental investigation was conducted on dodecyl ethoxy sulfates, as described in Chapter 7. Using viscosity and static and dynamic light scattering techniques, the effect of solution conditions (salt concentration and temperature) on the micelle shape and size of alkyl ethoxy sulfate surfactants were studied. It was found that the resulting equilibrium micelle structure is determined by an interplay between steric and electrostatic intramicellar interactions among the surfactant heads at the micelle surface. In addition, the effect of intermicellar interactions was accounted for in the light scattering

analysis using the DLVO potential. This experimental study provided an opportunity to gain a better understanding of the molecular-level interactions which determine the resulting micelle structure.

Finally, in Chapter 8, the key results of this thesis are summarized, and suggestions for future research in the area of ionic micellar solutions are presented.

Chapter 2

Extension of the Molecular-Thermodynamic Theory of Micellization to Ionic Surfactants

2.1 Introduction

As stressed in Chapter 1, ionic surfactants are widely used in diverse industrial and research applications. Clearly, there is a need for a theory which can accurately predict the behavior of these surfactants in aqueous solution, while retaining some computational simplicity. Our group has recently developed a molecular-thermodynamic theory to describe and predict micellization characteristics and micellar solution phase behavior of aqueous nonionic surfactant solutions.[6, 16] The central goal of this chapter is to extend this theory to incorporate ionic surfactants in an accurate and consistent manner. Specifically, the electrostatic contribution to the free energy of micellization, g_{elec}, must be quantified for ionic surfactants. The free energy of micellization, g_{mic}, is the free energy required to transfer a surfactant monomer into a micelle at infinite dilution. If the surfactant is ionic, the micelle is surrounded

by a diffuse ion cloud consisting of counterions, monomers, and salt ions, if salt is added. Note that intermicellar interactions, except for attractive mean-field interactions, are neglected in the molecular-thermodynamic theory. This neglect eventually led to the development of a new statistical-thermodynamic framework based on the McMillan-Mayer theory of multicomponent solutions, as described in Chapters 4 and 6.

The electrostatic contribution to the free energy of micellization, g_{elec}, can be calculated using the Poisson-Boltzmann (PB) equation to describe the distribution of ions in the ion cloud. The PB equation is a nonlinear differential equation which can be solved numerically.[24, 62, 63] However, a central goal of this chapter is to develop a model which is computationally simple. One option is to linearize the PB equation to obtain the well-known Debye-Hückel (DH) solution.[7, 8] While this solution is relatively simple to obtain, it is not accurate enough for the high surface charge densities typically encountered on a typical ionic micellar surface. Alternatively, several analytical approximations are available in the literature[21, 22, 23, 58, 59, 60] that afford ease of computation while not sacrificing quantitative accuracy. Some of these analytical approximations will be discussed in this chapter.

While an analytical approximation may be very close to the actual solution of the PB equation, there are some approximations inherent in the formulation of the PB equation itself. In particular, the ions in the cloud surrounding the micelle (including counterions, co-ions, and surfactant monomers) are treated as point charges.[57] In other words, they are assumed to have zero volume, and therefore, can approach infinitely close to the micellar surface and to each other. Consequently, the PB equation is expected to overpredict the counterion concentration at the micellar surface, thus reducing the head/head electrostatic repulsions more than is physically possible.[26, 27, 64] In order to overcome this problem, a model was developed which includes the finite size of the counterions at the micellar surface, representing a more realistic picture of the charged micelle and its ion cloud. This modification to the PB equation allows for more accurate predictions of micellization properties, such as the CMC, as well as for a better incorporation of the effect of added salt on these

properties.

Due to the electrostatic attractions between the oppositely-charged surfactant heads and their counterions, not all the surfactant molecules will be fully dissociated. In other words, some counterions will remain "bound" to the surface of the micelle. The distinction between bound and free ions constitutes a controversial issue in the field of colloid science, one that remains to be fully elucidated. In this chapter, this issue will be addressed by estimating the fraction of bound counterions based on the Gibbs Adsorption Equation. This approach is somewhat similar to that presented by Evans, Mitchell, and Ninham[22] and others,[23, 65] but here it is applied to the molecular model of micellization developed by our group, which includes a more detailed description of the micellization process, including the effect of finite counterion volume in the region of the micellar surface. In addition, a rigorous thermodynamic derivation of the expression for fractional counterion binding is presented which is lacking in the published literature.[22, 23, 65]

The remainder of this chapter is organized as follows. In Section 2.2, the phenomenological thermodynamic framework, originally developed for nonionic surfactant solutions, is described. In Section 2.3, the molecular model of micellization is presented, along with an extensive discussion of the various analytical approximations available for solving the PB equation and calculating g_{elec}. In addition, the Stern layer model, which accounts for the finite size of the counterions at the micelle surface, is derived in this section. Finally, in Section 2.4, a model for the prediction of fractional counterion binding is incorporated in the context of the molecular-thermodynamic theory of micellization of ionic surfactants.

2.2 Thermodynamic Framework

Previously, a thermodynamic free-energy description was developed by our group to describe the phase behavior and phase separation of nonionic micellar solutions.[6, 16, 17] This description is also applicable in the case of ionic micellar solutions. In this section, the salient features of this thermodynamic framework will be briefly reviewed.

The surfactant solution under consideration consists of N_w solvent (water) molecules and N_s surfactant molecules, which, depending upon the solution conditions, can form a distribution of micellar aggregates, $\{N_n\}$, where N_n denotes the number of micelles of aggregation number n, also known as n-mers. The total Gibbs free energy of the micellar solution can be written as follows

$$G = N_w\mu_w + N_1\mu_1 + \sum_{S=1}^{3}\sum_{l_c}\sum_{n>1} N_n(S,l_c)\mu_n(S,l_c) \tag{2.1}$$

where μ_w and μ_1 are the chemical potentials of solvent (water) molecules and surfactant monomers, respectively, $\mu_n(S,l_c)$ is the chemical potential of an n-mer of shape S (where $S = 3$ for spheres, 2 for cylinders, and 1 for bilayers) and micelle core radius l_c, and $N_n(S,l_c)$ is the number of n-mers of shape S and micelle core radius l_c. Note that $N_n(S,l_c)$ and $\mu_n(S,l_c)$ in Eq. (2.1) are summed over all possible values of S and l_c.

The total Gibbs free energy of the micellar solution can be modeled as the sum of three contributions, reflecting (i) the formation of the $\{N_n\}$ distribution of micellar aggregates in chemical equilibrium with each other and with the monomers in solution, (ii) the entropy of mixing micelles, surfactant monomers, and solvent molecules, and (iii) the attractive intermicellar interactions modeled at a mean-field level. The resulting Gibbs free energy is given by[6, 16, 17]

$$\begin{aligned} G &= N_w\mu_w^\circ + N_1\mu_1^\circ + \sum_{S=1}^{3}\sum_{l_c}\sum_{n>1} N_n(S,l_c)\mu_n^\circ(S,l_c) \\ &\quad + k_BT\left[N_w \ln X_w + \sum_{S=1}^{3}\sum_{l_c}\sum_{n>1} N_n(S,l_c)\ln X_n(S,l_c)\right] - \frac{CN_s\phi}{2} \end{aligned} \tag{2.2}$$

where μ_w° and μ_1° are the standard-state chemical potentials of a solvent molecule and a surfactant monomer, respectively, $\mu_n^\circ(S,l_c)$ is the standard-state chemical potential of an n-mer of shape S and micelle core radius l_c, X_w is the mole fraction of solvent, $X_n(S,l_c)$ is the mole fraction of n-mers of shape S and micelle core radius l_c, C is a mean-field interaction parameter reflecting the magnitude of the effective intermicellar

attractions, ϕ is the total surfactant volume fraction, k_B is the Boltzmann constant, and T is the absolute temperature.

The mass balance of the surfactant molecules must be maintained. Specifically,

$$N_s = N_1 + \sum_{S=1}^{3} \sum_{l_c} \sum_{n>1} n N_n(S, l_c) \tag{2.3}$$

The surfactant solution is in thermodynamic equilibrium, indicating that the Gibbs total free energy, G, is at its minimum value. That is, at a given temperature, T, pressure, p, N_w, and N_s, one has

$$dG\,|_{T,p,N_s,N_w} = 0 \tag{2.4}$$

Using Eq. (2.1) in Eq. (2.4) yields

$$0 = \mu_1 dN_1 + \sum_{S=1}^{3} \sum_{l_c} \sum_{n>1} \mu_n(S, l_c)\, dN_n(S, l_c) \tag{2.5}$$

Because N_s is held constant, Eq. (2.3) provides a connection between dN_1 and $dN_n(S, l_c)$. Hence, Eq. (2.5) becomes

$$\sum_{S=1}^{3} \sum_{l_c} \sum_{n>1} [\mu_n(S, l_c) - n\mu_1]\; dN_n(S, l_c) = 0 \tag{2.6}$$

Thus, for every n, S, and l_c, the following relation must be satisfied

$$\mu_n(S, l_c) = n\mu_1 \tag{2.7}$$

which is the mathematical statement of multiple chemical equilibrium.

The chemical potentials, $\mu_n(S, l_c)$ and μ_1, can be obtained by differentiating the free energy given in Eq. (2.2). That is, $\mu_n(S, l_c) = (\partial G / \partial N_n(S, l_c))_{T,p,N_w,\{N_{m\neq n}\}}$, which results in the following expressions for $\mu_n(S, l_c)$ and μ_1

$$\mu_n(S,l_c) = \mu_n^\circ(S,l_c) + k_BT\left[1+\ln X_n(S,lc) + n(X-1) - n\sum_{S=1}^{3}\sum_{l_c}\sum_{m} X_m(S,l_c)\right] + \frac{Cn}{2}\left[(1-\phi)^2-1\right] \quad (2.8)$$

$$\mu_1 = \mu_1^\circ + k_BT\left[1+\ln X_1 + (X-1) - \sum_{S=1}^{3}\sum_{l_c}\sum_{m} X_m(S,l_c)\right] + \frac{C}{2}\left[(1-\phi)^2-1\right] \quad (2.9)$$

Using Eqs. (2.8) and (2.9) in Eq. (2.7), the following expression is obtained for the micellar size distribution[6, 17, 56]

$$X_n(S,l_c) = \frac{(X_1 e)^n}{e}\exp\left[-\beta n g_{mic}(n,S,l_c)\right] \quad (2.10)$$

where $\beta = 1/k_BT$, and $g_{mic}(n,S,l_c) = (\mu_n^\circ(S,l_c)/n - \mu_1^\circ)$ is the free-energy change required to transfer a surfactant molecule from bulk solvent to a micelle of aggregation number n, shape S, and micelle core radius l_c. This free-energy change is known as the free energy of micellization, and will be evaluated based on the molecular model of micellization described in Section 2.3.

Using the micellar size distribution equation, Eq. (2.10), all the equilibrium micellar solution properties associated with it can be computed. In particular, the moments of the micellar size distribution are given by

$$M_k = X_1 + \sum_{S=1}^{3}\sum_{l_c}\sum_{n>1} n^k X_n(S,l_c) \quad (2.11)$$

Note that the zeroth moment corresponds to the total mole fraction of micelles and monomers. That is,

$$M_0 = X_1 + \sum_{S=1}^{3}\sum_{l_c}\sum_{n>1} X_n(S,l_c) \quad (2.12)$$

In addition, the first moment corresponds to the total mole fraction of surfactant, X,

and is given by

$$M_1 = X = X_1 + \sum_{S=1}^{3} \sum_{l_c} \sum_{n>1} nX_n(S, l_c) \tag{2.13}$$

Various average characteristics of the micellar size distribution which can be measured experimentally can be calculated from the moments defined in Eq. (2.11). For example, the number-average and weight-average micelle aggregation numbers, $\langle n \rangle_n$ and $\langle n \rangle_w$, respectively, are given by

$$\langle n \rangle_n = \frac{M_1}{M_0} \tag{2.14}$$

$$\langle n \rangle_w = \frac{M_2}{M_1} \tag{2.15}$$

The relative variance, Var, is a quantitative measure of the polydispersity of the micellar size distribution, and is given by

$$Var = \frac{M_3 M_1}{M_2^2} - 1 \tag{2.16}$$

It has been shown[6, 16] that monodisperse spherical micelles are characterized by $Var = 0.0$, whereas polydisperse cylindrical micelles are characterized by $Var = 0.5$.

Typically, one micelle shape is energetically favored over the other two shapes, so that all the micelles form in the optimal shape, S^*. In this case, it is not necessary to sum over all three shapes because only one micelle shape is present in solution. In addition, the distribution, $X_n(S^*, l_c)$, is usually sharply peaked at a specific value of $l_c = l_c^*$, the optimal micelle core radius. Hence, to a very good approximation, it can be assumed that all the micelles have the same shape, S^*, and the same micelle core radius, l_c^*. To determine the optimal shape, S^*, and the optimal micelle core radius, l_c^*, $X_n(S, l_c)$ is maximized with respect to S and l_c. By rewriting Eq. (2.10) as follows

$$X_n(S, l_c) = \left[X_1 \exp\left(-\beta g_{mic}(n, S, l_c) + 1\right)\right]^n / e \tag{2.17}$$

it is clear that X_n is maximized at the minimum value of $g_{mic}(n, S, l_c)$. In other words, S^* and l_c^* are given by the S and l_c values for which $g_{mic}(n, S, l_c)$ is minimized. The

minimization procedure is described in more detail in Section 2.3.1.

When all the micelles are assumed to be at the optimal S^* and l_c^*, Eq. (2.10) becomes

$$X_n \equiv X_n(S^*, l_c^*) = \frac{(X_1 e)^n}{e} \exp\left[-\beta n g_{mic}(n, S^*, l_c^*)\right] \tag{2.18}$$

The various moments fo the micellar size distribution are then given by

$$M_k = X_1 + \sum_{n>1} n^k X_n \tag{2.19}$$

From knowledge of the micelle size distribution, several experimentally measurable micellar properties can be predicted. For example, the critical micelle concentration, CMC, can be obtained from Eq. (2.18) by taking the natural log of X_n and retaining ony the terms that are of order n ($n \gg 1$). Specifically,

$$CMC \approx \exp\left[\beta g_{mic}(n, S^*, l_c^*) - 1\right] \tag{2.20}$$

The crossover surfactant concentration, X^*, signaling the transition from the dilute (nonentangled) to the semidilute (entangled) micellar solution regimes can be computed using Eq. (2.18) in the context of the theory developed in Ref. [10]. The critical point, which signals the onset of phase separation, is characterized by the critical surfactant concentration, X_c, and the critical temperature, T_c. At the critical point, thermodynamic stability requires that the two conditions, $(\partial^2 g/\partial X^2)_{T,p} = 0$ and $(\partial^3 g/\partial X^3)_{T,p} = 0$, should be satisfied, where $g = G/(N_w + N_s)$. By simultaneously solving these two equations, it is posible to deduce the values of X_c and the critical interaction parameter, C_c, for a given value of T_c. In order to make predictions using the thermodynamic framework described here, a model for the calculation of g_{mic} is required. This model is described in the next section.

2.3 Molecular Model of Micellization for Ionic Surfactants

A molecular model of micellization has been developed to calculate $g_{mic}(n, S, l_c)$.[16, 17] This model involves systematically calculating the magnitude and temperature dependence of the essential physical factors involved in the process of micellization, and is summarized below.

2.3.1 The Thought Process

The molecular model of micellization is used to calculate the free energy of micellization, g_{mic}, based on the chemical structure of the surfactant molecule and the solution conditions. Specifically, $g_{mic}(n, S, l_c)$ represents the free-energy change associated with the transfer of a surfactant molecule from the aqueous solvent to a micelle characterized by an aggregation number, n, shape, S, and micelle core radius, l_c, present in the aqueous solvent. A more negative value of g_{mic} results in a stronger tendency towards micellization. The magnitude of g_{mic} can be evaluated using a conceptual thought process which describes the formation of a micelle from individual surfactant monomers as a series of reversible steps, each associated with a physicochemical contribution to the micellization process. For a schematic representation of the micellization thought process, see Figure 2-1.

The following steps are involved:

1. Breaking the bonds between the surfactant heads and tails. The free-energy change associated with this step is considered to be equal in magnitude and opposite in sign to the free-energy change associated with reforming the bonds between the surfactant heads and tails, once the surfactant molecules have been incorporated into the micelle, and consequently, does not need to be quantified.

2. Transferring the surfactant hydrophobic tails, separately and independently from the heads, from bulk solvent to bulk hydrocarbon (representative of the micellar core). This is an attractive free-energy contribution that can be eval-

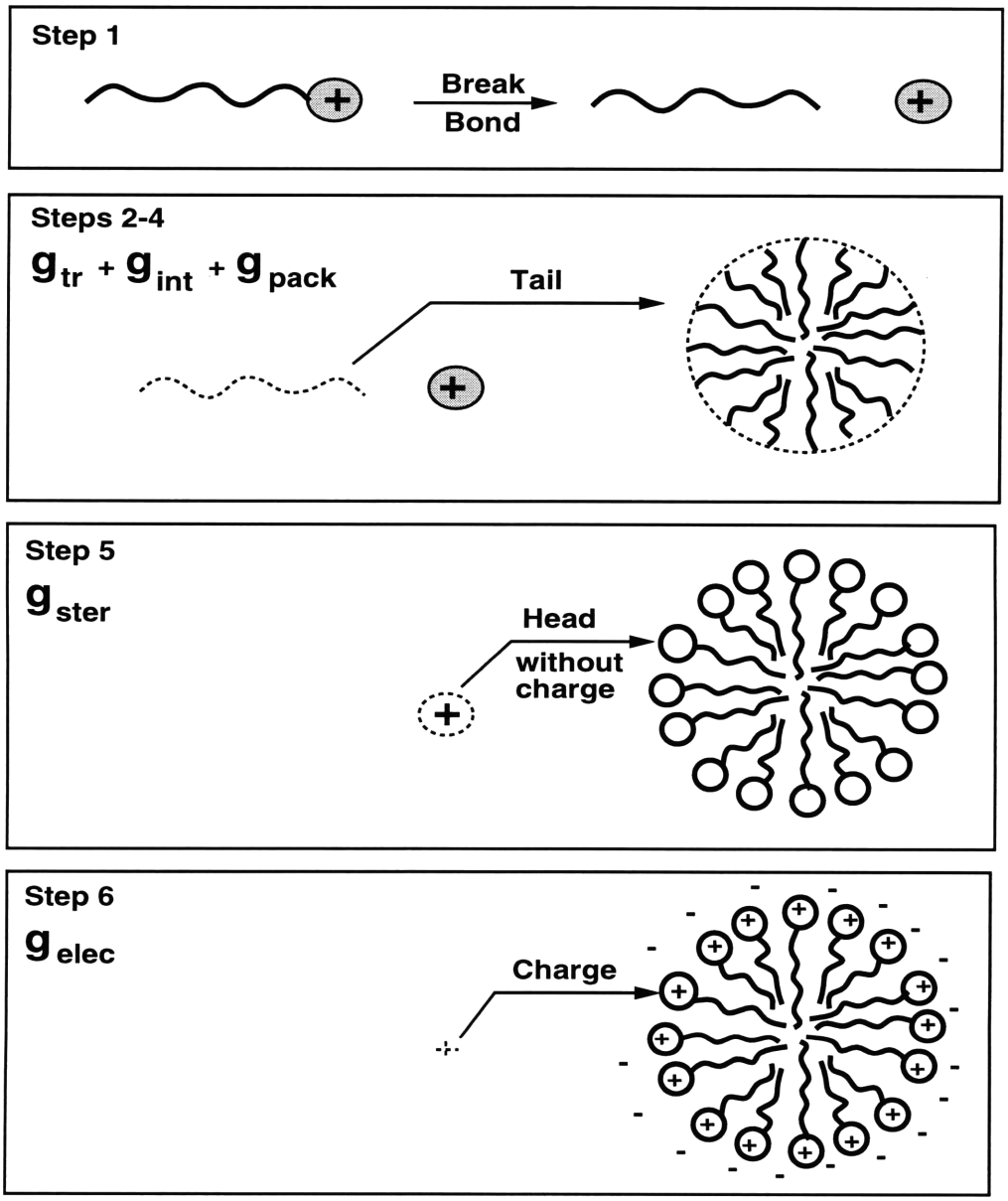

Figure 2-1: Schematic representation of the thought process to visualize the transfer of a charged surfactant monomer from aqueous solution at infinite dilution to the interior of a micelle.

uated using experimental data for the solubility of hydrocarbons in an aqueous solvent. The resulting expression is given by[3, 16]

$$g_{tr}/k_BT = [3.04 - 1.05(n_c - 1)](298/T) - [5.06 + 0.444(n_c - 1)] \qquad (2.21)$$

where n_c is the total number of carbon atoms in the tail.

3. Creating the interface between the micellar core and the surrounding solvent. This contribution is evaluated using the concept of a macroscopic interfacial free energy of a hydrocarbon-water interface, including its dependence on interfacial curvature. The interfacial free energy, g_{int}, is given by

$$g_{int}/k_BT = \frac{\sigma_0}{\left(1 + \frac{(S-1)\delta_T}{l_c}\right)} \left(\frac{a - a_0}{k_BT}\right) \qquad (2.22)$$

where σ_0 is the interfacial tension between bulk hydrocarbon and the solvent, δ_T is the Tolman distance (a measure of the interfacial thickness), a is the total interfacial area available per monomer at the micellar core-water interface, and a_0 is the interfacial area screened from contact with the solvent by the bond between the surfactant head and tail when the head is "reattached". The area available per surfactant molecule at the micellar core-water interface is given by

$$a = \frac{v_t\, S}{l_c} \qquad (2.23)$$

where v_t is the volume of the surfactant tail. For details on the calculation of v_t and δ_T, see References [17, 16].

4. Anchoring the surfactant tails to the interface formed in Step (3). In this step, the tails lose some of their conformational degrees of freedom. The resulting free energy of packing, g_{pack}, is calculated using a statistical-mechanical mean-field hydrocarbon chain packing calculation.[16, 66] For computational speed, the numerically-generated functions of $g_{pack}(l_c)$ are fitted to a second-order polyno-

mial for a range of n_c values between 4 and 18.[66] This yields

$$g_{pack}/k_BT = A_2(l_c/l_{max})^2 + A_1(l_c/l_{max}) + A_0 \tag{2.24}$$

where A_0, A_1, and A_2 are polynomial coefficients which depend on micellar shape as well as on the number of carbon atoms in the hydrocarbon chain, n_c, and l_{max} is the maximum (fully-extended) length of the hydrocarbon tail, given by $l_{max} = 1.54 + 1.265(n_c - 1)$, in Å.

5. Transferring the *uncharged* surfactant heads from their original positions in the solution to the interface between the micellar core and the solvent. The head/tail bonds are reformed, but, as mentioned earlier, the free-energy change associated with reforming the head/tail bonds is cancelled by the free-energy change of breaking these bonds in the first step. The presence of the heads at the interface results in steric and other nonelectrostatic interactions. As a first appoximation, only steric repulsions between the heads are considered (see [16]), and therefore, specific interactions, such as hydrogen bonding between the heads, are neglected. The free-energy change associated with these steric repulsions is calculated by treating the heads present at the interface as an ideal localized monolayer.[16] The resulting free-energy contribution, g_{st}, can be expressed as

$$g_{st}/k_BT = -\ln(1 - a_h/a) \tag{2.25}$$

where a_h is the effective cross-sectional area of the head. Note that in this step, as part of the thought process, the charges are left behind, so that the electrostatic interactions are calculated separately in the next step. The free-energy change associated with discharging the surfactant heads before transferring them is included in the calculation of the last step.

6. Charging the surfactant heads present at the micellar surface surrounded by a cloud of charged counterions. For nonionic surfactants, this step can be ignored. In the case of ionic surfactants, the charges, which were left behind in the

previous step, must now be restored to the uncharged surfactant heads residing on the micellar surface. Note that the free energy associated with discharging the surfactant heads in Step (5) is accounted for in this last step. The work involved in this step is the electrostatic free-energy contribution, g_{elec}, and its calculation, discussed in detail in the next section, is a central element of this chapter.

The sum of all the five free-energy contributions described above yields the free energy of micellization, $g_{mic}(n, S, l_c)$. Specifically,

$$g_{mic} = \frac{\mu_n^\circ}{n} - \mu_1^\circ = g_{tr} + g_{pack} + g_{int} + g_{st} + g_{elec} \tag{2.26}$$

As discussed in Section 2.2, it is convenient to determine the optimal l_c^* value, in order to simplify the calculation of the moments. Accordingly, for each of the three regular micelle shapes, g_{mic} is calculated and subsequently minimized with respect to l_c to determine the minimum free energy, $g_{mic}^*(S)$, and the corresponding optimal micelle core radius, l_c^*, for that particular micelle shape, S. The optimal micelle shape, S^*, corresponds to that associated with the lowest $g_{mic}^*(S, l_c^*)$ value. If the optimal shape, S^*, corresponds to a sphere, the micelles are assumed to be monodisperse spheres with an aggregation number $n_0 = 4\pi(l_c^*)^3/3v_t$. If the optimal shape, S^*, corresponds to an infinite cylinder, the micelles are polydisperse with aggregation numbers ranging from the minimum-sized spherical micelle of aggregation number $n_0 = 4\pi(l_c^*)^3/3v_t$ to infinity. In this case, $g_{mic}^*(n)$ is estimated by linearly interpolating between the g_{mic}^* values for spheres and infinite-sized cylinders. Specifically,

$$g_{mic}^{cyl}(n) = \frac{n_0}{n} g_{mic}(S = 3, l_c^*) + \frac{n - n_0}{n} g_{mic}(S = 2, l_c^*) \tag{2.27}$$

2.3.2 The Electrostatic Free Energy, g_{elec}

The electrostatic contribution, g_{elec}, represents the free-energy change associated with charging a surfactant molecule in a micelle surrounded by a cloud of ions. Note that in the McMillan-Mayer statistical-thermodynamic framework presented in Chapter 6,

g_{elec} is calculated for a bare micelle with no surrounding ion cloud. In other words, the standard state is defined differently. Hence, a different approach for calculating g_{elec} in the context of the McMillan-Mayer statistical-thermodynamic framework will be discussed in Chapter 6. The following discussion on the calculation of g_{elec} applies only to the molecular-thermodynamic theory presented in this chapter.

The ions (counterions and co-ions) surrounding the micelle are already fully-charged and arranged in their final spatial configuration, as if the micelle were already fully-charged. In that case, g_{elec} is equivalent to the reversible work, W, involved in bringing a charge into a region having an electrostatic potential, ψ, in the electrical double layer created between the micellar surface of charge and the ion cloud surrounding the micelle.[57] This is known as the Guntelberg charging process. In this approach, the work of charging is given by[57]

$$W = g_{elec} = \frac{1}{n}\int_0^{nze} \psi_o(q)\, dq - \frac{(ze)^2}{2\epsilon r_h} = a_{ch}\int_0^{ze/a_{ch}} \psi_o(\sigma)\, d\sigma - \frac{(ze)^2}{2\epsilon r_h} \qquad (2.28)$$

where ψ_o is the electrostatic potential at the surface of charge, q is the micelle charge (equal to nze when fully charged), σ is the surface charge density (equal to ze/a_{ch} when fully charged), e is the electronic charge, z is the surfactant valence, and a_{ch} is the area available to a surfactant molecule at the surface of charge. The negative term in Eq. (2.28) represents the free-energy change associated with discharging the surfactant head in the previous (fifth) step, where r_h is the radius of the surfactant head, and ϵ is the dielectric constant of the solvent. Because the monomer is discharged at infinite dilution, this free-energy change is simply the negative of the Born solvation energy of the monomer head. This contribution is typically negligible compared to the work of charging the micelle, but it is included for completeness. Note that in calculating g_{elec}, it is assumed that the surfactant charges are smeared over the surface of the micelle.

The next challenge is to calculate the electrostatic potential at the charged micelle surface, ψ_0. For this purpose, the classical Poisson-Boltzmann (PB) equation can be

utilized to describe the electric field around a charged micelle. Specifically,

$$\nabla^2 \psi(\vec{r}) = -\frac{4\pi e}{\epsilon} \sum_i c_i^o z_i \exp\left[\frac{-z_i e \psi(\vec{r})}{k_B T}\right] \tag{2.29}$$

where $\vec{r}$ is the location measured from the center of the micelle, c_i^o is the number concentration of ions of type i in the bulk solution far from the micelle, z_i is the valence of ions of type i, $\epsilon = 4\pi\epsilon_0\epsilon_r$ is the dielectric constant, where ϵ_r is the relative permittivity of water (78.5 at 25°C) and ϵ_0 is the vacuum permittivity ($8.854 \times 10^{-22} \mathrm{C}^2/\mathrm{J\AA}$). Equation (2.29) is general and can be applied to any electrolyte solution. The remainder of this chapter treats only symmetric surfactants, where $z_{surf} = -z_{counterion}$. Consequently, only the general notation z will be used, where z refers to the valence of the surfactant molecule (with $z_{counterion} = -z$). In addition, if salt is added, it is assumed to have the same valence as the surfactant molecule, that is, $z_{counterion,salt} = z_{counterion} = -z$ and $z_{coion,salt} = z_{surf} = z$.

The three types of micellar shapes considered here, spheres, infinite cylinders, and infinite bilayers, are axi-symmetric, which effectively reduces the solution of Eq. (2.29) to a one-dimensional problem. In other words, for a sphere, the only direction along which the potential varies is the radial distance from the center of the sphere. For the case of an infinite cylinder, the only direction along which the potential varies is the radial distance from the cylindrical axis. For inifinite bilayers, the only direction of interest is the distance normal to the planar bilayer. The scalar variable, r, is used for each of these three cases, such that the Laplacian operator on the left-hand side of Eq. (2.29) takes on the following form

$$\nabla^2 \psi(r) = \frac{\partial^2 \psi}{\partial r^2} + \frac{m}{r}\frac{\partial \psi}{\partial r} \tag{2.30}$$

where r is the scalar distance from the center of the micelle, and $m = S - 1$ is a shape factor (with $S = 3$ for spheres, 2 for infinite cylinders, and 1 for infinite bilayers).

The right-hand side of Eq. (2.29) describes the distribution of ions surrounding the charged micelle. This ion distribution (known as the Boltzmann distribution) neglects the finite volume of the counterions, an approximation which leads to exces-

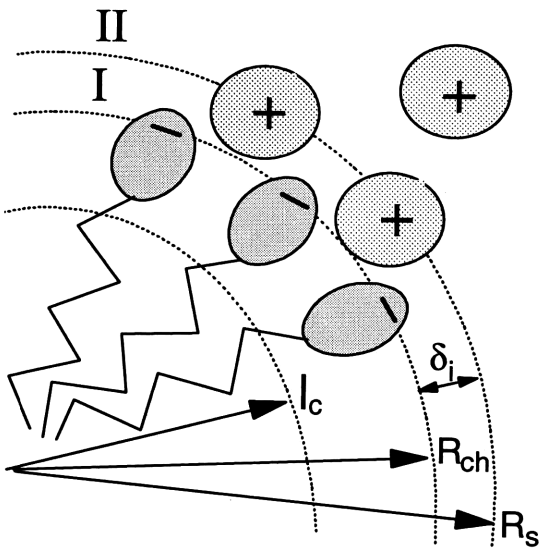

Figure 2-2: Section of the micellar interface, illustrating the pertinent regions involved in the Stern layer model: I indicates the Stern layer region, and II indicates the diffuse ion cloud region. l_c is the radius of the micelle core, R_{ch} is the radius of the surface of charge, δ_i is the radius of the hydrated counterion, and R_s is the radius of the outer edge of the Stern layer.

sive screening at the micellar surface. In order to provide the counterions with some volume, the original Poisson-Boltzmann equation was modified to include a Stern layer,[67, 26, 27] defined as the region immediately surrounding the micellar surface from which counterions are excluded. The Stern layer is illustrated in Figure 2-2, where region I refers to the Stern layer and region II refers to the diffuse ion cloud. The boundaries are defined by the radius of the surface of charge, R_{ch}, the radius of the hydrated counterion, δ_i, and the radius of the outer edge of the Stern layer, $R_s = R_{ch} + \delta_i$. The thickness of the Stern layer, δ_i, is approximately equal to the distance from the surface of charge to the center of the associated counterions, including hydration.

In the Poisson-Boltzmann model, the charge of an ion in the ion cloud is localized at the center of the ion. Because the centers of the ions do not penetrate the Stern layer region (region I), the right-hand side of Eq. (2.29) reduces to zero. In other

words, in region I, ψ satisfies the Laplace equation, that is,[64, 57]

$$\nabla^2 \psi_I(r) = 0 \tag{2.31}$$

where ψ_I represents the electrostatic potential within the Stern layer. From Gauss' Law at the charged surface of the micelle ($r = R_{ch}$), the following boundary condition is obtained (see Appendix A for a detailed derivation):[57]

$$\left(\frac{\partial \psi_I}{\partial r}\right)_{r=R_{ch}} = -\frac{4\pi\sigma}{\epsilon} = -\frac{4\pi z e}{\epsilon a_{ch}} \tag{2.32}$$

Note that the dielectric constant in region I is assumed to be equal to that in region II, which is equal to the bulk value, that is, $\epsilon_1 = \epsilon_2 = \epsilon$. The behavior of the dielectric constant is discussed in more detail in Section 2.3.3.

At $r = R_s$, where the Stern layer region (I) meets the diffuse ion cloud region (II), both the electrostatic potentials and the derivatives of the potentials must equal each other (see Appendix A). In other words,[64, 68]

$$\psi_I(R_s) = \psi_{II}(R_s) \tag{2.33}$$

and[1]

$$\left(\frac{\partial \psi_I}{\partial r}\right)_{r=R_s} = \left(\frac{\partial \psi_{II}}{\partial r}\right)_{r=R_s} \tag{2.34}$$

By integrating Eq. (2.31) subject to these boundary conditions (see Appendix A), the following expression is obtained for the electrostatic potential at the surface of charge:

[1]Note that if charges were physically present on the Stern layer surface (at $r = R_s$), the boundary condition given in Eq. (2.34) would have an additional contribution to account for the charge at $r = R_s$ (see Appendix A for details). In the model presented here, it is assumed that the charges are infinitesimally displaced from the Stern layer surface, and therefore, the additional contribution can be neglected.

$$\psi_I(R_{ch}) = \begin{cases} \psi_{II}(R_s) + \frac{4\pi e z \delta_i}{\epsilon a_{ch}(1+\delta_i/R_{ch})} & \text{, for a sphere} \\ \psi_{II}(R_s) + \frac{4\pi e z R_{ch}}{\epsilon a_{ch}} \ln(1+\delta_i/R_{ch}) & \text{, for an infinite cylinder} \\ \psi_{II}(R_s) + \frac{4\pi e z \delta_i}{\epsilon a_{ch}} & \text{, for an infinite bilayer} \end{cases} \quad (2.35)$$

where $\psi_{II}(R_s)$ is the electrostatic potential at the outer edge of the Stern layer. The Poisson-Boltzmann equation, Eq. (2.29), can then be utilized to solve for ψ_{II} in the diffuse ion cloud region (II) to obtain $\psi_{II}(R_s)$.

The electrostatic potential given in Eq. (2.35) can be integrated according to Eq. (2.28) to determine g_{elec}, Specifically (see Appendix A for details),

$$\beta g_{elec} = \beta g_{elec,II} + \frac{\kappa s}{2} \mathcal{F}(S) - \frac{(ze)^2}{2\epsilon r_h k_B T} \quad (2.36)$$

where $g_{elec,II}$ is the electrostatic free energy contribution due to the ion cloud region (II) and $\mathcal{F}(S)$ is a function which depends on the shape, S, of the micelle, given by

$$\mathcal{F}(S) = \begin{cases} \delta_i(1+\delta_i/R_{ch}) & \text{, for } S\text{=3 (sphere)} \\ R_{ch}(1+\delta_i/R_{ch})\ln(1+\delta_i/R_{ch}) & \text{, for } S\text{=2 (infinite cylinder)} \\ \delta_i & \text{, for } S\text{=1 (infinite bilayer)} \end{cases} \quad (2.37)$$

where s is a dimensionless surface charge density (see Appendix A for details), given by

$$s = \frac{4\pi e^2 z^2}{\epsilon \kappa a_{ch} k_B T (1+\delta_i/R_{ch})^m} \quad (2.38)$$

and κ^{-1} is the Debye screening length, where

$$\kappa^2 = \frac{8\pi c_i^\circ e^2 z^2}{\epsilon k_B T} \quad (2.39)$$

where c_i° is the concentration of ions in the bulk, including the surfactant monomers. In other words, $c_i^\circ = c_{salt} + c_1$, where c_{salt} is the concentration of added salt and c_1 is the concentration of the surfactant monomers. Note that κ^{-1} has units of length, and is a measure of the thickness of the ion cloud. At low concentrations, c_i° is low,

and the ion cloud surrounding the micelle is relatively thick. Conversely, at high salt concentrations, c_i° is high, and the ion cloud is thin.

As stated above, $g_{elec,II}$ is the electrostatic free energy due to the ion cloud region (II). To calculate $g_{elec,II}$, the integral in Eq. (2.28) is applied to the diffuse-ion cloud region. Specifically,

$$\beta g_{elec,II} = \frac{a_{ch}}{k_B T} \int_0^\sigma \psi_{II}(R_s)\, d\sigma \tag{2.40}$$

In order to determine $\psi_{II}(R_s)$, the electrostatic potential must be calculated according to Eq. (2.29), subject to the following boundary conditions (see Appendix A for details).[57, 21]

(i) at $r = R_s$, the potential must be continuous, as described in Eq. (2.34). In addition, the value of this derivative is given by Gauss' law, as follows,

$$\left(\frac{\partial \psi_{II}}{\partial r}\right)_{r=R_s} = \left(\frac{\partial \psi_I}{\partial r}\right)_{r=R_s} = \frac{-4\pi z e}{\epsilon a_{ch}(1+\delta_i/R_{ch})^m} \tag{2.41}$$

(ii) as $r \to \infty$, the potential decays to zero due to electroneutrality in the bulk, that is,

$$\psi_{II}(r \to \infty) = 0 \tag{2.42}$$

$$\left(\frac{\partial \psi_{II}}{\partial r}\right)_{r\to\infty} = 0 \tag{2.43}$$

Recall that Eq. (2.29) is a nonlinear differential equation, and an analytical solution for ψ_{II} cannot be realized. Instead, Eq. (2.29) can be solved numerically, which is computationally expensive, or analytical approximations can be utilized. ψ_{II} can then be integrated according to Eq. (2.40) to obtain $g_{elec,II}$. Several different analytical approximations are available in the literature. Among these, four widely-used approximations were selected for study. The first is a solution by Evans and Ninham[21] based on an expansion in powers of $1/\kappa R_s$ around the planar solution ($m = 0$), which is analytical. This solution will be denoted as the EMN83 approximation, and is

given by

$$\beta g_{elec,II}(\text{EMN83}) = 2\ln\left[(s/2) + (1+s^2/4)^{1/2}\right] + \frac{4}{s}\left[1 - (1+s^2/4)^{1/2}\right] - \frac{4m}{\kappa R_s s}\ln\left(\frac{1+(1+s^2/4)^{1/2}}{2}\right) \quad (2.44)$$

In a subsequent publication, Evans, Mitchell, and Ninham[22] amended their previous solution with a slightly different approximation. This solution, referred to as the EMN84 approximation, is given by

$$\begin{aligned}\beta g_{elec,II}(\text{EMN84}) &= y_0 - 2\left(\frac{w+1}{w-1}\right)^{1/2} + \frac{8}{s}\left(1+\frac{2}{\kappa R_s}\right)^{1/2} \\ &\quad -\frac{8m}{\kappa R_s s}\left[\ln\left((w+1)^{1/2} + \frac{s}{2(w-1)^{1/2}}\right) - \ln 2^{1/2}\left(1+(1+\frac{2}{\kappa R_s})^{1/2}\right)\right]\end{aligned} \quad (2.45)$$

where $w = \cosh(y_0/2)$, and y_0 is the scaled surface potential, obtained from the following expression

$$\cosh(y_0/2) = \left[\left(1+\frac{2}{\kappa R_s}\right)^2 + \frac{s^2}{4}\right]^{1/2} - \frac{2}{\kappa R_s} \quad (2.46)$$

More recently, Mitchell and Ninham[58] added additional curvature correction terms to the 1983 approximation (to order $1/(\kappa R_s)^2$). This solution, referred to hereafter as the EMN89 approximation, is given by

$$\begin{aligned}\beta g_{elec,II}(\text{EMN89}) &= \text{Eq. (2.44)} + m^2/(\kappa R_s)^2\left[1/s - 8/s^3 + 8/(s^3(1+s^2/4)^{1/2})\right] \\ &\quad -\frac{2m(m-1)}{s(\kappa R_s)^2} f[(1+s^2/4)^{1/2}]\end{aligned} \quad (2.47)$$

where

$$f(x) = 2\int_1^x \frac{\ln[(1+t)/2]}{t^2-1}\,dt \quad (2.48)$$

Hayter[23] contributed a fourth approximate expression based on a renormaliza-

tion of the planar result corresponding to the EMN approach. Specifically,

$$\begin{aligned}\beta g_{elec,II}(\text{Hayter}) &= y_0 - \frac{4m}{\kappa R_s s}\left\{\left(1+x_0^2(u+1)^2/4\right)^{1/2} - (1+x_0^2)^{1/2} + 2\ln\left(\frac{u+1}{2}\right)\right\} \\ &\quad -\frac{4m}{\kappa R_s s}\left\{\ln[1+(1+x_0^2)^{1/2}] - \ln\left[1+\left(1+x_0^2(u+1)^2/4\right)^{1/2}\right]\right\}\end{aligned} \tag{2.49}$$

where s is given in Eq. (2.38), and x_0 and y_0 are the scaled radius and surface potential, respectively, and are given by

$$x_0 = \kappa R_s \tag{2.50}$$

$$y_0 = 2\ln\left[u+(u^2-1)^{1/2}\right] \tag{2.51}$$

u is calculated from the following implicit equation

$$s = \frac{4}{x_0}\left(\frac{u-1}{u+1}\right)^{1/2}\left[1+\left(1+\left(\frac{x_0(u+1)}{2}\right)^2\right)^{1/2}\right] \tag{2.52}$$

Each of the four approximations described above can be studied separately to determine which is most appropriate for use in the micellar solution case. There are two critieria that could be used to determine the best approximation: (i) select the approximation which most closely matches the exact solution of the Poisson-Boltzmann equation, or (ii) select the approximation which yields the most accurate predictions of micellar solution properties, such as the CMC. In other words, due to its inherent limitations, the PB equation itself may not be the most accurate model of the electrostatic field surrounding a micelle, such that criterion (ii) may be more appropriate than criterion (i).

The major variables on which g_{elec} depends are l_c, the micll core radius, and κ, a measure of the ionic strength of the solution. Hence, the behavior of the various analytical approximations to the PB equation will be studied for a range of l_c and κ. First, each approximation will be compared with the numerical solution to the PB equation by calculating g_{elec} as a function of l_c/l_{max} for a fixed κ. As an illustration, an

SDS solution at the CMC will be considered. In this case, $c_i^\circ = CMC(SDS)$ =8mM at $T = 25°C$, resulting in $\kappa = 0.0294\text{Å}^{-1}$. The radius of charge is given by $R_{ch} = l_c + d_{ch}$, where $d_{ch}(SDS) = 3.7\text{Å}$ is the distance from the tail to the location of the charge (including the first CH_2 group), and δ_I (Na^+) = 1.85Å. Figure 2-3 shows g_{elec} calculated from Eq. (2.36) using the various approximations for $g_{elec,II}$. Specifically, $g_{elec,II}$ is given by Eq. (2.44) for EMN83 ($\cdots$), Eq. (2.45) for EMN84 ($- \cdot\cdot - \cdot\cdot -$), Eq. (2.47) for EMN89 ($- - -$), and Eq. (2.49) for the Hayter ($- \cdot - \cdot -$) approximations. These are compared with the numerical solution to the Poisson-Boltzmann equation (—). The EMN83 solution clearly yields the closest agreement with the numerical PB solution at the larger l_c values, but deviates significantly from it for $l_c/l_{max} < 0.85$. The behavior of g_{elec} as a function of l_c is important to the minimization procedure for determining $g_{mic}(l_c^*)$. At the smaller l_c values, it may be safer to use one of the other approximations, which, although they underestimate g_{elec} with respect to the numerical PB solution, exhibit a dependence on l_c similar to that of the numerical solution.

As mentioned above, in addition to its dependence on l_c, g_{elec} also depends on κ. The dependence on κ is not as important as the dependence on l_c/l_{max} for the minimization of g_{mic}. However, it is important for the determination of the CMC, since κ is a function of $c_i^\circ \approx$ CMC when no salt is added. To study the behavior of g_{elec} over a range of c_i° values, the approximations for g_{elec} are analyzed over a range of CMC predictions, which depend on both l_c and κ. Each g_{elec} approximation was used in g_{mic} to calculate the CMC for dodecyl ethoxy sulfates at 50°C, where the number of ethylene oxide (EO) groups in the head varies from zero to four. Note that the range of l_c values over which g_{mic} was minimized was restricted to $0.5l_{max} \leq l_c \leq l_{max}$. The results are presented in Figure 2-4 for the EMN83 ($\cdots$), EMN84 ($- \cdot\cdot - \cdot\cdot -$), EMN89 ($- - -$), and Hayter ($- \cdot - \cdot -$) approximations, and for the numerical solution to the PB equation (—)[2]. The experimental CMC values are denoted by the circles.[69]

[2]Note that g_{elec} depends on κ, which, in turn, depends on the monomer concentration through the concentration of ions, c_i°. However, g_{elec} is required to calculate the surfactant monomer concentration. In other words, g_{elec} and the monomer concentration must be solved simultaneously through an iterative procedure. In order to speed up the calculations, the CMC is used to approximate the

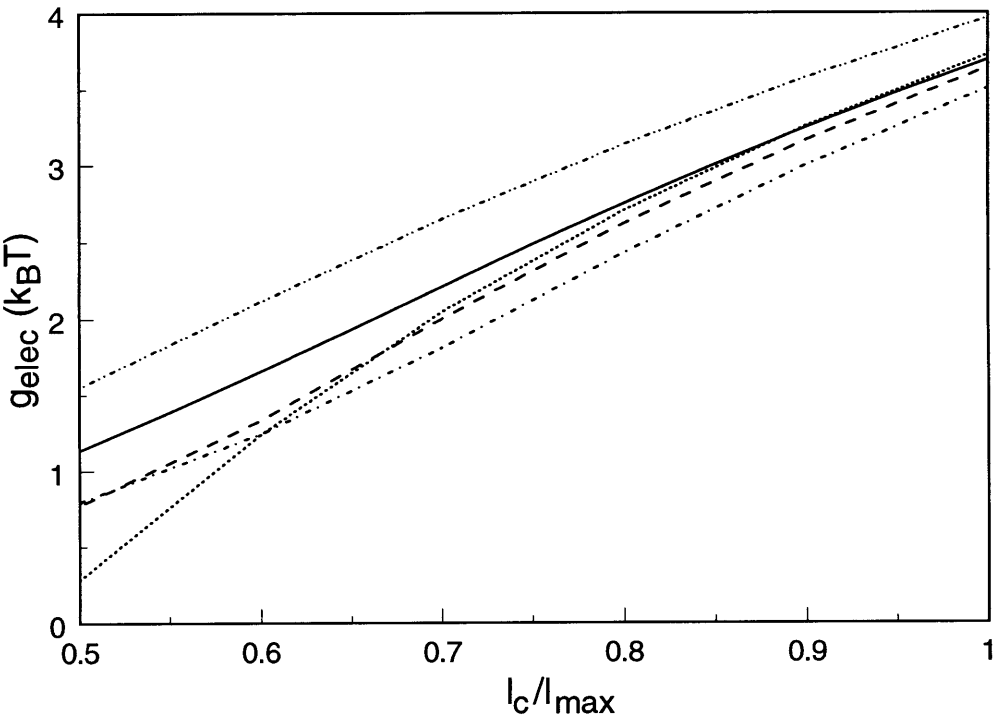

Figure 2-3: Calculation of g_{elec} as a function of l_c/l_{max} for SDS at 25°C using the numerical solution to the Poisson-Boltzmann equation (—), and the EMN83 ($\cdots$), EMN84 ($- \cdot\cdot - \cdot\cdot -$), EMN89 ($- - -$), and Hayter ($- \cdot - \cdot -$) approximations.

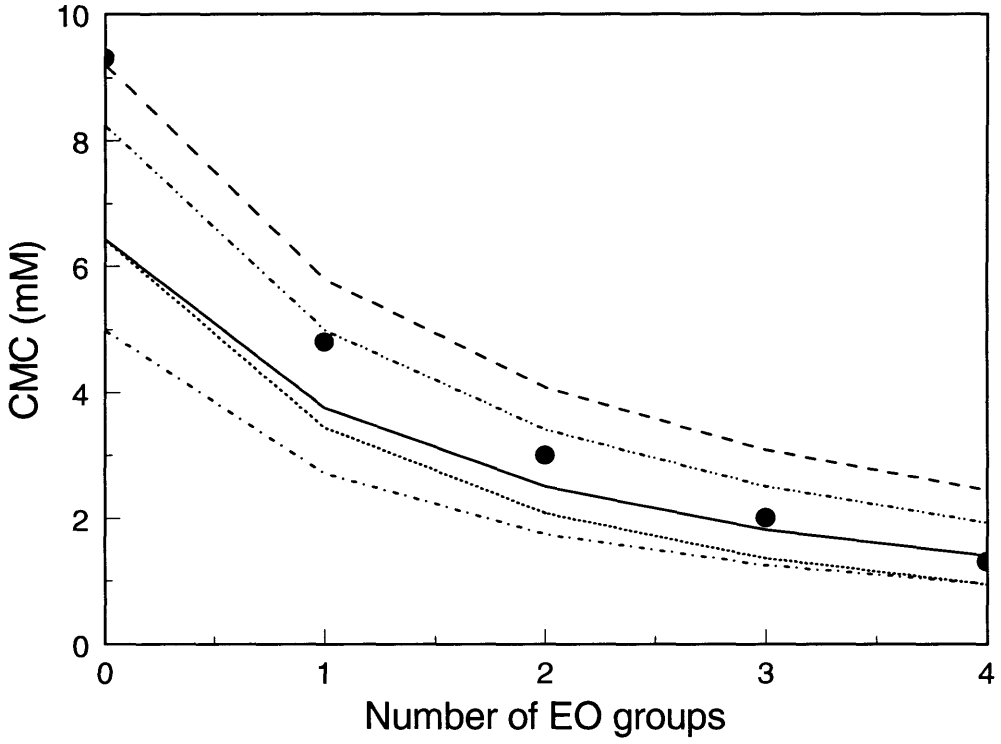

Figure 2-4: Predicted CMC as a function of the number of EO groups in the head for aqueous solutions of dodecyl ethoxy sulfates at 50°C. Predictions were made using the EMN83 (···), EMN84 (– ·· – ·· –), EMN89 (– – –), and Hayter (– · – · –) approximations and the numerical solution to the PB equation (—). Experimental CMC values are denoted by the circles.

Figure 2-4 indicates that the numerical solution to the PB equation consistently underpredicts the CMC. The EMN84 and EMN89 approximations overestimate g_{elec} compared with the numerical PB solution, and therefore, predict higher CMC values. In fact, the EMN84 approximation mathematically compensates for the limitations of the Poisson-Boltzmann model, resulting in fairly accurate CMC predictions. The EMN83 and the Hayter approximations both underestimate g_{elec} compared with the numerical PB solution, and therefore predict CMC values which are even lower than those predicted by the numerical PB solution. Note that as the number of EO groups increases, all the CMC predictions become much closer to each other. This reflects the fact that the surfactant charges are displaced farther away from the micellar core, and therefore, electrostatic effects become less important.

Because the EMN84 approximation predicts CMC values which are very close to the experimental values, it was chosen as the best approximation for use in additional studies. However, it should be kept in mind that this approximation overestimates the true numerical solution to the PB equation, and, in so doing, *mathematically* corrects the Poisson-Boltzmann predictions, resulting in better CMC predictions. For comparison, the EMN83 approximation was also used in the additional studies, because at larger l_c values, it closely resembles the numerical PB solution. However, this approximation should also be used with caution, since, during the minimization of g_{mic}, the micelle may have a tendency to favor smaller l_c values for which the calculated g_{elec} becomes very small (see Figure 2-3).

The EMN84 and the EMN83 approximations were also used to study the effect of varying the counterion size. In Figure 2-5, the predicted CMC is shown for dodecyl sulfate surfactants with various counterions ($C_{12}H_{25}SO_4X$, or XDS, where X= Li, Na, K, or Cs.[64]) The dark-shaded bars represent experimental CMC values.[70] The striped bars represent CMC predictions made with the EMN84 approximation, and the dotted bars represent CMC predictions made with the EMN83 approximation.

---

monomer concentration. In the calculations presented in Figure 2-4, the CMC was used in place of the monomer concentration for all the analytical approximations, but the numerical solution was calculated with the actual monomer concentration. If the numerical solution was calculated with the CMC, the numerical predictions would decrease by approximately 10%.

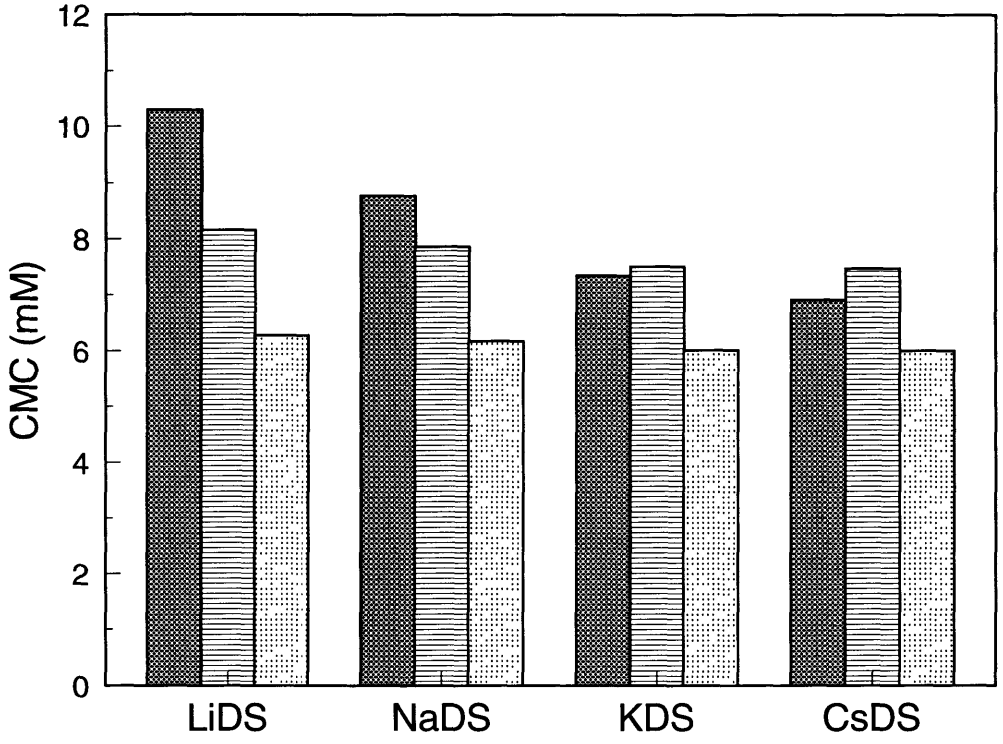

Figure 2-5: Predicted CMC of dodecyl sulfate surfactants having different counterions at 40°C. Predictions were made with the EMN84 approximation (striped bars) and the EMN83 approximation (dotted bars). The dark-shaded bars represent the experimental values.

Again, because the EMNM84 approximation mathematically corrects the limitations of the PB equation by overestimating g_{elec}, it results in better CMC predictions than those of the EMN83 approximation, which is very close to the numerical PB solution(see Figure 2-3). Note that the CMC decreases as the hydrated radius of the counterion decreases (δ_i = 2.35Å, 1.85Å, 1.32Å, and 1.27Å for Li, Na, K, and Cs, respectively[71]). This is due to the fact that smaller counterions can approach closer to the micellar surface, thereby screening the head/head electrostatic repulsions more effectively. In other words, as δ_i decreases, it is easier to form a micelle, and therefore, the CMC is lower. Figure 2-5 also illustrates the effect of including a Stern layer in the model. The Stern layer allows not only for a more accurate calculation of g_{elec}, and hence, of the CMC, but also introduces counterion specificity.

Solution conditions can have a strong effect on micellar size. In particular, it is well known[9] that the addition of salt screens the surfactant charges, allowing spherical micelles to grow into cylindrical micelles. For SDS, this sphere-to-rod transition occurs at approximately 0.5M NaCl.[9, 72, 73] Figure 2-6 shows the effect of adding NaCl on the predicted relative variance of the micellar size distribution, with a Stern layer (—) and with no Stern layer (– – –).

As discussed in Section 2.2, a variance of 0.0 corresponds to monodisperse, spherical micelles, while a variance of 0.5 corresponds to polydisperse, elongated cylindrical micelles. As can be seen in Figure 2-6, the model without a Stern layer actually predicts the micellar shape transition quite accurately as compared with experimental measurements which indicate that it occurs at 0.5M NaCl. In comparison, the Stern layer model appears to inhibit growth of the micelles from spheres into cylinders. Indeed, the Stern layer increases the repulsive electrostatic interactions between the surfactant heads such that much more NaCl must be added to screen the charges and allow the micelles to grow. This behavior is true regardless of the analytical approximation (or numerical solution) used to calculate g_{elec}.

Although the Stern layer model is instrumental in achieving accurate CMC predictions, it is clearly missing an important element to accurately predict micellar growth. Recall that in the thermodynamic framework described in Section 2.2, only mean-

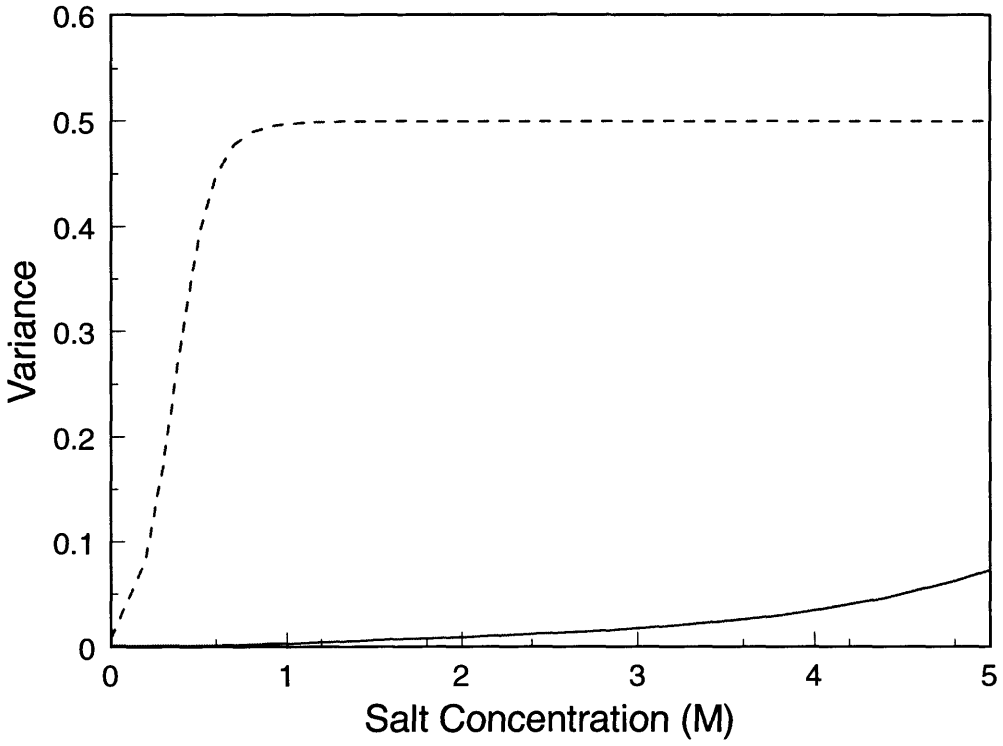

Figure 2-6: Predicted relative variance of the micellar size distribution for an aqueous SDS solution at 25°C as a function of NaCl concentration with (—) and without (– – –) a Stern layer.

field attractive intermicellar interactions are included in the model. Electrostatic intermicellar interactions, which can be quite long-ranged, are neglected. Clearly, a new approach to systematically address the impact of intermicellar interactions based on rigorous statistical-thermodynamic principles is needed. This was the motivation for developing the McMillan-Mayer statistical-thermodynamic framework presented in Chapters 4 through 6. However, the molecular-thermodynamic theory presented in this chapter is still valuable in that the equations that must be solved are relatively simple. Accordingly, it can provide accurate predictions of many micellar solution properties in a matter of seconds. In addition, several minor modifications can be made to the Stern layer model to improve predictions. These are discussed in the next section.

2.3.3 Modifications to the Poisson-Boltzmann Model

Size of the Stern Layer

In the previous section, the width of the Stern Layer was chosen to be the radius of the hydrated counterion. In addition, the surface of the micelle was assumed to be smooth, and the Stern layer surface was measured from the surface of charge. In reality, the surfactant head layer is a fluid region consisting of surfactant heads, water molecules, and counterions. Therefore, the width of the Stern layer may fluctuate. There is some evidence[74, 75] that the surfactant heads themselves are hydrated. Indeed, in the case of metal electrodes, certain ions, such as Cs^+ and Cl^-, prefer to lose their hydration sheaths and contact the surfactant heads directly. Other ions, such as Na^+ and F^-, prefer to retain their hydration sheaths and remain separated from the surfactant heads by the surfactant's hydration layer.[57] In addition, the surfactant head may contain some atoms which sterically inhibit the counterions from directly contacting the surface of charge. Of course, it is also possible that the charge is not localized at one position, but is shared among several atoms. Figure 2-7 illustrates the micellar interfacial region for the case where a charged sulfate group is the terminal group on the surfactant head.

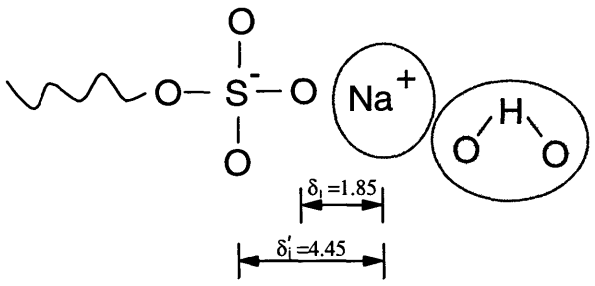

Figure 2-7: Expanded schematic view of the micellar interface for a surfactant with a charged sulfate group as the terminal group in the head. Measurements are in Å.

In order to test the effect of the Stern layer width, CMC predictions were made for dodecyl ethoxy sulfate surfactants with a Stern layer width of 4.45Å, which is equal to the radius of the hydrated counterion plus the distance that the oxygen atom extends from the charged sulfur atom (see Figure 2-7). For comparison, predictions were also made with a Stern layer width of 1.85Å, which includes only the radius of the hydrated counterion. Note that this is the same δ_i value used in the predictions illustrated in Figures 2-3 and 2-4. Figure 2-8 illustrates predictions made using the EMN84 approximation with Stern layer widths of $\delta_i = 4.45$Å ($- - -$) and $\delta_i = 1.85$Å ($- \cdot \cdot - \cdot \cdot -$), and using the EMN83 approximation with Stern layer widths of $\delta_i = 4.45$Å ($- - -$) and $\delta_i = 1.85$Å ($\cdots$). For comparison, experimental CMC values are also shown (circles). Note that the predictions with $\delta_i = 1.85$Å are the same as those presented in Figure 2-4.

For the EMN84 approximation, it can be seen that increasing the width of the Stern layer increases the CMC. This is due to the fact that a larger Stern layer prevents the counterions from shielding the surfactant charges as effectively, thereby making it more difficult to form a micelle, resulting in a higher CMC. Increasing the Stern layer width improves the CMC predictions made with the EMN84 model for zero EO groups. The EMN84 approximation overestimates the CMC for higher numbers of EO groups, although the effect becomes negligible as electrostatics are less important for the larger numbers of EO groups. In contrast to the behavior exhibited by the EMN84 approximation, the larger Stern layer actually resulted in lower CMC predictions for the EMN83 approximation over much of the EO range

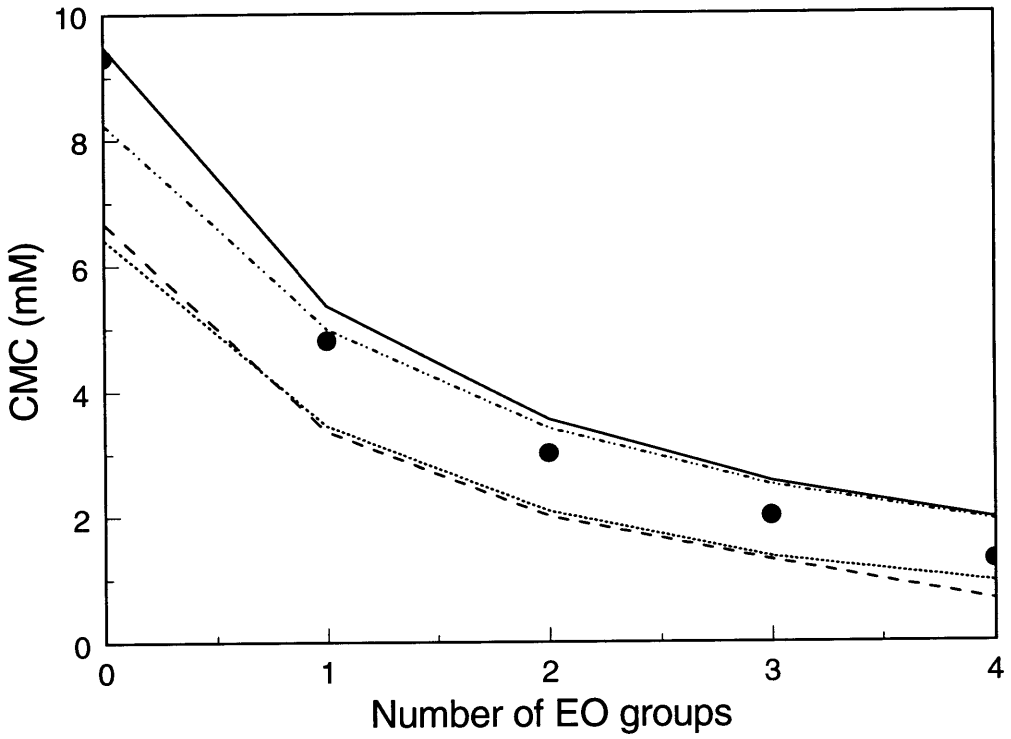

Figure 2-8: Predicted CMC as a function of the number of EO groups in the head for aqueous solutions of dodecyl ethoxy sulfates at 50°C. Predictions were made using the EMN84 approximation with a Stern layer width of $\delta_i = 1.85$Å$(- \cdot\cdot - \cdot\cdot -)$ and $\delta_i = 4.45$Å$(—)$, and using the EMN83 approximation with a Stern layer width of $\delta_i = 1.85$Å$(\cdots)$ and $\delta_i = 4.45$Å$(- - -)$. Experimental CMC values are denoted by circles.

examined. This result is an artifact of the minimization procedure. Recall that the EMN83 approximation deviates from the numerical solution at small radii (see Figure 2-3). When the Stern layer width is increased, the electric field is stronger, and the micelle compensates by shrinking to very small radii where g_{elec}(EMN83) becomes very small. This behavior is an illustration of the need to select an approximation which is accurate over the entire range of l_c values, in order to obtain the correct minimization. The Stern layer width could be increased further by including some water of hydration around the sulfate group. However, recall that the Stern layer model prevents micellar growth (see Figure 2-6), an effect which would be worse for a larger Stern layer. All of these factors should be considered when deciding on an appropriate value for δ_i.

Dielectric Constant

In the Poisson-Boltzmann equation, the solvent is treated as a structureless continuum characterized by a uniform dielectric constant, ϵ. This treatment ignores two important effects. [76, 77] The first effect is that, in reality, ϵ will decrease as the strength of the electric field, E, increases. That is, at high electric fields, the water dipoles become oriented in the direction of the applied electric field, so that any applied potential (for example, that resulting from other ions present in the solution) would have little or no effect on these dipoles. This is known as dielectric saturation, and may occur at the charged micellar surface where the high local density of the charged surfactant heads can generate strong electric fields. The second effect on ϵ is due to the presence of counterions in the head layer, as a result of which the water molecules structure around the ions, thus inducing a decrease in the value of ϵ.

Several attempts have been made to model the variation of ϵ with the electric field strength and the ionic concentration. For example, empirical relationships have been developed where the dielectric constant is decreased depending on the concentration of the ions.[76] However, in order to develop a truly predictive theory, the introduction of additional parameters should be avoided. An alternative approach is to define certain regions surrounding the micelle and assign a different dielectric constant to

each, with the outermost layer having a dielectric constant corresponding to that of bulk water. This approach is appropriate for the present model, in which a region surrounding the micelle has already been defined for the Stern layer. The Stern layer model can be revised such that the dielectric constant inside the Stern layer, region I, has a value ϵ_1, and the dielectric constant in region II has a different value, ϵ_2 (see Figure 2-2). In this revised description, the boundary conditions must be modified to incorporate the difference in the dielectric constants (see Appendix A for details). Specifically, Eq. (2.32) becomes

$$\left(\frac{\partial \psi_I}{\partial r}\right)_{r=R_{ch}} = -\frac{4\pi\sigma}{\epsilon_1} = -\frac{4\pi z e}{\epsilon_1 a_{ch}} \tag{2.53}$$

and Eq. (2.34) becomes

$$\epsilon_1 \left(\frac{\partial \psi_I}{\partial r}\right)_{r=R_s} = \epsilon_2 \left(\frac{\partial \psi_{II}}{\partial r}\right)_{r=R_s} \tag{2.54}$$

Following the same procedure as in Section 2.3.2 with these modified boundary conditions, the following expression for g_{elec} is obtained (compare with Eq. (2.36))

$$\beta g_{elec} = \beta g_{elec,II} + \frac{\kappa s}{2}\frac{\epsilon_2}{\epsilon_1}\mathcal{F}(S) - \frac{(ze)^2}{2\epsilon_2 r_h k_B T} \tag{2.55}$$

where $\mathcal{F}(S)$ is given in Eq. (2.37).

$\beta g_{elec,II}$ can be obtained from a solution of the Poisson-Boltzmann equation using any of the analytical approximations discussed previously. Note that s must be calculated using the dielectric constant in region II, ϵ_2.

The value of the dielectric constant in the Stern layer, ϵ_1, will be much lower than that of bulk water because the water molecules will be aligned with the strong electric field. Indeed, experimental measurements indicate that the dielectric constant at the micellar interface is approximately $4.12 \times 10^{-19} C^2/J\text{Å}$ at 25°C, which is equal to $3.67 \times 10^{-19} C^2/J\text{Å}$ at 50°C. For comparison, bulk water has a dielectric constant of $7.79 \times 10^{-19} C^2/J\text{Å}$ at 50°C. It is likely that the dielectric constant will gradually increase from $3.67 \times 10^{-19} C^2/J\text{Å}$ up to $7.79 \times 10^{-19} C^2/J\text{Å}$ throughout the Stern layer

region. In order to approximate this behavior, a linear variation in ϵ was assumed from $\epsilon = 3.67 \times 10^{-19} C^2/J\text{Å}$ at $r = R_{ch}$ up to $\epsilon = 7.79 \times 10^{-19} C^2/J\text{Å}$ at $r = R_s$. ϵ_1 was then assigned the average value, that is, $\epsilon_1 = \langle\epsilon\rangle = 5.79 \times 10^{-19} C^2/J\text{Å}$.

CMC predictions were made with $\epsilon_1 = 5.79 \times 10^{-19} C^2/J\text{Å}$ and $\epsilon_2 = 7.79 \times 10^{-19} C^2/J\text{Å}$ for dodecyl ethoxy sulfate surfactants at 50°C. Results are presented in Figure 2-9 for the EMN84 approximation (—) and for the EMN83 approximation (– – –). For comparison, the CMC predictions made with a uniform dielectric constant are also shown for the EMN84 approximation (– ·· – ·· –) and the EMN83 approximation (· · ·). The circles denote the experimental CMC measurements. Note that the predicitons with the uniform dielectric constant for both approximations are the same as those presented in Figure 2-4. As can be seen, for both of these analytical approximations, reducing the dielectric constant in region I increases the CMC, because the ability of the water molecules to shield the electric field is reduced. In fact, reducing the dielectric constant to the value at the micellar surface, $\epsilon_1 = 3.67 \times 10^{-19} C^2/J\text{Å}$, would increase the electric field too much. A moderate change in ϵ, such as $\epsilon_1 = 5.79 \times 10^{-19} C^2/J\text{Å}$ yields the most accurate representation of the electric field surrounding the micelle.

2.4 Fractional Counterion Binding

When ionic surfactant molecules aggregate to form a micelle, a fraction of the counterions dissociate from the surfactant molecules and distribute freely in solution, while the remainder bind to the micellar surface in order to reduce the electrostatic repulsions between the charged surfactant heads. Indeed, experimental evidence indicates that micelles are only ionized to a degree of 20 to 50% of their full charge.[23, 47, 78] However, a *quantitative* distinction between bound and unbound counterions remains an unresolved issue, subject to different interpretations.[79, 80, 81, 82] For example, "bound" ions may be considered to be those which are physically attached to specific sites at the micelle surface. An alternative picture includes those ions which, although not physically attached, are attracted to the micelle surface through electrostatic in-

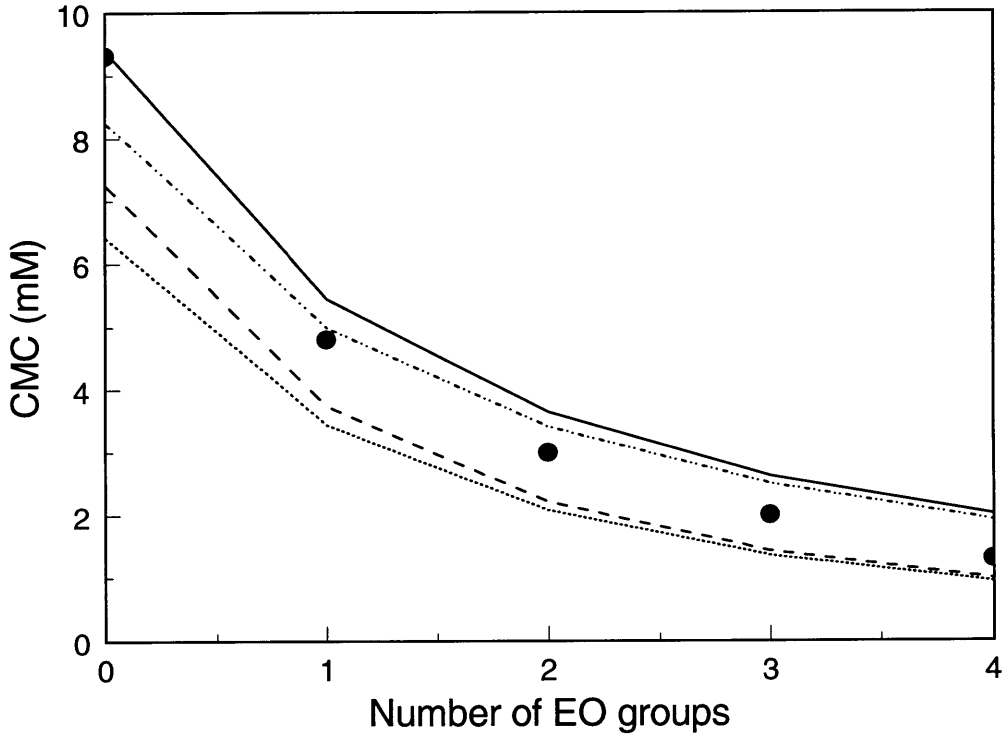

Figure 2-9: Predicted CMC as a function of the number of EO groups in the head for aqueous solutions of dodecyl ethoxy sulfates at 50°C using the EMN84 approximation (—) and the EMN83 approximation (– – –) with a lower dielectric constant in the Stern layer region ($\epsilon_1 = 5.79 \times 10^{-19} C^2/J\text{Å}$). Predictions made with a uniform dielectric constant equal to the bulk value are also shown for the EMN84 approximation (– ·· – ·· –) and for the EMN83 approximation (· · ·). The circles denote experimental CMC values.

teractions to such a degree that they are not free to move independently in solution. Experimental estimates of counterion binding vary widely, as different experimental methods probe different regions of the micellar/water interface.[83]

Theoretically, there are two competing pictures of the micellization process. The first picture assumes that the counterions participate along with the surfactant molecules in the micellization process,[81, 84] and therefore, should be included as part of the micelle itself. In this case, the thermodynamic framework presented in Section 2.2 would have to be altered to include the counterions as part of the micelle, as described in Appendix C. The second picture assumes that the micelle is formed from the bare surfactant molecules only, with the counterions participating in the micellization process indirectly through their presence in the diffuse ion cloud surrounding the micelle, as described in Section 2.3.[22, 65] In this picture, the counterions are in thermodynamic equilibrium with the micelle throughout the micellization process, as accounted for in the calculation of g_{elec}. Hence, a certain fraction of counterions are very close to the surface of charge and can be viewed as thermodynamically "bound" to the micelle surface.

The second picture is consistent with the micellization description presented in Section 2.3. In this description, a thermodynamic competition for the counterions exists between (i) binding to the micelle surface to reduce the micellar surface charge density, and (ii) dispersing in solution to maximize entropy and satisfy their own solvation energy.[65] In order to quantify this thermodynamic equilibrium, fundamental surface chemistry principles are used in the next section to define "bound" counterions, based on the Gibbs adsorption equation.

2.4.1 The Gibbs Adsorption Equation

The Gibbs adsorption equation is based on the Gibbs free energy of an interface in equilibrium with two bulk phases. Although the Gibbs adsorption equation was derived for a macroscopic interface, as in the case of the interface between a bulk oil phase and a bulk water phase, the approximation is made here that it can also be applied to a microscopic interface such as that associated with the micellar interface.

In the Stern layer model, the bound counterions reside at the outer edge of the Stern layer (at $r = R_s$ in Figure 2-2). The inner phase includes the surfactant molecules in the micelle and the water molecules residing between the surfactant heads and the counterions. The outer phase includes counterions, water molecules, and coions if salt is added. In calculating g_{elec}, the assumption was made that the dielectric constant in the Stern layer is equal to the bulk value, which implies that the concentration of the water molecules within the Stern layer is equivalent to the bulk concentration of water. Accordingly, the adsorption of water molecules on the dividing surface is zero.[85] By convention, the location of the Gibbs dividing surface is typically selected such that the adsorption of the solvent is zero.[85] However, since there is no solvent (water) adsorption on the dividing surface, this requirement is automatically satisfied. Note also that the Gibbs dividing surface has no volume.[85]

At this surface, the following equation is obtained for the surface excess Gibbs free energy[85]

$$d\underline{G}^{\sigma} = -\underline{S}^{\sigma} dT - \underline{A}^{\sigma} d\sigma + \sum \mu_j dN_j^{\sigma} \tag{2.56}$$

where σ is the surface tension at the surface $r = R_s$, $\underline{A}^{\sigma}$ is the total surface area, $\underline{S}^{\sigma}$ is the surface excess entropy, N_j^{σ} is the excess number of molecules of type j at this surface, and μ_j is the chemical potential of component j residing at this surface, which is equal to the chemical potential of component j in the bulk due to thermodynamic equilibrium. The summmation in Eq. (2.56) is over all the components adsorbed at the surface. Note that the original equation for the Gibbs' free energy of the surface also includes some curvature terms, but, by the appropriate selection of the Gibbs' dividing surface, these terms become negligible.[85]

The surface excess Gibbs free energy can be rewritten in terms of chemical potentials as follows

$$\underline{G}^{\sigma} = \sum \mu_j N_j^{\sigma} \tag{2.57}$$

and its differential is given by

$$d\underline{G}^{\sigma} = \sum \mu_j dN_j^{\sigma} + \sum N_j^{\sigma} d\mu_j \tag{2.58}$$

By combining Eq. (2.58) with Eq. (2.56), the Gibbs adsorption Equation is obtained, that is,[86]

$$-\underline{S}^{\sigma} dT - \underline{A}^{\sigma} d\sigma - \sum N_j^{\sigma} d\mu_j = 0 \tag{2.59}$$

At constant temperature, the number of ions bound per surface area, known as the Gibbs Surface Excess, Γ_i, is calculated from Eq. (2.59) as follows[86, 87]

$$\Gamma_i = \frac{N_i^{\sigma}}{\underline{A}^{\sigma}} = -\left(\frac{\partial \sigma}{\partial \mu_i}\right)_{T,\mu_{j\neq i}} \tag{2.60}$$

The fractional counterion binding, α_B, is defined as the number of ions bound per number of surfactant molecules in the micelle, N, that is, $\alpha_B = N_i^{\sigma}/N$. Using Eq. (2.60) for N_i^{σ}, the following equation is obtained for α_B

$$\alpha_B = \frac{N_i^{\sigma}}{N} = -a^{\sigma}\left(\frac{\partial \sigma}{\partial \mu_i}\right)_T \tag{2.61}$$

where $a^{\sigma} = \underline{A}^{\sigma}/N$ is the surface area per surfactant molecule at the surface of interest, located at $r = R_s$. Note that for the remainder of this analysis, the derivatives are taken at constant $\mu_{j\neq i}$, which is left out of the equations in order to simplify the notation.

The chemical potential of the ions is given by

$$\mu_i = \mu_i^{\circ}(T) + k_B T \ln c_i^{\circ} \tag{2.62}$$

$$d\mu_i\,|_T = \frac{k_B T}{c_i^{\circ}} dc_i^{\circ}\,|_T \tag{2.63}$$

where μ_i° is the standard-state chemical potential of the ions. In Eq. (2.62), the assumption was made that the ions behave ideally because they are relatively dilute. This assumption may not be very accurate because the ions may have very long-range electrostatic interactions. In order to gain more accuracy, Eq. (2.62) could be

based on activities rather than on concentrations,[87, 79, 80] but this would require additional parameters. For the purposes of calculating binding at or near the CMC, the dilute approximation appears reasonable.

Using Eq. (2.63) in Eq.(2.61) the following relation is obtained

$$\alpha_B = \frac{-a^\sigma c_i^\circ}{kT}\left(\frac{\partial\sigma}{\partial c_i^\circ}\right)_T \tag{2.64}$$

The surface tension at the surface of interest ($r = R_s$) is affected by electrostatic and steric interactions among the counterions adsorbed at the surface. Hence, the surface tension in Eq. (2.64) can be written as a sum of both of these two contributions. Specifically,

$$\sigma = \sigma_{elec} + \sigma_{ster} \tag{2.65}$$

where σ_{elec} and σ_{ster} are the "effective surface tensions" due to electrostatic interactions and steric interactions, respectively. Recall that throughout this analysis, the micelle is fixed in its equilibrium state. That is, l_c and the area per surfactant molecule are fixed at their optimal values (l_c^* and a^*). Since a is fixed, the steric interactions between the counterions remain fixed. Thus, in the derivative of σ, the major contribution is due to changes in the electrostatic surface tension, that is,

$$d\sigma = d\sigma_{elec} \tag{2.66}$$

The surface tension is equivalent to the free energy of a surface per unit area. Hence, the electrostatic free energy at the surface of interest, g^σ_{elec}, can be used to calculate σ_{elec}, as follows

$$a^\sigma \sigma_{elec} = g^\sigma_{elec} \tag{2.67}$$

Thus, at constant a^σ,

$$d\sigma_{elec} = \frac{dg^\sigma_{elec}}{a^\sigma} \tag{2.68}$$

Utilizing Eq. (2.68) in Eq. (2.64), the following expression for the fractional coun-

terion binding is obtained

$$\alpha_B = -\frac{c_i^\circ}{k_B T}\left(\frac{\partial g_{elec}^\sigma}{\partial c_i^\circ}\right)_T \tag{2.69}$$

This equation can be further simplifed in terms of the Debye screening length, κ^{-1}. Noting that,

$$\kappa^2 = \frac{8\pi c_i^\circ e^2 z^2}{\epsilon k T} \tag{2.70}$$

Equation (2.69) can be rewritten as follows,[22]

$$\alpha_B = -\frac{\kappa}{2}\left(\frac{\partial \beta g_{elec}^\sigma}{\partial \kappa}\right)_T \tag{2.71}$$

Equation 2.71 is the same expression found in Refs. [22] and [23], but here a more complete derivation was presented. The next step is to evaluate the quantity g_{elec}^σ, the electrostatic free energy of interactions among the counterions directly surrounding the micelle, which is described in the next section.

2.4.2 Calculation of g_{elec}^σ

g_{elec}^σ is the electrostatic free energy at the surface of interest, which is the outer edge of the Stern layer region ($r = R_s$ in Figure 2-2). The electrostatic free energy at $r = R_s$ is equal to the electrostatic free-energy contribution due to the diffuse ion cloud region, $g_{elec,II}$. In other words,

$$\alpha_B = -\frac{\kappa}{2}\left(\frac{\partial \beta g_{elec,II}}{\partial \kappa}\right)_T \tag{2.72}$$

Any of the approximations for the evaluation of $g_{elec,II}$ discussed in Section 2.3.2 can be utilized to calculate counterion binding. In this analyis, EMN84 will be used because it exhibited the most accurate behavior. Use of the EMN84 approximation in Eq. (2.72) results in the following expression for the counterion binding[22]

$$\alpha_B = \frac{s}{2}\left(\frac{\partial y_0}{\partial w}\right)\left(\frac{\partial w}{\partial s}\right) + \left(\frac{\partial w}{\partial s}\right)\left(\frac{s}{(w+1)^{1/2}(w-1)^{3/2}}\right) + \frac{4}{s\kappa R_s(1+\frac{2}{\kappa R_s})^{1/2}}$$
$$-\frac{4}{s}\left(1+\frac{2}{\kappa R_s}\right)^{1/2} - \frac{2m}{\kappa R_s}\left[\frac{\left(\frac{\partial w}{\partial s}\right)\frac{1}{(w+1)^{1/2}} + \frac{1}{(w-1)^{1/2}} - \frac{s/2}{(w-1)^{3/2}}\left(\frac{\partial w}{\partial s}\right)}{(w+1)^{1/2} + \frac{s/2}{(w-1)^{1/2}}}\right]$$
$$+\frac{4m}{s(\kappa R_s)^2}\frac{1}{\left[1+\frac{2}{\kappa R_s}+(1+\frac{2}{\kappa R_s})^{1/2}\right]} \tag{2.73}$$

where

$$\left(\frac{\partial y_0}{\partial w}\right) = \frac{2\left(1+\frac{w}{(w^2-1)^{1/2}}\right)}{w+(w^2-1)^{1/2}} \tag{2.74}$$

and

$$\left(\frac{\partial w}{\partial s}\right) = \frac{\left(1+\frac{2}{\kappa R_s}\right)\left(\frac{2}{s\kappa R_s}\right)+\frac{s}{4}}{\left[\left(1+\frac{2}{\kappa R_s}\right)^2+\frac{s^2}{4}\right]^{1/2}} - \frac{2}{s\kappa R_s} \tag{2.75}$$

The s in Eqs. (2.73)-(2.75) represents the dimensionless surface charge density of the counterions, given in Eq. (2.38). Alternatively, one could assume that only the bound counterions contribute to g^{σ}_{elec}. In this case, s would be reduced by the fraction of counterions bound, that is, $s' = \alpha_B s$. Note that including α_B in the quantity s' causes this to become a nonlinear problem. In that case, the derivative in Eq. (2.72) which was easily calculated analytically in Eq. (2.73) becomes a nonlinear differential equation which must be solved numerically. Results using the full charge, s, and the partial charge, s', will be compared in the next section.

2.4.3 Comparison with Experiments

Figure 2-10 shows the predicted and experimental fractional counterion binding of sodium octyl sulfate (SOS, $C_{12}H_{25}OSO_3Na$) at 25°C with varying salt (NaCl) concentrations. Predictions were made using Eq. (2.73) with a fully-charged micelle, s (—), and with a partially-charged micelle, s' (– – –). The circles denote experimental

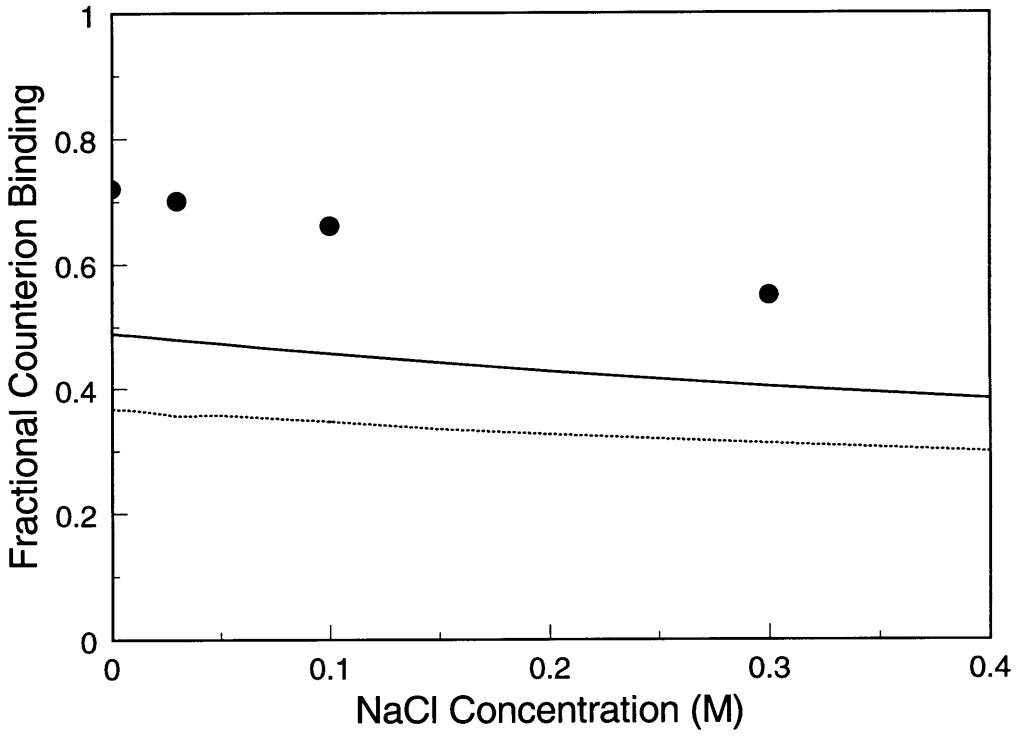

Figure 2-10: Counterion binding predictions for sodium octyl sulfate (SOS) as a function of NaCl concentration for a fully-charged micelle (—) and a partially-charged micelle (– – –). The circles denote experimental counterion binding values.

values.[22, 23] The counterion binding gradually decreases as the concentration of salt is increased. This trend is probably due to the fact that the electrostatic attractions between the negatively charged sulfate groups and the positively charged sodium counterions will be weakened by the additional screening, such that fewer counterions are attracted to the surface. Although both approximations consistently underpredict counterion binding, they capture the downward trend in α_B with added salt. Possible reasons for the underprediction are discussed below. Note that the predictions based on s', the partially-charged micelle, are lower than those based on s, the fully-charged micelle. This is reasonable, since g^{σ}_{elec} will be lower for a partially-charged micelle than for a fully-charged micelle, and therefore, fewer counterions would be attracted to the micellar surface, thus resulting in lower α_B values.

Figure 2-11 shows fractional counterion binding predictions for several cationic surfactant systems with a fully-charged micelle (striped bars) and a partially-charged micelle (dotted bars). Predictions are compared with experimental results (dark-shaded bars).[22, 23, 47, 78] Surfactant systems examined include cetyltrimethylammonium bromide (CTAB, $C_{16}H_{33}N(CH_3)_3Br$), myristyltrimethylammonium bromide (MTAB, $C_{14}H_{29}N(CH_3)_3Br$), cetyltrimethylammonium chloride (CTACl, $C_{16}H_{33}N(CH_3)_3Cl$), and dodecyltrimethylammonium bromide (DTAB, $C_{12}H_{25}N(CH_3)_3Br$), with and without added sodium chloride (NaCl). The counterion binding predictions generally underestimate the experimental results, except for the case of DTAB and CTACl. Possible reasons for the underprediction are discussed below. It is interesting that the α_B predictions for DTAB and CTACl are higher than the experimentally measured α_B values. However, it is important to note that experimental measurements of α_B are less accurate when no salt is added. In any case, the results in Figures 2-10 and 2-11 indicate that the model based on the fully-charged micelle yields better predictions than that based on the partially-charged micelle.

The experimental techniques utilized to obtain counterion binding values often have errors in the range of 10-20%.[83] In addition, different techniques can yield different results for the same system, depending on which region of the micellar interface the technique is probing. It is likely that the underprediction of the theoretical re-

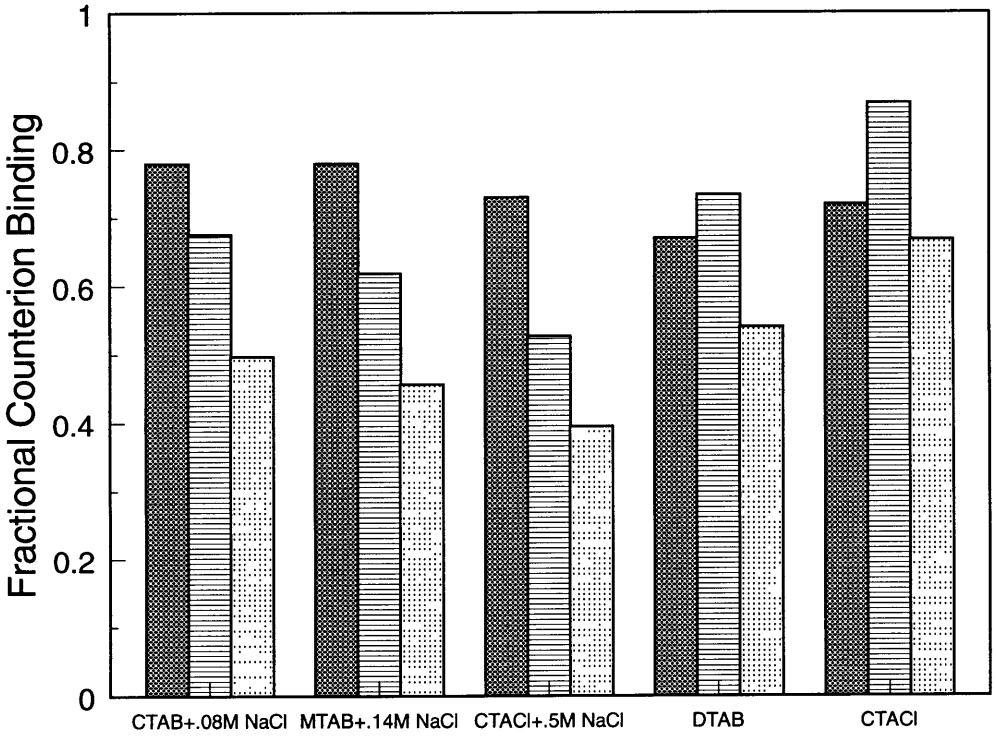

Figure 2-11: Counterion binding predictions for several cationic surfactant systems for a fully-charged micelle (striped bars) and a partially-charged micelle (dotted bars). Experimental counterion binding values are denoted by the dark-shaded bars.

sults is due to the fact that the model does not represent the same counterion binding that is being measured. In other words, the experimental technique probably probes a region that is farther away from the micelle surface than the Stern layer, thereby including more counterions in the binding value that is measured. However, it is valuable to note that the model, in general, captures the experimental trends quite nicely.

2.5 Conclusions

In this chapter, a molecular-thermodynamic theory for the micellization of ionic surfactants was presented. The electrostatic contribution to the free energy of micellization was described using the Poisson-Boltzmann equation. In order to correct for some inherent limitations of the PB equation, a Stern layer was included in the model. The Stern layer approach represents a valuable correction to the Poisson-Boltzmann equation. Specifically, it results in more accurate CMC predictions, and it provides counterion specificity. However, it also inhibits the growth of ionic micelles from spheres into cylinders upon the addition of salt. In addition, it underestimates the degree of counterion binding. There are alternative approaches to predicting counterion binding, such as that using a Langmuir isotherm,[88, 89] but these require additional adjustable parameters. The model presented here contains no adjustable parameters, yet it adequately predicts the observed experimental trends in counterion binding.

The Stern layer model improves on the Poisson-Boltzmann equation only through the excluded volume at the micellar surface. However, the counterions may also exhibit excluded-volume effects throughout the micellar solution which are not accounted for. The molecular-thermodynamic framework presented in this chapter includes only mean-field attractive intermicellar interactions. Electrostatic and excluded-volume intermicellar interactions are neglected, which could have a significant effect on the resulting micellar shape and size. To address this issue, an alternative statistical-thermodynamic framework which incorporates electrostatic and

excluded-volume intermicellar interactions was developed based on the McMillan-Mayer theory of multicomponent solutions. This framework is described in detail in Chapters 4 through 6. It is important to keep in mind, however, that the molecular-thermodynamic theory presented in this chapter is quite valuable because the equations are relatively simple, and predictions can be made in a matter of seconds.

The predictions presented in this chapter focused primarily on the CMC's of some typical ionic surfactants. The molecular-thermodynamic theory is also capable of predicting a wide range of surfactant solution properties for a variety of ionic, nonionic, and zwitterionic surfactants. To enhance the usefulness of this theory, it has been incorporated into a user-friendly computer program, program PREDICT, for industrial use which is described in the next chapter.

Chapter 3

User-Friendly Computer Program to Predict Surfactant Solution Properties

3.1 Introduction

In Chapter 2, a molecular-thermodynamic theory to describe and predict micellization and micellar solution phase behavior of aqueous surfactant solutions [16, 56] was presented. The molecular model of micellization, described in Section 2.3, accounts explicitly for the effects of surfactant molecular structure and solution conditions on the physical driving forces which control micelle formation and growth.[16, 56] The thermodynamic framework, described in Section 2.2, accounts explicitly for the effects of intermicellar interactions (described at a mean-field level) and multiple chemical equilibrium on the micellar size distribution as well as on the equilibrium bulk thermodynamic properties of the micellar solution.[6] In addition to predicting bulk surfactant solution properties, a molecular-thermodynamic theory to predict surface tensions of aqueous solutions containing nonionic surfactants has been developed.[61] The predictions of both the theory for the bulk and the theory for the surface were found to be in good agreement with available experimental data for a variety of

surfactant systems.[10, 16, 17, 18, 61]

In order to make these theoretical advances accessible to all those interested in surfactant design, manufacturing, and formulation, some of the theoretical predictive capabilities have been incorporated into a "user-friendly" computer program known as program PREDICT. This program can be utilized with relative ease to predict a broad spectrum of surfactant solution properties for a variety of surfactant types and solution conditions. Predicted surfactant solution properties include: (i) the critical micellar concentration (CMC), (ii) the micelle shape, size, and size distribution, (iii) the monomer concentration, (iv) the crossover surfactant concentration signaling the transition from the dilute to the semidilute micellar solution regimes, (v) the critical surfactant concentration for phase separation, and (vi) the surface tension of nonionic surfactant solutions. In addition, some of these fundamental surfactant solution properties can be correlated to industrially-relevant surfactant performance characteristics, such as viscosity or skin irritation. Accordingly, with the use of program PREDICT, the surfactant scientist in industry or academia can obtain valuable information on surfactant solution properties while greatly reducing tedious and time-consuming experimentation.

The remainder of this chapter is organized as follows. In Section 3.2, program PREDICT is described, including a summary of its predictive capabilities and an explanation of the inputs required to run the program. In Section 3.3, several examples of predictions made by program PREDICT are presented, along with a comparison with available experimental data. Finally, conclusions are presented in Section 3.4.

3.2 Program PREDICT

3.2.1 Predictive Capabilities

Program PREDICT can be utilized to predict micellar solution properties of nonionic, ionic, and zwitterionic hydrocarbon-based surfactants under a variety of solution conditions. Note that program PREDICT can also be utilized in the case of

fluorocarbon-based surfactants, but this case will not be addressed in this chapter.

Given the surfactant molecular structure and the solution conditions, the following properties can be predicted using program PREDICT:

1. Bulk solution properties such as the critical micellar concentration (CMC).

2. Equilibrium micellar characteristics such as the optimal micellar shape, size, and size distribution.

3. Phase behavior characteristics such as the critical surfactant concentration signalling the onset of phase separation, and the crossover surfactant concentration marking the transition from the dilute (nonentangled) to the semidilute (entangled) micellar solution regimes.

4. Surface tensions of aqueous solutions containing hydrocarbon-based nonionic surfactants.

Program PREDICT is designed to be "user-friendly" to both those interested solely in predicting solution properties of surfactant types already incorporated into the program, as well as to those who are interested in incorporating new surfactant structures which are relevant to their specific needs. For both types of users, minimal knowledge of the underlying theoretical details is required. Instead, what is required is knowledge of the surfactant molecular structure and the solution conditions, which serve as inputs to the program (see Section 3.2.2). This greatly reduces the level of expertise and amount of computational effort required to make predictions of surfactant solution properties. For a flow diagram of program PREDICT, see Figure 3-1.

In order to facilitate the use of program PREDICT, it was written in FORTRAN for use on a typical personal computer. The necessary calculations are performed in a matter of seconds. The operation of program PREDICT is interactive, that is, the program leads the user through a series of questions in order to gather the relevant data and determine which properties need to be predicted. The output is in a tabular format. First, the inputs are listed, then the free-energy calculations

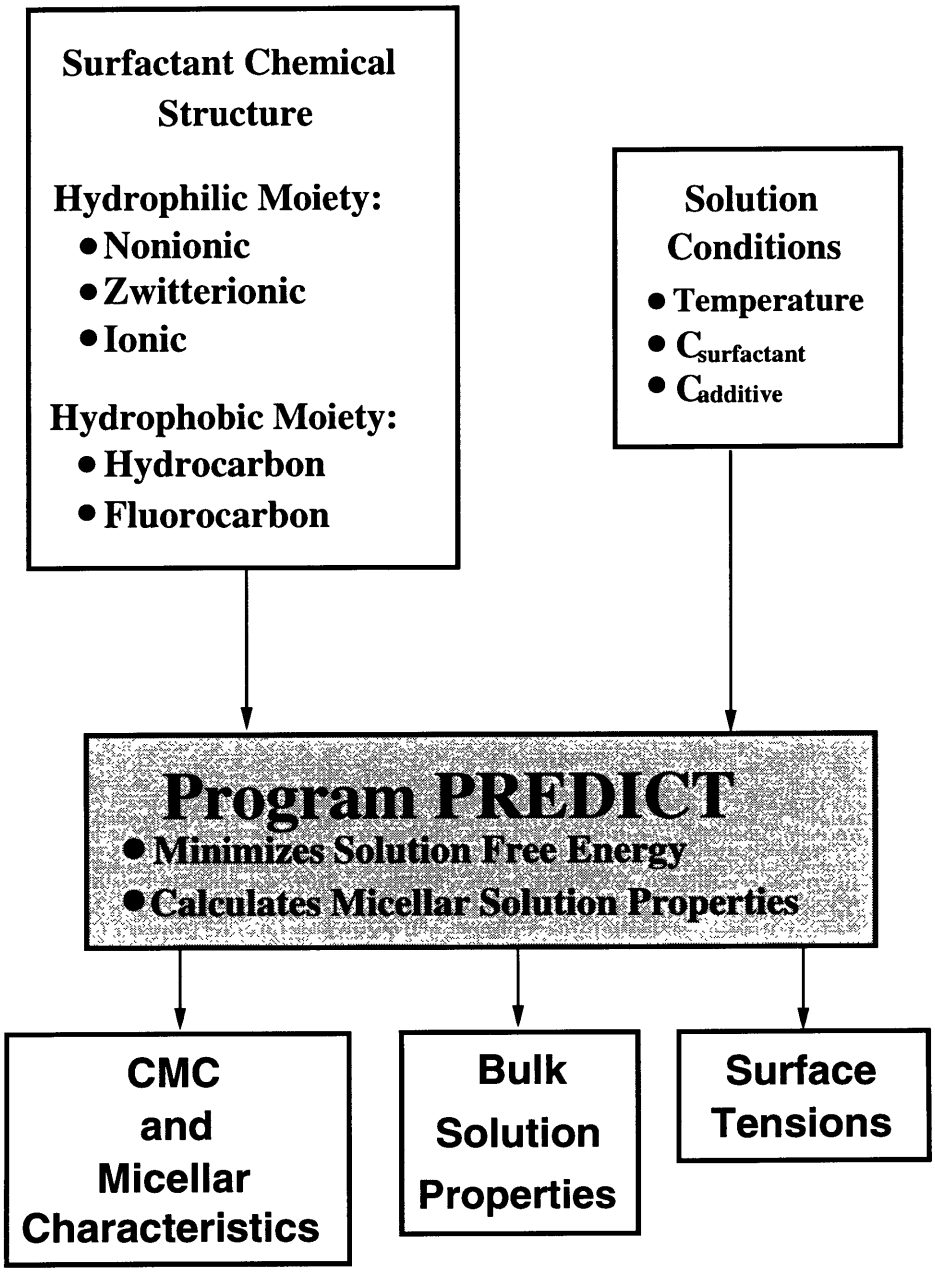

Figure 3-1: Flow Diagram of Program PREDICT.

are presented, and finally the desired predicted properties are displayed. After the output is displayed, the user has the option of repeating the calculations using new adjusted molecular parameters or solution conditions. For later use, the outputs are saved in a data file.

3.2.2 Inputs to Program PREDICT

In order to operate program PREDICT, the user needs to input information about the surfactant molecular structure and the desired solution conditions. Regarding the surfactant molecular structure, descriptions of both the surfactant head and tail are needed. To describe the tail of a hydrocarbon-based surfactant, the user needs to simply input the total number of carbon atoms, n_c, comprising the tail. To describe the head, the user needs to input the effective cross-sectional area of the head, a_h, for all classes of surfactants. If the head is nonionic, no additional inputs are required. However, if the head is ionic, the distance between the position of the charge in the head and the beginning of the tail (including the length of the CH_2 group adjacent to the head), d_{charge}, as well as the valence, z, constitute additional required inputs. In addition, due to the presence of the Stern layer (see Section 2.3.2), the type of counterion (Na^+, Br^-, etc.) must be specified. If the head is zwitterionic, the distance between the two charges comprising the dipole in the head, d_{sep}, is a required input. The surfactant head molecular parameters, a_h, d_{charge}, and d_{sep}, can be calculated from the known bond lengths and bond angles of the various chemical groups comprising the head. If the head is particularly complex, it is often convenient to make use of commercially available molecular-simulation software to carry out these calculations. For a summary of the molecular parameters which need to be input in the case of nonionic, ionic, and zwitterionic surfactants, see Figure 3-2 and Table 3.1.

Additional inputs may be needed to predict certain properties, including the critical surfactant concentration for phase separation, X_c, the crossover surfactant concentration for entanglements, X^*, and the surface tension, σ. For a summary of the additional required inputs, see Table 3.2.

Regarding solution conditions, the user needs to input the temperature, the to-

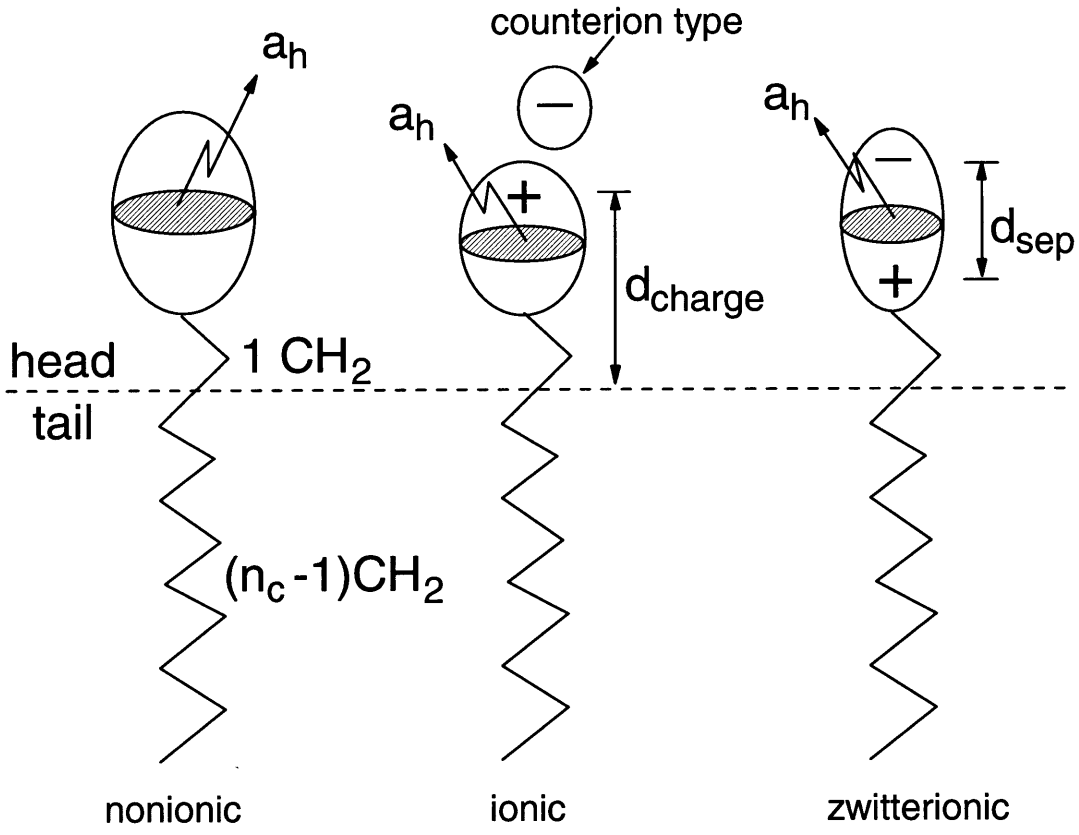

Figure 3-2: Illustration of surfactant molecular parameters.

Table 3.1: Required surfactant molecular inputs for Program PREDICT: n_c is the total number of carbon atoms in the tail, a_h is the effective cross-sectional area of the head, z is the valence of the head, d_{charge} is the distance between the position of the charge in the head and the beginning of the tail (including the length of the CH_2 group adjacent to the head), and d_{sep} is the distance between the two charges comprising the dipole in the zwitterionic head. In addition, for ionic surfactants, the type of counterion must be specified.

Nonionic	Ionic	Zwitterionic
n_c	n_c	n_c
a_h	a_h	a_h
	z	d_{sep}
	d_{charge}	
	counterion	

Table 3.2: Additional required inputs to predict the critical surfactant concentration for phase separation, X_c, the crossover surfactant concentration, X^*, and the surface tension, $\sigma(X)$: T_c is the critical temperature for phase separation, l_{hg} is the length of the head including the first CH_2 group adjacent to the head, ξ is the micellar "chain" persistence length, and $\sigma(X)$ is a surface tension value at a total surfactant concentration, X.

Property	Required Input
X_c	T_c
X^*	l_{hg}, ξ
Surface Tension	$\sigma(X), X$

tal concentration of surfactant, and the type and concentration of any additive (for example, salt).

Using the inputs described above, program PREDICT can be utilized to predict a wide range of surfactant solution properties. Several examples of these predictive capabilities, including a comparison with available experimental data, are presented next.

3.3 Comparison with Experiments

3.3.1 Critical Micellar Concentration

Program PREDICT was utilized to predict CMC's of some widely-used, representative nonionic, ionic, and zwitterionic surfactants. In this section, some examples are presented.

The nonionic surfactants examined belong to the alkyl poly(ethylene oxide), C_iE_j, family. These surfactants possess a hydrophilic head consisting of j ethylene oxide (CH_2CH_2O, or EO) groups, and an alkyl tail consisting of i carbon atoms. The effective cross-sectional areas of the E_j heads, $a_h(j)$, were estimated as a function of j in the following manner. For the relatively short E_3 head, a_h was estimated by assuming a fully-extended (all trans) conformation of the PEO head, and then utilizing the known bond lengths and bond angles of an EO group, resulting in a

value of $a_h(j = 3) = 26.9\text{Å}^2$. For the longer and more flexible E_j heads ($j \geq 4$), a_h was estimated as a function of j by utilizing a recently proposed[16] scaling law based on an E_6 head. Specifically, $a_h(j \geq 4) = a_h(j = 6)\,(j/6)^{0.8}$, with $a_h(j = 6) = 38.1\text{Å}^2$. Figure 3-3 shows predicted CMC's at 25°C of aqueous solutions of C_iE_j surfactants as a function of the number of EO groups, j, for $i = 8$ (solid line), $i = 10$ (dashed line), and $i = 12$ (dotted line). The circles, triangles, and stars denote experimental CMC values for C_8E_j, $C_{10}E_j$, and $C_{12}E_j$, respectively.[90, 91, 92]

The ionic surfactants examined belong to the sodium alkyl sulfate, $C_iH_{2i+1}SO_4Na$, family. Figure 3-4 shows predicted CMC's (line) at 25°C of aqueous solutions of $C_iH_{2i+1}SO_4Na$ as a function of the number of carbon atoms, i, in the tail. The circles denote experimental CMC values.[19] To make these predictions, values of $z = 1$, $d_{charge} = 3.7\text{Å}$, and $a_h = 25\text{Å}^2$ were input into program PREDICT.

The alkyl betaine family, $C_iH_{2i+1}N^+(CH_3)_2CH_2COO^-$, was used as a representative zwitterionic surfactant family. Figure 3-5 shows predicted CMC's (line) at 25°C of aqueous solutions of $C_iH_{2i+1}N^+(CH_3)_2CH_2COO^-$ as a function of the number of carbon atoms, i, in the tail. The circles denote experimental CMC values.[19] To make these predictions, values of $d_{sep} = 2.5\text{Å}$, and $a_h = 32\text{Å}^2$ were input into program PREDICT. In Figures 3-4 and 3-5, the observed systematic deviation of the predicted CMC's from the experimental ones as n_c increases can be attributed to an overestimation of the Tolman distance, δ_T (see Ref. [17] for details).

In addition to analyzing reagent-grade surfactants, program PREDICT can be utilized to estimate CMC values of commercial surfactants, where impurities (chemical heterogeneity) are typically present. Table 3.3 compares predicted CMC's to experimental CMC's[1] at 25°C for aqueous solutions of four representative commercial surfactants, including zwitterionic surfactants from the Zwittergent family and nonionic surfactants from the MEGA family. In view of the chemical heterogeneity of these surfactants, their average molecular structure was utilized as an input to program PREDICT. For Zwittergent, the molecular parameters input into program

[1]The experimental CMC values were taken from *A Guide to the Properties and Uses of Detergents in Biology and Biochemistry*, J. Neugebauer,CALBIOCHEM Corporation, 1990.

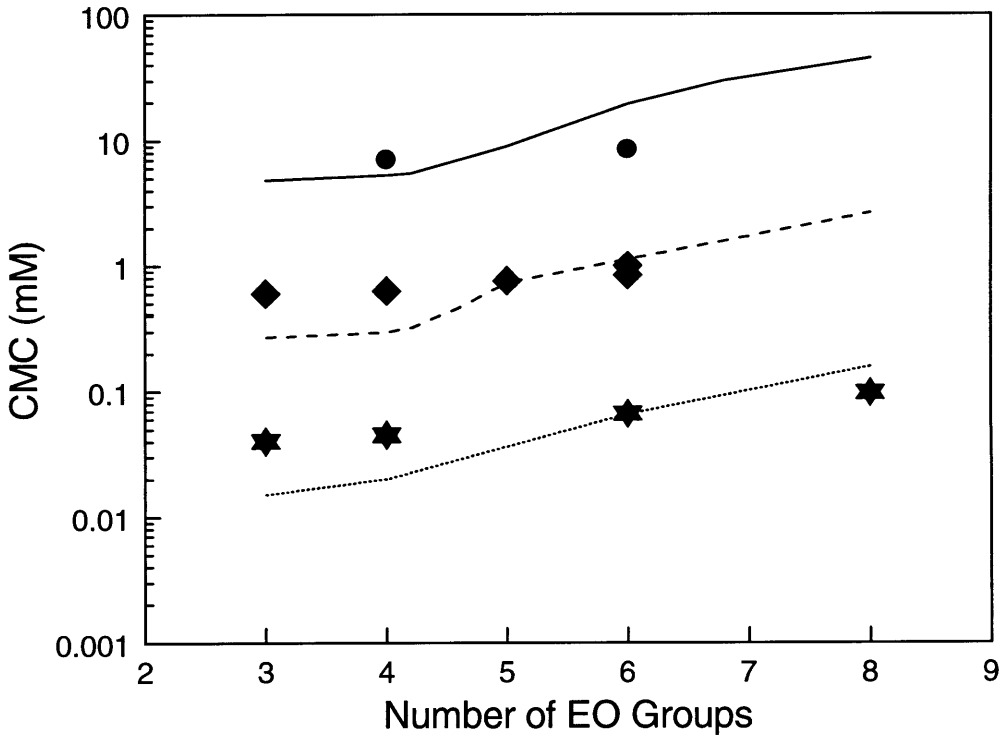

Figure 3-3: Predicted CMC as a function of the number of ethylene oxide (EO) groups, j, in the head, for aqueous solutions of C_8E_j (—), $C_{10}E_j$ (- - -), and $C_{12}E_j$ ($\cdots$) at 25°C. Experimental CMC values are denoted by circles for C_8E_j, triangles for $C_{10}E_j$, and stars for $C_{12}E_j$.

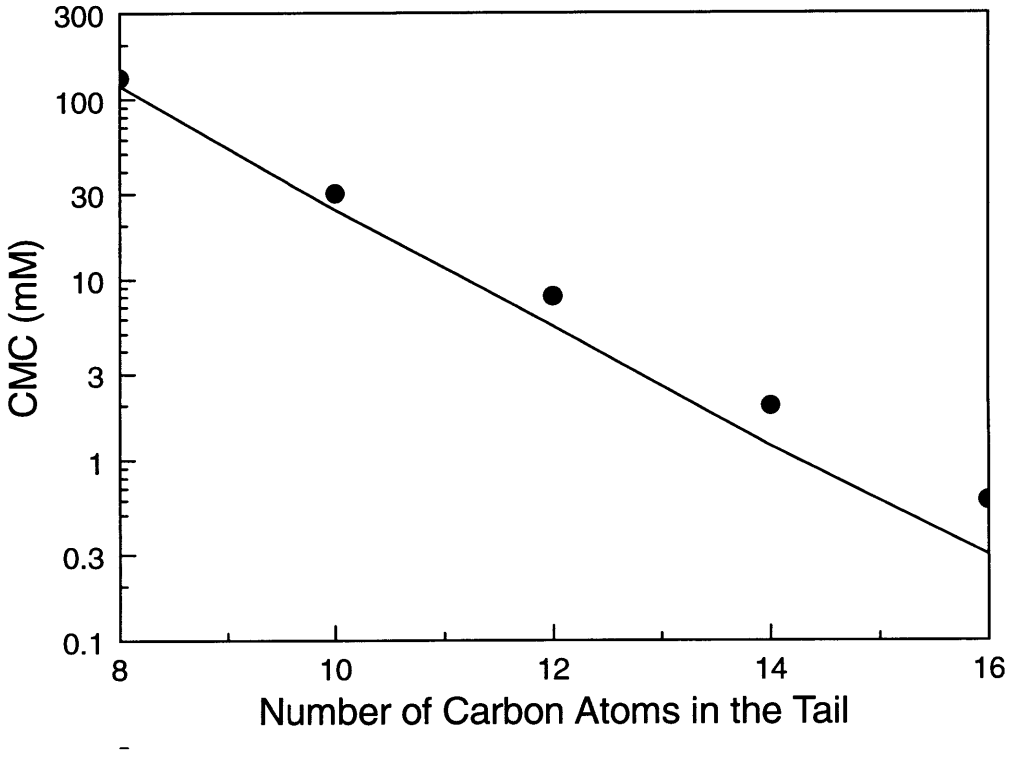

Figure 3-4: Predicted CMC as a function of the number of carbon atoms in the tail, i, for aqueous solutions of sodium alkyl sulfates ($C_iH_{2i+1}SO_4Na$) at 25°C. The line represents the theoretical predictions, and the circles denote experimental CMC values.

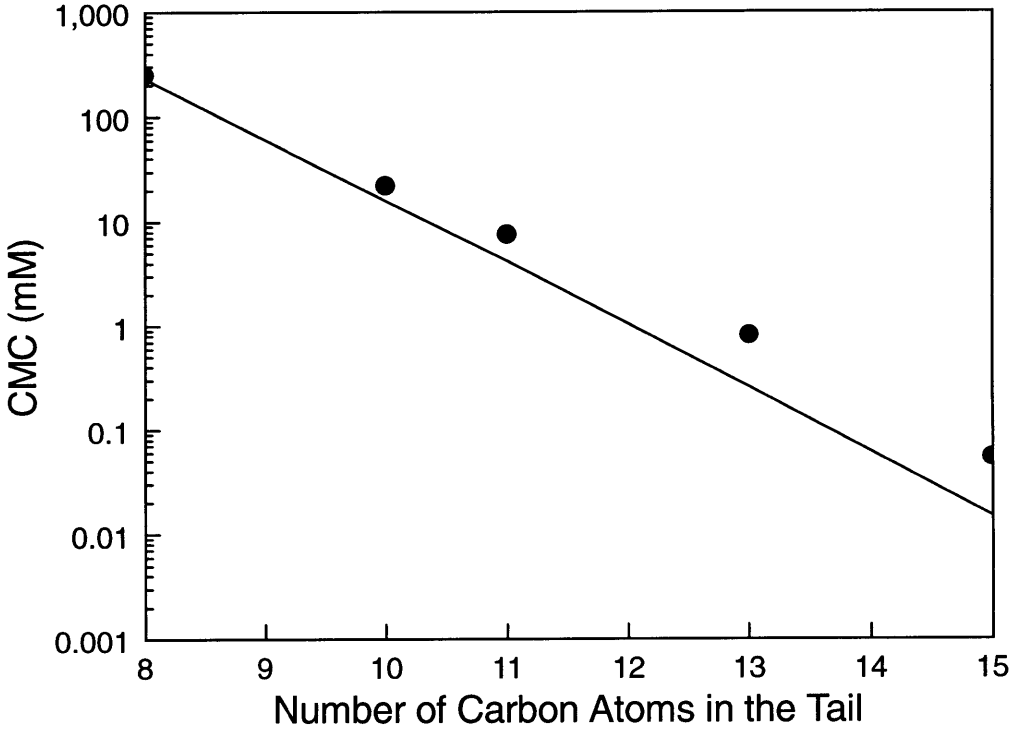

Figure 3-5: Predicted CMC as a function of the number of carbon atoms in the tail, i, for aqueous solutions of alkyl betaines ($C_i\ H_{2i+1}N^+(CH_3)_2CH_2COO^-$) at 25°C. The line represents the theoretical predictions, and the circles denote experimental CMC values.

PREDICT include $n_c = 8$ or 14, $d_{sep} = 5.03$Å, and $a_h = 32.2$Å^2. For the MEGA surfactants, the molecular parameters $n_c = 8$ or 9 and $a_h = 40$Å^2 were input into program PREDICT. As can be seen from Table 3.3, program PREDICT provides reasonable estimations of the CMC's of these chemically heterogeneous commercial surfactants.

Table 3.3: Examples of CMC predictions at 25°C for aqueous solutions of four representative commercial surfactants along with the experimental CMC values (see footnote on page 79).

Commercial Surfactant Type	Predicted CMC (mM)	Experimental CMC (mM)
Zwittergent - 8 $C_8H_{17} - N^+(CH_3)_2(CH_2)_3SO_3^-$	284	330
Zwittergent - 14 $C_{14}H_{29} - N^+(CH_3)_2(CH_2)_3SO_3^-$	0.1	0.1-0.4
MEGA - 8 $C_8H_{17} - CON(CH_3)CH_2(CH(OH))_4OH$	23	19-25
MEGA - 9 $C_9H_{19} - CON(CH_3)CH_2(CH(OH))_4OH$	6	6-7

Changes in solution conditions can have marked effects on the CMC of the surfactant solution. With the aid of program PREDICT, the user can manipulate solution conditions by varying the temperature or additive type and concentration. As an illustration of this capability, Figure 3-6 shows the effect of adding sodium chloride, NaCl, on the CMC of an aqueous solution of sodium dodecyl sulfate, SDS. The line corresponds to the predicted CMC at 25°C as a function of NaCl concentration, and the circles denote experimental CMC values.[93, 94] As the salt concentration increases, the electrostatic repulsions between the charged sulfate heads decrease, making micelle formation more favorable. Consequently, the CMC decreases, as predicted quite accurately by program PREDICT.

As can be seen, the CMC predictions presented in Figures 3-3 through 3-6 and Table 3.3 constitute a reasonably good representation of the experimental CMC data.

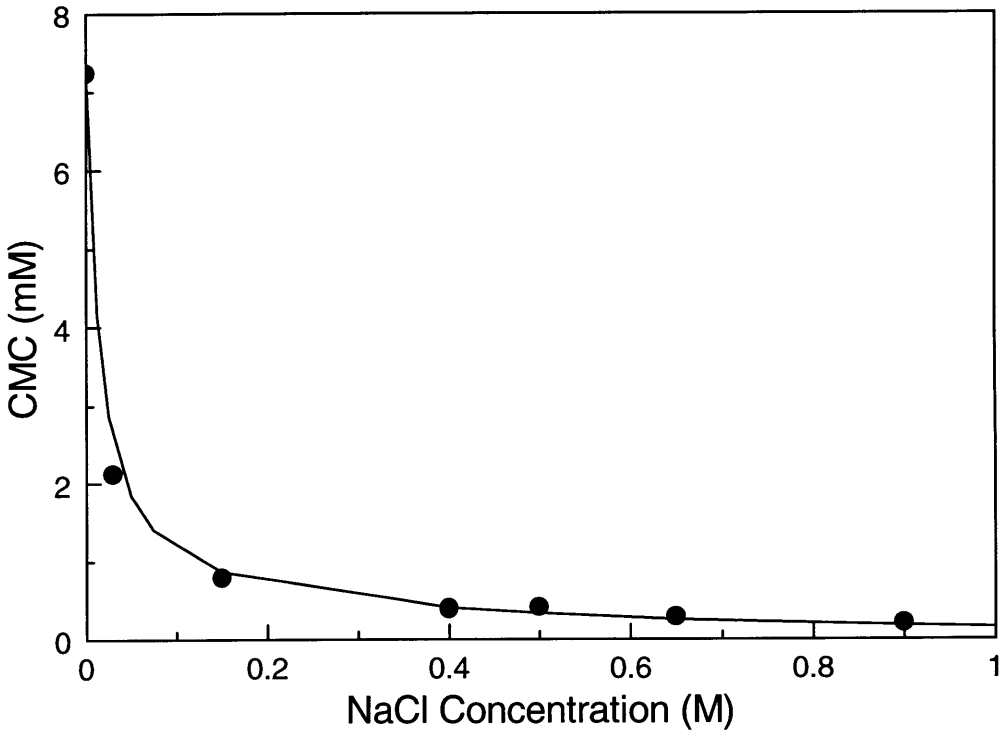

Figure 3-6: Predicted CMC as a function of salt (NaCl) concentration for aqueous solutions of sodium dodecyl sulfate ($C_{12}H_{25}SO_4Na$) at 25°C. The line represents the theoretical predictions, and the circles denote experimental CMC values.

3.3.2 Characteristics of the Micellar Size Distribution

A very challenging and still controversial aspect of micellar solution phase behavior involves the extent of micellar growth and associated degree of polydispersity of C_iE_j nonionic micelles in aqueous solutions. As discussed in Section 2.2, the relative variance of the micellar size distribution, Var, constitutes a quantitative measure of polydispersity. In particular, elongated, polydisperse cylindrical micelles are characterized by $Var = 0.5$, whereas small, monodisperse spherical micelles are characterized by $Var = 0$.

As illustrated in Figure 3-7, program PREDICT can be utilized to predict the temperature variation of the relative variance of the micellar size distribution for $C_{12}E_j$ surfactants in aqueous solutions, where $j = 5$, 6, 7, and 8. In particular, for $j = 6$, 7, and 8, the narrow temperature range over which the relative variance changes rapidly from 0 to 0.5, corresponds to a sphere-to-cylinder micellar shape transition. The experimentally determined shape transition temperatures (see the dashed arrows in Figure 3-7) are 18°C,[95] 34°C,[14] and 50°C[96] for $C_{12}E_6$, $C_{12}E_7$, and $C_{12}E_8$, respectively. As can be seen, program PREDICT is capable of predicting the micellar shape transition behavior quite accurately.

3.3.3 Crossover Surfactant Concentration

At certain temperatures, increasing surfactant concentration may cause the micelles present in aqueous solutions of C_iE_j surfactants to grow into cylindrical microstructures, which may elongate sufficiently to overlap and form an entangled mesh. This, in turn, can dramatically alter the rheological behavior of the micellar solution. In order to quantitatively characterize the relatively broad surfactant concentration region separating the nonentagled and entangled micellar solution regimes, it is customary to single out a crossover surfactant concentration, X^*, based on excluded-volume considerations, associated with the initial contact of micellar volumes.[10] Program PREDICT is capable of predicting the crossover surfactant concentration, as illustrated in Figure 3-8. In addition to the inputs involving the surfactant molecular

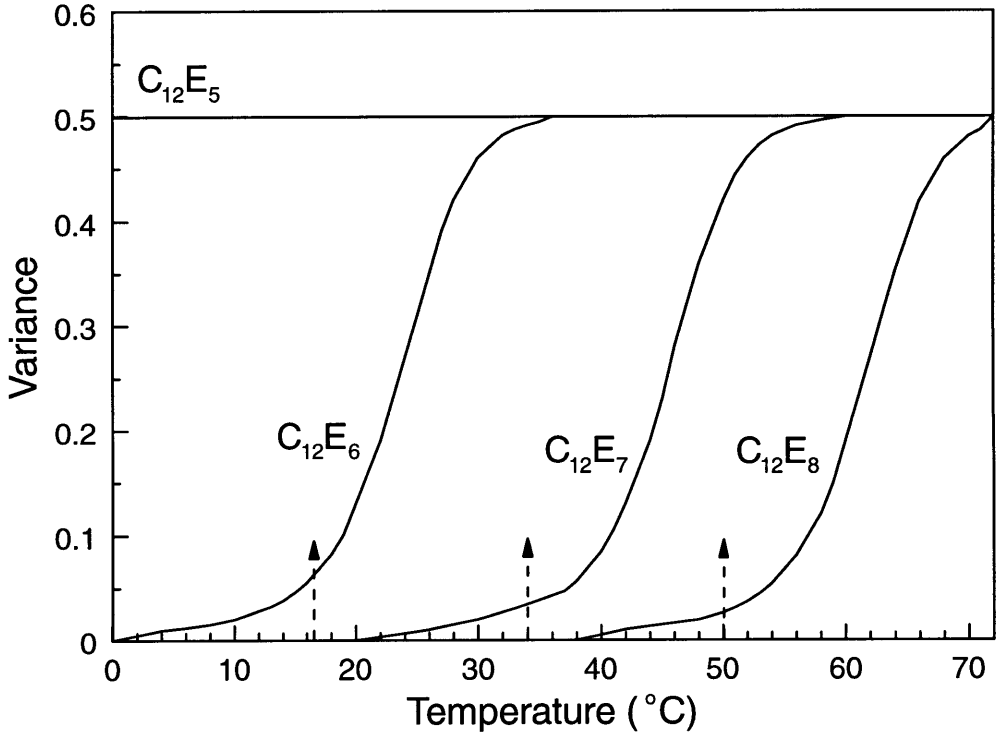

Figure 3-7: Predicted relative variance of the micellar size distribution of $C_{12}E_j$ ($j = 5$, 6, 7, and 8) micelles in aqueous solution as a function of temperature (solid lines). The dashed arrows denote the experimentally determined shape transition temperatures for $j = 6$, 7, and 8.

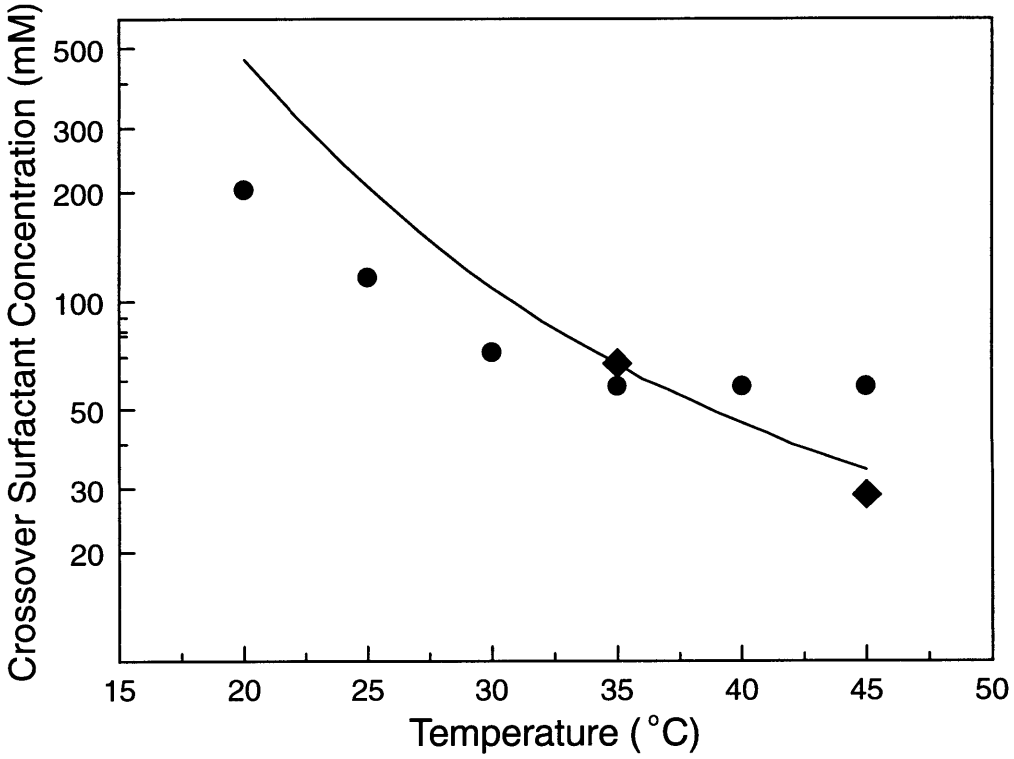

Figure 3-8: Predicted crossover surfactant concentration as a function of temperature for aqueous solutions of $C_{12}E_6$. The line represents the theoretical predictions for a micellar persistence length of 200Å. The circles (diamonds) denote experimental values deduced from light scattering (viscosity) measurements.

structure and the solution conditions described in Section 3.2.2, the prediction of X^* requires the user to input the micellar persistence length, ξ, which constitutes a measure of micellar flexibility, as well as the length of the head, l_{hg}, including the first CH_2 group adjacent to the head (see Table 3.2).

Figure 3-8 illustrates the prediction of X^* as a function of temperature for $C_{12}E_6$, where a typical value of $\xi = 200$Å was input into program PREDICT. In addition, values for l_{hg} in the range 9.7-11.5Å were input into program PREDICT, depending on the temperature. Experimentally, X^* can only be deduced indirectly from observed changes in certain solution properties with surfactant concentration as the solution traverses the nonentangled to entangled transition region. Since this transition region is relatively broad, the experimentally deduced X^* values are meaningful only to within about 20%. With this in mind, Figure 3-8 shows experimental deductions of X^* as a function of temperature for $C_{12}E_6$ based on determinations of micellar diffusion coefficients using quasi-elastic light scattering (circles) and viscosity measurements (diamonds).[10] Considering the theoretical and experimental limitations discussed above, the X^* versus T predictions presented in Figure 3-8 provide a fair representation of the experimental data, and, as such, provide a useful practical guideline.

3.3.4 Critical Surfactant Concentration

Program PREDICT can also predict characteristics of the critical point, signalling the macroscopic separation of the micellar solution into two coexisting micellar solution phases. Specifically, if the user inputs the critical temperature, T_c (in addition to the required inputs regarding surfactant molecular structure and solution conditions), program PREDICT can be utilized to calculate the critical surfactant concentration, X_c. Figure 3-9 illustrates the prediction of X_c in the case of several C_iE_j nonionic surfactants. In this example, the critical temperature values input into program PREDICT are 44 and 58°C for $C_{10}E_5$ and $C_{10}E_6$, respectively, and 23, 50, 67, 77°C for $C_{12}E_5$, $C_{12}E_6$, $C_{12}E_7$, and $C_{12}E_8$, respectively.[16] As can be seen, the X_c predictions (left-hatched bars) compare favorably with the experimental data (white bars).[12,

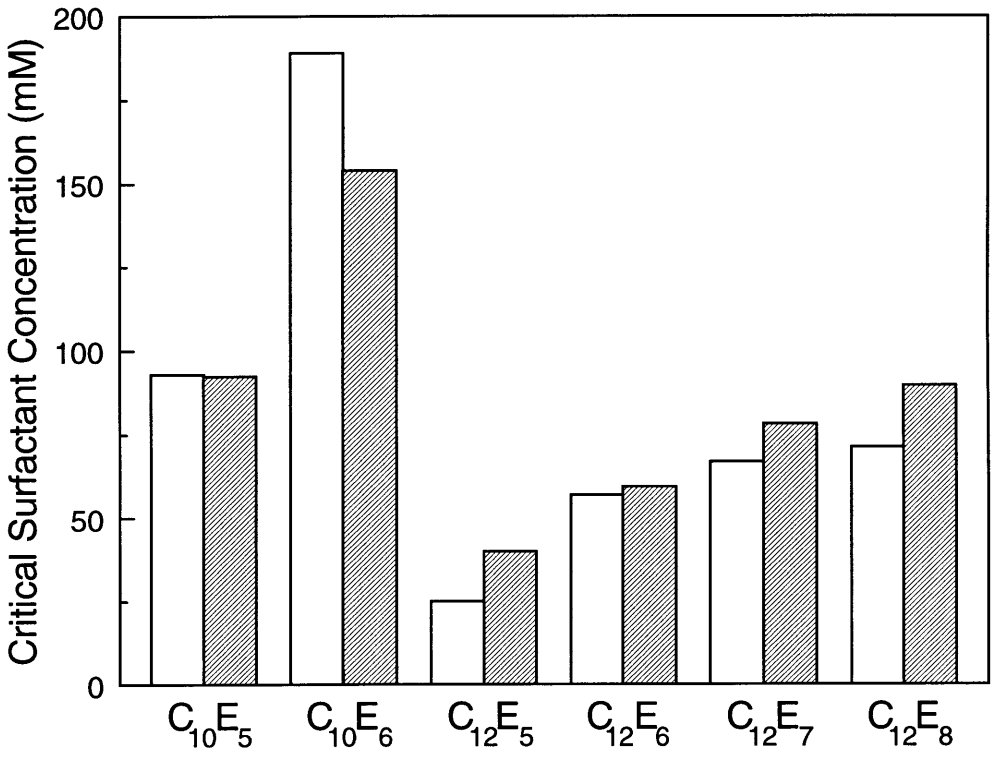

Figure 3-9: Predicted critical surfactant concentration for aqueous solutions of various C_iE_j surfactants. The left-hatched bars denote theoretical predictions, and the white bars denote experimental values.

14, 15, 97, 98]

3.3.5 Surface Tension

For nonionic hydrocarbon-based surfactants in aqueous solutions, program PREDICT can be utilized to predict surface tensions as a function of surfactant concentration. The user needs to input a single surface tension value and its corresponding surfactant concentration, and then program PREDICT can predict the surface tension at any other surfactant concentration requested by the user. Figure 3-10 illustrates the predicted surface tension (line) at 25°C as a function of surfactant concentration for aqueous solutions of $C_{12}E_6$. In order to make these predictions, a surface tension value of 35 dyn/cm at a surfactant concentration of X =0.0556mM was input into program PREDICT. As can be seen, the predictions compare favorably with the experimentally measured[61] surface tension values (see circles in Figure 3-10).

3.3.6 Correlation between Predictions and Applied Surfactant Performance Characteristics

The fundamental micellar solution properties predicted by program PREDICT are closely related to the performance behavior of surfactant systems in many practical applications. For example, CMC's and micelle shape and size can be related to detergency, skin irritation, and viscosity characteristics.[99, 100, 101, 102] Surface properties of surfactant solutions can be related to foaming, wetting, emulsification, and solubilization characteristics.[99, 102] In this section, some examples of these useful correlations will be presented.

As mentioned above, micellar size can be correlated to solution viscosity. As described in Section 1.2, some micelles may exhibit growth with increasing temperature or surfactant concentration. When micellar growth is significant, the micelles may elongate sufficiently to overlap and form an entangled mesh, dramatically altering the rheological behavior of the micellar solution. Figure 3-11 shows the predicted number-average micellar aggregation number, $\langle n \rangle_n$, together with experimental vis-

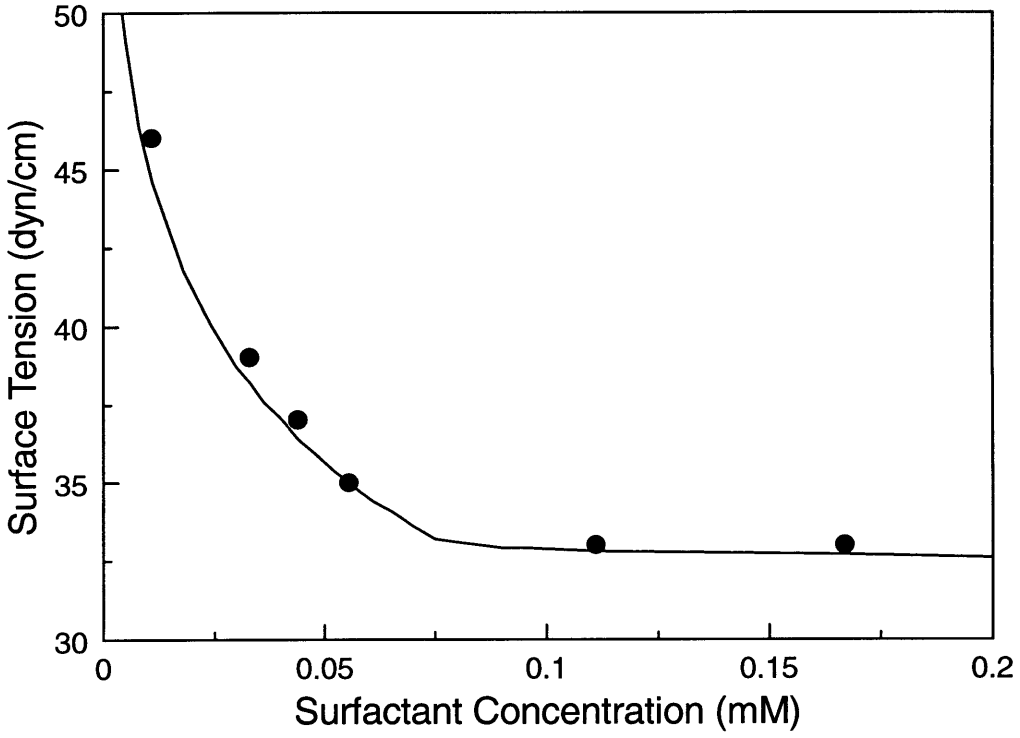

Figure 3-10: Predicted surface tension as a function of surfactant concentration at 25°C for aqueous solutions of $C_{12}E_6$. The line represents the theoretical predictions, and the circles denote experimental values.

cosity measurements, for a series of tetradecyl poly(ethylene oxide) surfactants, $C_{14}E_j$, as a function of j, the number of ethylene oxide (EO) groups.[102] As j increases, both the predicted $\langle n \rangle_n$ values and the observed solution viscosity decrease. While program PREDICT does not predict solution viscosity directly, it does predict the variation of $\langle n \rangle_n$ with j. This variation reflects the observed change in viscosity with j, and thus provides a useful indicator of the rheological behavior of the micellar solution.

It has been shown that skin irritation is associated with the diffusion of single surfactant monomers across the skin.[101] To model this phenomenon, researchers have measured the diffusion of surfactants across a collagen membrane, a useful model of the skin. In Figure 3-12, the SDS monomer concentration in aqueous solution, predicted using program PREDICT, is plotted as a function of the concentration of added NaCl (solid line) at 25°C. On the secondary Y-axis, the experimentally measured flux of SDS across a collagen membrane is also plotted as a function of NaCl concentration (circles).[100] As the salt concentration increases, the CMC of SDS decreases due to a decrease in the electrostatic repulsions between the charged SDS polar heads (see Figure 3-6), and consequently, the SDS monomer concentration also decreases. The trend of the predicted SDS monomer concentration matches the observed trend in SDS diffusion across the collagen film. Since skin irritation is reduced when surfactant diffusion is minimized, the predictions imply that skin irritation may also be reduced when the surfactant monomer concentration is minimized through the addition of salt. Although we cannot predict the complex skin irritation phenomenon directly, this example demonstrates our ability to correlate fundamental predicted surfactant properties, such as the monomer concentration, to more practical performance characteristics, such as surfactant diffusion across a collagen film.

3.4 Conclusions

As the need for a detailed understanding of surfactant solution behavior increases, the surfactant technologist is faced with the challenge of modeling the complex behavior

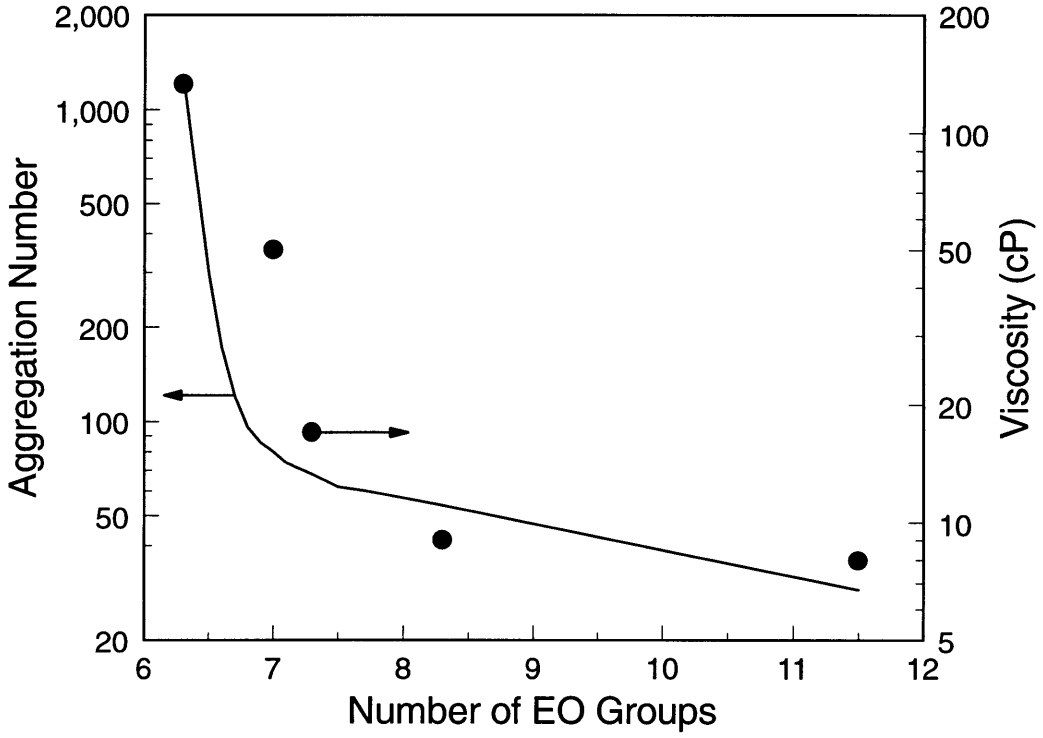

Figure 3-11: Number-average micelle aggregation number, $\langle n \rangle_n$, predicted using program PREDICT (solid line), and experimental viscosity values (circles) as a function of j for $C_{14}E_j$ nonionic surfactants in aqueous solution at 25°C.

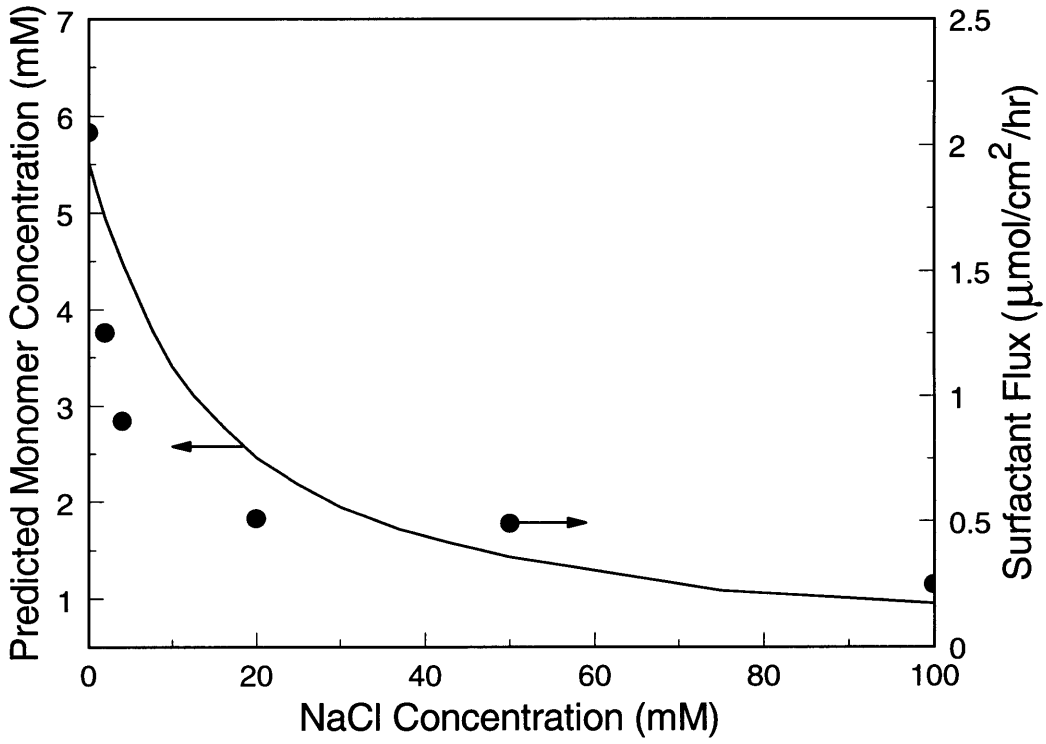

Figure 3-12: SDS monomer concentration in aqueous solution predicted using program PREDICT (solid line), and experimental flux of SDS across a collagen membrane (circles), as a function of NaCl concentration at 25°C.

of these systems. With this need in mind, a comprehensive molecular-thermodynamic theory of micellar solution behavior has been developed. As described in Chapter 2, this theory combines a molecular model of micellization with a thermodynamic description of micellar solution phase behavior. To further enhance the practical utility of these theories, they have been incorporated into program PREDICT, a "user-friendly" computer program for industrial use.

As demonstrated in Section 3.3, program PREDICT is fairly accurate in predicting a wide range of surfactant solution properties, including the CMC, the micellar shape, size, and size distribution, the crossover surfactant concentration, and phase separation characteristics. In addition, program PREDICT can also quantify quite accurately the surface behavior of aqueous solutions containing nonionic surfactants. Moreover, the surfactant technologist can correlate these predicted fundamental micellar solution properties to industrially relevant surfactant performance characteristics such as viscosity and skin irritation.

The availability of program PREDICT should facilitate the design of new surfactants possessing desirable properties by alleviating the need for *a priori* synthesis and characterization. In addition, the speed and relative ease with which surfactant solution properties can be predicted using program PREDICT should aid in greatly reducing the level of experimentation required to evaluate the performance of the new surfactants.

Chapter 4

McMillan-Mayer Statistical-Thermodynamic Framework for Multicomponent Solutions

4.1 Introduction

As discussed in Chapter 2, the molecular-thermodynamic theory of micellization is capable of accurately predicting a wide range of micellar solution properties for both ionic and nonionic surfactant solutions (see Chapter 3 for several examples). In the thermodynamic component of the theory (described in detail in Section 2.2), the Gibbs free energy of the micellar solution is decomposed into three contributions: formation, mixing, and interactions. Although this approach has been highly successful in describing a wide range of micellar solution properties, particularly for nonionic surfactants, splitting the solution nonidealities into mixing and interaction free-energy contributions without a rigorous underlying statistical-mechanical basis can sometimes lead to ambiguities. Specifically, when the model is unable to describe some aspect of the experimentally observed micellar solution behavior, such as the

growth of ionic surfactant micelles with added salt, it is difficult to unambiguously determine if the source of the discrepancy lies in the mixing or in the interactions contributions to the micellar solution Gibbs free energy. In addition, the intermicellar interactions have only been accounted for at a mean-field level of description. Moreover, excluded-volume, electrostatic, and other specific intermicellar interactions have been neglected.

In view of the above, a theoretical framework for the calculation of the micellar solution Gibbs free energy has been developed based on rigorous statistical-mechanical principles in the context of the McMillan-Mayer theory of multicomponent solutions. An advantage of this theoretical framework is that the approximations made in constructing the solution Gibbs free energy model are clearly delineated, and therefore, in principle, it is possible to systematically improve upon the theory, if needed. In addition, the theoretical framework allows for the implementation of a variety of excess free energy models. Determining the optimal model for the excess free energy requires a tradeoff between accuracy and computational complexity. In other words, a complex model may have a high degree of accuracy for all types of surfactants, but may be computationally difficult to handle. A more simple phenomenological model may be computationally fast, but would have to be specialized for each type of surfactant. In this chapter, as well as in Chapters 5 and 6, an excess free energy model is presented which is somewhat computationally complex, and yields an accurate description of micellar solution behavior over a wide range of surfactant concentrations and other solution conditions. Indeed, a similar theoretical framework has already been successfully applied to model solute partitioning in phase-separated surfactant solutions.[103]

In the next section, a general description of the McMillan-Mayer theory and its application to multicomponent solutions will be presented. Specifically, the McMillan-Mayer theory is utilized to develop a general statistical-thermodynamic framework for the calculation of the solution Gibbs free energy. In Section 4.3, the statistical-thermodynamic framework developed in Section 4.2 is implemented in the case of aqueous micellar solutions. This statistical-thermodynamic framework will then be

used in Chapter 5 to model the behavior of nonionic micellar solutions, and in Chapter 6 to model the behavior of ionic micellar solutions.

4.2 Basic Principles

For many multicomponent fluids of practical interest, such as dilute colloidal dispersions and micellar solutions, one of the components, referred to as the solvent, is present at a much higher concentration than those of the other components, referred to as the solutes. There are several levels of approximation to approach the statistical-mechanical problem of constructing a free energy model for such systems. A widely-used approximation involves treating the solvent as a background, or continuum, through which the solute molecules interact with each other. Properties of the solvent molecules are averaged, and are therefore not accounted for explicitly in the statistical-mechanical analysis. As a result, the interactions between the solute molecules now include not only the "bare" solute-solute interactions, which are present when the solutes are located in vacuum, but also additional interactions due to the presence of the solvent. The resulting effective interaction potential between the solute molecules, $W^{(\{N_\sigma\})}$, where $\{N_\sigma\} = \{N_1, N_2, ..., N_n\}$ is a shorthand notation for the various numbers of solute molecules, is known as the *potential of mean force*[104] and is a required input to the theory. $W^{(\{N_\sigma\})}$ can be quite complex, since it must reflect the properties of the solvent, such as its structure and the manner in which it restructures in the presence of the solutes, in addition to its dependence on the thermodynamic state of the system (for example, on temperature and pressure). Consequently, approximations are typically required to model $W^{(\{N_\sigma\})}$.

Once an expression for the potential of mean force is available, the next step is to construct the free energy of a system consisting of molecules interacting via this potential. There are many approximate free energy models for various molecular systems,[5, 105, 106] such as hard-sphere and Lennard-Jones fluids, but these models are strictly only applicable to particles interacting in vacuum, rather than embedded in a solvent. In view of this, it would be extremely useful to be able to apply the

models for particles *interacting in vacuum* to particles *interacting in a solvent.* The McMillan-Mayer theory establishes such a connection.[104, 107]

In the remainder of this section, the basic results of the McMillan-Mayer theory are summarized, with details of the derivations left to Appendix D. In what follows, Greek indices (σ,α) refer only to solute species, the index w refers to the solvent (that is, water), and all other Latin indices (i,j) refer to both solvent and solute species.

In the McMillan-Mayer theory, the natural independent variables of the system are temperature, T, volume, $V^\dagger$, $\{N_\sigma\}$, and the chemical potential of the pure solvent, μ_w°. Note that $V^\dagger = V(T, p + \Pi, \{N_\sigma\}, N_w)$ is the total volume of the solution at $T, p + \Pi, \{N_\sigma\}$, and N_w, where Π is the osmotic pressure of the solution and N_w is the number of solvent molecules. In other words, $V^\dagger$ is the volume of the solution in osmotic equilibrium with pure solvent at T, p, and N_w. The reason for this selection of variables will become apparent later in the paper. The free energy associated with this set of independent variables is a Legendre transform[108] of the Helmholtz free energy, A, whose natural variables are T, $V^\dagger$, $\{N_\sigma\}$, and N_w. If N_w is transformed to its conjugate variable,μ_w°, then the Helmholtz free energy, A, is transformed into the McMillan-Mayer free energy, F, that is,

$$F = A - N_w \mu_w^\circ \tag{4.1}$$

In order to evaluate the McMillan-Mayer free energy, F, it will be decomposed into IDEAL and EXCESS contributions, F^{ID} and F^{EX}, where $F = F^{ID} + F^{EX}$. An IDEAL solution is defined as one in which the solute molecules do not interact with each other. The IDEAL contribution to the McMillan-Mayer free energy is given by[103][1]

$$F^{ID}(T, V^\dagger, \{N_\sigma\}, \mu_w^\circ) = \sum_\sigma N_\sigma \mu_\sigma^\ominus + k_B T \sum_\sigma N_\sigma \left(\ln(c_\sigma^\dagger / c_\sigma^\ominus) - 1 \right) - p(T, \{0\}, \mu_w^\circ) V^\dagger \tag{4.2}$$

[1]Note that Eq. (8) in Ref. [103] contains two typographical errors: (i) it is missing the $-pV^\dagger$ term, which is the last term given in Eq. (4.2), and (ii) μ_w should be replaced by μ_w°.

where $\mu_\sigma^\ominus$ is the standard-state chemical potential of solute σ corresponding to a concentration $c_\sigma^\ominus$, $c_\sigma^\dagger = N_\sigma/V^\dagger$ is the concentration of solute σ, k_B is the Boltzmann constant, T is the absolute temperature, and $p(T, \{0\}, \mu_w^\circ)$ is the pressure of the pure solvent at T and μ_w°, where $\{0\}$ denotes zero solute concentrations. Note that the standard-state chemical potential of solute σ, $\mu_\sigma^\ominus$, is chosen to be solute molecules dissolved in solvent molecules at concentration $c_\sigma^\ominus$, usually chosen to be 1 mol/L, in a hypothetical standard state in which the solute molecules do not interact with each other. This standard state is frequently utilized to model electrolyte solutions.[109]

An EXCESS property is defined as the difference between the property of the actual system and that of an IDEAL system at the same T, $V^\dagger$, $\{N_\sigma\}$, and μ_w°. In particular, the EXCESS McMillan-Mayer free energy, F^{EX}, is given by

$$F^{EX}(T, V^\dagger, \{N_\sigma\}, \mu_w^\circ) = F(T, V^\dagger, \{N_\sigma\}, \mu_w^\circ) - F^{ID}(T, V^\dagger, \{N_\sigma\}, \mu_w^\circ) \tag{4.3}$$

In the system of interest, referred to hereafter as the *"solvent"* system, the solute molecules interact with each other through a potential of mean force, $W^{(\{N_\sigma\})}$, which depends on the positions and orientations of all the solute molecules in the system. Consider a system in which the solute molecules are placed in vacuum but still interact with each other through the same potential, $W^{(\{N_\sigma\})}$. This system will be referred to hereafter as the *"vacuum"* system. In what follows, properties of the vacuum system will carry a tilde to distinguish them from those of the solvent system. For example, the Helmholtz free energy of the vacuum system will be denoted by $\tilde{A}$.

The central result of the McMillan-Mayer theory is the following relation[104]

$$F^{EX}(T, V^\dagger, \{N_\sigma\}, \mu_w^\circ) \;=\; \tilde{A}^{res}(T, V, \{N_\sigma\}) \tag{4.4}$$

where the superscript res denotes the residual property of the vacuum system, that is, the difference between the property of the actual vacuum system and that of an ideal vacuum system at the same T, V, and $\{N_\sigma\}$. Note that the volume of the vacuum system is $V(T, p, \{N_\sigma\})$, evaluated at a different pressure than the volume of the solvent system, $V^\dagger(T, p + \Pi, \{N_\sigma\}, N_w)$. Note also that the "vacuum" system

depends on one less variable than the solvent system because it contains one less component, namely, the solvent.

Equation (4.4) establishes a relation between the residual Helmholtz free energy of a vacuum system and the EXCESS McMillan-Mayer free energy of a solvent system. Accordingly, a model for the residual Helmholtz free energy of solute molecules *in vacuum* can be utilized to calculate the EXCESS McMillan-Mayer free energy of solute molecules interacting *through solvent.* In theory, therefore, a complete model for the system of interest has been developed. Specifically, given T, $V^\dagger$, $\{N_\sigma\}$, and μ_w° of a system, Eqs. (4.2), (4.3), and (4.4) can be utilized to calculate F, from which other thermodynamic properties, such as the chemical potentials and the osmotic pressure, can then be obtained. The difficulty in implementing this approach in practice, however, is that μ_w° is not a convenient, experimentally-accesible variable. Instead, in a typical experiment, the independent variables which are most easily manipulated are temperature, T, pressure, p, the numbers of solute molecules, $\{N_\sigma\}$, and the number of solvent molecules, N_w. The free energy associated with this set of independent variables is the Gibbs free energy, G, and therefore, in order to effectively model the thermodynamic behavior of the system, a model is required for the Gibbs free energy rather than the McMillan-Mayer free energy. Consequently, in order to make a connection with actual experimental measurements, a relation between the McMillan-Mayer free energy, F, and the Gibbs free energy, G, is required.

As in the case of F, in order to derive an expression for G, its ideal and excess contributions will be computed separately. As before, an ideal solution is defined as one in which there are no interactions between the solute molecules. Note, however, that an "ideal" solution is different from the "IDEAL" solution defined earlier, in spite of the fact that in both systems the solutes do not interact with each other. This difference reflects the fact that the solvent molecules can still interact with themselves as well as with the solute molecules, and the effect of these interactions depends on the thermodynamic variables which are held constant. For the ideal solution, these variables are T, p, $\{N_\sigma\}$, and N_w, while for the IDEAL solution, the variables are T, $V^\dagger$, $\{N_\sigma\}$, and μ_w°.

The ideal Gibbs free energy, G^{id}, is given by[103]

$$G^{id}(T,p,\{N_\sigma\},N_w) = N_w\mu_w^{id} + \sum N_\sigma\mu_\sigma^{id} \quad (4.5)$$

$$= N_w\mu_w^\circ + \sum_\sigma N_\sigma\mu_\sigma^\circ + k_BT\sum_\sigma N_\sigma(\ln m_\sigma - 1) \quad (4.6)$$

where μ_w^{id} is the ideal chemical potential of water, μ_σ^{id} is the ideal chemical potential of solute σ, μ_i° is the standard-state chemical potential of component i ($i = w$ or σ), and $m_\sigma = N_\sigma/N_w$ is the "molality" of solute σ. Eq. (4.6) is obtained from Eq. (4.5) by expanding μ_w^{id} to leading order in m_σ. For the solvent, the standard state is chosen to be pure solvent at the system T and p. For a solute species, the standard state is chosen to be a solute molecule at infinite dilution in the solvent at the system T and p. Note that $\mu_\sigma^\ominus$ (at $c_\sigma^\ominus$) in Eq. (4.2) and μ_σ° (at infinite dilution) in Eq. (4.6) are related through the following expression[109]

$$\mu_\sigma^\circ = \mu_\sigma^\ominus - k_BT\ln c_\sigma^\ominus V_w \quad (4.7)$$

where $V_w = V(T,p,\{0\},N_w)/N_w$ is the volume per molecule in pure solvent (water).

From G^{id}, all the other thermodynamic properties of the ideal system can be determined. For example, one finds that

$$\mu_\sigma^{id} = \left(\frac{\partial G^{id}}{\partial N_\sigma}\right)_{T,p,\{N_{\alpha\neq\sigma}\},N_w} = \mu_\sigma^\circ + k_BT\ln m_\sigma \quad (4.8)$$

and

$$\mu_w^{id} = \left(\frac{\partial G^{id}}{\partial N_w}\right)_{T,p,\{N_\sigma\}} = \mu_w^\circ - k_BTm \quad (4.9)$$

where $m = \sum_\sigma m_\sigma$ is the total solute molality.

In addition, an excess property is defined, denoted by a superscript ex, to differentiate it from the superscript EX utilized earlier, as the difference between the property of the actual system and the property of an ideal system at the same T, p,

$\{N_\sigma\}$, and N_w. Specifically,

$$G^{ex}(T,p,\{N_\sigma\},N_w) = G(T,p,\{N_\sigma\},N_w) - G^{id}(T,p,\{N_\sigma\},N_w) \quad (4.10)$$

The excess Gibbs free energy can be obtained from the EXCESS McMillan-Mayer free energy through the appropriate thermodynamic transformations (see Appendix D for a detailed derivation).[107] This yields

$$\begin{aligned} G^{ex}(T,p,\{N_\sigma\},N_w) &= F^{EX}(T,V^\dagger,\{N_\sigma\},\mu_w^\circ) - \int_p^{p+\Pi} V(T,p',\{N_\sigma\},N_w)\,dp' \\ &\quad +\Pi V^\dagger - Nk_BT\ln\frac{V^\dagger}{V_wN_w} \end{aligned} \quad (4.11)$$

The advantage of rewriting G^{ex} in this form is that F^{EX} can be related to the residual Helmholtz free energy of solute molecules interacting in vacuum with potentials equal to the potentials of mean force [see Eq. (4.4)]. Therefore, one can apply all the available models for dilute fluids directly to solute molecules interacting in a solvent.

From the excess Gibbs free energy expression given in Eq. (4.11), one can obtain the following expression for the excess chemical potential of solute σ, μ_σ^{ex} (see Appendix D for a detailed derivation)

$$\begin{aligned} \mu_\sigma^{ex} &= \left(\frac{\partial G^{ex}}{\partial N_\sigma}\right)_{T,p,\{N_{\alpha\neq\sigma}\},N_w} \\ &= \mu_\sigma^{EX} - \int_p^{p+\Pi}\overline{V}_\sigma(p')\,dp' - k_BT\ln\frac{V^\dagger}{V_wN_w} \end{aligned} \quad (4.12)$$

where $\overline{V}_\sigma(p')$ is the partial molar volume of solute σ at pressure p'. Similarly, the excess chemical potential of the solvent, μ_w^{ex}, is given by (see Appendix D)

$$\begin{aligned} \mu_w^{ex} &= \left(\frac{\partial G^{ex}}{\partial N_w}\right)_{T,p,\{N_\sigma\}} \\ &= k_BTm - \int_p^{p+\Pi}\overline{V}_w(p')\,dp' \end{aligned} \quad (4.13)$$

where $\overline{V}_w(p')$ is the partial molar volume of the solvent at pressure p'.

The total chemical potentials of the solutes and the solvent include both the ideal contributions (from Eqs. (4.8) and (4.9)) and the excess contributions (from Eqs. (4.12) and (4.13)), as shown below for solute σ

$$\begin{aligned} \mu_\sigma = \mu_\sigma^{id} + \mu_\sigma^{ex} &= \mu_\sigma^\circ + k_B T \ln m_\sigma + \mu_\sigma^{EX} \\ &\quad - \int_p^{p+\Pi} \overline{V}_\sigma(p')\, dp' - k_B T \ln \frac{V^\dagger}{V_w N_w} \end{aligned} \tag{4.14}$$

and for the solvent

$$\mu_w = \mu_w^{id} + \mu_w^{ex} = \mu_w^\circ - \int_p^{p+\Pi} \overline{V}_w(p')\, dp' \tag{4.15}$$

In summary, it has been shown that the McMillan-Mayer theory allows one to use the thermodynamic properties of a system in vacuum to predict the thermodynamic properties of a system in a continuum solvent. In the next section, the results derived in this section will be used to construct a Gibbs free energy model for an aqueous micellar solution.

4.3 Application to Micellar Solutions

In the previous section, a general statistical-thermodynamic framework for constructing a Gibbs free energy model of a solution, given the potentials of mean force between the solute species, was described. In this section, the general aspects of implementing this theoretical framework in the case of aqueous micellar solutions will be discussed. In particular, the chemical potentials of the solute species (micelles and monomers) are calculated and utilized, along with the principle of multiple chemical equilibrium, to obtain an expression for the micellar size distribution and its moments.

The surfactant-water micellar system is modeled as a multicomponent solution containing: (i) N_w water molecules, (ii) N_1 surfactant monomers, and (iii) a distribution of $\{N_n\}$ surfactant micelles of aggregation number n also referred to as n-mers, where $\{N_n\}$ is a shorthand notation for the various numbers of n-mers,

$\{N_1, N_2, ..., N_n\}$. *Note that the subscript σ utilized in Section 4.2 is now replaced by the subscript n.*

Micelles are self-assembling aggregates which continually exchange surfactant molecules with each other and with the monomers in solution. These material exchanges must satisfy the principle of multiple chemical equilibrium, that is,[5]

$$\mu_n = n\mu_1 \tag{4.16}$$

where μ_n is the chemical potential of an n-mer, and μ_1 is the chemical potential of a monomer. The chemical potential of an n-mer is obtained from Eq. (4.14) with $\sigma = n$, where $n = 1$ for the monomers and $n > 1$ for the micelles. The chemical potential of water is given in Eq. (4.15).

In Eqs. (4.14) and (4.15), $\overline{V}_n$ and $\overline{V}_w$ are the partial molar volumes of an n-mer and water, respectively, which, in general, can be complicated functions of solute concentration, pressure, and temperature. Consequently, to evaluate the volume terms in Eqs. (4.14) and (4.15), a model for the volumetric behavior of the solution is required. In general, the total volume of the solution, V, is given by

$$V = N_w\overline{V}_w + \sum_{n=1}^{\infty} N_n\overline{V}_n \tag{4.17}$$

Since the micellar solutions considered in this thesis are assumed to be quite dilute, solute concentration effects on the partial molar volumes, $\overline{V}_w$ and $\overline{V}_n$, can be neglected. In addition, pressure effects on $\overline{V}_w$ and $\overline{V}_n$ will also be neglected, since these should not be significant at the atmospheric conditions typically encountered experimentally. With these assumptions in mind, $\overline{V}_w = V_w$, the volume occupied by a water molecule, which is taken to be a constant, $V_w \approx \Omega_w = 30\text{Å}^3$. Similarly, the partial molar volume of a surfactant monomer, $\overline{V}_1$, is equal to Ω_s, the volume occupied by a surfactant monomer, independent of surfactant concentration and pressure.

Regarding a micelle of aggregation number, n, it is assumed that: (i) the partial molar volume, $\overline{V}_n$, is equal to the sum of the partial molar volumes of its n constituent surfactant molecules, and (ii) the partial molar volume of a surfactant molecule in a

micelle is equal to that of a free surfactant monomer in solution. In other words, (i) and (ii) imply that $\overline{V}_n = n\overline{V}_1 = n\Omega_s$.

Combining these volumetric approximations, the total volume of the micellar solution is given by

$$V(T,p,\{N_n\},N_w) = V^{\dagger}(T,p+\Pi,\{N_n\},N_w) = N_w\Omega_w + N_s\Omega_s \qquad (4.18)$$

Note that the neglect of pressure effects (incompressibility assumption) in Eq. (4.18) also implies that the solute concentrations utilized in the McMillan-Mayer theory, $c_n^{\dagger} = N_n/V^{\dagger}$, are equal to the solute concentrations in the actual system, $c_n = N_n/V$.

In the context of the model for the volumetric behavior of the micellar solution given in Eq. (4.18), the chemical potential expressions in Eqs. (4.14) and (4.15) can be simplified (the pressure integrals can be easily carried out). Specifically,

$$\mu_n = \mu_n^o + k_B T \ln c_n\Omega_w + \mu_n^{EX} - n\Pi\Omega_s \qquad (4.19)$$

and

$$\mu_w = \mu_w^{\circ} - \Pi\Omega_w \qquad (4.20)$$

Note that the natural log terms in Eq. (4.14) have been combined in Eq. (4.19) to transform from molalities, $m_n = N_n/N_w$, to concentrations, $c_n = N_n/V$.

The micelle ($n > 1$) and monomer ($n = 1$) chemical potential expressions in Eq. (4.19) can be utilized in the chemical equilibrium condition, $\mu_n = n\mu_1$, to obtain the following expression for the micellar size distribution

$$\Omega_w c_n = (\Omega_w c_1)^n \exp\{-\beta(\mu_n^{\circ} - n\mu_1^{\circ}) - \beta(\mu_n^{EX} - n\mu_1^{EX})\} \qquad (4.21)$$

Note that the osmotic pressure contribution in Eq. (4.19) cancels out in Eq. (4.21). Equation (4.21) defines the entire micellar size distribution in terms of the concentra-

tions of n-mers for any $n > 1$. The first term, $(\Omega_w c_1)^n$, corresponds to the entropic cost associated with localizing n monomers at one position to form the n-mer, and the exponential term reflects the free-energy advantage associated with forming the n-mer. This last term includes both an ideal (infinite dilution) contribution and an EXCESS contribution. If there were no interactions among the various n-mers, then the EXCESS contribution would be zero, and the "traditional" expression for the micellar size distribution equation would be recovered.

Up to this point, the only approximation made involves the use of Eq. (4.18) for the volumetric behavior of the micellar solution. Consequently, Eq. (4.21) can be applied to any micellar solution which satisfies Eq. (4.18). To complete the calculation, models are required for the standard-state chemical potential difference, $\mu_n^\circ - n\mu_1^\circ$, and for the EXCESS chemical potential difference, $\mu_n^{EX} - n\mu_1^{EX}$, appearing in Eq. (4.21). The calculation of these quantities is discussed in Chapter 5 for nonionic surfactants, and in Chapter 6 for ionic surfactants.

Chapter 5

Application of the McMillan-Mayer Statistical-Thermodynamic Framework to Nonionic Micellar Solutions

5.1 Introduction

In Chapter 4, the McMillan-Mayer theory was utilized to construct a statistical-thermodynamic framework for the calculation of the Gibbs free energy of a micellar solution. Using this framework, an expression for the micellar size distribution was derived. All that is needed now is a model for the calculation of the standard-state and EXCESS chemical potentials. In this chapter, a model will be derived and tested for nonionic micellar solutions which exhibit one-dimensional micellar growth in the presence of excluded-volume and attractive intermicellar interactions. A model for ionic micellar solutions which includes electrostatic and excluded-volume intermicellar interactions will be presented in Chapter 6.

The remainder of this chapter is organized as follows. In Section 5.2, the difference in the standard-state chemical potentials of an n-mer and n monomers will be analyzed for the case of spherocylindrical micelles. In Section 5.3, the EXCESS chemical potentials of n-mers and monomers will be derived, based on excluded-volume and attractive intermicellar interactions. Expressions for the moments of the micellar size distribution will be presented in Section 5.4. Interestingly, as discussed in Section 5.5, in the limit of extensive micellar growth, expressions for the micellar size distribution and its moments corresponding to the well-known phenomenological "ladder model" are recovered. Micellar solution phase separation will be discussed in Section 5.6, where expressions for the spinodal curve, the critical point, and the coexistence curve will be derived. In Section 5.7, a qualitative analysis of the effect of excluded-volume intermicellar interactions on the monomer and micelle concentrations and on the weight-average micelle aggregation numbers for a typical nonionic surfactant will be presented. In addition, quantitative predictions of CMC's, micellar size distribution polydispersity, critical surfactant concentrations signalling the onset of phase separation, and the osmotic compressibility of aqueous micellar solutions of alkyl poly(ethylene oxide) nonionic surfactants will be presented and compared with experimental data. Finally, the key results of this chapter will be summarized in Section 5.8.

5.2 Standard-State Chemical Potential

Each n-mer has a distinct standard-state chemical potential, μ_n°, which is equal to the chemical potential of a micelle of aggregation number n at infinite dilution in water. In the micellar size distribution equation, Eq. (4.21), the relevant quantity is the difference between the standard-state chemical potential of an n-mer and that of n monomers. This difference, per surfactant molecule, is referred to as the free energy of micellization, g_{mic}.[16] Specifically,

$$g_{mic}(n) = (\mu_n^\circ - n\mu_1^\circ)/n \tag{5.1}$$

g_{mic} represents the free-energy change when a surfactant molecule is transferred from the aqueous solvent to a micelle of aggregation number n present at infinite dilution in the solvent. The magnitude of g_{mic} can be evaluated using the thought process described in Section 2.3, which models the formation of a micelle from individual surfactant monomers as a series of reversible steps, each associated with a physico-chemical contribution to the micellization process.[16]

The calculation[16] of g_{mic} depends on the micellar core radius, l_c, and on the micelle shape, S, which can be a sphere ($S = 3$) or an infinite cylinder ($S = 2$). (Theoretically, the shape can also be an infinite bilayer ($S = 1$), but this case will not be addressed here since it is not relevant to the experimental systems examined in this thesis.) g_{mic} is then minimized with respect to l_c and S to determine the optimal micellar core radius, l_c^*, and shape, S^*, of the micelle. Note that the optimal l_c^* value for a sphere may be different from that corresponding to an infinite cylinder. As previously discussed in Section 2.2, it would be instructive to sum over all the possible l_c values rather than forcing all the micelles to adopt the optimal l_c^*. However, when intermicellar interactions are included in the model, this process becomes computationally prohibitive. In order to obtain analytical expressions for the moments of the micellar size distribution, it is assumed that all $l_c = l_c^*$. Note that, for large aggregation numbers, it has been shown[5] that this is a very good approximation because the distribution over l_c is very sharply peaked at l_c^*.

If the optimal shape, S^*, corresponds to a sphere, the spherical micelles are assumed to be monodisperse with an aggregation number, n_0, derived from geometric considerations. Specifically, $n_0 = 4\pi(l_c^*)^3/3v_t$, where v_t is the volume of the surfactant tail. If the optimal shape, S^*, corresponds to an infinite cylinder, the micelles can be quite polydisperse, with aggregation numbers ranging from $n = n_0$ to infinity. In this case, $g_{mic}^{cyl}(n)$ is estimated by linearly interpolating between the g_{mic} values corresponding to a sphere and an infinite cylinder, namely,[16]

$$g_{mic}^{cyl}(n) = \frac{n_0}{n} g_{sph} + \frac{(n - n_0)}{n} g_{cyl} \tag{5.2}$$

where g_{sph} is the optimal micellization free energy, $g_{mic}(l_c^*, S^* = 3)$, of a sphere, and g_{cyl} is the optimal micellization free energy, $g_{mic}(l_c^*, S^* = 2)$, of an infinite cylinder.

5.3 EXCESS Chemical Potential

The EXCESS chemical potential of an n-mer, μ_n^{EX}, can be calculated from the EXCESS McMillan-Mayer free energy, F^{EX}, as follows

$$\beta\mu_n^{EX} = \left(\frac{\partial\beta F^{EX}}{\partial N_n}\right)_{T,V^\dagger,\{N_{m\neq n}\},\mu_w^\circ} \tag{5.3}$$

where $\beta = 1/k_BT$ (recall that, according to Eq. (4.18), $V^\dagger = V$). F^{EX} can be obtained by integrating over the osmotic pressure of the micellar solution, Π, with respect to the total solute concentration, c, that is,[103, 107, 108]

$$\frac{\beta F^{EX}}{N} = \int_0^c \left(\frac{\beta\Pi}{c'} - 1\right)\frac{dc'}{c'} \tag{5.4}$$

where $N = \sum_{n=1} N_n$ and $c = \sum_{n=1} c_n$ are the total number and total concentration of aggregates (*micelles and monomers*), respectively. In order to model Π, the virial equation of state is used because it provides a reasonable, mathematically tractable representation of the nonidealities arising from solute-solute interactions in a *dilute* micellar solution. Specifically,[103]

$$\beta\Pi = c + \sum_{n=1}^{\infty}\sum_{m=1}^{\infty} B_{nm}^{(2)} c_n c_m + \sum_{n=1}^{\infty}\sum_{m=1}^{\infty}\sum_{p=1}^{\infty} B_{nmp}^{(3)} c_n c_m c_p + \cdots \tag{5.5}$$

where $B_{nm}^{(2)}$ is the second-virial coefficient between aggregates of aggregation numbers n and m, and $B_{nmp}^{(3)}$ is the third-virial coefficient between aggregates of aggregation numbers n, m, and p. Note that the first term in Eq. (5.5) represents the IDEAL contribution to the osmotic pressure ($\beta\Pi^{ID} = c$), while the additional terms represent the EXCESS contribution, $\beta\Pi^{EX}$. As discussed above, the micellar solution is dilute, and therefore, the contributions of the third- and higher-order virial coefficients in

Eq. (5.5) can be neglected. For convenience, hereafter, the superscript (2) is dropped from the second-virial coefficient, that is, $B_{nm}^{(2)} \equiv B_{nm}$.

Using Eq. (5.5) for $\beta\Pi$ in Eq. (5.4) yields

$$\frac{\beta F^{EX}}{V} = \sum_{n=1}^{\infty}\sum_{m=1}^{\infty} B_{nm}c_n c_m \tag{5.6}$$

The EXCESS chemical potential, μ_n^{EX}, can then be obtained using Eq. (5.6) in Eq. (5.3) (recall that $c_n = N_n/V$). This yields

$$\beta\mu_n^{EX} = 2\sum_{m=1}^{\infty} B_{nm}c_m \tag{5.7}$$

In a typical micellar solution, the interaction potentials reflect three types of interactions: (i) hard-core, steric repulsions, (ii) electrostatic repulsions, and (iii) attractions. This chapter focuses on nonionic surfactants, for which electrostatic interactions are negligible. Consequently, the EXCESS chemical potential is divided into hard-core (HC) and attractive (att) contributions, each characterized by its own second-virial coefficient. Specifically,

$$\beta\mu_n^{EX} = \beta\mu_n^{EX,HC} + \beta\mu_n^{EX,att} \tag{5.8}$$

Equations (5.8) and (5.7) indicate that

$$\beta\mu_n^{EX} = 2\sum_{m=1}^{\infty} B_{nm}^{HC}c_m + 2\sum_{m=1}^{\infty} B_{nm}^{att}c_m \tag{5.9}$$

where B_{nm}^{HC} and B_{nm}^{att} are the hard-core and attractive contributions to the second-virial coefficient, respectively.

The attractive contribution, B_{nm}^{att}, in Eq. (5.9) is estimated utilizing a mean-field approximation. Specifically,

$$B_{nm}^{att} = -\frac{nmC(T)\Omega_s}{2k_BT} \tag{5.10}$$

where the attractive interaction between an n-mer and an m-mer is assumed to be proportional to the number of pairwise interactions ($nm/2$) associated with the n-mer and the m-mer. Use of this simple form for the attractive intermicellar interactions implies averaging over all possible micellar configurations, a reasonable assumption for *isotropic* micellar solutions which lack both positional and orientational long-range order. $C(T)$ in Eq. (5.10) is a phenomenological parameter reflecting the magnitude of the attraction between two surfactant molecules, in units of k_BT. Note that $C(T)$ in Eq. (5.10) is multiplied by the volume of a surfactant molecule, Ω_s, in order to express the virial coefficient in volumetric units. Using Eq. (5.10) for B_{nm}^{att} in the second summation of Eq. (5.9) yields the attractive contribution to the EXCESS chemical potential, that is,

$$\beta\mu_n^{EX,att} = -n\frac{C(T)\Omega_s}{k_BT}\sum_{m=1}^{\infty} mc_m \tag{5.11}$$

where $\sum_{m=1}^{\infty} mc_m = c_s$, the total surfactant concentration.

The hard-core repulsive contribution is somewhat more difficult to quantify because nonionic micelles often exhibit growth from monodisperse spheres into flexible, polydisperse cylindrical aggregates. The model for the repulsive interactions should be applicable to the full range of shapes and sizes. Gelbart *et al.* have developed[44, 110] a description of the hard-core, repulsive interactions between cylindrical micelles by modeling them as rigid spherocylinders, consisting of a cylindrical body of length L_n and cross-sectional radius R_m, terminating in two hemispherical end-caps of radius R_m. Note that $R_m = l_c^* + l_{hg}$, where l_{hg} is the length of the surfactant head. In this model, the smallest micelle that can form is a sphere ($L_n = 0$) having aggregation number $n_0 = 4\pi(l_c^*)^3/(3v_t) \approx 4\pi R_m^3/(3\Omega_s)$.

For the spherocylindrical micelle case, the excluded-volume contribution, $\beta\mu_n^{EX,HC}$ can be written as

$$\beta\mu_n^{EX,HC} = 2B_{n1}^{HC}c_1 + 2\sum_{m=n_0}^{\infty} B_{nm}^{HC}c_m \tag{5.12}$$

where the second-virial coefficients, B_{n1}^{HC} and B_{nm}^{HC}, are given by[111, 110, 103] (see

Appendix F.1 for details)

$$B_{n1}^{HC} = \frac{\Omega_s \gamma^2}{2}(n + n_0^{2/3}) , \quad n \geq n_0 \tag{5.13}$$

and

$$B_{nm}^{HC} = \frac{2\pi d^3}{3} + \frac{\pi d^2}{2}(L_n + L_m) + \frac{\pi}{4} d L_n L_m , \quad n, m \geq n_0 \tag{5.14}$$

where $d = 2R_m$, and $\gamma = (1 + 1/n_0^{1/3})$ is a geometric factor associated with the smallest micelle of aggregation number n_0. Note that for the case of spherical micelles, $B_{n1}^{HC}(sph)$ can be obtained from Eq. (5.13) with $n = n_0$, and $B_{nm}^{HC}(sph)$ can be obtained from Eq. (5.14) with $L_n = L_m = 0$.

Utilizing Eq. (5.13), along with the fact that $B_{11}^{HC} = 4\Omega_s$, in Eq. (5.12) with $n = 1$, the following expression is obtained for the hard-core EXCESS chemical potential of a monomer (see Appendix F.1 for details).

$$\beta\mu_1^{EX,HC} = 8\Omega_s c_1 + \Omega_s \gamma^2 (c_s - c_1) + \Omega_s \gamma^2 n_0^{2/3} (c - c_1) \tag{5.15}$$

where $c_s = c_1 + \sum_{m=n_0}^{\infty} m c_m$ is the total surfactant concentration, and $c = c_1 + \sum_{m=n_0}^{\infty} c_m$ is the total aggregate concentration. Note that for the case of monodisperse spherical micelles, $n_0(c - c_1) = c_s - c_1$, and the EXCESS chemical potential of a monomer becomes $\beta\mu_1^{EX,HC}(sph) = 8\Omega_s c_1 + \Omega_s \gamma^3 (c_s - c_1)$.

Utilizing Eqs. (5.13) and (5.14) in Eq. (5.12), the following expression is obtained for the hard-core EXCESS chemical potential of a spherocylindrical micelle of aggregation number $n \geq n_0$,

$$\beta\mu_n^{EX,HC} = \Omega_s \gamma^2 (n + n_0^{2/3}) c_1 + \frac{4\pi d^3}{3} \sum_{m=n_0}^{\infty} c_m + \pi d^2 \sum_{m=n_0}^{\infty} c_m (L_n + L_m) + \frac{\pi}{2} d \sum_{m=n_0}^{\infty} c_m L_n L_m \tag{5.16}$$

Note that for the case of monodisperse spherical micelles, $\beta\mu_n^{EX,HC}(sph)$ can be obtained from Eq. (5.16), with $n = n_0$ and $L_n = L_m = 0$. Using a geometric relation for L_n (see Appendix F.1 for details), the following relation between $\mu_n^{EX,HC}$ and n is

obtained

$$\begin{aligned}\beta\mu_n^{EX,HC} &= \Omega_s\gamma^2 n_0^{2/3}c_1 + \frac{2\pi d^3}{9}(c-c_1) + \frac{8\Omega_s}{3}(c_s-c_1) \\ &\quad + n\left(\Omega_s\gamma^2 c_1 + \frac{8\Omega_s}{3}(c-c_1) + \frac{8\Omega_s^2}{\pi d^3}(c_s-c_1)\right) \end{aligned} \tag{5.17}$$

5.4 Micellar Size Distribution and its Moments

The EXCESS chemical potentials, μ_n^{EX} and μ_1^{EX}, are now fully defined through Eqs. (5.8), (5.11), (5.15), and (5.16), and can be utilized to evaluate the micellar size distribution through Eq. (4.21). The attractive contribution to the EXCESS chemical potential in Eq. (5.11) was computed in the context of a mean-field approximation, and was shown to depend solely on the total surfactant concentration, $c_s = \sum_{m=1}^{\infty} mc_m$. As a result, this contribution cancels out when used in Eq. (4.21). Specifically,

$$\mu_n^{EX,att} - n\mu_1^{EX,att} = -nC(T)\Omega_s \sum_{m=1}^{\infty} mc_m + n\left[C(T)\Omega_s \sum_{m=1}^{\infty} mc_m\right] = 0 \tag{5.18}$$

In view of Eq. (5.18), only the hard-core, repulsive interactions contribute to the EXCESS chemical potentials appearing in the size-distribution equation. This hard-core contribution can be conveniently written as a linear function of the micelle aggregation number, n. Specifically, for the case of spherocylindrical micelles, one obtains

$$\beta(\mu_n^{EX} - n\mu_1^{EX}) = \beta(\mu_n^{EX,HC} - n\mu_1^{EX,HC}) = A_0^{cyl} - nA_1^{cyl} \tag{5.19}$$

where

$$A_0^{cyl} = \Omega_s\gamma^2 n_0^{2/3}c_1 + \frac{2\pi d^3}{9}(c-c_1) + \frac{8\Omega_s}{3}(c_s-c_1) \tag{5.20}$$

and

$$A_1^{cyl} = \left[8 - \gamma^2(2 + n_0^{2/3})\right]\Omega_s c_1 + \Omega_s\gamma^2 c_s + \Omega_s\gamma^2 n_0^{2/3} c - \frac{8\Omega_s}{3}(c - c_1) - \frac{8\Omega_s^2}{\pi d^3}(c_s - c_1) \tag{5.21}$$

For the case of monodisperse spheres, A_0^{sph} and A_1^{sph} can be obtained directly from Eqs. (5.20) and (5.21) by making use of the fact that $n = n_0 = \pi d^3/(6\Omega_s)$ and $n_0(c - c_1) = c_s - c_1$. Specifically, $A_0^{sph} = \Omega_s\gamma^2 n_0^{2/3} c_1 + 4\Omega_s(c_s - c_1)$ and $A_1^{sph} = [12 - \gamma^2(1 + \gamma)]\Omega_s c_1 + \Omega_s\gamma^3 c_s - 4\Omega_s c$.

Note that A_0^{cyl} and A_1^{cyl} in Eqs. (5.20) and (5.21) are dimensionless quantities which are independent of n. When very few micelles are present in the solution, A_0^{cyl} and A_1^{cyl} are very small, since, as $c_s \to 0$, $c_1 \approx c \approx c_s$, and therefore, A_0^{cyl} and $A_1^{cyl} \to 0$.

Utilizing Eqs. (5.19) and (5.1) in Eq. (4.21), the following expression is obtained for the micellar size distribution of spherocylindrical micelles

$$\Omega_w c_n = (\Omega_w c_1)^n \exp\{-\beta n g_{mic}(n) - (A_0^{cyl} - nA_1^{cyl})\} \tag{5.22}$$

with $g_{mic}(n) = g_{mic}^{cyl}(n)$ given in Eq. (5.2). Note that Eq. (5.22) is also applicable to monodisperse spherical micelles of aggregation number n_0, with $g_{mic}^{cyl}(n)$ replaced by $g_{sph} = g_{mic}(l_c^*, s^* = 3)$, and A_0^{cyl} and A_1^{cyl} replaced by A_0^{sph} and A_1^{sph}, respectively.

By substituting the expression for $g_{mic}^{cyl}(n)$ given in Eq. (5.2) in Eq. (5.22), the following convenient form is obtained for the micellar size distribution of spherocylindrical micelles

$$c_n = \frac{q^n}{K} \tag{5.23}$$

where

$$K = \Omega_w \exp[\beta n_0(g_{sph} - g_{cyl}) + A_0^{cyl}] \tag{5.24}$$

and

$$q = (\Omega_w c_1) \exp[-\beta g_{cyl} + A_1^{cyl}] \tag{5.25}$$

Equations (5.23)-(5.25) describe the effect of excluded-volume interactions on the micellar size distribution of spherocylindrical micelles through the parameters A_0^{cyl} and A_1^{cyl}. It is noteworthy that, in the absence of excluded-volume interactions (the "ideal case"), $A_0^{cyl} = A_1^{cyl} = 0$, and one recovers the well-known expressions for c_n, q, and K.[9] Interestingly, Gelbart *et al.* obtained[44] a similar expression for the size distribution of spherocylindrical micelles by utilizing the same model for the excluded-volume interactions with an alternative equation of state.[1] However, they only considered the relatively high surfactant concentration limit, and hence, neglected the monomer excluded-volume contributions. In addition, the spherocylindrical micelles at these conditions were assumed to be sufficiently long such that the effect of the excluded-volume contributions associated with the hemispherical end-caps could be neglected. Consequently, their expressions for A_0^{cyl} and A_1^{cyl} are slightly different from those given in Eqs. (5.20) and (5.21).

In order to better characterize the spherocylindrical micellar system, it is useful to introduce various moments of the micellar size distribution. In general, the kth moment of the micellar size distribution is given by

$$M_k = \sum_{n=1}^{\infty} n^k c_n \tag{5.26}$$

From these moments, one can calculate various average characteristics of the micellar size distribution, which can be measured experimentally. For example,[6]

[1] Gelbart et al.[44, 110] utilized the "y-expansion"[112] which rescales the virial expansion in terms of a new concentration variable, thus incorporating the effect of higher-order terms. For the relatively dilute surfactant solutions of interest in this chapter, the two approaches yield similar results.

$$\langle n \rangle_n = \frac{M_1}{M_0} \tag{5.27}$$

$$\langle n \rangle_w = \frac{M_2}{M_1} \tag{5.28}$$

and

$$Var = \frac{M_3 M_1}{M_2^2} - 1 \tag{5.29}$$

where $\langle n \rangle_n$ is the number-average micellar aggregation number, $\langle n \rangle_w$ is the weight-average micellar aggregation number, and Var is the relative variance of the micellar size distribution, constituting a measure of micellar-size polydispersity.

For spherocylindrical micelles, M_k in Eq. (5.26) is given by

$$M_k^{cyl} = c_1 + \sum_{n=n_0}^{\infty} n^k c_n \tag{5.30}$$

Expressions for $\langle n \rangle_n$, $\langle n \rangle_w$, and Var corresponding to spherocylindrical micelles can be obtained by using Eq. (5.30) for M_k^{cyl} (with $k = 0,1,2$, and 3) in Eqs. (5.27)-(5.29), respectively.

Utilizing Eq. (5.23) in Eq. (5.30) with $k = 0$ and $k = 1$, expressions for c and c_s, respectively, can be derived. Specifically,

$$c = M_0^{cyl} = c_1 + \sum_{n=n_0}^{\infty} \frac{q^n}{K} = c_1 + \frac{q^{n_0}}{K(1-q)} \tag{5.31}$$

and

$$c_s = M_1^{cyl} = c_1 + \sum_{n=n_0}^{\infty} n\frac{q^n}{K} = c_1 + \frac{q^{n_0}}{K(1-q)^2}[n_0(1-q)+q] \tag{5.32}$$

Equation (5.23), describing the size distribution of spherocylindrical micelles, can

also be utilized to define a critical micellar concentration (or CMC). Specifically, by taking the natural log of c_n in Eq. (5.23), and keeping only terms that are of order n, because $n \gg 1$, one can show[16, 9] that the CMC (in units of mole fraction) is given by

$$CMC \approx \exp\left(\beta g_{cyl} - A_1^{cyl}\right) \tag{5.33}$$

where $g_{cyl} = g_{mic}(l_c^*, s^* = 2)$. In view of the fact that A_1^{cyl} depends on surfactant concentration (see Eq. (5.21)), it is necessary to set $c_s = CMC$ and solve Eq. (5.33) iteratively.

Note that Eqs. (5.27)-(5.33) are also applicable to monodisperse spherical micelles of aggregation number n_0, with g_{cyl} replaced by $g_{sph} = g_{mic}(l_c^*, s^* = 3)$, and A_0^{cyl} and A_1^{cyl} replaced by A_0^{sph} and A_1^{sph}, respectively.

In summary, using Eqs. (5.24) and (5.25), along with Eqs. (5.20) and (5.21), in Eq. (5.32), one obtains an implicit equation relating c_1 and c_s. Note that solving Eq. (5.32) requires the simultaneous solution of Eq. (5.31), since K and q depend on A_0^{cyl} and A_1^{cyl}, respectively, which, in turn, are functions of c. Solving this set of equations numerically, one can, in principle, calculate c_1 as a function of c_s, which can then be inserted back in Eq. (5.23) to obtain the entire distribution of micellar sizes, $\{c_n\}$, as a function of c_s and T. Illustrative example calculations of (i) the variation of c_1 with c_s, (ii) the CMC, and (iii) characteristics of the micellar size distribution, including c, $\langle n \rangle_w$, and Var, will be presented in Section 5.7.

5.5 Limit of Extensive Micellar Growth

It is instructive to consider the limiting case of extensive spherocylindrical micellar growth, in which $\langle n \rangle_w \gg n_0$. For this purpose, it is convenient to introduce a concentration, c_b, which corresponds to the maximum monomer concentration attainable in this limit. Therefore, $\Omega_w c_b$ is equivalent to the CMC defined in Eq. (5.33), that

is,[9, 6]

$$\Omega_w c_b = \exp(\beta g_{cyl} - A_1^{cyl}) \tag{5.34}$$

In view of Eqs. (5.25) and (5.34), it follows that $q = c_1/c_b$. Note that c_b is a function of the total surfactant concentration, c_s, through the excluded-volume parameter, A_1^{cyl} (see Eq. (5.21)). In particular, as c_s increases, the excluded-volume term, A_1^{cyl}, increases, and c_b decreases. At high c_s values, the monomer concentration, c_1, approaches its maximum value, c_b, and hence $q \approx 1$. In order to explore this limiting behavior, it is useful to introduce a parameter $f = 1 - q$. Substituting $q = 1 - f$ in Eq. (5.32), c_s can be expressed in terms of this new parameter as follows

$$c_s = c_1 + \frac{(1 - n_0 f)}{K}\left(\frac{n_0}{f} + \frac{1 - f}{f^2}\right) \tag{5.35}$$

In the limit of extensive micellar growth, $q \approx 1$, and $f \ll 1$. Expanding the right-hand side of Eq. (5.35) in powers of f (to leading order in f), and rearranging terms, the following expression is obtained for f[9]

$$f = [K(c_s - c_1)]^{-1/2} \tag{5.36}$$

At high surfactant concentrations, $(c_s - c_1) \approx c_s$, and, by utilizing Eq. (5.36) in Eq. (5.23), one obtains the following remarkably simple expression for c_n[9]

$$c_n^{cyl} = \frac{1}{K}\exp\left[-n\,(Kc_s)^{-1/2}\right] \ , \quad n \gg n_0 \tag{5.37}$$

Consequently, in the limit of extensive micellar growth, the micellar size distribution, $\{c_n\}$, is a monotonically decreasing exponential function of n. Using Eq. (5.37) in Eq. (5.26), the following expression for the kth moment is obtained:

$$M_k^{cyl} = \frac{k!}{K}\,(c_s K)^{(k+1)/2} \ , \quad n \gg n_0 \tag{5.38}$$

In particular, the zeroth moment is given by $M_0^{cyl} = c = (c_s/K)^{1/2}$. The parameter K provides a quantitative measure of the ability of the spherocylindrical micelles to

grow.[9] Recall that K is a function of the surfactant concentration, c_s, through the excluded-volume contribution, A_0^{cyl} (see Eqs. (5.24) and (5.20)). In the ideal case, when $A_0^{cyl} = 0$, K does not depend on c_s, and c increases as the square root of c_s. However, when $A_0^{cyl} > 0$, as c_s increases, K also increases, thus reducing the rate at which c increases with c_s.

In addition, in the limit of extensive micellar growth, the average micellar aggregation numbers are given by

$$\langle n \rangle_n = \frac{M_1^{cyl}}{M_0^{cyl}} = (c_s K)^{1/2} \tag{5.39}$$

$$\langle n \rangle_w = \frac{M_2^{cyl}}{M_1^{cyl}} = 2\,(c_s K)^{1/2} \tag{5.40}$$

Equations (5.39) and (5.40), along with Eq. (5.24), indicate that excluded-volume interactions affect these aggregation numbers through the growth parameter, K, which depends on A_0^{cyl}. When $A_0^{cyl} = 0$ (ideal case), both $\langle n \rangle_n$ and $\langle n \rangle_w$ increase as the square-root of the total surfactant concentration, c_s. However, in the presence of excluded-volume interactions, A_0^{cyl} increases as c_s increases (see Eq. (5.20)), which, in turn, leads to an increase of K with c_s. As a result, in the presence of excluded-volume interactions, $\langle n \rangle_w$ and $\langle n \rangle_n$ are not only larger, but also increase at a rate faster than $c_s^{1/2}$ with increasing c_s. Interestingly, although excluded-volume interactions separately affect both $\langle n \rangle_w$ and $\langle n \rangle_n$, in the limit of extensive micellar growth, their ratio, $\langle n \rangle_w / \langle n \rangle_n$, remains equal to 2 (see Eqs. (5.39) and (5.40)), a well-known finding corresponding to the ideal case.[9, 6] In addition, the relative variance of the micellar size distribution, Var, has a value of 0.5 even in the presence of excluded-volume interactions, which is another well-known finding corresponding to the ideal case.[9, 6]

5.6 Micellar Solution Phase Separation

5.6.1 Spinodal Curve and Critical Point

Nonionic surfactants, particulary those of the alkyl poly(ethylene oxide) variety, can phase separate into a micelle-rich phase coexisting with a micelle-poor phase by varying temperature and/or surfactant concentration. The phase separation behavior can be quantified by making use of thermodynamic stability requirements. The spinodal curve is obtained from the following requirement[108]

$$\left(\frac{\partial \mu_1}{\partial c_s}\right)_{T,p} = 0 \tag{5.41}$$

The critical point is obtained from the following additional requirement[108]

$$\left(\frac{\partial^2 \mu_1}{\partial c_s^2}\right)_{T,p} = 0 \tag{5.42}$$

The derivatives of the monomer chemical potential in Eqs. (5.41) and (5.42) can be taken directly using Eq. (4.19), with $n = 1$. The following expression is then obtained for the spinodal curve

$$\left(\frac{\partial \mu_1}{\partial c_s}\right)_{T,p} = \left(\frac{\partial \mu_1^{EX}}{\partial c_s}\right)_{T,p} + \frac{k_B T}{c_1}\left(\frac{\partial c_1}{\partial c_s}\right)_{T,p} - \Omega_s \left(\frac{\partial \Pi}{\partial c_s}\right)_{T,p} = 0 \tag{5.43}$$

At constant temperature and pressure, the Gibbs-Duhem equation requires that $(\partial \mu_w / \partial c_s)_{T,p,N_w}$ vanishes at the spinodal.[108] Since the standard-state chemical potential, $\mu_w^\circ(T,p)$, depends only on T and p, Eq. (4.20) indicates that $(\partial \mu_w / \partial c_s)_{T,p,N_w} = -\Omega_w \left(\partial \Pi / \partial c_s\right)_{T,p,N_w} = 0$. Hence, the last term in Eq. (5.43) can be set to zero.

A second differentiation of Eq. (5.43), with $(\frac{\partial \Pi}{\partial c_s})_{T,p} = 0$ as explained above, with respect to c_s yields the additional expression required to evaluate the critical point, that is,

$$\left(\frac{\partial^2 \mu_1}{\partial c_s^2}\right)_{T,p} = \left(\frac{\partial^2 \mu_1^{EX}}{\partial c_s^2}\right)_{T,p} - \frac{k_B T}{c_1^2}\left(\frac{\partial c_1}{\partial c_s}\right)_{T,p}^2 + \frac{k_B T}{c_1}\left(\frac{\partial^2 c_1}{\partial c_s^2}\right)_{T,p} = 0 \tag{5.44}$$

For the micellar solutions exhibiting phase separation considered in this chapter, the micelles are cylindrical in shape.[13, 12, 113] Therefore, in what follows, the micelles are modeled as spherocylinders, so the results derived in Sections 5.3-5.4 for this micellar shape will be used. Recall that the monomer EXCESS chemical potential includes both attractive (Eq. (5.11) with $n = 1$) and repulsive (Eq. (5.15)) contributions, that is,

$$\begin{aligned}\mu_1^{EX} &= \mu_1^{EX,att} + \mu_1^{EX,HC} \\ &= k_BT\Omega_s\gamma^2 c_s + k_BT\Omega_s\gamma^2 n_0^{2/3} c + k_BT\Omega_s\left[8 - \gamma^2(1 + n_0^{2/3})\right] c_1 - C(T)\Omega_s c_s\end{aligned} \tag{5.45}$$

Utilizing Eq. (5.45) for μ_1^{EX} in Eq. (5.43), the following expression is obtained for the spinodal curve

$$\Omega_s\left(\gamma^2 - \frac{C(T)}{k_BT}\right) + \Omega_s\gamma^2 n_0^{2/3}\left(\frac{\partial c}{\partial c_s}\right)_{T,p} + \left\{\Omega_s[8 - \gamma^2(1 + n_0^{2/3})] + \frac{1}{c_1}\right\}\left(\frac{\partial c_1}{\partial c_s}\right)_{T,p} = 0 \tag{5.46}$$

The critical point is then obtained from the following additional requirement, obtained by utilizing Eq. (5.45) for μ_1^{EX} in Eq. (5.44)

$$\Omega_s\gamma^2 n_0^{2/3}\left(\frac{\partial^2 c}{\partial c_s^2}\right)_{T,p} + \left\{\Omega_s[8 - \gamma^2(1 + n_0^{2/3})] + \frac{1}{c_1}\right\}\left(\frac{\partial^2 c_1}{\partial c_s^2}\right)_{T,p} - \frac{1}{c_1^2}\left(\frac{\partial c_1}{\partial c_s}\right)_{T,p}^2 = 0 \tag{5.47}$$

Note that c and c_1, as well as their derivatives with respect to c_s, which appear in Eqs. (5.46) and (5.47), can be calculated from Eqs. (5.31) and (5.32), respectively (see Appendix E for details).

Typically, both c and c_1 depend on solution conditions such as temperature through the free energy of micellization, g_{mic}. Given models for $g_{mic}(T)$ and the attraction parameter, $C(T)$, one can predict both the critical temperature, T_c, and the critical surfactant concentration, c_s^{crit}, by simultaneously solving Eqs. (5.46) and

(5.47), utilizing the expressions for the derivatives given in Appendix E. Alternatively, given the critical temperature, T_c, solving Eq. (5.47) yields the critical surfactant concentration, c_s^{crit}. Then, Eq. (5.46) can be utilized to solve for the attraction parameter at the critical point, $C^{crit}(T_c)$. Illustrative calculations of the critical surfactant concentration are presented in Section 5.7.2.

5.6.2 Coexistence Curve

The coexistence curve can be obtained through the requirements of thermodynamic equilibrium. Specifically, the temperature, the pressure, and the chemical potential of each component present in the two coexisting micellar phases A and B should be equal, namely,

$$\mu_n^A = \mu_n^B , \quad n \geq 1 \tag{5.48}$$

and

$$\mu_w^A = \mu_w^B \tag{5.49}$$

Recall that due to the multiple chemical equilibrium condition (see Eq. (4.16)), requiring $\mu_1^A = \mu_1^B$ is equivalent to requiring $\mu_n^A = n\mu_1^A = n\mu_1^B = \mu_n^B$ for any n. Hence, Eq. (5.48) can be replaced by the following requirement

$$\mu_1^A = \mu_1^B \tag{5.50}$$

In addition, specifying the water chemical potentials in phases A and B is equivalent to specifying the osmotic pressures of phases A and B (see Eq. (4.20)). Hence, Eq. (5.49) can be replaced by

$$\Pi^A = \Pi^B \tag{5.51}$$

The monomer chemical potential, μ_1, is given in Eq. (4.19) with n =1, with μ_1^{EX}

given in Eq. (5.45). Utilizing the resulting expressions in Eq. (5.50) yields

$$\Omega_s\gamma^2(c_s^A - c_s^B) + \Omega_s\gamma^2 n_0^{2/3}(c^A - c^B) + \Omega_s(8 - \gamma^2(1 + n_0^{2/3}))(c_1^A - c_1^B) - \frac{C(T)\Omega_s}{k_BT}(c_s^A - c_s^B) + \ln\frac{c_1^A}{c_1^B} = 0 \qquad (5.52)$$

where the superscripts A and B indicate the values of c_1, c, and c_s in phases A and B, respectively.

The osmotic pressure, Π, is obtained directly from the virial equation of state used in Section 5.3 to model the attractive and repulsive intermicellar interactions. Utilizing the second-virial coefficients corresponding to the attractive interactions (see Eq. (5.10)), along with those corresponding to the hard-core repulsive interactions (see Eqs. (5.13) and (5.14)), in Eq. (5.5), truncated at quadratic order in concentration, results in the following expression for the osmotic pressure

$$\begin{aligned}\beta\Pi &= c - \frac{C(T)\Omega_s c_s^2}{2k_BT} + \Omega_s\gamma^2 c_s c_1 + \Omega_s\gamma^2 n_0^{2/3} c c_1 + \Omega_s[4 - \gamma^2(1 + n_0^{2/3})]c_1^2 \\ &\quad + \frac{\pi d^3}{9}(c - c_1)^2 + \frac{8\Omega_s}{3}(c - c_1)(c_s - c_1) + \frac{4\Omega_s^2}{\pi d^3}(c_s - c_1)^2 \qquad (5.53)\end{aligned}$$

Utilizing Eq. (5.53) in Eq. (5.51) yields

$$\begin{aligned}0 &= c^A - c^B - \frac{C(T)\Omega_s}{2k_BT}\left[(c_s^A)^2 - (c_s^B)^2\right] \\ &\quad + \Omega_s\gamma^2\left[c_s^A c_1^A - c_s^B c_1^B\right] + \Omega_s\gamma^2 n_0^{2/3}\left[c^A c_1^A - c^B c_1^B\right] \\ &\quad + \Omega_s(4 - \gamma^2(1 + n_0^{2/3}))\left[(c_1^A)^2 - (c_1^B)^2\right] + \frac{\pi d^3}{9}\left[(c^A - c_1^A)^2 - (c^B - c_1^B)^2\right] \\ &\quad + \frac{8\Omega_s}{3}\left[(c^A - c_1^A)(c_s^A - c_1^A) - (c^B - c_1^B)(c_s^B - c_1^B)\right] \\ &\quad + \frac{4\Omega_s^2}{\pi d^3}\left[(c_s^A - c_1^A)^2 - (c_s^B - c_1^B)^2\right] \qquad (5.54)\end{aligned}$$

Accordingly, given a model for the attraction parameter, $C(T)$, a simultaneous solution of Eqs. (5.52) and (5.54) at a fixed temperature and pressure yields the two coexisting concentrations, c_s^A and c_s^B. Repeating this calculation for a range of temperatures generates the entire coexistence curve in the temperature-concentration

plane.

Note that Eq. (5.53) can also be utilized to derive an expression for the osmotic compressibility of the micellar solution in the one phase region, $(\frac{\partial \Pi}{\partial c_s})^{-1}_{T,p}$. By differentiating Eq. (5.53) with respect to c_s, we obtain the following result

$$\begin{aligned}\left(\frac{\partial \Pi}{\partial c_s}\right)^{-1}_{T,p} &= \beta\left\{\left(\frac{\partial c}{\partial c_s}\right)_{T,p} - \frac{C(T)\Omega_s}{k_B T}c_s + \Omega_s\gamma^2\left[c_1 + c_s\left(\frac{\partial c_1}{\partial c_s}\right)_{T,p}\right]\right. \\ &+\Omega_s\gamma^2 n_0^{2/3}\left[c_1\left(\frac{\partial c}{\partial c_s}\right)_{T,p} + c\left(\frac{\partial c_1}{\partial c_s}\right)_{T,p}\right] + 2\Omega_s(4-\gamma^2(1+n_0^{2/3}))c_1\left(\frac{\partial c_1}{\partial c_s}\right)_{T,p} \\ &+\frac{2\pi d^3}{9}(c-c_1)\left[\left(\frac{\partial c}{\partial c_s}\right)_{T,p} - \left(\frac{\partial c_1}{\partial c_s}\right)_{T,p}\right] + \frac{8\Omega_s}{3}(c-c_1)\left[1-\left(\frac{\partial c_1}{\partial c_s}\right)_{T,p}\right] \\ &\left.+\frac{8\Omega_s}{3}(c_s-c_1)\left[\left(\frac{\partial c}{\partial c_s}\right)_{T,p} - \left(\frac{\partial c_1}{\partial c_s}\right)_{T,p}\right] + \frac{8\Omega_s^2}{\pi d^3}(c_s-c_1)\left[1-\left(\frac{\partial c_1}{\partial c_s}\right)_{T,p}\right]\right\}^{-1}\end{aligned} \tag{5.55}$$

As stated earlier, the derivatives of c and c_1 with respect to c_s are given in Appendix E.

If the temperature dependence of $C(T)$ is known in the one-phase region (that is, for $T < T_c$ in the case of the alkyl poly(ethylene oxide) surfactants considered in this thesis), then solving Eq. (5.55) at a given value of c_s yields the osmotic compressibility for temperatures less than T_c. Illustrative calculations for both the coexistence curve and the osmotic compressibility are presented in Section 5.7.2.

5.7 Results

In this section, the theoretical results derived in Sections 5.4 and 5.6 are appplied to aqueous micellar solutions of alkyl poly(ethylene oxide) surfactants, a representative, widely-used class of nonionic surfactants. First, a qualitative analysis of the effect of excluded-volume interactions is presented. Then, micellar solution properties, such as the CMC, the relative variance of the micellar size distribution, the critical surfactant concentration for phase separation, and the osmotic compressibility, are quantitatively predicted and compared to experimental data.

5.7.1 Excluded-Volume Contribution

As a representative example, aqueous solutions of the nonionic surfactant $C_{12}E_6$, $CH_3(CH_2)_{11}(OCH_2CH_2)_6$-OH, were examined at 20°C. Using Eq. (5.32), the monomer concentration, c_1, was predicted as a function of the total surfactant concentration, c_s, and plotted in Figure 5-1 (solid line). In addition, the same prediction was made assuming ideal behavior, that is, in the absence of excluded-volume interactions (dashed line in Figure 5-1). Two main conclusions can be drawn from these predictions. First, the monomer concentration is lower when excluded-volume interactions are accounted for, indicating that such interactions encourage free surfactant monomers to form micelles. Second, as the total surfactant concentration increases, the monomer concentration initially increases both in the presence and in the absence of excluded-volume interactions. However, beyond the CMC (signalled in Figure 5-1 by the abrupt changes in the slopes of each curve), the monomer concentration remains constant in the ideal case, while it decreases in the presence of excluded-volume interactions.

In general, as micelle formation becomes more favorable from a free-energy perspective, larger micelles are formed.[3] Indeed, this is also true in the present case. Figure 5-2 depicts the micelle concentration, $c - c_1$, predicted using Eq. (5.31), as a function of c_s for the ideal case (dashed line) and in the presence of excluded-volume interactions (solid line). In the ideal case, as more surfactant molecules are added, they aggregate to form new micelles, such that the overall micelle concentration increases. When excluded-volume interactions are considered, as c_s increases, the micelle concentration increases at a slower rate. This indicates that instead of forming new micelles, the additional surfactant molecules are incorporated into already existing micelles, thus inducing micellar growth. This is further corroborated in Figure 5-3, which shows predictions of the weight-average micellar aggregation number, $\langle n \rangle_w$, as a function of c_s. Indeed, Figure 5-3 reveals that, for a given c_s value, when excluded-volume interactions are accounted for (solid line) the micelles that form have larger aggregation numbers than those corresponding to the ideal case (dashed line).[44]

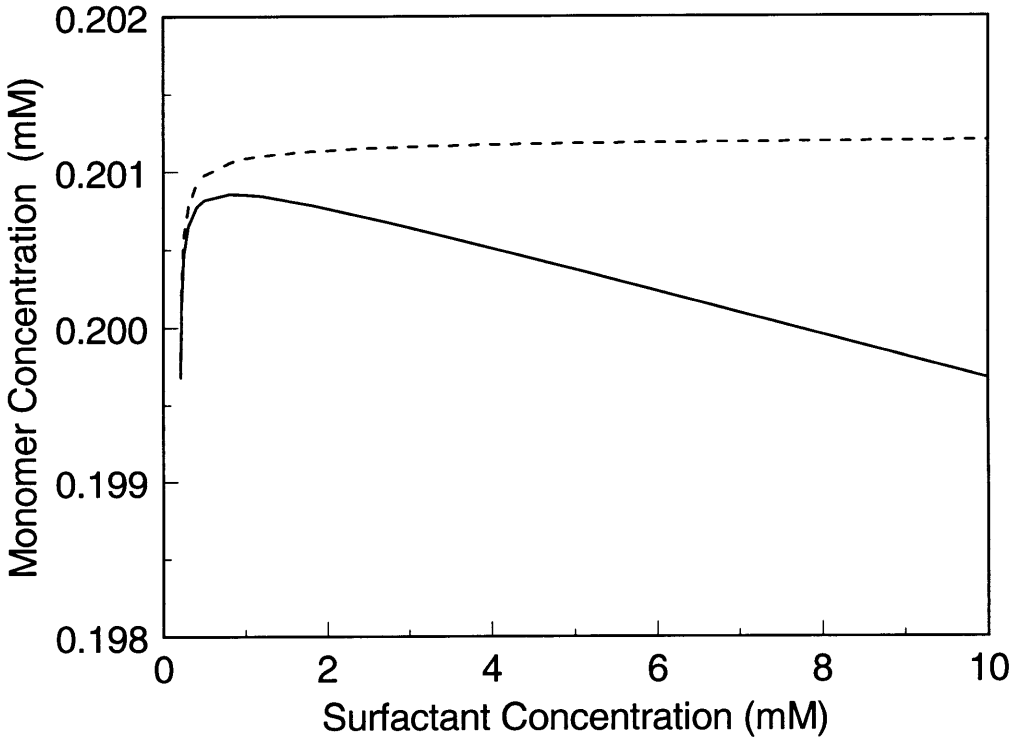

Figure 5-1: Predicted monomer concentration, c_1, as a function of total surfactant concentration, c_s, for an aqueous solution of $C_{12}E_6$ at 20°C. Predictions were made using the excluded-volume model (—) and the ideal solution model (- - -), which has zero excluded volume.

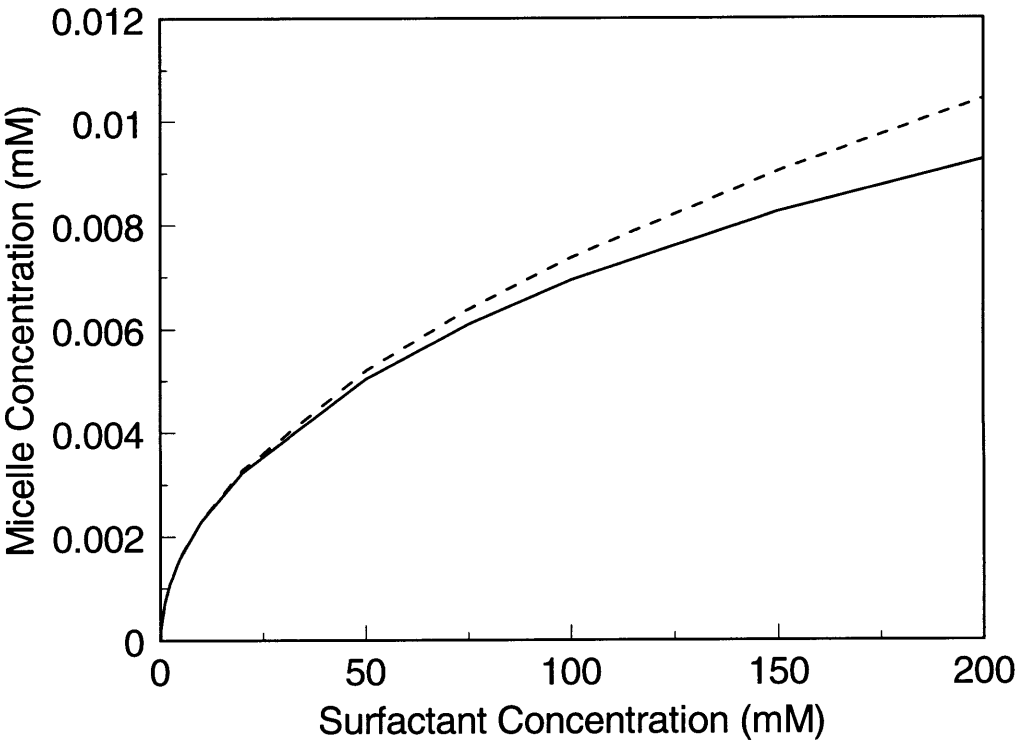

Figure 5-2: Predicted micelle concentration, $c - c_1$, as a function of total surfactant concentration, c_s, for an aqueous solution of $C_{12}E_6$ at 20°C. Predictions were made using the excluded-volume model (—) and the ideal solution model (- - -), which has zero excluded volume.

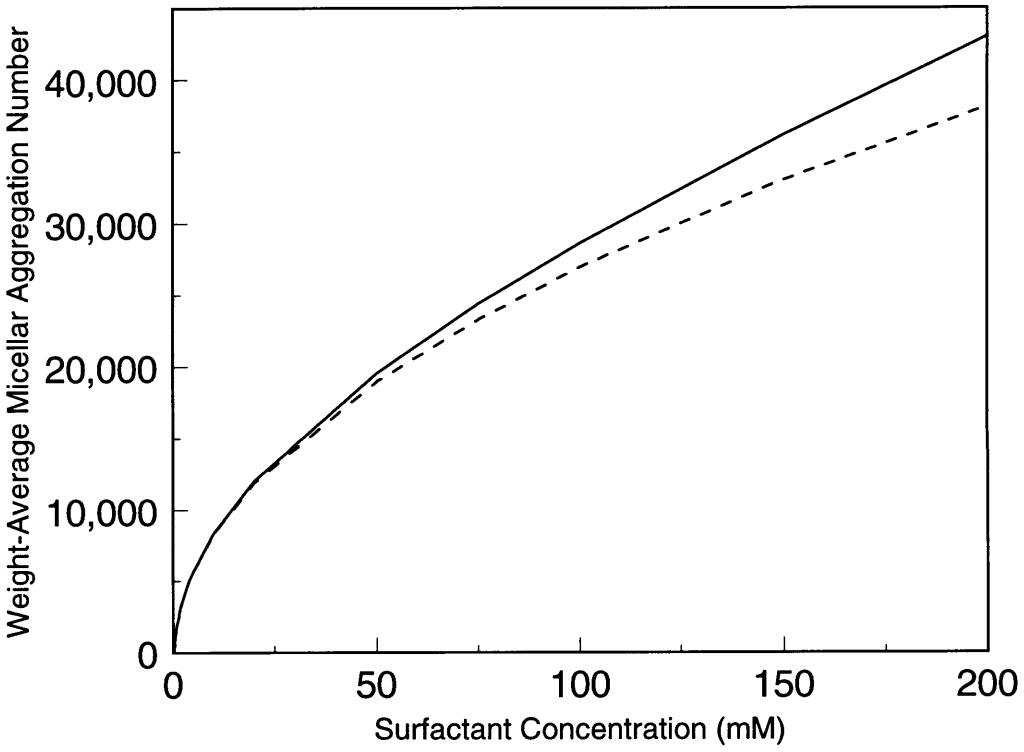

Figure 5-3: Predicted weight-average micellar aggregation number, $\langle n \rangle_w$, as a function of total surfactant concentration, c_s, for an aqueous solution of $C_{12}E_6$ at 20°C. Predictions were made using the excluded-volume model (—) and the ideal solution model (- - -), which has zero excluded volume.

The results in Figures 5-1 through 5-3 indicate that the overall effect of excluded-volume interactions is to encourage micellar growth, since a solution containing fewer, larger micelles excludes less volume than one containing a larger number of smaller micelles. This is a general result which should be applicable to any micellar system in the presence of excluded-volume interactions. However, it should be kept in mind that the predictions presented here were made using a particular excluded-volume model, namely, that corresponding to rigid spherocylinders treated at the second-virial expansion level of approximation. This derivation assumes that: (i) third- and higher-order body interactions can be neglected, and (ii) micelle flexibility can be neglected. In order to test the validity and range of applicablility of assumptions (i) and (ii) corresponding to the excluded-volume description presented above, other excluded-volume models were analyzed.

First, to examine assumption (i), the third-virial coefficient corresponding to rigid spherocylinders[44] was utilized in Eq. (5.5) to account for the effect of three-body interactions. The various EXCESS chemical potentials were then obtained following a procedure similar to that described in Section 5.3, and predictions for the micellar size distribution, analogous to those presented in Figures 5-1 through 5-3, were made. As expected, at relatively low surfactant concentrations, no difference was observed between the predictions made in the context of the second-order and third-order virial equations. Only when the surfactant concentration exceeded about 200 mM, which is approximately 1000 times the CMC, did the predictions made using the third-order virial equation begin to deviate from those made using the second-order virial equation. This clearly indicates that, for the relatively dilute surfactant concentrations of interest in this paper (0-100mM), it is reasonable to neglect three-body excluded-volume effects.

Second, to examine assumption (ii), an equation of state for flexible, hard-sphere chains[114, 115] was utilized, instead of the virial equation of state, to investigate the effect of micellar flexibility on the theoretical predictions. Similar to the finding regarding the third-virial coefficient contribution, deviations from the rigid case were only observed at surfactant concentrations greater than $\approx$ 200 mM. At these relatively

high surfactant concentrations, the flexible model predicted slightly higher monomer concentrations and higher micellar aggregation numbers than the virial equation approach, indicating that the nonideal contributions were even stronger for this equation of state. However, for the relatively low surfactant concentrations of interest in this paper (0-100mM), is is reasonable to neglect micellar flexibility.

In summary, the virial equation of state truncated at quadratic order in the context of an excluded-volume model for rigid spherocylinders is adequate for the calculation of micellar solution characteristics at the solution conditions of interest in this paper. Carrying out these additional calculations was also valuable in demonstrating the versatility of the McMillan-Mayer theory and the relative ease with which alternative models of intermicellar interactions and micellar flexibility can be analyzed in the context of this statistical-thermodynamic framework.

5.7.2 Comparison with Experiments

In this section, the excluded-volume model is utilized to make several quantitative predictions of micellar solution characteristics. The molecular parameters, Ω_s, n_0, and g_{mic}, of the C_iE_j surfactants examined in this chapter (i = 10, 12, and 16; j = 4-9) were determined using the molecular model of micellization presented in Section 2.3.[16, 17] g_{mic} has a strong dependence on temperature, while n_0 and Ω_s are approximately constant over the range of temperatures examined. Specifically, n_0 = 34, 48, and 84 for C_{10}, C_{12}, and C_{16}, respectively, and $\Omega_s = v_t + v_{head}$, where v_t = 312Å^3, 366Å^3, and 473Å^3 for C_{10}, C_{12}, and C_{16}, respectively, and $v_{head} = (42.3 + 63.5j)$Å^3. Note that the -$CH_2$ group adjacent to the poly(ethylene oxide) head has been included as part of the head.[16]

Figure 5-4 shows predicted CMC's at 20°C corresponding to aqueous solutions of C_iE_j surfactants as a function of the number of ethylene oxide (EO) groups, j, for i = 10 (solid line), i = 12 (dashed line), and i = 16 (dotted line). The circles, diamonds, and stars denote experimental values for $C_{10}E_j$, $C_{12}E_j$, and $C_{16}E_j$, respectively.[16, 90, 91] Note that the theory consistently captures the trend of increasing CMC with increasing j.

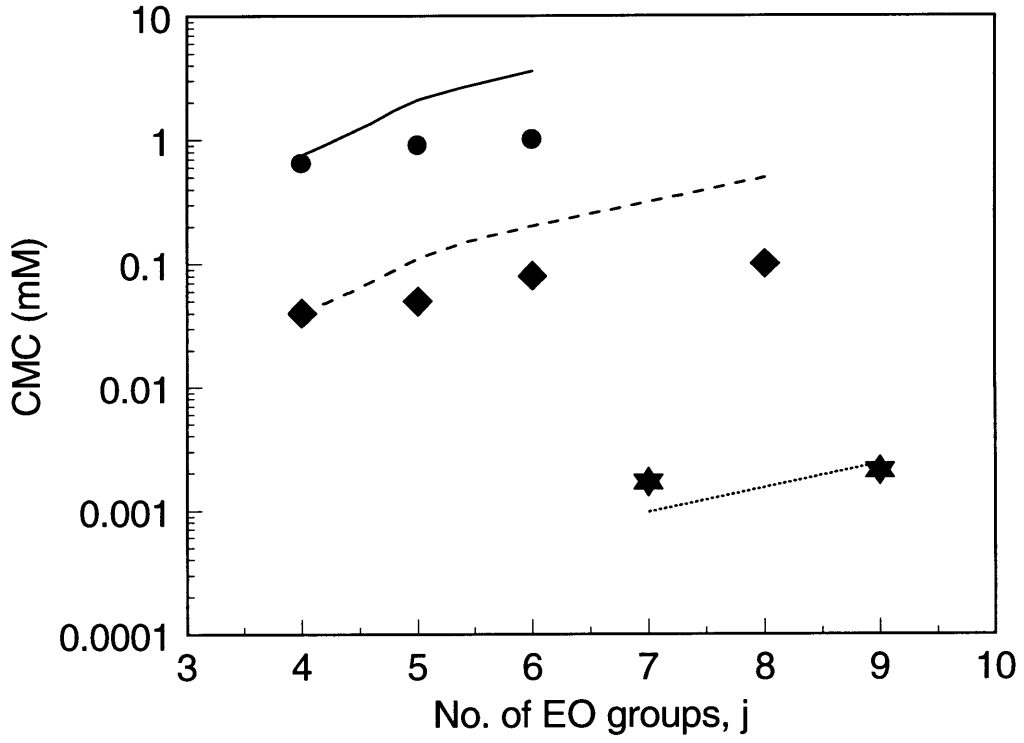

Figure 5-4: Predicted CMC as a function of the number of ethylene oxide (EO) groups, j, for aqueous solutions of $C_{10}E_j$ (—), $C_{12}E_j$ (- - -), and $C_{16}E_j$ ($\cdots$) at 20°C. Experimental values are denoted by circles for $C_{10}E_j$, diamonds for $C_{12}E_j$, and stars for $C_{16}E_j$.

As discussed in Section 5.4, the relative variance of the micellar size distribution, Var, constitutes a quantitative measure of polydispersity. In particular, elongated, polydisperse cylindrical micelles are characterized by $Var = 0.5$, whereas small, monodisperse spherical micelles are characterized by $Var = 0$. Figure 5-5 illustrates the predicted temperature variation of the relative variance of the micellar size distribution for $C_{12}E_j$ surfactants in aqueous solutions, where $j = 5$, 6, 7, and 8. In particular, for $j = 6$, 7, and 8, the narrow temperature range over which the relative variance changes rapidly from 0 to 0.5 corresponds to a sphere-to-cylinder micellar shape transition. The experimentally determined shape transition temperatures (indicated by the various arrows in Figure 5-5) are 16°C,[95] 34°C,[14] and 50°C[96] for $C_{12}E_6$, $C_{12}E_7$, and $C_{12}E_8$, respectively. As can be seen, the theory is capable of predicting the micellar shape transition behavior quite accurately.

The critical behavior of several aqueous solutions of C_iE_j surfactants was predicted by solving Eqs. (5.46) and (5.47). As discussed in Section 5.6, the quantites c_1 and c depend on temperature through $g_{mic}(T)$. Consequently, in order to make these predictions, experimental values of the critical temperatures, T_c, served as inputs to the theory. Then, Eq. (5.47) was used to solve for the critical surfactant concentration. Figure 5-6 illustrates the predictions of the critical surfactant concentration for several C_iE_j surfactants. The experimental critical temperature values are 21°C,[15] 44°C,[15] and 58°C[97] for $C_{10}E_4$, $C_{10}E_5$, and $C_{10}E_6$, respectively, and 3.5°C,[35, 36] 25°C,[14] 50°C,[14] 62°C,[14] and 77°C[12, 113] for $C_{12}E_4$, $C_{12}E_5$, $C_{12}E_6$, $C_{12}E_7$, and $C_{12}E_8$, respectively. The theoretical predictions are given by the left-hatched bars, and the experimental values are given by the white bars.[14, 15, 97, 12, 113, 98] As can be seen, the theory yields accurate predictions for the critical behavior of C_iE_j surfactants. It should also be noted that the predicted coexistence curves corresponding to the aqueous C_iE_j micellar solutions examined (not shown) were relatively flat, in accordance with experimental observations.[14, 12, 113]

In order to gain a quantitative understanding of the mean-field attraction parameter, $C(T)$, experimental values[13] for $c_s^A(T)$ and $c_s^B(T)$ were used in Eq. (5.52) to predict $C(T)$ as a function of T ($> T_c$). The predictions close to the critical

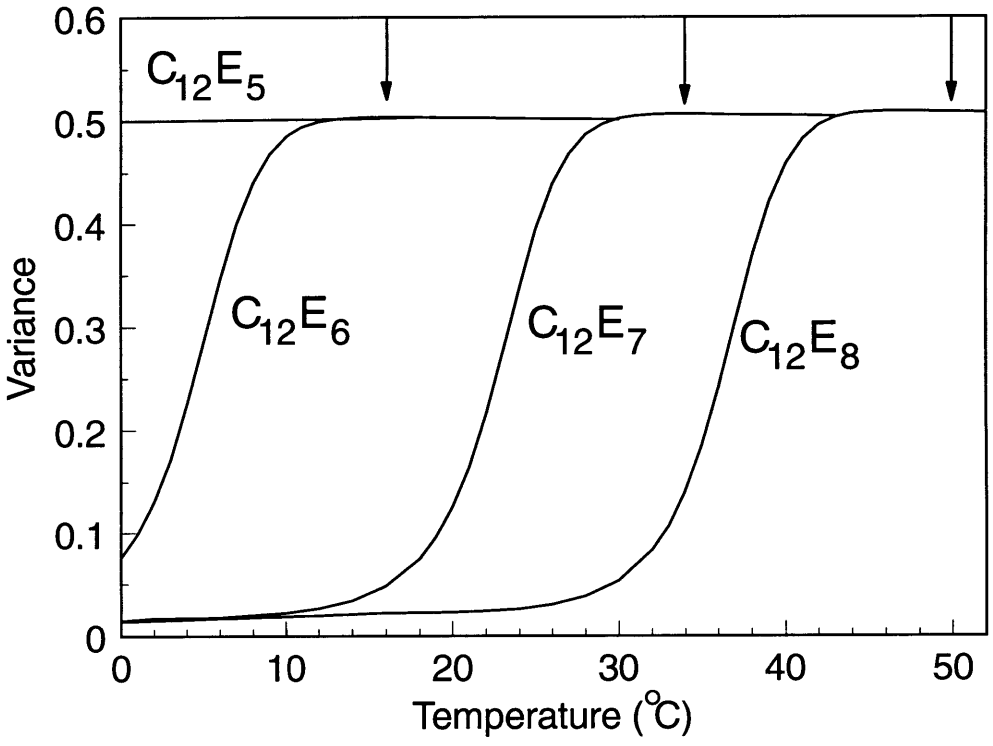

Figure 5-5: Predicted relative variance of the micellar size distribution of $C_{12}E_j$ (j = 5, 6, 7, and 8) micelles in aqueous solution as a function of temperature (solid lines). The arrows denote the experimentally determined shape transition temperatures for j = 6, 7, and 8.

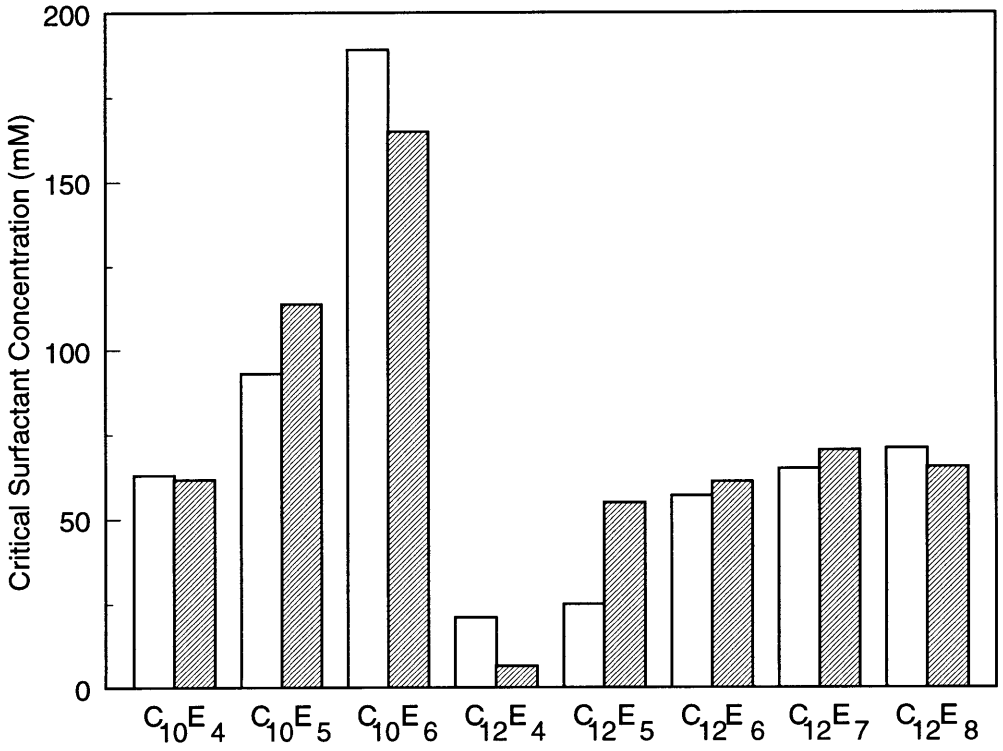

Figure 5-6: Predicted critical surfactant concentration for aqueous solutions of various C_iE_j surfactants. The left-hatched bars denote theoretical predictions, and the white bars denote experimental values.

point ($T - T_c < 2°C$) indicated a linear dependence on temperature (specifically, $C(T)/k_B = 0.45T - 141$, in units of °K). This expression for $C(T)$ was assumed to be applicable for $T < T_c$ as well, and was utilized in Eq. (5.55) to predict the osmotic compressibility along the critical isochore, for which the surfactant concentration is equal to the critical concentration ($c_c = 57$mM,[13]) for temperatures in the range $15°C < T < T_c$. Predictions of the osmotic compressibility are shown in Figure 5-7 (solid line) and compared to experimental data from Ref. [113] (stars) and from Ref. [13] (diamonds). The expected divergence of the osmotic compressibility as the temperature approaches T_c is clearly observed. The predictions follow the experimental data closely, indicating that the linear dependence on temperature found for $C(T)$ at $T > T_c$ is a reasonable approximation, even when extrapolated to temperatures which are less than T_c. In addition, because the osmotic compressibility and the coexistence curve represent two independent characteristics of the micellar solution, the agreement of the osmotic compressibility predictions with experiments can be interpreted as an independent validation of the present theory.

5.8 Conclusions

In summary, a statistical-thermodynamic framework to model nonionic micellar solutions, based on the McMillan-Mayer theory of multicomponent solutions, has been developed. The advantage of this approach is that it clearly delineates the ideal and excess contributions to the solution Gibbs free energy, thus allowing, in principle, for successive improvements of the theory as equations of state of increasing complexity and accuracy are implemented. In addition, this statistical-thermodynamic framework allows for the quantitative analysis of the effect of intermicellar interactions on micellar solution characteristics, such as micelle formation, micellar size distribution, and micellar solution phase separation.

In the calculations presented in this chapter, intermicellar interactions were modeled in the context of a virial equation of state, truncated at quadratic order. In particular, attractive intermicellar interactions were modeled using a mean-field de-

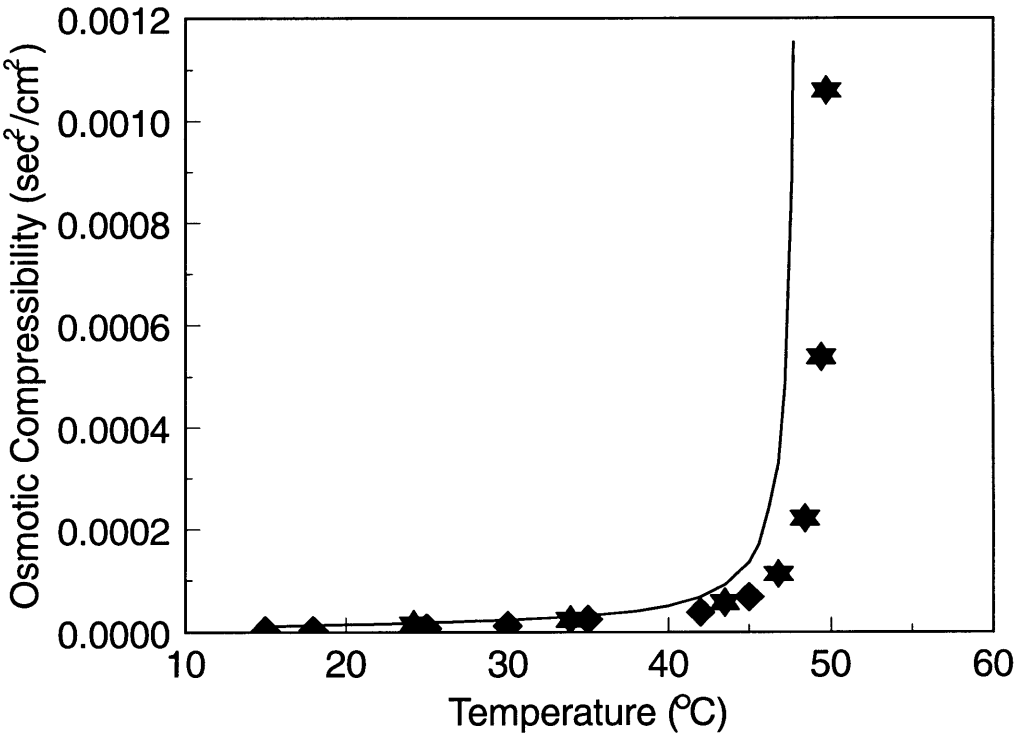

Figure 5-7: Predicted osmotic compressibility along the critical isochore, $c_s^c = 57\text{mM}$, as a function of temperature for an aqueous solution of $C_{12}E_6$ (—). Experimental values are denoted by stars and diamonds.

scription, while repulsive intermicellar interactions were described using a model for excluded-volume interactions between rigid spherocylinders. It was shown that the inclusion of excluded-volume intermicellar interactions has a profound effect on the micellar size distribution. Specifically, excluded-volume interactions encourage micellar growth, resulting in fewer, larger micelles. The theory was compared to an earlier phenomenological model (the ladder model[9]) which was developed for an ideal system devoid of excluded-volume intermicellar interactions. In particular, in the limit of extensive micellar growth, the expressions for the average micellar aggregation numbers and the relative variance of the micellar size distribution were found to have exactly the same mathematical form as those predicted by the ladder model. The only difference is that, in the presence of excluded-volume interactions, the growth parameter, K, depends on surfactant concentration and more readily promotes micellar growth. It is interesting that a micellar solution model based on an entirely different thermodynamic framework leads to the same limiting behavior.

In addition, several quantitative predictions of micellar solution characteristics were made and found to compare favorably with experimental data. These include (i) the CMC, (ii) the variance of the micellar size distribution, (iii) the critical surfactant concentration for phase separation, and (iv) the osmotic compressibility for aqueous solutions of alkyl poly(ethylene oxide) nonionic surfactants. In view of this, for the dilute micellar solutions examined in this chapter, the model for intermicellar interactions presented here constitutes a reasonable approximation. However, if more concentrated micellar solutions are investigated, then alternative models of intermicellar interactions may need to be considered. As better descriptions of the interactions occuring between nonionic micelles are developed, they can be incorporated into the statistical-thermodynamic framework presented here.

Chapter 6

Application of the McMillan-Mayer Statistical-Thermodynamic Framework to Ionic Micellar Solutions

6.1 Introduction

In this chapter, the McMillan-Mayer statistical-thermodynamic framework described in Chapter 4 will be applied to an ionic surfactant solution. One of the key results of the theory presented in Chapter 4 is an explicit expression for the micellar size distribution equation, given in Eq. (4.21) and repeated below for completeness

$$\Omega_w c_n = (\Omega_w c_1)^n \exp\left(-\beta(\mu_n^\circ - n\mu_1^\circ) - \beta(\mu_n^{EX} - n\mu_1^{EX})\right) \tag{6.1}$$

where $\beta = 1/k_B T$, c_n is the concentration of micelles of aggregation number n, c_1 is the concentration of monomers, μ_n° and μ_1° are the standard-state chemical potentials of micelles and monomers, respectively, and μ_n^{EX} and μ_1^{EX} are the EXCESS chemical

potentials of micelles and monomers, respectively. Equation (6.1) is general, that is, given an appropriate model for the various chemical potentials involved, Eq. (6.1) can be implemented for any micellar solution. In Chapter 5, a model was developed to implement Eq. (6.1) in the case of nonionic micellar solutions. In this model, the difference in standard-state chemical potentials, $(\mu_n^\circ - n\mu_1^\circ)/n$, is equivalent to g_{mic}, the free energy of micellization. The EXCESS chemical potentials included hard-core intermicellar interactions, described using a spherocylinder excluded-volume model, and attractive intermicellar interactions described using a mean-field approach. In this chapter, a model for the standard-state and EXCESS chemical potentials appropriate for *ionic* surfactants, including contributions due to hard-core and electrostatic intermicellar interactions, will be developed.

Recall that a molecular-thermodynamic theory for ionic micellar solutions was presented in Chapter 2. This theory resulted in accurate predictions of CMC's, but strongly underestimated micellar growth for ionic surfactants, particularly in the presence of added salt. The McMillan-Mayer statistical-mechanical approach presented here corrects some of the limitations of the molecular-thermodynamic theory presented in Chapter 2, yielding more accurate predictions of micellar growth in the presence of added salt. Specifically, in the molecular-thermodynamic theory presented in Chapter 2, only the ions immediately surrounding the micelle were assigned a finite volume (through the Stern layer). In the McMillan-Mayer approach, the excluded volume of *all* the charged solutes, including counterions, monomers, micelles, and salt ions, are incorporated in the model. More importantly, electrostatic intermicellar interactions, which were neglected in the molecular-thermodynamic theory presented in Chapter 2, are treated in the McMillan-Mayer approach. Note that the standard-state chosen in the McMillan-Mayer approach is different than that utilized in the molecular-thermodynamic theory presented in Chapter 2. In particular, in the McMillan-Mayer approach, the ion cloud is not included in the standard state. This will be discussed in more detail in Section 6.2.1.

The remainder of this chapter is organized as follows. Section 6.2 presents a general definition of the various constituents of the ionic surfactant solution, and

a description of a general thought process for implementing the McMillan-Mayer statistical-thermodynamic framework in the case of ionic surfactants. In addition, various methods for calculating the electrostatic contribution to the EXCESS chemical potentials will be discussed. In Section 6.3, the Debye-Hückel (DH) approximation will be utilized to evaluate the electrostatic contribution to the EXCESS chemical potentials. In Section 6.4, a modified Poisson-Boltzmann (PB) equation which accounts for the finite size of the ions will be derived, and then utilized to calculate the electrostatic contribution to the EXCESS chemical potentials. Both the DH and the modified PB descriptions will be used to make qualitative predictions to assess the effect of electrostatic intermicellar interactions on the micellar size distribution. In addition, some quantitative CMC predictions will be made and compared with experimental CMC values. Finally, in Section 6.5, the key results of the chapter will be summarized.

6.2 General Description of an Ionic Surfactant Solution

6.2.1 Definition of System

The ionic surfactant solution consists of three or four types of charged solutes: (i) surfactant monomers, (ii) surfactant micelles, (iii) counterions, and (iv) coions, if salt is added. Note that counterions are those ions whose charge is opposite to that of the surfactant ions, while coions are those ions whose charge is equal to that of the surfactant ions. For example, in a solution containing sodium dodecyl sulfate (SDS) and NaCl, sodium (Na^+) is the counterion and chlorine ($Cl-$) is the coion. The notation used in this chapter to describe the various charged solutes is summarized below in Table 6.1. Note that for spherocylindrical micelles, the radius of charge and the hard-core radius refer to the cross-sectional radius of the cylindrical body.

The following reasonable assumptions have been made to simplify the calculations:

- The surfactant molecules in the micelles are assumed to be fully-extended. In

Table 6.1: Summary of the notation used in this chapter to describe the various charged solutes, where c_n is the concentration of n-mers, c_1 is the concentration of monomers, c_c is the concentration of counterions, c_{co} is the concentration of coions, c_s is the total surfactant concentration, and c_{salt} is the concentration of added salt. R_{ch} is the micelle radius of charge, r_h is the monomer radius of charge, R is the micelle hard-core radius, R_1 is the monomer hard-core radius, r_i is the radius of charge and the hard-core radius of an ion, Ω_s is the volume of the surfactant molecule, Ω_i is the volume of an ion, and z is the valence of the surfactant molecule.

Ionic Species	Concentration	Valence	Radius of Charge	Hard-Core Radius	Hard-Core Volume
micelle (n-mer)	c_n	nz	R_{ch}	R	$n\Omega_s$
monomer	c_1	z	r_h	R_1	Ω_s
counterion	$c_c = c_s + c_{salt}$	$-z$	r_i	r_i	Ω_i
coion	$c_{co} = c_{salt}$	z	r_i	r_i	Ω_i

other words, it is assumed that $l_c^* = l_{max}$, which is the natural conformation for most ionic surfactants within a micelle, except at very high salt concentrations. Indeed, this conformation reduces repulsive electrostatic head/head interactions occurring at the micellar interface. The reasons for making this assumption are further discussed in Section 6.2.3.

- In treating excluded-volume interactions, the surfactant monomers are treated as effective spheres of radius R_1. Note that the hard-core monomer volume includes the volume of the *entire* surfactant molecule, including the tail ($\Omega_s = 4\pi R_1^3/3$), whereas the radius of charge is based *only* on the charged monomer head ($r_h = [a_h/\pi]^{1/2}$), where a_h is the cross-sectional area of the head. The reason for this minor distinction is that the charge remains on the surfactant head, and therefore, r_h is the relevant dimension for the electrostatic calculations. However, the tail contributes to the excluded volume, and therefore, for the excluded-volume calculations, R_1 is the relevant dimension. Note that r_h is typically 2-4 Å, while R_1 is typically 5-8Å. It should be noted that the predictions of micelle size can be sensitive to the value of R_1, and therefore, the distinction between R_1 and r_h can be important.

- The counterions and coions are assumed to be spheres having the same radius, r_i, in order to simplify the calculations. This is a reasonable approximation because the micelles are much larger than both the counterions and the coions, and therefore, are expected to dominate the excluded-volume interactions.

- Both the salt and the ionic surfactant are assumed to be symmetric electrolytes with the same valence. That is, if the surfactant is monovalent (as is the case for most ionic surfactants), the salt must also be monovalent. This assumption is made for practical convenience, since most commonly encountered ionic surfactants and salts are monovalent. Theoretically, the model presented in this chapter can be extended to treat asymmetric salts, but then, the equations derived in Sections 6.3.1 and 6.4.2 need to be modified accordingly.

The standard state of the surfactant solution is chosen to be a state of infinite dilution in water. That is, μ_n° and μ_1° must be evaluated at infinite dilution, defined here as a bare charged micelle (or monomer) in water *with no surrounding ion cloud.* The difference in standard-state chemical potentials, $(\mu_n^\circ - n\mu_1^\circ)/n$, represents the free energy of micellization at infinite dilution, in the absence of counterions or coions. As mentioned earlier, this standard state is different from the standard state defined in the context of the molecular-thermodynamic theory presented in Chapter 2, which included the ion cloud. The new standard state is chosen because *all* interparticle interactions, including interactions with the ion cloud, will be included as part of the EXCESS chemical potentials. Accordingly, the EXCESS chemical potential of an n-mer (where $n = 1$ corresponds to a monomer) will now include interactions between (i) n-mer/m-mer, (ii) n-mer/monomer, (iii) n-mer/counterion, and (iv) n-mer/coion. Note that this modification of the standard state will require a different model for g_{elec}, which will be discussed further in Section 6.2.2.

The intermicellar interactions considered in this chapter include both electrostatic and hard-core (excluded-volume) repulsive interactions. For ionic systems, it is also possible that attractive, van der Waal's-type intermicellar interactions may operate at very high salt concentrations. However, for the solution conditions considered in

this chapter, the attractive intermicellar interactions should be negligible.

In order to keep track of the various ionic species and their contributions to the standard-state and EXCESS chemical potentials, it is useful to construct a thought process which represents the formation of an n-mer from n monomers in an ionic surfactant solution. This thought process breaks down the micellization process into several steps, each step associated with one of the chemical potential quantities that needs to be evaluated. A detailed description of the thought process is presented in the next section.

6.2.2 Thought Process

The formation of a charged n-mer from n charged monomers is broken down into three steps (refer to Figure 6-1): (i) transferring n charged monomers from the surfactant solution to infinite dilution, (ii) assembling the n charged monomers into a charged n-mer at infinite dilution, and (iii) transferring the charged n-mer from infinite dilution back into solution.

In the first step, the n charged monomers are transferred to infinite dilution in water, a process which is exactly opposite to that associated with calculating the EXCESS chemical potential of these n monomers, $-n\mu_1^{EX}$. In the second step, at infinite dilution, the charged n-mer is assembled from the n charged monomers, a process which is equivalent to that associated with calculating the difference in their standard-state chemical potentials, $(\mu_n^\circ - n\mu_1^\circ)$. Finally, in the third step, the charged n-mer is transferred from infinite dilution back into solution, a process which is equivalent to that associated with calculating the EXCESS chemical potential of the n-mer, μ_n^{EX}. Breaking the micellization process into these three steps allows us to calculate each of the associated chemical potential quantities separately.

The total change in chemical potential from the initial state (n charged monomers in solution) to the final state (charged n-mer in solution) can be viewed as the reversible work (equivalent to a free-energy change) involved in forming the charged n-mer from the n charged monomers in solution. This work, W_{1-3}, is equivalent to the difference in the standard-state and EXCESS chemical potentials associated with

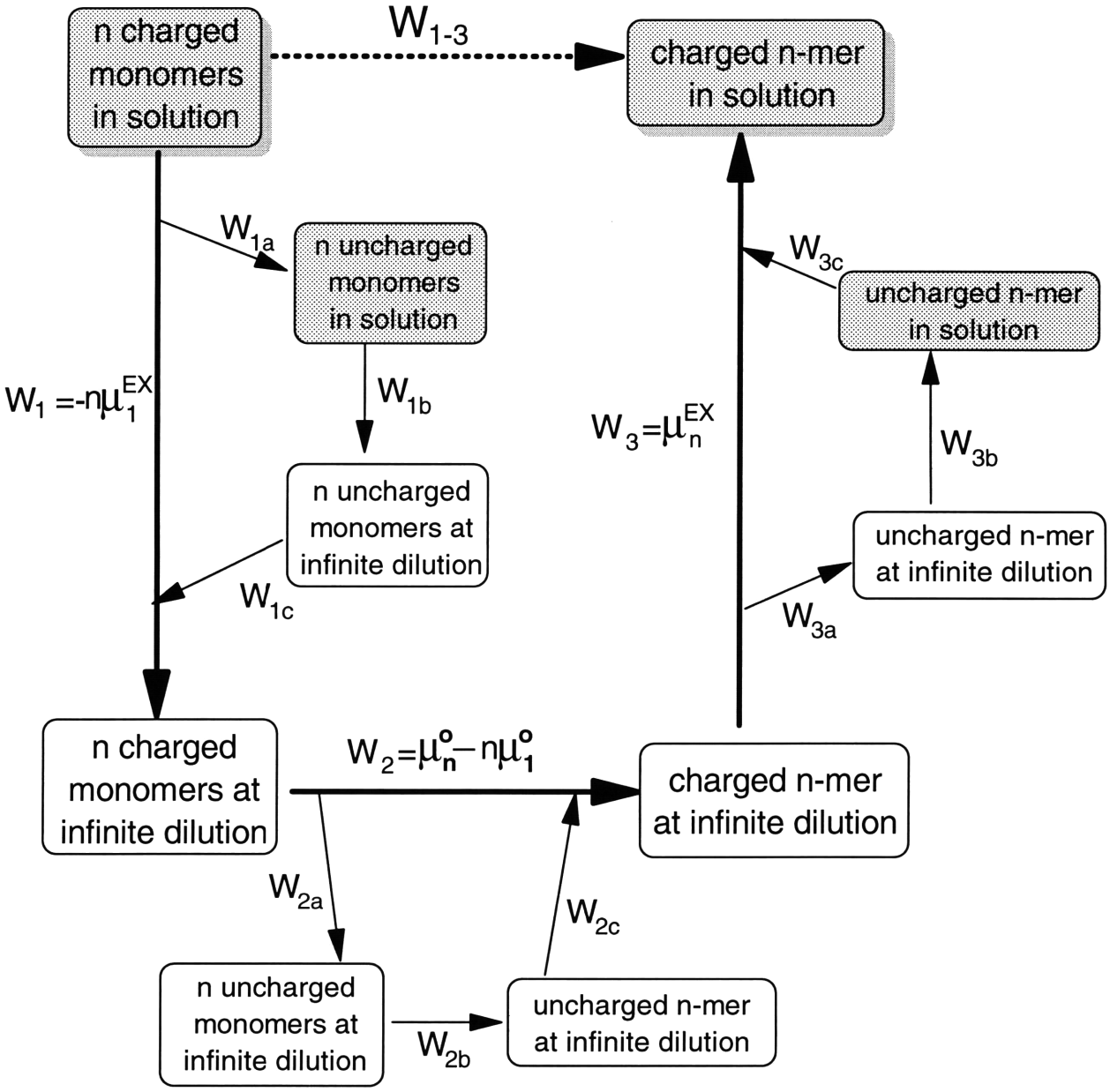

Figure 6-1: Schematic representation of the thought process to visualize the formation of a charged n-mer from n charged monomers in solution.

the n-mer and the n monomers. Specifically,

$$W_{1-3} = \mu_n^\circ - n\mu_1^\circ + \mu_n^{EX} - n\mu_1^{EX} \tag{6.2}$$

Note that $-\beta W_{1-3}$ is the quantity appearing in the exponent of the micellar size distribution expression given in Eq. (6.1). Next, the calculation of each step is described in detail.

Step 1: Transferring n charged monomers to infinite dilution

In the first step, n charged monomers are transferred from an aqueous micellar solution to infinite dilution in water, defined as the standard state. In other words, the interactions between the monomers and all other solutes, including micelles, other monomers, counterions, and coions, are "turned off". This step is equivalent to the negative of the EXCESS chemical potential of the n monomers, $-n\mu_1^{EX}$, including hard-core (HC) and electrostatic ($elec$) interactions. In other words,

$$W_1 = -n\mu_1^{EX} = -n\mu_1^{EX,HC} - n\mu_1^{EX,elec} \tag{6.3}$$

In order to evaluate these quantities separately, this step is further broken down into three substeps. The model for excluded-volume interactions treats the micelles and monomers as uncharged bodies. Therefore, in order to evaluate $\mu_1^{EX,HC}$, the monomers are first discharged in solution. In other words, the electrostatic interactions between the monomers and all other charged species, including micelles, other monomers, counterions, and coions, are "turned off". The work associated with discharging the n monomers is W_{1a}, and its calculation will be discussed in Section 6.2.3.

In the second substep, the uncharged monomers are transferred from solution to infinite dilution. Because the monomers have already been discharged, only steric interactions are accounted for in this substep. In other words, the excluded-volume interactions between the monomers and the micelles, other monomers, counterions, and coions are "turned off". Hence, the work involved in this substep is the negative

of the hard-core EXCESS chemical potential. That is,

$$W_{1b} = -n\mu_1^{EX,HC} \tag{6.4}$$

The hard-core EXCESS chemical potential was already evaluated in Chapter 5 for the case of nonionic micelles. The same model will be utilized here, along with an additional contribution arising from the excluded volume of the counterions and the coions. In this model, the micelles are treated as rigid spherocylinders consisting of a cylindrical body of variable length capped with two hemispheres of total aggregation number n_0. Thus, the minimum-sized micelle is a sphere with an aggregation number equal to n_0. As discussed in Section 6.2.1, the monomers are treated as effective spheres with a radius $R_1 = (3\Omega_s/4\pi)^{1/3}$, where Ω_s is the volume of a surfactant molecule. This model results in the following expression for $\mu_1^{EX,HC}$ (see Eq. (F.15) in Appendix F.2)

$$\mu_1^{EX,HC} = \frac{4\pi}{3}(R_1 + r_i)^3 c_i + 8\Omega_s c_1 + \Omega_s\gamma^2(c_s - c_1) + \Omega_s\gamma^2 n_0^{2/3}(c - c_1) \tag{6.5}$$

where c is the zeroth moment of the micellar size distribution, c_i is the total concentration of counterions and coions ($c_i = c_c + c_{co} = c_s + 2c_{salt}$), and $\gamma = (1 + 1/n_0^{1/3})$. Note that Eq. (6.5) is very similar to Eq. (5.15), with an additional contribution (the first term) due to the excluded volume of the counterions and the coions.

In the third substep, the n uncharged monomers are recharged at infinite dilution. Because there are no other ions at infinite dilution, the work involved in this substep is simply the Born solvation energy of the n monomers.[57] That is,

$$W_{1c} = n\frac{(ze)^2}{2\epsilon r_h} \tag{6.6}$$

where ϵ is the dielectric constant of the solvent, e is the electronic charge, and r_h is the radius of the monomer head. Recall that r_h is the radius of the monomer head only, while the radius used for the excluded-volume calculations, R_1, is the radius of

the entire monomer.

Combining the contribution associated with discharging the n monomers in solution with that associated with charging the n monomers at infinite dilution results in the negative of the electrostatic EXCESS chemical potential of the monomers. That is,

$$W_{1a} + W_{1c} = -n\mu_1^{EX,elec} \tag{6.7}$$

In other words, discharging the n monomers in solution and then recharging them at infinite dilution is the same as "turning-off" the electrostatic interactions between the n monomers and all the other charged solutes. The work involved in the entire first step is the negative of the total EXCESS chemical potential of the n monomers, that is,

$$\begin{aligned} W_1 &= W_{1a} + W_{1b} + W_{1c} \\ &= -n(\mu_1^{EX,HC} + \mu_1^{EX,elec}) = -n\mu_1^{EX} \end{aligned} \tag{6.8}$$

Step 2: Formation of the micelle (n-mer) at infinite dilution

In this step, the n charged monomers aggregate to form a charged n-mer at infinite dilution. This process represents the difference in standard-state chemical potentials, $\mu_n^\circ - n\mu_1^\circ$, which is equivalent to ng_{mic}, the free energy of micellization at infinite dilution, that is,

$$W_2 = \mu_n^\circ - n\mu_1^\circ = ng_{mic} \tag{6.9}$$

Recall that, as discussed in Section 6.2.1, the standard state is defined differently than the standard state defined in the context of the molecular-thermodynamic theory presented in Chapter 2, and therefore, the calculation of g_{mic} must be modified accordingly. Specifically, there is no ion cloud in the current model, and hence, g_{mic} is the free energy associated with forming the bare micelle at infinite dilution. Because there is no ion cloud, the electrostatic contribution, g_{elec}, will be dealt with as a separate contribution. The other contributions to g_{mic} are the same as those described in Section 2.3. This distinction is illustrated in the thought process by dividing the

calculation of $W_2 = \mu_n^\circ - n\mu_1^\circ$ into three substeps.

In the first substep, the n charged monomers are discharged at infinite dilution in order to evaluate the electrostatic contribution to the free energy of micellization separately. This discharging is simply the reverse work of charging the n monomers in Step 1c, and is given by

$$W_{2a} = -n\frac{(ze)^2}{2\epsilon r_h} \tag{6.10}$$

It may seem redundant to compute both W_{2a} and W_{1c}, since they cancel each other, but it is important to include both of these substeps in order to determine separate expressions for $\mu_1^{EX,elec}$ and g_{elec}.

In the second substep, the n uncharged monomers are assembled to form an uncharged n-mer at infinite dilution. The work in this substep includes all the contributions to the free energy of micellization, except for the electrostatic contribution, denoted as g_{mic}°. Specifically,

$$W_{2b} = ng_{mic}^\circ = n(g_{trans} + g_{int} + g_{pack} + g_{ster}) \tag{6.11}$$

The calculation of these contributions was described in detail in Section 2.3. g_{mic}° has been calculated for three regular micellar shapes: spheres, infinite cylinders, and infinite bilayers. Typically, bilayers are not formed by ionic surfactants at the solution conditions examined here. For the other two shapes, the optimal shape is determined by comparing the g_{mic}° values corresponding to a sphere, g_{sph}°, and an infinite cylinder, g_{cyl}°. If g_{sph}° is lower, then the resulting micelles are assumed to be monodisperse spheres with an aggregation number $n_0 = 4\pi l_c^3/3v_t$ (with $l_c = l_{max}$, as explained in Section 6.2.1). If g_{cyl}° is lower, then the resulting micelles exhibit one-dimensional growth and are modeled as spherocylinders. In this case, g_{mic}° is estimated by linearly interpolating between g_{sph}° and g_{cyl}°, as follows

$$g_{mic}^\circ = \frac{n_0}{n}g_{sph}^\circ + \frac{n - n_0}{n}g_{cyl}^\circ \tag{6.12}$$

In the third substep, the uncharged n-mer is charged at infinite dilution. The work

involved in this substep is the Born Solvation Energy of the micelle, $W_{2c} = BSE$. Although it is difficult to model the Born Solvation Energy of a spherocylinder, it is not necessary to evaluate it explicitly because it will cancel with a similar contribution in Step 3.

The sum of the contributions in substeps 2a and 2c is equal to g_{elec}, the electrostatic contribution to the free energy of micellization at infinite dilution, namely,

$$W_{2a} + W_{2c} = ng_{elec} = BSE - n\frac{(ze)^2}{2\epsilon r_h} \tag{6.13}$$

As discussed above, because there is no ion cloud in the current model, this g_{elec} is different than the g_{elec} defined in the context of the molecular-thermodynamic theory described in Chapter 2.

The free energy of micellization, g_{mic}, is obtained by summing up all the work contributions involved in Step 2, that is,

$$W_2 = \mu_n^\circ - n\mu_1^\circ = ng_{mic} = ng_{mic}^\circ + BSE - n\frac{(ze)^2}{2\epsilon r_h} \tag{6.14}$$

Step 3. Transferring the micelle (n-mer) to solution

In the third and last step, the charged n-mer is transferred from infinite dilution to the solution containing other micelles, monomers, counterions, and coions. In other words, the interactions between the n-mer and all the other solutes are "turned on", which is equivalent to calculating the micelle (n-mer) EXCESS chemical potential, including hard-core and electrostatic intermicellar interactions. That is,

$$W_3 = \mu_n^{EX} = \mu_n^{EX,HC} + \mu_n^{EX,elec} \tag{6.15}$$

In order to evaluate these quantities separately, this step is further broken down into three substeps. In the first substep, the charged n-mer is discharged at infinite dilution. The work involved in this substep is the negative of the Born Solvation Energy of the n-mer, that is,

$$W_{3a} = -BSE \tag{6.16}$$

As noted above, this work contribution will exactly cancel W_{2c}. As with the case for the monomers, it is important conceptually to consider both of these substeps in order to determine separate expressions for g_{elec} and μ_n^{EX}.

In the second substep, the uncharged n-mer is transferred from infinite dilution to solution. Because the n-mer has been discharged, only excluded-volume interactions are accounted for in this substep. Accordingly, the work involved in this substep is equal to the EXCESS hard-core chemical potential of the n-mer, that is,

$$W_{3b} = \mu_n^{EX,HC} \tag{6.17}$$

As with the case for the monomers, the excluded-volume model that was developed for nonionic surfactants will be used here, with additional contributions resulting from the excluded volume of the counterions and the coions. Treating the ions as spheres of radius r_i results in the following expression for $\mu_n^{EX,HC}$ (compare with Eq. (F.19) in Appendix F.2)

$$\begin{aligned}\mu_n^{EX,HC} &= (R+r_i)^2\left(\frac{4\pi r_i}{3}+\frac{n\Omega_s}{R^2}\right)c_i + +\Omega_s\gamma^2 n_0^{2/3}c_1 + \frac{2\pi d^3}{9}(c-c_1) + \frac{8\Omega_s}{3}(c_s-c_1) \\ &\quad +n\left(\Omega_s\gamma^2 c_1 + \frac{8\Omega_s}{3}(c-c_1) + \frac{8\Omega_s^2}{\pi d^3}(c_s-c_1)\right)\end{aligned} \tag{6.18}$$

where R is the hard-core radius of the micelle (n-mer), and $d = 2R$ is the hard-core diameter of the n-mer. Note that Eq. (6.18) is very similar to Eq. (5.17), with an additional contribution (the first term) due to the excluded volume of the counterions and the coions.

In the third substep, the uncharged n-mer is charged in solution. In other words, the electrostatic interactions between the n-mer and all the other charged solutes, including other micelles, monomers, counterions, and coions are "turned on". This substep combined with substep 3a results in the electrostatic EXCESS chemical potential of the n-mers, that is,

$$W_{3a} + W_{3c} = \mu_n^{EX,elec} \tag{6.19}$$

The work involved in the entire third step is the total EXCESS chemical potential of the n-mers, that is,

$$\begin{aligned} W_3 &= W_{3a} + W_{3b} + W_{3c} \\ &= \mu_n^{EX,HC} + \mu_n^{EX,elec} = \mu_n^{EX} \end{aligned} \tag{6.20}$$

Finally, each of the three steps are combined to obtain the following expression for W_{1-3}

$$\begin{aligned} W_{1-3} &= W_1 + W_2 + W_3 = \mu_n^\circ - n\mu_1^\circ + \mu_n^{EX} - n\mu_1^{EX} \\ &= ng_{mic} + (\mu_n^{EX,elec} - n\mu_1^{EX,elec}) + (\mu_n^{EX,HC} - n\mu_1^{EX,HC}) \end{aligned} \tag{6.21}$$

6.2.3 Electrostatic EXCESS Chemical Potentials

Up to this point, the thought process described in Section 6.2.2 is completely general. Any model for the electrostatic EXCESS chemical potentials can be used within this framework. There are several approaches to calculating $\mu_n^{EX,elec}$ and $\mu_1^{EX,elec}$. For example, one could use a liquid-state theory approach where the charged species exhibit a Coulombic interaction. The EXCESS chemical potential is then obtained by summing over all pairwise interactions. This approach is described in Appendix G.1. Interestingly, it can be shown that this approach leads to the same expressions for $\mu_n^{EX,elec}$ and $\mu_1^{EX,elec}$ as those resulting from the charging approach that will be utilized here (see Appendix G.1 for details). Alternatively, one could use a virial equation of state, similar to that used for the hard-core interactions, as discussed in Section 5.3. This approach is summarized in Appendix G.2, along with an explanation of why it will not be utilized here.

As indicated above, a charging process will be utilized to calculate $\mu_n^{EX,elec}$ and $\mu_1^{EX,elec}$. In this process, the central micelle (or monomer) is gradually brought from zero to full charge while interacting with a diffuse, fully-charged ion cloud. The ion cloud consists of all the other charged species in solution, including counterions, coions, monomers, *and micelles.* Including the micelle in the ion cloud is an ap-

proximate way to account for micelle/micelle electrostatic interactions. That is, the central micelle interacts with each component of the ion cloud, which also includes other micelles. For the micelles in the ion cloud, the distribution of the charges over the micellar surface is neglected. In other words, the micelles in the ion cloud are assumed to have a charge of nze localized at their center, irrespectively of their shape. This is a fairly good approximation for spherical micelles at dilute concentrations. However, this approach is less accurate for elongated micelles because the orientations of the micelles in the ion cloud relative to the central micelle are neglected. In either case, including the micelles in the ion cloud will at least account for the additional screening provided by these charged solutes. In general, the work associated charging an n-mer (micelle) is given by

$$W_{charge}^{mic} = \int_0^{nze} \psi_{mic}(R_{ch})\, dq \tag{6.22}$$

where $\psi_{mic}(R_{ch})$ is the electrostatic potential at the micelle surface of charge, and q is the micelle charge as it is raised from zero to full charge (nze). Similarly, the work associated with charging a monomer is given by

$$W_{charge}^{mon} = \int_0^{ze} \psi_{mon}(r_h)\, dq \tag{6.23}$$

where $\psi_{mon}(r_h)$ is the electrostatic potential at the monomer surface of charge, and q is the monomer charge as it is raised from zero to full charge (ze).

This charging process will be used to calculate W_{1a} in substep 1a, where the n monomers are discharged in solution, and to calculate W_{3c} in substep 3c, where the n-mer (micelle) is charged in solution. Specifically,

$$W_{1a} = -nW_{charge}^{mon} = -n\int_0^{ze} \psi_{mon}(r_h)\, dq \tag{6.24}$$

$$W_{3c} = W_{charge}^{mic} = \int_0^{nze} \psi_{mic}(R_{ch})\, dq \tag{6.25}$$

Note that W_{1a} in Eq. (6.24) is the negative of the integral because the monomers are discharged.

The electrostatic EXCESS chemical potential of the n-mers is obtained by using Eqs. (6.16) and (6.25) in Eq. (6.19), as follows

$$\mu_n^{EX,elec} = -BSE + \int_0^{nze} \psi_{mic}(R_{ch})\, dq \tag{6.26}$$

Similarly, the electrostatic EXCESS chemical potential of the monomers is obtained by using Eqs. (6.6) and (6.24) in Eq. (6.7) (dividing by n), as follows

$$\mu_1^{EX,elec} = \frac{-(ze)^2}{2\epsilon r_h} + \int_0^{ze} \psi_{mon}(r_h)\, dq \tag{6.27}$$

Using Eq. (6.14) for g_{mic}, Eqs. (6.5) and (6.18) for $\mu_1^{EX,HC}$ and $\mu_n^{EX,HC}$, respectively, and Eqs. (6.27) and (6.26) for $\mu_1^{EX,elec}$ and $\mu_n^{EX,elec}$, respectively, in Eq. (6.21), the following expression is obtained for W_{1-3}

$$W_{1-3} = n g_{mic}^{\circ} + \int_0^{nze} \psi_{mic}(R_{ch})\, dq - n \int_0^{ze} \psi_{mon}(r_h)\, dq + (A_0 - nA_1) k_B T \tag{6.28}$$

where A_0 and A_1 are excluded-volume parameters, which, for spherocylindrical micelles, are given by (see Appendix F.2)

$$A_0^{cyl} = \frac{4\pi}{3} r_i (R + r_i)^2 c_i + \Omega_s \gamma^2 n_0^{2/3} c_1 + \frac{2\pi d^3}{9}(c - c_1) + \frac{8\Omega_s}{3}(c_s - c_1) \tag{6.29}$$

$$\begin{aligned} A_1^{cyl} = {} & \frac{4\pi}{3}\left[(R_1 + r_i)^3 - (R + r_i)^2 \frac{R}{n_0}\right] c_i + [8 - \gamma^2(2 + n_0^{2/3})]\Omega_s c_1 \\ & + \Omega_s \gamma^2 c_s + \Omega_s \gamma^2 n_0^{2/3} c - \frac{8\Omega_s}{3}(c - c_1) - \frac{8\Omega_s^2}{\pi d^3}(c_s - c_1) \end{aligned} \tag{6.30}$$

Note that these expressions are slightly different from the A_0^{cyl} and A_1^{cyl} expressions given in Eqs. (5.20) and (5.21) due to the additional excluded-volume effect of the counterions and coions. When $c_i = 0$, the original expressions for A_0^{cyl} and A_1^{cyl} are recovered (see Appendix F for details).

As discussed in Section 6.2.2, the minimum-sized micelle is a spherocylinder consisting only of the two endcaps, that is, a sphere with an aggregation number equal to n_0, where $n_0 = 4\pi l_c^3/(3v_t)$. In this case, A_0^{sph} and A_1^{sph} can be obtained directly

from Eqs. (6.29) and (6.30) by making use of the fact that $n = n_0 = \pi d^3/(6\Omega_s)$ and $n_0(c - c_1) = c_s - c_1$. Specifically, $A_0^{sph} = 4\pi r_i(R + r_i)^2 c_i/3 + \Omega_s \gamma^2 n_0^{2/3} c_1 + 4\Omega_s(c_s - c_1)$, and $A_1^{sph} = 4\pi[(R_1 + r_i)^3 - (R + r_i)^2 R/n_0]c_i/3 + [12 - \gamma^2(1 + \gamma)]\Omega_s c_1 + \Omega_s \gamma^3 c_s - 4\Omega_s c$. Note that these expressions are slightly different from the A_0^{sph} and A_1^{sph} expressions given in Chapter 5 due to the additional excluded-volume effect of the counterions and coions. When $c_i = 0$, the original expressions for A_0^{sph} and A_1^{sph} are recovered.

Equation (6.28) can be implemented in Eq. (6.1) to obtain the following expression for the micellar size distribution which is applicable to both spherical and spherocylindrical micelles

$$\Omega_w c_n = (\Omega_w c_1)^n \exp\left(-\beta n g^{\circ}_{mic} - \beta \int_0^{nze} \psi_{mic}(R_{ch})\, dq + \beta n \int_0^{ze} \psi_{mon}(r_h)\, dq - (A_0 - nA_1)\right) \tag{6.31}$$

As discussed previously in Section (2.2), it would be instructive to sum over all the possible l_c values for $c_n(l_c)$, rather than forcing all c_n to be at the same l_c^*. However, this process is computationally very tedious, particularly when intermicellar interactions are included. In order to simplify the calculations, it is assumed that all $l_c = l_c^*$. As discussed in Section 6.2.1, it was assumed that $l_c^* = l_{max}$. The reason behind this assumption can be understood by examining Eq. (6.31). To determine the optimal l_c value, one should maximize $c_n(l_c)$, which is equivalent to maximizing the exponential term in Eq. (6.31). However, when intermicellar interactions are included, the exponential term, and hence, the optimal l_c^* value, depend on n. It was found that A_0 and A_1 have very little effect on the resulting l_c^* value. Therefore, in the case of nonionic surfactants presented in Chapter 5, l_c^* can be determined based on minimizing g_{mic} (that is, maximizing -g_{mic}). However, for ionic surfactants, the integral terms in Eq. (6.31) have a strong effect on l_c^*, and therefore, cannot be neglected. Hence, for the models presented in this chapter, it is assumed that $l_c^* = l_{max}$, in order to reduce computational complexity. As discussed earlier in Section 6.2.1, this is a reasonable approximation, because l_{max} is the most favorable l_c value for most ionic surfactants in a micelle in order to reduce the electrostatic

repulsions among the charged surfactant heads at the micellar interface.

The main remaining challenge then is to calculate the electrostatic potential at the micelle or monomer surfaces of charge. This can be accomplished by using the Poisson-Boltzmann (PB) equation. However, it is first simpler to utilize the analytical Debye-Hückel (DH) solution to the PB equation to calculate $\psi_{mic}(R_{ch})$ (or $\psi_{mon}(r_h)$). This is done in Section 6.3. Following that, in Section 6.4, a modified Boltzmann distribution is used to calculate $\psi_{mic}(R_{ch})$ (or $\psi_{mon}(r_h)$). An examination of the advantages and disadvantages of each approach will be undertaken in their respective sections.

6.3 Debye-Hückel Approximation

6.3.1 Debye-Hückel Solution

In order to evaluate the electrostatic potential at the micelle (or monomer) surface of charge, we begin with the Poisson-Boltzmann equation, given in Eq. (2.29) and repeated here for completeness[57, 24]

$$\nabla^2 \psi(r) = \frac{-4\pi e}{\epsilon} \sum_j c_j^\circ z_j \exp\left[\frac{-z_j e\psi(r)}{k_B T}\right] \tag{6.32}$$

where c_j° is the bulk concentration of ions of type j, and z_j is their valence. The Debye-Hückel model will be developed for both spherical and spherocylindrical micelles, the most likely micelle shapes for the solution conditions examined here. Because these shapes are axi-symmetric, the PB equation is written in terms of the radial scalar variable, r. Note that the summation in Eq. (6.32) is over all the charged solutes listed in Table 6.1.

Expanding the summation over all the charged solutes listed in Table 6.1, Eq. (6.32) becomes

$$\nabla^2 \psi = -\frac{4\pi e}{\epsilon}\left[(c_{salt} + c_s)(-z)\exp\left(\frac{ze\psi}{k_B T}\right) + c_{salt} z \exp\left(\frac{-ze\psi}{k_B T}\right)\right.$$

$$+c_1 z \exp\left(\frac{-ze\psi}{k_B T}\right) + \sum_{n=n_0}^{\infty} c_n nz \exp\left(\frac{-nze\psi}{k_B T}\right)\Bigg] \qquad (6.33)$$

where $n_0 = 4\pi l_{max}^3/3v_t$ is the aggregation number of the minimum-sized spherical micelle, and the summation is over all the spherocylindrical n-mers.

Because the ion cloud contains ions of different valences, that is, z and nz, solving the PB equation becomes more difficult than in the symmetric valence case, and the common analytical approximations discussed in Section 2.3.2 are no longer applicable. In order to obtain an analytical solution, Eq. (6.33) must be linearized, following the Debye-Hückel approach. In other words, it is assumed that the electrostatic potential, ψ, in Eq. (6.33) is small enough to enable an expansion of the exponential terms. This yields

$$\begin{aligned} \nabla^2 \psi &= -\frac{4\pi ez}{\epsilon}\Bigg[-(c_{salt} + c_s)\left(1 + \frac{ze\psi}{k_B T}\right) + c_{salt}\left(1 - \frac{ze\psi}{k_B T}\right) \\ &\quad + c_1\left(1 - \frac{ze\psi}{k_B T}\right) + \sum_{n=n_0}^{\infty} nc_n\left(1 - \frac{nze\psi}{k_B T}\right)\Bigg] \end{aligned} \qquad (6.34)$$

Recall that $c_s = c_1 + \sum_{n=n_0}^{\infty} nc_n$, and $M_2 = c_1 + \sum_{n=n_0}^{\infty} n^2 c_n$, where M_2 is the second moment of the micellar size distribution, which allows for the following simplification of Eq. (6.34)

$$\nabla^2 \psi = \frac{8\pi e^2 z^2}{\epsilon k_B T}\left[c_{salt} + \frac{(c_s + M_2)}{2}\right]\psi \qquad (6.35)$$

Equation (6.35) can be rewritten as

$$\nabla^2 \psi = \kappa^2 \psi \qquad (6.36)$$

where κ is the inverse Debye screening length, given by

$$\kappa^2 = \frac{8\pi e^2 I}{\epsilon k_B T} \qquad (6.37)$$

and I is the ionic strength of the micellar solution, given by

$$I = \frac{z^2}{2}(2c_{salt} + c_s + M_2) \tag{6.38}$$

The expression for I in Eq. (6.38) can be understood physically as follows. The ionic strength is the sum of the concentration of all the ions in the solution multiplied by the square of their valence. c_{salt} is multiplied by 2 to account for both the cations and the anions of the added salt. The second moment corresponds to the square of the aggregation number, representing the valence of the micelles, multiplied by the concentration of the micelles. Hence, in Eq. (6.38), c_s corresponds to the contribution of the surfactant counterions, and M_2 corresponds to the contribution of the micelles and the monomers.

The Debye-Hückel equation, Eq. (6.36), can be solved for both spherical and cylindrical geometries, subject to the following boundary conditions.[57, 22] In the bulk solution (as $r \to \infty$), due to electroneutrality,[57, 116]

$$\psi(r) = 0 \tag{6.39}$$

At the micelle radius of charge ($r = R_{ch}$), one has[57, 116]

$$\frac{\partial \psi}{\partial r} = \frac{-4\pi e z}{\epsilon a_{ch}} \tag{6.40}$$

where a_{ch} is the surface area per surfactant head at the surface of charge, and is given by

$$a_{ch} = \frac{S v_t}{l_c}\left(\frac{R_{ch}}{l_c}\right)^{S-1} \tag{6.41}$$

where l_c is the length of the surfactant tail (assumed to be equal to l_{max}), v_t is the volume of the surfactant tail, and S is the shape factor ($S = 2$ for an infinite cylinder, and $S = 3$ for a sphere).

Integrating Eq. (6.36) twice, subject to the boundary conditions given in Eqs. (6.39) and (6.40), the electrostatic potential at the micelle radius of charge, R_{ch}, is obtained.

Specifically,

$$\psi_{mic}(R_{ch}) = \frac{4\pi e z R_{ch}}{\epsilon a_{ch}(1+\kappa R_{ch})} = \frac{q}{\epsilon R_{ch}(1+\kappa R_{ch})} \text{ , for spheres} \tag{6.42}$$

$$\psi_{mic}(R_{ch}) = \frac{4\pi e z}{\kappa a_{ch}\epsilon}\frac{K_0(\kappa R_{ch})}{K_1(\kappa R_{ch})} = \frac{2\lambda}{\kappa R_{ch}\epsilon}\frac{K_0(\kappa R_{ch})}{K_1(\kappa R_{ch})} \text{ , for infinite cylinders} \tag{6.43}$$

where q is the charge of the micelle ($q = nze$), λ is the charge per unit length of the cylindrical micelle, that is, $\lambda = q/L$, and K_0 and K_1 are the zeroth-order and first-order Modified Bessel Functions of the Second Kind, respectively.

Integrating these expressions for $\psi_{mic}(R_{ch})$ as the micelle charge, q, is increased from zero to full charge (nze), the work of charging the micelles, W_{3c}, is obtained, as follows (where we have made use of the geometric relations $na_{ch} = 4\pi R_{ch}^2$ for spheres, and $na_{ch} = 2\pi R_{ch}L$ for cylinders)

$$\int_0^{nze} \psi_{mic}(R_{ch})\, dq = nsk_BT\frac{\kappa R_{ch}}{2(1+\kappa R_{ch})} \text{ , for spheres} \tag{6.44}$$

$$\int_0^{nze} \psi_{mic}(R_{ch})\, dq = nsk_BT\frac{K_0(\kappa R_{ch})}{K_1(\kappa R_{ch})} \text{ , for infinite cylinders} \tag{6.45}$$

where s is a dimensionless surface charge density, given by

$$s = \frac{4\pi e^2 z^2}{\epsilon\kappa a_{ch} k_B T} \tag{6.46}$$

Note that the expression for s in Eq. (6.46) is the same as the one given in Eq. (2.38), with $\delta_i = 0$, since there is no need for a Stern layer in the McMillan-Mayer approach.

Since the micelles in this model are finite spherocylinders, the work of charging is estimated by linearly interpolating between Eq (6.44) for spheres and Eq. (6.45) for infinite cylinders. This is the same interpolation model that was used in calculating

g°_{mic} for spherocylindrical micelles. Specifically,

$$\int_0^{nze} \psi_{mic}(R_{ch})\, dq \;=\; n_0 \frac{s_{sph} k_B T \kappa R_{ch}}{2(1+\kappa R_{ch})} + (n-n_0) s_{cyl} k_B T \frac{K_0(\kappa R_{ch})}{K_1(\kappa R_{ch})} \text{ , for spherocylinders} \tag{6.47}$$

where s_{sph} and s_{cyl} are the dimensionless surface charge densities in the hemispherical endcaps and in the cylindrical body of the spherocylindrical micelle, respectively. Note that in the limiting case of monodisperse spheres, $n = n_0$, and Eq. (6.47) reduces to

$$\int_0^{nze} \psi_{mic}(R_{ch})\, dq \;=\; n_0 \frac{s_{sph} k_B T \kappa R_{ch}}{2(1+\kappa R_{ch})} \text{ , for spheres} \tag{6.48}$$

The monomer discharging term, W_{1a}, can also be solved with the Debye-Hückel approximation, by assuming that a monomer behaves as an effective spherical ion with a radius equal to that of the head, $r_h = (a_h/\pi)^{1/2}$. The electrostatic potential at the resulting monomer surface of charge can be obtained from Eq. (6.42) by substituting the appropriate parameters for the monomer, that is,

$$\psi_{mon}(r_h) \;=\; \frac{q_{mon}}{\epsilon r_h (1+\kappa r_h)} \tag{6.49}$$

where $q_{mon} = ez$ is the charge of the monomer.

The work involved in discharging n monomers is obtained by using Eq. (6.49) in Eq. (6.24) and integrating. This yields

$$-n\int_0^{ze} \psi_{mon}(r_h)\, dq \;=\; -n \frac{e^2 z^2}{2\epsilon r_h (1+\kappa r_h)} \tag{6.50}$$

We now have all the information required to evalulate the total work associated with forming the spherocylindrical micelle. Using Eqs. (6.47) and (6.50) in Eq. (6.31),

the following expression is obtained for the micellar size distribution

$$\Omega_w c_n = (\Omega_w c_1)^n \exp\left[-\beta n g^\circ_{mic} - (E_0^{cyl} - nE_1^{cyl}) - (A_0^{cyl} - nA_1^{cyl})\right] \tag{6.51}$$

where

$$E_0^{cyl} = n_0 \left(\frac{s_{sph}\kappa R_{ch}}{2(1+\kappa R_{ch})} - \frac{s_{cyl} K_0(\kappa R_{ch})}{K_1(\kappa R_{ch})} \right) \tag{6.52}$$

$$E_1^{cyl} = \frac{(ez)^2}{2\epsilon k_B T r_h (1+\kappa r_h)} - \frac{s_{cyl} K_0(\kappa R_{ch})}{K_1(\kappa R_{ch})} \tag{6.53}$$

and with g°_{mic} given in Eq. (6.12).

Note that when $z = 0$, $s = 0$, and both E_0^{cyl} and E_1^{cyl} vanish. In that limit, Eq. (6.51) reduces to the nonionic case given in Eq. (5.22). Equation (6.51) is also applicable to the case of monodisperse spherical micelles with $g^\circ_{mic} = g^\circ_{sph}$, and A_0^{cyl}, A_1^{cyl}, E_0^{cyl}, and E_1^{cyl} replaced by A_0^{sph}, A_1^{sph}, E_0^{sph}, and E_1^{sph}, respectively. Note that E_0^{sph} and E_1^{sph} can be obtained from Eqs. (6.52) and (6.53) by neglecting the contribution from the cylindrical region. That is, $E_0^{sph} = (n_0 s_{sph}\kappa R_{ch})/[2(1+\kappa R_{ch})]$, and $E_1^{cyl} = (ez)^2/[2\epsilon k_B T r_h(1+\kappa r_h)]$.

It is convenient to rewrite Eq. (6.51) in the following manner (compare with Eq. (5.23)):

$$c_n = \frac{q^n}{K} \tag{6.54}$$

where

$$q = \Omega_w c_1 \exp\left(-\beta g^\circ_{cyl} + A_1^{cyl} + E_1^{cyl}\right) \tag{6.55}$$

$$K = \Omega_w \exp\left(\beta n_0 (g^\circ_{sph} - g^\circ_{cyl}) + A_0^{cyl} + E_0^{cyl}\right) \tag{6.56}$$

When there are no charge effects, $E_0^{cyl} = E_1^{cyl} = 0$, and Eqs. (6.55) and (6.56) reduce to the nonionic case given in Eqs. (5.25) and (5.24). The moments of the micellar

size distribution can now be written as

$$M_k^{cyl} = c_1 + \sum_{n=n_0}^{\infty} n^k c_n \tag{6.57}$$

which is identical to Eq. (5.30). Hence, the same expressions for c and c_s given in Eqs. (5.31) and (5.32) also apply here. That is,

$$c = M_0^{cyl} = c_1 + \sum_{n=n_0}^{\infty} \frac{q^n}{K} = c_1 + \frac{q^{n_0}}{K(1-q)} \tag{6.58}$$

and

$$c_s = M_1^{cyl} = c_1 + \sum_{n=n_0}^{\infty} n\frac{q^n}{K} = c_1 + \frac{q^{n_0}}{K(1-q)^2}[n_0(1-q)+q] \tag{6.59}$$

Note that similar expressions for c_n, c, and c_s can be derived for monodisperse spherical micelles by replacing g°_{mic} with g°_{sph}, and A_0^{cyl}, A_1^{cyl}, E_0^{cyl}, and E_1^{cyl} with A_0^{sph}, A_1^{sph}, E_0^{sph}, and E_1^{sph}, respectively.

The micellar size distribution can also be characterized by the number-average micellar aggregation number, $\langle n \rangle_n$, the weight-average micellar aggregation number, $\langle n \rangle_w$, and the relative variance, Var, given in Eqs. (5.27)-(5.29) and repeated here for clarity

$$\langle n \rangle_n = \frac{M_1}{M_0} \tag{6.60}$$

$$\langle n \rangle_w = \frac{M_2}{M_1} \tag{6.61}$$

and

$$Var = \frac{M_3 M_1}{M_2^2} - 1 \tag{6.62}$$

As described in Section 5.4, Eq. (6.54) can be utilized to define a CMC. Specifically, by taking the natural log of c_n in Eq. (6.54), and keeping only terms that are of order

n, because $n \gg 1$, one can show[16, 9] that the CMC (in units of mole fraction) is given by

$$CMC \approx \exp\left(\beta g^{\circ}_{cyl} - A_1^{cyl} - E_1^{cyl}\right) \tag{6.63}$$

In view of the fact that A_1^{cyl} and E_1^{cyl} depend on surfactant concentration, it is necessary to set $c_s = CMC$ and solve Eq. (6.63) iteratively. This was fairly straightforward for the case of nonionic surfactants described in Chapter 5 where $E_1^{cyl} = 0$. However, in the case of ionic surfactants, the calculation of E_1^{cyl} can be fairly complex, causing the iteration routine to be very time-consuming. Instead, an alternative definition of the CMC is utilized.[19] Specifically, the CMC was defined to be the surfactant concentration at which the monomer concentration is equal to 95% of the total surfactant concentration (that is, 5% of the surfactant molecules have formed micelles).

6.3.2 Predictions of Micellar Solution Properties

The expressions given in Eqs. (6.58)-(6.62) can now be used to make predictions of several characteristics associated with the micellar size distribution. A typical ionic surfactant, sodium dodecyl sulfate (SDS, $C_{12}H_{25}SO_4Na$), was used as a model surfactant to study the effect of electrostatic intermicellar interactions. For example, in Figure 6-2, predictions of the monomer concentration of SDS are plotted as a function of total surfactant (SDS) concentration. The dashed line corresponds to predictions where the ion cloud consists only of monomers and counterions, and the solid line corresponds to predictions where the micelles are also included in the ion cloud. In other words, the dashed line predictions neglect micelle/micelle electrostatic interactions (at the ion cloud approximate level of description adopted here), while the solid line predictions include them. Note that there is no added salt, and hence, the counterions are the Na^+ ions dissociated from the surfactant (SDS) molecules. At low surfactant concentrations, as the surfactant concentration increases, the monomer concentration increases concomitantly. At a certain surfactant concentration, the CMC is reached, beyond which micelles begin to form. When micelle/micelle interac-

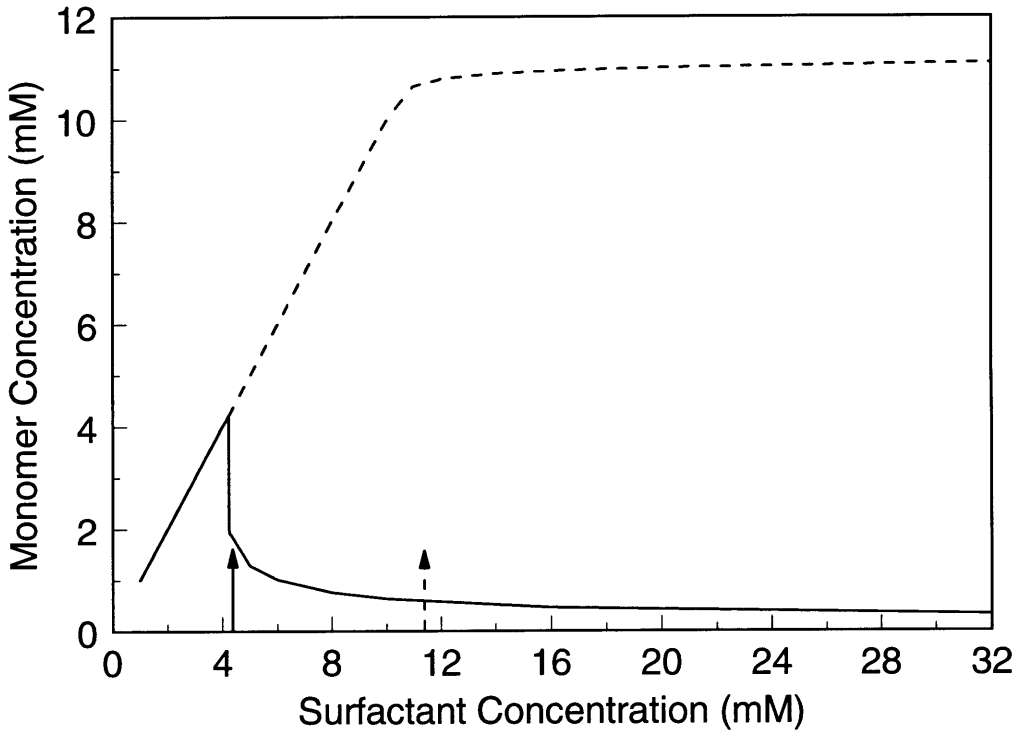

Figure 6-2: Predicted monomer concentration, c_1, as a function of total surfactant concentration, c_s, for an aqueous solution of SDS at 25°C. Predictions were made where the ion cloud consists only of monomers and counterions (- - -), and where the ion cloud also includes micelles (—). The dashed and solid arrows denote the corresponding predicted CMC values.

tions are neglected, the monomer concentration levels off to an almost constant value beyond the CMC (see dashed arrow in Figure 6-2), indicating that all the additional surfactant goes to form micelles. In contrast, when the micelles are included in the ion cloud, the CMC is reached at a much lower surfactant concentration (see solid arrow in Figure 6-2). In addition, the monomer concentration exhibits a sharp decrease above the CMC. Including the micelles in the ion cloud results in additional screening of the electrostatic repulsions among the surfactant heads at the micellar interface, thus making micelle formation more favorable, thereby resulting in a lower CMC. The monomer concentration decreases above the CMC because many of the monomers form micelles once it is more favorable to do so. Note that this decrease in monomer concentration above the CMC has been observed experimentally, although typically, a more gradual decrease is observed.[25]

The sharp peak in the monomer concentration at the CMC is due to the fact that the Debye-Hückel approximation overestimates the screening ability of all the charged solutes in the ion cloud, which particularly affects the micelles in the ion cloud. Specifically, the Boltzmann distribution treats all the ions in the ion cloud (including other micelles) as point ions. As such, these point ions can approach very closely to the micelle and to each other. In other words, the micelles present in the ion cloud are over-screening, resulting in a drastic reduction in the monomer concentration. On the other hand, there are no micelles in the ion cloud for the predictions illustrated by the dashed curve in Figure 6-2, and therefore, it does not exhibit the sharp peak. This point-ion approximation will be further discussed in Section 6.4.

Since the monomer concentration decreases with total surfactant concentration beyond the CMC when electrostatic intermicellar interactions are accounted for, the micelle concentration $(c - c_1)$ increases with total surfactant concentration, as illustrated in Figure 6-3. The dashed line represents the micelle concentration where the ion cloud consists only of monomers and counterions, and the solid line represents the micelle concentration where micelles are also included in the ion cloud. As before, there is no added salt, and therefore, the counterions are the Na^+ ions dissociated

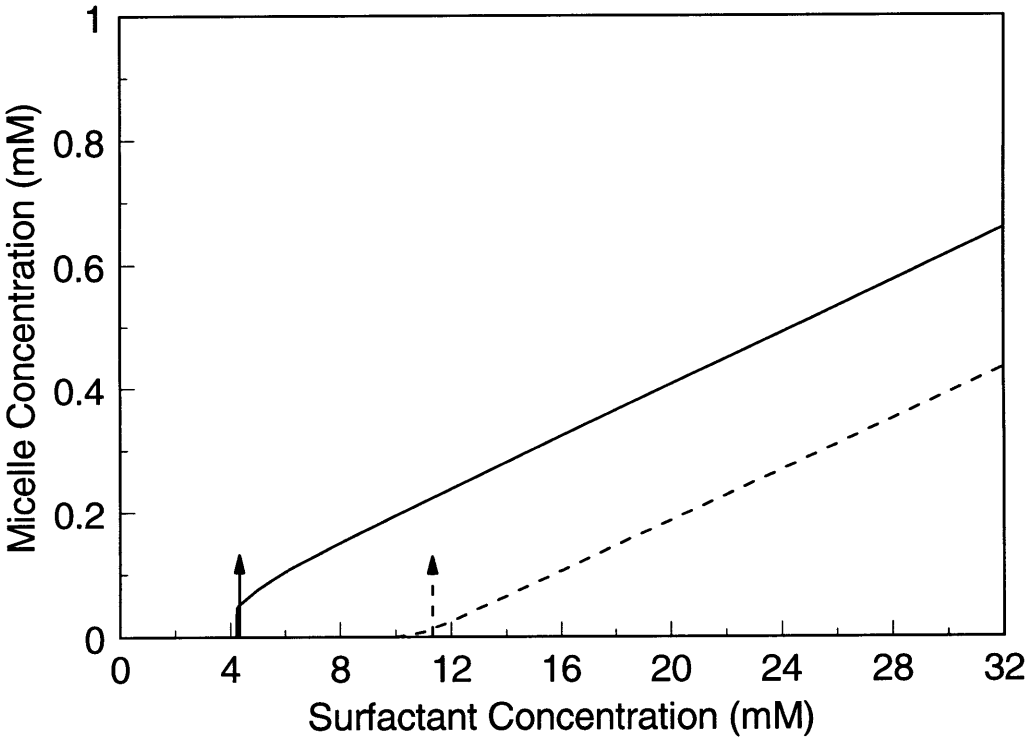

Figure 6-3: Predicted micelle concentration, $(c - c_1)$, as a function of total surfactant concentration, c_s, for an aqueous solution of SDS at 25°C. Predictions were made where the ion cloud consists only of monomers and counterions (- - -), and where the ion cloud also includes micelles (—). The dashed and solid arrows denote the corresponding predicted CMC values.

from the surfactant molecules. Below the CMC, micelles have not yet formed, and therefore, the micelle concentration is zero. When electrostatic intermicellar interactions are accounted for (solid line), the micelles contribute to the screening making it more favorable to form micelles. Hence, the CMC is lower, and micelles form at a lower surfactant concentration, thus resulting in a higher micelle concentration. Note that the jump in the micelle concentration at the CMC for predictions including intermicellar interactions (solid line) is an artifact of the sharp decrease in the monomer concentration, due to the point-charge approximation, discussed earlier with regard to Figure 6-2.

Figures 6-2 and 6-3 illustrate the fact that including intermicellar interactions reduces the CMC predictions. This is also the case when salt is added, as illustrated in Figure 6-4 for SDS at 25°C in a NaCl aqueous solution. The dashed line represents the CMC predictions where the ion cloud consists of monomers, counterions, and coions only, while the solid line represents CMC predictions where micelles are also included in the ion cloud. The diamonds denote experimental CMC values. Clearly, at low salt concentrations, including electrostatic intermicellar interactions results in much lower CMC predictions. Interestingly, as the salt concentration increases, the two lines coincide, indicating that the effect of including electrostatic intermicellar interactions becomes negligible. The salt concentration is much higher than the micelle concentration at this point, and therefore, the salt ions screen the electrostatic intermicellar interactions.

Intermicellar interactions, both of the electrostatic and hard-core variety, can also have an effect on the average micelle size. Predictions of the weight-average micellar aggregation number, $\langle n \rangle_w$, are shown in Figure 6-5 for a 10mM SDS aqueous NaCl solution as a function of the NaCl concentration. As discussed in Chapter 2, adding salt to an ionic micellar solution typically causes the spherical micelles to grow into elongated cylindrical structures. The dotted line in Figure 6-5 represents predicted $\langle n \rangle_w$ values using the Stern layer model described in Chapter 2, which does not include electrostatic or excluded-volume intermicellar interactions. As discussed earlier in Section 2.3.2, the Stern layer model strongly underestimates micelle size,

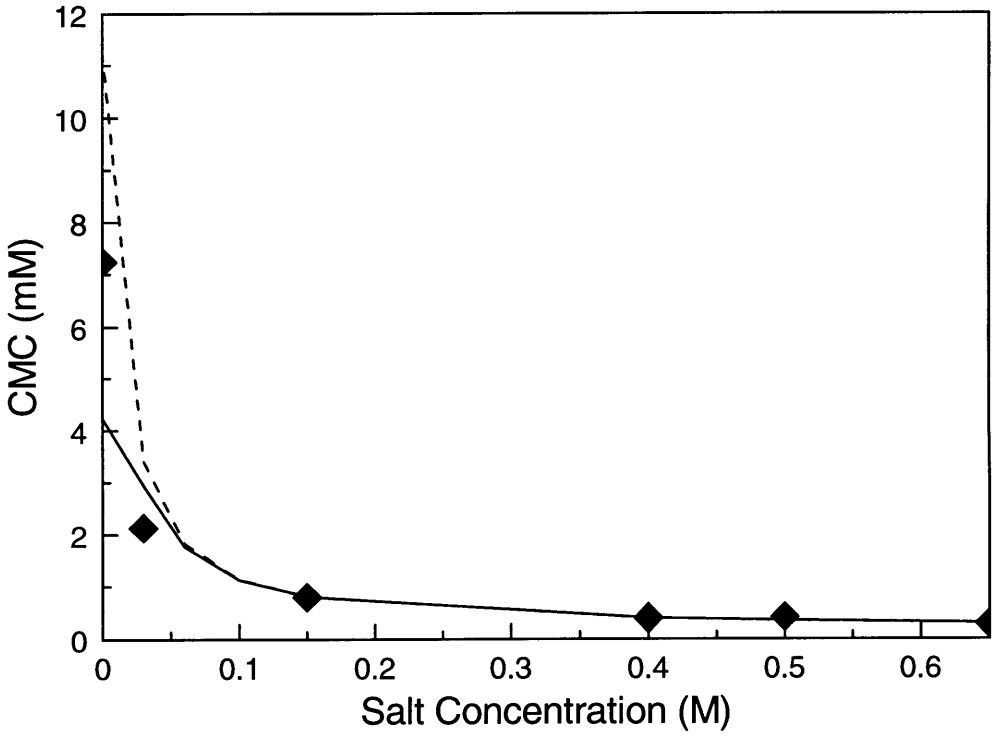

Figure 6-4: Critical micelle concentration (CMC) as a function of NaCl concentration for aqueous solutions of SDS at 25°C. CMC predictions were made using a model where the ion cloud consists only of monomers, counterions, and coions (- - -), and where the ion cloud also includes micelles (—). The diamonds represent experimental CMC values.

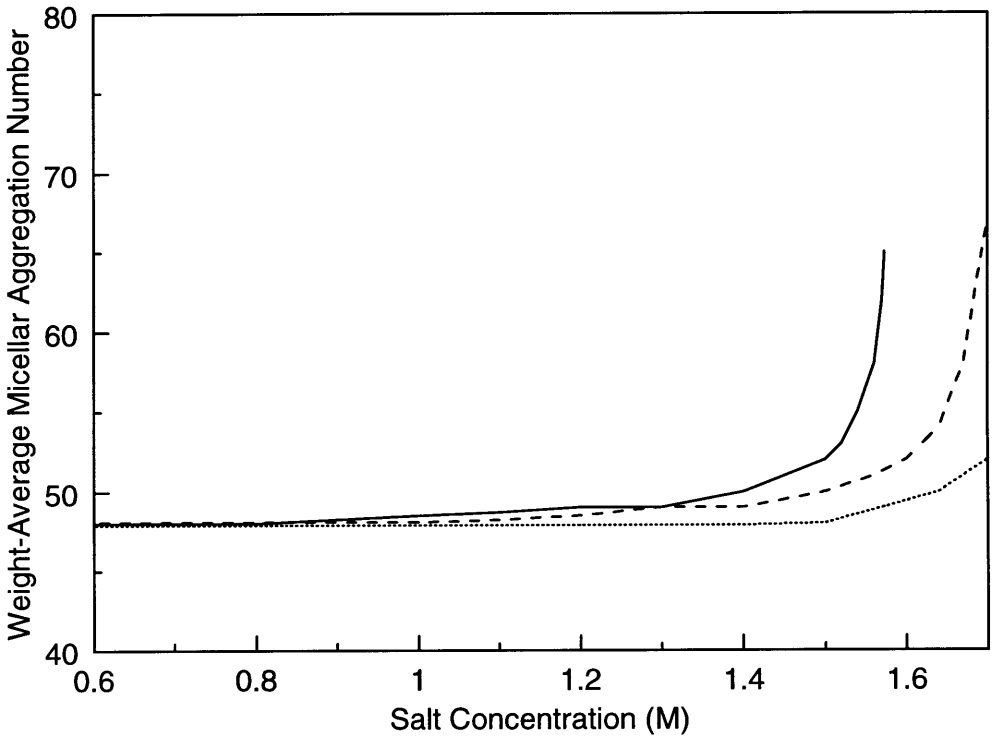

Figure 6-5: Predicted weight-average micellar aggregation number, $\langle n \rangle_w$, as a function of NaCl concentration for SDS in aqueous solution at 25°C. Predictions were made using a model where the ion cloud consists only of monomers, counterions, and coions (- - -), and where the ion cloud also includes micelles (—). These were compared against predictions made using the molecular-thermodynamic theory with a Stern layer presented in Chapter 2 which does not account for either hard-core or electrostatic intermicellar interactions ($\cdots$).

resulting in predictions of no growth in this salt concentration region. The dashed line represents $\langle n \rangle_w$ predictions using the model presented in this section with only monomers, counterions, and salt ions in the ion cloud. In other words, excluded-volume interactions are present among all the solutes, but electrostatic intermicellar interactions are neglected in the dashed line predictions.

As with the case for the nonionic surfactants discussed in Chapter 5, excluded-volume intermicellar interactions encourage micellar growth, as exhibited by a significant increase in $\langle n \rangle_w$ at about 1.6M NaCl (see the dashed line in Figure 6-5). Interestingly, including electrostatic intermicellar interactions (by including the micelles in the ion cloud) further encourages micellar growth, as shown by the solid line which has a sharp increase at approximately 1.5M NaCl. In other words, including the micelles in the ion cloud provides additional electrostatic screening, which allows the charged surfactant heads to approach closer to each other at the micellar interface, leading to micellar growth. Experimental measurements indicate that SDS micelles exhibit growth at approximately 0.5M NaCl.[9, 72, 73] Although the McMillan-Mayer approach with the Debye-Hückel model presented in this section still underestimates micelle size, it represents a significant improvement over the growth predictions of the molecular-thermodynamic theory with a Stern layer presented in Chapter 2.

Note that at the higher salt concentrations, including electrostatic intermicellar interactions has little impact on the CMC predictions (see Figure 6-4), but results in larger $\langle n \rangle_w$ predictions (see Figure 6-5). This is due to the fact that the $\langle n \rangle_w$ predictions were made at a surfactant concentration of 10mM, which is at least 10 times higher than the CMC of SDS at the higher salt concentrations. Consequently, more micelles are present in the ion cloud, and can contribute more significantly to the screening.

6.4 Modified-Poisson Boltzmann Equation

6.4.1 General Discussion

The Debye-Hückel approach presented in the previous section is useful due to its analytical nature, and could be implemented for both spherical and cylindrical micellar geometeries. However, some of the approximations necessary to obtain an analytical solution were fairly severe. Specifically, the linearization approximation used in the Debye-Hückel approach is really valid only for regions of low electrostatic potential ($ez\psi \ll k_BT$). As such, it is not a good approximation for the potentials at the surface of a micelle, which are typically of the order of 100-200mV, corresponding to $ez\psi$ in the range of 4 to 8 k_BT. To accurately calculate this relatively high surface potential, the full Poisson-Boltzmann equation should be used instead, necessitating a numerical solution. An additional approximation is that the Boltzmann distribution assumes that the ions in the ion cloud have no size, that is, they were treated as point ions. This may be acceptable for small ions such as Na^+ or Cl^-, but not for micelles. In other words, the micelles in the ion cloud were treated as point ions of valence nz. This is a severe approximation that should be improved. In addition, if the model is to be consistent with the evaluation of the hard-core EXCESS chemical potentials, the finite volume of all the solutes in the ion cloud should be included.

Therefore, in this section, a modified Boltzmann distribution will be derived which incorporates the effect of the finite size of the solutes in the ion cloud. This will be utilized in conjunction with the Poisson equation to numerically solve for the electrostatic EXCESS chemical potentials of the micelles or the monomers.

Including the finite size of the solutes in the ion cloud represents a complicated numerical problem which has not yet been fully resolved. For spherocylindrical micelles, the model would have to account for the respective orientation of the micelles in the ion cloud with respect to the central micelle. Clearly, this is a complicated electrostatics problem, and will not be addressed here. Instead, the micelles will be assumed to be monodisperse spheres. The aggregation number, n, of these micelles is based on the micellar core, $n = 4\pi l_c^3/3v_t$, where l_c is the length of the surfac-

tant tail (assumed to be equal to l_{max}), and v_t is the volume of the surfactant tail. Because the aggregation number is fixed, this approach cannot be used to model micellar growth. Hence, in the analysis which follows, the predictions will be limited to solution conditions at which the optimal micellar shape is spherical.

6.4.2 Modified Boltzmann Distribution

The Poisson equation can be used to describe the electrostatic potential at the surface of a micelle. Specifically, for a spherically-symmetric distribution of ions,[57, 68]

$$\nabla^2\psi(r) = \frac{-4\pi}{\epsilon}\sum_j ez_jc_j(r) \tag{6.64}$$

where ϵ is the dielectric constant of the solution, e is the electronic charge, z_j is the valence of ion j, and $c_j(r)$ is the concentration of ion j at radial position r measured from the center of the central micelle (or monomer). As mentioned above, the micelles are assumed to be spherical, and therefore, the Poisson equation is radially symmetric. The summation in Eq. (6.64) is over all the ions in the solution, including counterions, coions, monomers, and micelles. The Poisson equation sums over the interactions of the micelle with each ion in the ion cloud, assuming that the charge of each ion in the ion cloud is localized at position r.

To evaluate the concentration distribution, $c_j(r)$, one can make use of the electrochemical equilibrium existing between ions in the bulk and ions close to the central micelle (or monomer). That is,[117, 118]

$$\mu_j(r) = \mu_j \tag{6.65}$$

where $\mu_j(r)$ is the chemical potential of ion j at radial position r measured from the center of the central micelle (or monomer), and μ_j is the chemical potential of ion j in the bulk. Within the context of the McMillan-Mayer theory, the chemical potential of solute j is obtained from Eq. (4.14), where Eq. (4.18) is used for the volume of the

solution. Specifically,

$$\mu_j = \mu_j^\circ + k_B T \ln[c_j \Omega_w] + \mu_j^{EX} - \Pi \Omega_j \tag{6.66}$$

and

$$\mu_j(r) = \mu_j^\circ + k_B T \ln[c_j(r) \Omega_w] + \mu_j^{EX}(r) - \Pi(r) \Omega_j \tag{6.67}$$

where c_j and $c_j(r)$ are the concentrations of ion j in the bulk and at position r, respectively, and Π and $\Pi(r)$ are the osmotic pressures in the bulk and at position r, respectively. Note that $j = 1$ for monomers, n for n-mers, c for counterions, and *co* for coions. Because all concentrations are relatively dilute, it has been shown[118] that the difference in osmotic pressures is negligible, and therefore, it can be assumed that $\Pi \approx \Pi(r)$. Using Eqs. (6.66) and (6.67) in Eq. (6.65), the following expression is obtained for the concentration distribution of ion j in the ion cloud

$$c_j(r) = c_j \exp\left[\beta\left(\mu_j^{EX,elec} - \mu_j^{EX,elec}(r)\right) + \beta\left(\mu_j^{EX,HC} - \mu_j^{EX,HC}(r)\right)\right] \tag{6.68}$$

In order to calculate the ion distribution given in Eq. (6.68), the various EXCESS chemical potentials must be evaluated.

The hard-core EXCESS chemical potentials can be obtained from the virial equation of state, as described in Chapter 5 and in Appendix F. Specifically,

$$\mu_j^{EX,HC} = 2 k_B T \sum_k B_{jk}^{HC} c_k \tag{6.69}$$

where B_{jk}^{HC} is the excluded-volume contribution to the second-virial coefficient between species j and k, and the summation is over all other solutes. Thus, the difference between the hard-core EXCESS chemical potentials in the bulk and at position r is given by

$$\mu_j^{EX,HC} - \mu_j^{EX,HC}(r) = 2 k_B T \sum_k B_{jk}^{HC} \left(c_k - c_k(r)\right) \tag{6.70}$$

The electrostatic EXCESS chemical potential difference can be obtained using a

charging process as described in Section 6.2, resulting in the following expression

$$\mu_j^{EX,elec} - \mu_j^{EX,elec}(r) = \int_0^{q_j} \psi_b \, dq - \int_0^{q_j} \psi(r) \, dq \tag{6.71}$$

where $\psi(r)$ is the electrostatic potential at position r and ψ_b is the electrostatic potential in the bulk. In other words, the difference in electrostatic EXCESS chemical potentials is equal to the difference in the work of charging ion j in the bulk and the work of charging ion j at position r. Due to electroneutrality in the bulk, $\psi_b = 0$, and therefore, the first integral in Eq. (6.71) can be neglected. The electrostatic potential $\psi(r)$ is determined by the central micelle (or monomer) being charged, and therefore, does not vary with q_j, the charge on ion j in the ion cloud. Hence, Eq. (6.71) becomes

$$\mu_j^{EX,elec} - \mu_j^{EX,elec}(r) = 0 - \psi(r) \int_0^{q_j} dq \tag{6.72}$$

$$= -\psi(r) q_j \tag{6.73}$$

The charge on ion j can be written as $q_j = ez_j$, and Eq. (6.73) becomes

$$\mu_j^{EX,elec} - \mu_j^{EX,elec}(r) = -ez_j\psi(r) \tag{6.74}$$

By using Eqs. (6.70) and (6.74) in Eq. (6.68), the following expression is obtained for the distribution of ion j

$$c_j(r) = c_j \exp\left[\frac{-ez_j\psi(r)}{k_BT}\right] \exp\left[2\sum_k B_{jk}^{HC}(c_k - c_k(r))\right] \tag{6.75}$$

Recall that all micelles, monomers, and ions are assumed to be spherical. As discussed in Appendix F, the excluded volume between two spheres is given by $B_{jk}^{HC} = 2\pi(r_j + r_k)^3/3$, where r_j is the radius of species j and r_k is the radius of species k. The excluded volume between two spheres of the same size can be further simplified in terms of the volume of the sphere. For example, $B_{11}^{HC} = 2\pi(2R_1)^3/3 = 4\Omega_s$. Similarly, $B_{nn}^{HC} = 4n\Omega_s$ and $B_{cc}^{HC} = 4\Omega_i$, where Ω_i is the volume of a counterion or coion. Expanding the summation term in Eq. (6.75) over all the solutes involved, including

monomers, micelles, counterions, and coions, results in the following expressions for the distributions of each charged solute

$$c_1(r) = c_1 e^{-y(r)} \exp\left[8\Omega_s(c_1 - c_1(r)) + \frac{4\pi}{3}(R_1 + R)^3(c_n - c_n(r)) + \frac{4\pi}{3}(R_1 + r_i)^3(c_c - c_c(r) + c_{co} - c_{co}(r))\right] \quad \text{, for monomers} \tag{6.76}$$

$$c_n(r) = c_n e^{-ny(r)} \exp\left[\frac{4\pi}{3}(R_1 + R)^3(c_1 - c_1(r)) + 8n\Omega_s(c_n - c_n(r)) + \frac{4\pi}{3}(R + r_i)^3(c_c - c_c(r) + c_{co} - c_{co}(r))\right] \quad \text{, for micelles} \tag{6.77}$$

$$c_c(r) = c_c e^{y(r)} \exp\left[\frac{4\pi}{3}(R_1 + r_i)^3(c_1 - c_1(r)) + \frac{4\pi}{3}(R + r_i)^3(c_n - c_n(r)) + 8\Omega_i(c_c - c_c(r) + c_{co} - c_{co}(r))\right] \quad \text{, for counterions} \tag{6.78}$$

$$c_{co}(r) = c_{co} e^{-y(r)} \exp\left[\frac{4\pi}{3}(R_1 + r_i)^3(c_1 - c_1(r)) + \frac{4\pi}{3}(R + r_i)^3(c_n - c_n(r)) + 8\Omega_i(c_c - c_c(r) + c_{co} - c_{co}(r))\right] \quad \text{, for coions} \tag{6.79}$$

where $y = ez\psi/k_BT$ is a dimensionless electrostatic potential, written in terms of the valence of the surfactant molecule, z.

Because the ion concentrations, $c_j(r)$ for $j = 1, n, c, co$, appear explicitly in the excluded-volume correction terms in Eqs. (6.76)-(6.79), the four ion distributions are coupled and would have to be solved simultaneously with the Poisson equation, making this a difficult computational challenge. Therefore, in order to simplify the calculations, the traditional Boltzmann distribution is used to describe the ion concentrations appearing in the excluded-volume correction terms in Eqs. (6.76)-(6.79). Specifically, $c_j(r) \approx c_j \exp\left[\frac{-z_j y(r)}{z}\right]$. Although this is approximate, it is appropriate for use in the excluded-volume terms, because these are only correction terms that only slightly modify the actual ion distributions. The ion concentration distributions

then become

$$c_1(r) = c_1 e^{-y(r)} \exp\left[8\Omega_s c_1(1-e^{-y}) + \frac{4\pi}{3}(R_1+R)^3 c_n(1-e^{-ny}) + \frac{4\pi}{3}(R_1+r_i)^3(c_c(1-e^{y}) + c_{co}(1-e^{-y}))\right] \quad \text{, for monomers} \tag{6.80}$$

$$c_n(r) = c_n e^{-ny(r)} \exp\left[\frac{4\pi}{3}(R_1+R)^3 c_1(1-e^{-y}) + 8n\Omega_s c_n(1-e^{-ny}) + \frac{4\pi}{3}(R+r_i)^3(c_c(1-e^{y}) + c_{co}(1-e^{-y}))\right] \quad \text{, for micelles} \tag{6.81}$$

$$c_c(r) = c_c e^{y(r)} \exp\left[\frac{4\pi}{3}(R_1+r_i)^3 c_1(1-e^{-y}) + \frac{4\pi}{3}(R+r_i)^3 c_n(1-e^{-ny}) + 8\Omega_i(c_c(1-e^{y}) + c_{co}(1-e^{-y}))\right] \quad \text{, for counterions} \tag{6.82}$$

$$c_{co}(r) = c_{co} e^{-y(r)} \exp\left[\frac{4\pi}{3}(R_1+r_i)^3 c_1(1-e^{-y}) + \frac{4\pi}{3}(R+r_i)^3 c_n(1-e^{-ny}) + 8\Omega_i(c_c(1-e^{y}) + c_{co}(1-e^{-y}))\right] \quad \text{, for coions} \tag{6.83}$$

The concentrations in Eqs. (6.80)-(6.83) can now be substituted in the Poisson Equation, Eq. (6.64), as follows

$$\nabla^2\psi(r) = -\left(\frac{4\pi ez}{\epsilon}\right)[c_1(r) + nc_n(r) + c_{co}(r) - c_c(r)] \tag{6.84}$$

Using Eqs. (6.80)-(6.83) in Eq. (6.84) results in the following modified PB equation

$$\nabla^2\psi(r) = -\left(\frac{4\pi ez}{\epsilon}\right)\left[c_1 B_1(y) e^{-y} + nc_n B_n(y) e^{-ny} - c_c B_i(y) e^{y} + c_{co} B_i(y) e^{-y}\right] \tag{6.85}$$

where the $B_j(y)$ coefficients are the excluded-volume correction factors, given by

$$B_1(y) = \exp\left[8\Omega_s c_1(1-e^{-y}) + \frac{4\pi}{3}(R_1+R)^3 c_n(1-e^{-ny}) + \frac{4\pi}{3}(R_1+r_i)^3(c_c(1-e^{y}) + c_{co}(1-e^{-y}))\right] \tag{6.86}$$

$$B_n(y) = \exp\left[\frac{4\pi}{3}(R_1+R)^3 c_1(1-e^{-y}) + 8n\Omega_s c_n(1-e^{-ny}) + \frac{4\pi}{3}(R+r_i)^3(c_c(1-e^{y}) + c_{co}(1-e^{-y}))\right] \quad (6.87)$$

$$B_i(y) = \exp\left[\frac{4\pi}{3}(R_1+r_i)^3 c_1(1-e^{-y}) + \frac{4\pi}{3}(R+r_i)^3 c_n(1-e^{-ny}) + 8\Omega_i(c_c(1-e^{y}) + c_{co}(1-e^{-y}))\right] \quad (6.88)$$

Note that because the counterions and the coions were assumed to have the same size, they give rise to the same excluded-volume correction factor, that is, $B_c = B_{co} = B_i$.

The modified PB equation, Eq. (6.85), can now be used to solve for ψ_{mic} and ψ_{mon}, which, in turn, can be used in Eq. (6.31) to calculate the micelle size distribution. The boundary conditions for this problem were given in Eqs. (6.39) and (6.40). a standard finite element method[119] is used to solve Eq. (6.85). In this method, Eq. (6.85) is replaced with a finite difference equation which is solved over a mesh of points covering the entire range of the problem. In order to use this method, the range of the problem must be transformed from an infinite range (from $r = R_{ch}$ to $r \to \infty$) to a finite range (from $w = 0$ to $w = 1/\kappa R_{ch}$) by using the transformation $w = 1/\kappa r$. In this case, Eq. (6.85) becomes

$$w^4 \frac{\partial^2 y}{\partial w^2} = \frac{-\left[c_1 B_1(y) e^{-y} + n c_n B_n(y) e^{-ny} - c_c B_i(y) e^{y} + c_{co} B_i(y) e^{-y}\right]}{\left[c_1 + n^2 c_n + c_{co} + c_c\right]} \quad (6.89)$$

Recall that $y = ez\psi/k_BT$ is the dimensionless electrostatic potential. The value of y at each point on the mesh is gradually adjusted until the entire mesh is brought to close agreement with the finite difference equation and with each boundary condition. This solution method is used to solve for both $\psi_{mic}(R_{ch})$ and $\psi_{mon}(r_h)$, which are then used in conjunction with Eq. (6.31) to calculate various characteristics of the micellar size distribution.

Treating the solutes in the ion cloud as point ions ($R = R_1 = r_h = 0$) results in $B_1 = B_n = B_i = 1$. In this limit, Eq. (6.85) becomes the traditional Poisson-

Boltzmann equation, that is,

$$\nabla^2\psi(r) = -\left(\frac{4\pi ez}{\epsilon}\right)\left[c_1 e^{-y} + nc_n e^{-ny} - c_c e^{y} + c_{co} e^{-y}\right] \tag{6.90}$$

Equation (6.90) is the same as Eq. (6.32), where $y = ez\psi/k_BT$, and the summation has been carried out over all the charged solutes.

6.4.3 Predictions of Micellar Solution Properties

The modified Poisson-Boltzmann equation, Eq. (6.85), was used to calculate several characteristics of the micellar size distribution for the same model ionic surfactant used earlier, SDS. Figure 6-6 illustrates predictions of the monomer concentration for SDS as a function of total surfactant concentration for the case where the ion cloud consists of monomers and counterions only (dashed line), and for the case where the ion cloud also includes other micelles (solid line). For both cases, at low surfactant concentrations, below the CMC (see the dashed and solid lines in Figure 6-6), as the surfactant concentration increases, the monomer concentration increases concomitantly. When intermicellar electrostatic interactions are neglected (dashed line), as the surfactant concentration increases further, micelles begin to form, and the monomer concentration levels out to a constant value (at higher surfactant concentrations not shown in this scale). In other words, all the additional surfactant molecules form micelles. In contrast, when micelles are included in the ion cloud (solid line), once micelles begin to form, as the surfactant concentration increases, there is a marked decrease in the monomer concentration. This is due to the additional screening provided by the micelles in the ion cloud, thus making it more favorable to form micelles, and inducing more monomers to aggregate into micelles. This behavior is qualitatively very similar to that found with the Debye-Hückel approximation (compare with Fig. 6-2). However, when micelles are included in the ion cloud in the modified PB solution, the decrease in monomer concentration above the CMC is not as sharp as it is in the context of the DH solution. Because the finite size of the micelles is accounted for in the modified PB solution, the screening provided

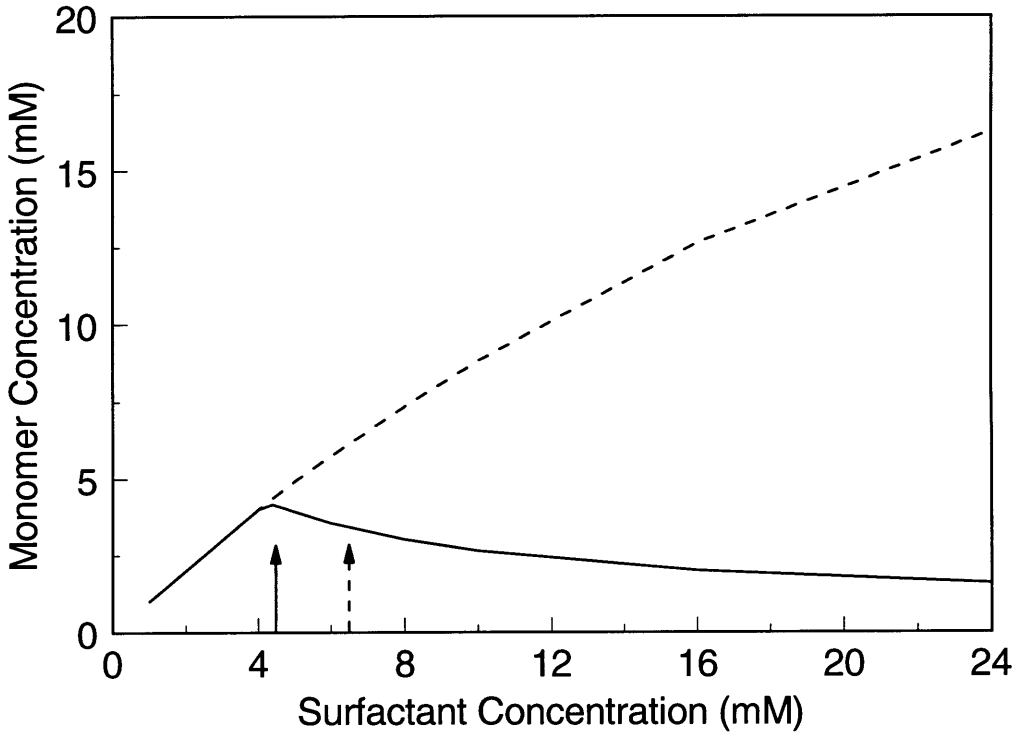

Figure 6-6: Predicted monomer concentration, c_1, as a function of total surfactant concentration, c_s, for an aqueous solution of SDS at 25°C. Predictions were made using a model where the ion cloud consists only of monomers and counterions (- - -), and where the ion cloud also includes micelles (—). The dashed and solid arrows denote the corresponding predicted CMC values.

by the micelles in the ion cloud is more realistic. In addition, the electrostatic potential, ψ, is not linearized, as it is in the DH solution, and therefore, the modified PB equation provides a more accurate representation of ψ. Both of these effects result in a much smoother decrease in monomer concentration.

The predicted decrease in monomer concentration leads to a corresponding increase in micelle concentration, as illustrated in Figure 6-7. The dashed line represents predictions made for the case where the ion cloud consists of monomers and counterions only, and the solid line represents predictions made where micelles are also included in the ion cloud. Clearly, including electrostatic intermicellar interactions results in an increase in the micelle concentration as micelle formation becomes more favorable. Again, this is the same qualitative behavior found with the DH approximation (compare with Figure 6-3). In addition, as the surfactant concentration increases further, more micelles are formed, resulting in even more screening. At these high surfactant concentrations, the effect of intermicellar interactions becomes even more pronounced, as indicated by the widening of the gap between the solid and the dashed lines.

Note that the CMC value predicted where the ion cloud contains only monomers and counterions (6.4mM, dashed arrow in Figure 6-6) is lower than that predicted using the DH model (11.3mM, dashed arrow in Figure 6-2). Interestingly, when micelles are also included in the ion cloud, the difference in CMC predictions is quite small (4.4mM for the modified PB model, solid arrow in Figure 6-6, and 4.2mM for the DH model, solid arrow in Figure 6-2). The additional screening provided by including the micelles in the ion cloud reduces the CMC considerably, regardless of the model used to calculate it. However, at higher surfactant concentrations, when more micelles are present, including the finite size of the micelles in the ion cloud will have a significant impact on the resulting micellar size distribution predictions (compare Figure 6-7 with Figure 6-3).

To compare the CMC predictions with experimental CMC values, the CMC was also predicted for SDS in aqueous NaCl solutions at 25°C, as illustrated in Fig. 6-8. The dashed line represents CMC predictions where only monomers, counterions,

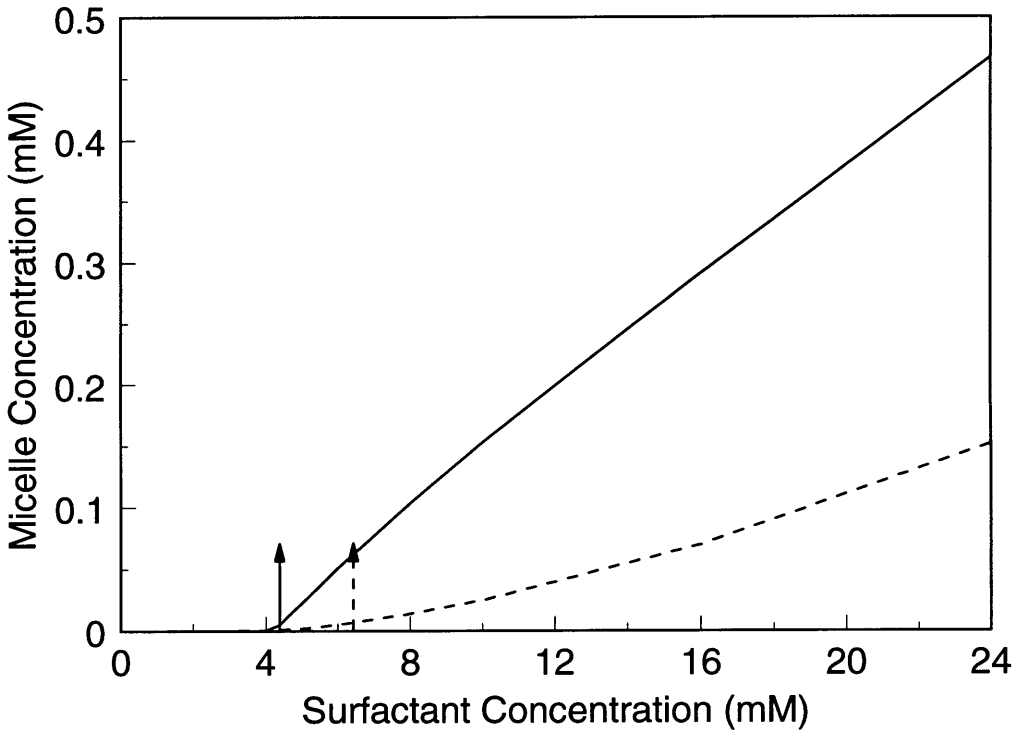

Figure 6-7: Predicted micelle concentration, $c - c_1$, as a function of total surfactant concentration, c_s, for an aqueous solution of SDS at 25°C. Predictions were made using a model where the ion cloud consists only of monomers and counterions (- - -), and where the ion cloud also includes micelles (—). The dashed and solid arrows denote the corresponding predicted CMC values.

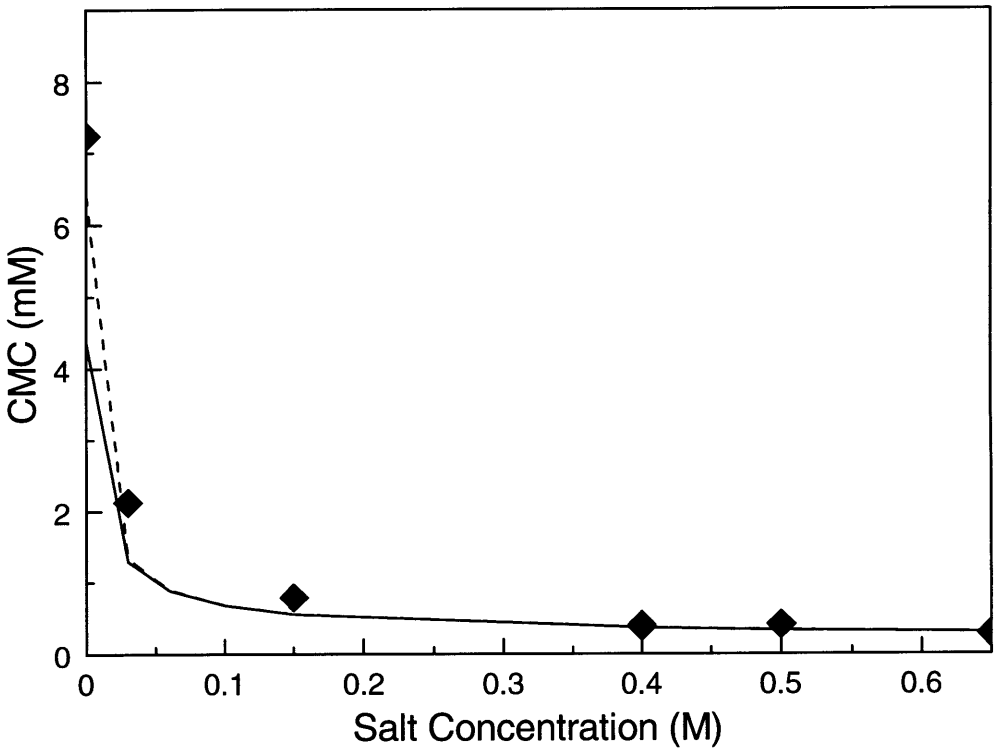

Figure 6-8: Critical micelle concentration (CMC) as a function of NaCl concentration for aqueous solutions of SDS at 25°C. CMC predictions were made using a model where the ion cloud consists only of monomers, counterions, and coions (- - -), and where the ion cloud also includes micelles (—).The diamonds represent experimental CMC values.

and coions are included in the ion cloud, and the solid line represents CMC predictions where micelles are also included in the ion cloud. The diamonds represent experimental CMC values. At very low salt concentrations, including intermicellar interactions clearly affects the CMC predictions, lowering the CMC by almost 2mM. Again, including the micelles in the ion cloud provides more screening, thus making it more favorable to form micelles, and hence reducing the CMC. The predictions which include the electrostatic intermicellar interactions underestimate the CMC when compared to the experimental measurements. Even so, this analysis has been helpful in assessing the impact of the electrostatic intermicellar interactions. Interestingly, as the salt concentration increases, the salt molecules dominate the screening, and the difference between the solid line and the dashed line diminishes. Clearly, at higher salt concentrations, it makes little difference whether the micelles are included in the ion cloud or not. Note, however, that the concentration of micelles at the CMC is very low. At higher surfactant concentrations, the concentration of micelles is much higher, and the effect of including intermicellar interactions, even in salt solutions, may become important.

To test the effect of the excluded-volume corrections, predictions were also made using the full PB equation solved numerically, with $B_1 = B_n = B_i = 0$. It was found that neglecting the excluded-volume corrections results in slightly lower CMC predictions. When the solutes in the ion cloud (including micelles) have no volume, they can approach infinitely close to each other and to the central micelle, thereby screening more effectively than when they have a finite size. Consequently, micelle formation becomes more favorable, resulting in a lower CMC.

The modified PB equation can only be applied to spherical micelles, and therefore, is unable to predict micellar growth. Therefore, it is important to use both the DH model and the modified PB model. For spherical micelles, the modified PB approach is more accurate, because it does not linearize the potential, and also treats the finite volume of the solutes in the ion cloud. On the other hand, the DH model is more versatile, in that it can also treat spherocylindrical micelles. Clearly, what is needed in the future is an accurate model of the potential which can also be implemented

in the case of elongated micelles. In any case, the two approaches presented in this chapter represent a useful "first step" in the modeling of electrostatic intermicellar interactions.

6.5 Conclusions

In this chapter, we have implemented the general statistical-thermodynamic framework developed in Chapter 4 in the case of ionic micellar solutions. Due to their long range, electrostatic intermicellar interactions are more difficult to model than the shorter-ranged attractive and excluded-volume interactions considered in Chapter 5 in the case of nonionic micellar solutions. Several different approaches to modeling electrostatic intermicellar interactions were discussed. Indeed, due to its versatility, the statistical-thermodynamic framework developed in Chapter 4 is well-suited to testing various models. The Debye-Hückel approximation and a modified Poisson-Boltzmann equation were used to model the electrostatic potential around the micellar surface. The modified PB equation provides a more accurate description because it does not linearize the potential and it includes the finite size of the charged solutes. On the other hand, the Debye-Hückel approximation is more versatile because it is analytical and can be used to model elongated micelles. The CMC's predicted by both models when no salt is present underestimate the experimentally-measured CMC values. In fact, the molecular-thermodynamic framework with the Stern layer presented in Chapter 2 actually predicts more accurate CMC's. However, including the electrostatic intermicellar interactions significantly improves the predictions of micelle size, which was underpredicted in the context of the molecular-thermodynamic theory presented in Chapter 2. In conclusion, for convenient, fast predictions, the molecular-thermodynamic theory presented in Chapter 2 is useful. However, the McMillan-Mayer approach presented in this chapter is more accurate for predicting micellar solution properties above the CMC where intermicellar interactions may become significant.

Chapter 7

Investigations of Micelle Shape and Size in Aqueous Solutions of Dodecyl Ethoxy Sulfates

7.1 Introduction

The predictions presented in the preceding chapters were compared against experimental data from various sources found in the literature. As such, there may be some variation in the purity of the surfactants investigated which could affect the measured micellar properties. In addition, different experimental methods may yield slightly different values for the same micellar property. In view of these limitations, it would be valuable to obtain a set of consistent, reliable experimental data for a family of surfactants of high purity. With this in mind, an investigation into the micellar properties of dodecyl ethoxy sulfates was conducted and is described in this chapter. Alkyl ethoxy sulfates represent an important and interesting family of surfactants, both scientifically and commercially.[120, 121] Due to the unique chemical structure of their hydrophilic heads, these surfactants exhibit a behavior which is intermediate between that of nonionic and ionic surfactants. Specifically, the head consists of a variable number of non-charged ethoxy (EO) groups capped

by a charged sulfate group, while the tail consists of a straight-chain hydrocarbon (that is, $C_{12}H_{25}(OCH_2CH_2)_nOSO_3Na$, where n is the number of EO groups). The lengths of both the head and the tail groups can be varied in order to tune the hydrophilic/hydrophobic character of these surfactants to achieve a specific desired behavior.

By varying the number of EO groups in the surfactant head, one may study the interplay of steric and electrostatic head/head interactions at the micelle surface. In particular, when the number of EO groups is small, the presence of the charged sulfate groups results in strong electrostatic interactions among the surfactant heads. Increasing the number of EO groups in the head displaces the charged sulfate group from the micelle surface, thus diluting its effect. In addition, because the EO groups are typically hydrated, they can be quite bulky. Accordingly, the overall effect of increasing the number of EO groups is to both weaken the electrostatic interactions and enhance the steric interactions among the surfactant heads. This interesting interplay between steric and electrostatic head/head interactions at the micelle surface is ultimately responsible for the resulting micelle shape and size. Typically, ionic surfactants form spherical micelles in aqueous solution in order to reduce the electrostatic repulsions among the charged heads at the micelle surface.[9, 72] As discussed in Chapter 2, it has been shown[9, 72, 122, 123, 49, 124] that the addition of salt screens these electrostatic repulsions, which results in a reduction of the critical micelle concentration (CMC) and allows the charged spherical micelles to grow into more elongated, rod-like structures. This "sphere-to-rod" transition has been well-documented in the case of sodium dodecyl sulfate micelles,[9, 72] but has not been thoroughly investigated in the case of alkyl ethoxy sulfate micelles.

Although alkyl ethoxy sulfates represent the second most important group of anionic sufactants commercially,[121] relatively few systematic experimental investigations have been conducted on this interesting class of surfactants. Most of the work to date has involved primarily surface tension and CMC measurements,[120, 125, 126] as well as Krafft point studies.[127] Relatively little effort has been devoted to a systematic investigation of the shape and size of micelles formed by alkyl ethoxy sulfates

in aqueous solution. Early work indicated that the micelles of dodecyl ethoxy sulfate surfactants containing 1 to 10 EO groups form small, spherical micelles in 0.1M NaCl aqueous solution.[128] To quantitatively determine the effect of salt concentration on micelle size, a thorough light scattering study was conducted[129] on dodecyl ethoxy sulfates with one, two, and four EO groups. However, this study focused only on the effect of intermicellar interactions, and assumed that micellar growth was negligible under the conditions examined. Recent investigations of micellar growth have shown[130, 131] that dodecyl ethoxy sulfate micelles containing two EO groups exhibit a distinct sphere-to-rod transition in the presence of multivalent counterions, such as Ca^{2+} and Al^{3+}. However, this investigation was conducted at a relatively low surfactant concentration, and hence, intermicellar interactions were assumed to be negligible.

In the study described in this chapter, previous work is extended by introducing three new elements. First, the quantitative analysis incorporates *both* intermicellar interactions and micellar growth. Second, two *independent* experimental methods (light scattering and viscosity) are utilized in order to verify the effect of salt concentration and temperature on micelle shape and size. Third, four different shape models (spheres, prolate ellipsoids, oblate ellipsoids, and spherocylinders) are examined and compared in order to determine the relative likelihood of one-dimensional versus two-dimensional growth. These four micellar shapes were considered because they span a plausible range of possible shapes for which the micelle average hydrodynamic radius can be quantitatively deduced.

A serious challenge associated with studying alkyl ethoxy sulfates involves obtaining pure samples. In particular, most synthesis procedures result in surfactants that contain a distribution of EO groups in the head, as well as a distribution of hydrocarbon tail lengths. This polydispersity can have a significant effect on the observed solution properties of the surfactants.[132, 133] Unless the samples are well-characterized, this heterogeneity may cause ambiguities in the analysis of the experimental results. In order to minimize this potential problem, pure, monodisperse samples of alkyl ethoxy sulfates were synthesized by Witco, Inc. specifically for the studies described

in this chapter. The surfactants investigated consist of a dodecyl ($C_{12}H_{25}$) tail and 1, 2, 4, or 6 EO groups. Hereafter, these dodecyl ethoxy sulfates will be abbreviated as E1S for one EO group, E2S for two EO groups, and so on.

Interestingly, one of the surfactants examined, E1S, was observed to phase separate at high salt (NaCl) concentrations. Phase separation of aqueous ionic micellar solutions is fairly unusual, typically only occurring at very high salt concentrations, such as 4-5M salt.[134, 135] The phase separation of the aqueous E1S micellar solution is more similar to the coacervation typically observed in polyelectrolyte solutions or surfactant/polymer mixtures.[136, 137] In coacervation, the micelle-rich phase is very concentrated. It consists of hydrated elongated micelles which align with each other in some kind of long-range order.[136] Although a thorough investigation of this coacervation phenomenon is beyond the scope of this thesis, some cloud-point measurements were conducted to map out the coexistence curve (see Section 7.4.2).

The remainder of this chapter is organized as follows. In Section 7.2, the materials and experimental methods are described. In Section 7.3, the theoretical aspects associated with the interpretation of the light scattering and viscosity measurements are presented. In Section 7.4, the quantitative analysis of the light scattering data is explained, followed by a thorough discussion of the light scattering and viscosity experimental results. Finally, concluding remarks are presented in Section 7.5.

7.2 Materials and Methods

7.2.1 Sample Preparation

The dodecyl ethoxy sulfates investigated were synthesized by Witco, Inc. specifically for this study and used without further purification. The starting materials were monodisperse dodecyl poly(ethylene oxide) surfactants of a very high purity obtained from Nikko Chemicals, Tokyo. These surfactants were then sulfated and analyzed for composition by Witco, Inc. It was found that the final material was 92-99% sulfated and contained approximately 3-6% residual sodium sulfate salts. However, because a

relatively large amount of NaCl was added to all the solutions studied, the residual sodium sulfate salt should have a negligible effect on the micellar solution properties. Aqueous surfactant solutions were prepared using deionized water which was futher purified using a Milli-Q ion-exchange system. These solutions were stored at 4°C and utilized within 48 hours. The sodium chloride used was of the analytical reagent grade from Mallinckrodt, Paris, KY. Prior to use, the salt was roasted at 450°C for 12 hours to remove organic impurities.

Before use, all glassware were immersed in a 1N NaOH-ethanol bath for at least 8 hours, then in a 1N nitric acid bath for another 8 hours, followed by a thorough rinsing with Milli-Q water. The glassware were then dried in an oven.

7.2.2 Dynamic Light Scattering

Dynamic (quasielastic) light scattering measurements were performed at a scattering angle $\theta = 90°$, using an apparatus consisting of a Lexel model 95 2W argon laser ($\lambda = 514$nm), a goniometer, and an autocorrelator (model BI-9000AT, Brookhaven Instruments, Holtsville, NY). The temperature of the samples was stabilized to within ± 0.1°C by a circulating ethylene glycol bath. To minimize interference from dust, the samples were filtered through a 0.2μm filter three times into a scattering cell that had been rinsed with acetone. The collective diffusion coefficient, D_c, was extracted from the measured autocorrelation function using the cumulants analysis method[9, 138] with a quadratic fit. The average hydrodynamic radius of the micelles, R_H, was deduced from the measured collective diffusion coefficient by accounting for the effect of intermicellar interactions (see Section 7.3.1).

7.2.3 Static Light Scattering

In the static light scattering measurements, the total scattered light intensity was measured at $\theta = 90°$ using the same apparatus that was described above. The intensity of the scattered light is used to calculate the Rayleigh ratio of the micellar solution, $\mathcal{R}$, by comparing with the scattering from a reference liquid having a known

Rayleigh ratio. Specifically,[139]

$$\mathcal{R} = \frac{\langle I(\theta) \rangle}{\langle I_{ref}(\theta) \rangle} \mathcal{R}_{ref} \left(\frac{n}{n_{ref}} \right)^2 - \mathcal{R}_0 \tag{7.1}$$

where $\langle I(\theta) \rangle$ is the average scattered light intensity of the micellar solution, $\langle I_{ref}(\theta) \rangle$ is the average scattered light intensity of the reference liquid (toluene), $\mathcal{R}_{ref}$ is the Rayleigh ratio of toluene at the appropriate experimental conditions, n is the refractive index of the micellar solution, n_{ref} is the refractive index of toluene, and $\mathcal{R}_0$ is the Rayleigh ratio of the aqueous salt solution in the absence of micelles. Values of $\mathcal{R}_{ref}$ and n_{ref} are available in the literature.[140, 141, 142] Note that, in general, the Rayleigh ratio depends on the angle of the scattered light. However, for all the measurements described in this chapter, the micelles are much smaller than the wavelength of the scattered light, and therefore, the dependence of $\mathcal{R}$ on θ can be neglected.

The Rayleigh ratio can be utilized to obtain the apparent molecular weight of the micelles, M_{app}, as follows[139, 143, 144]

$$\frac{Kc}{\mathcal{R} - \mathcal{R}_0} = \frac{1}{k_B T} \frac{\partial \Pi}{\partial c} = \frac{1}{M_{app}} \tag{7.2}$$

where c is the concentration of surfactant in g/cm^3, $(\partial \Pi / \partial c)$ is the inverse osmotic compressibility, k_B is the Boltzmann constant, T is the absolute temperature, and K is an optical constant, given by[139, 143]

$$K = \frac{4\pi n^2 \left(\frac{\partial n}{\partial c} \right)_T^2}{N_A \lambda^4} \tag{7.3}$$

where $(\partial n / \partial c)_T$ is the refractive index increment, λ (=514nm) is the wavelength of the incident light, and N_A is Avogadro's number. The average micellar aggregation number was obtained from the apparent molecular weight by accounting for the effect of intermicellar interactions, as discussed in Section 7.3.1.

The refractive index increment, $(\partial n / \partial c)_T$, was measured using an ABBE Refrac-

tometer (American Optical Corporation, Buffalo, NY) connected to a water bath having a $\pm 0.01°C$ temperature stability (see Tables 7.1 and 7.2 for a list of the measured $(\partial n/\partial c)_T$ values).

Table 7.1: The refractive index increment, $(\partial n/\partial c)_T$, and the solvent viscosity, η_0, for the various NaCl concentrations examined at a temperature of 25°C. The blank entries correspond to solution conditions which were not examined for that surfactant.

NaCl $[M]$	$\left(\frac{\partial n}{\partial c}\right)_T [cm^3/g]$ for E1S	$\left(\frac{\partial n}{\partial c}\right)_T [cm^3/g]$ for E2S	η_0 $[cP]$
0.1	0.167	0.148	0.900
0.2	0.184	0.154	0.909
0.3	0.177	0.158	0.917
0.4	0.198	0.150	0.925
0.5	–	0.157	0.933
0.6	–	0.158	0.941

Table 7.2: The refractive index increment, $(\partial n/\partial c)_T$, and the solvent viscosity, η_0, at the various temperatures examined at a NaCl concentration of 0.6M NaCl. The blank entries correspond to solution conditions which were not examined for that surfactant.

Temperature $[°C]$	$\left(\frac{\partial n}{\partial c}\right)_T [cm^3/g]$ for E4S	$\left(\frac{\partial n}{\partial c}\right)_T [cm^3/g]$ for E6S	η_0 $[cP]$
25	0.115	0.131	0.941
34	0.117	0.124	0.782
38	–	0.121	0.721
40	0.119	0.119	0.690
44	0.120	0.116	0.646
45	0.120	0.115	0.634
46	0.120	–	0.623

7.2.4 Viscosity

The kinematic viscosities of the aqueous surfactant solutions were measured using Cannon-Ubbelohde capillary viscometers immersed in a water bath having a temperature stability of ±0.01°C. The viscometer containing the sample was immersed in the water bath for at least 20 minutes prior to taking a measurement, to allow the surfactant solution to come to thermal equilibrium. Dilutions (by volume) were prepared directly in the viscometer. The time it takes for the sample to flow through the capillary was measured to the nearest 0.1s, and was then converted to kinematic viscosity values using a calibration constant. The viscosity of the surfactant solution was obtained by multiplying the kinematic viscosity by the density of the solution.[145] To avoid the need for kinetic energy corrections, flow times were kept above 200s by varying the diameters of the capillaries of the viscometers used. The viscosity of each sample was measured at least four times, until the standard deviation among the readings was less than 2%.

7.2.5 Cloud-Point Measurements

The coexistence curve for the liquid-liquid phase separation of E1S in a 0.9M NaCl aqueous solution was determined according to the cloud-point method, which consists of visually identifying the temperature at which solutions of known E1S concentration became cloudy when the temperature is lowered. Each sample was placed in a transparent water bath whose temperature was controlled to within 0.01°C. Initially, each sample was heated to a high temperature so that it exhibited a single, clear, homogeneous phase. The temperature was then gradually lowered until the solution started to cloud at a temperature T_{cloud}. Note that at each step the sample was first stirred thoroughly, with a magnetic stirrer, to ensure temperature homogeneity, and subsequently observed for any signs of cloudiness with the stirrer turned off. Over the range of surfactant concentrations investigated, T_{cloud} was found to be in the range 50-60°C. At this high temperature, E1S was unstable, making it impossible to obtain reproducible results. Indeed, hydrolysis of E1S was detected with pH test papers.

Accordingly, to improve accuracy, many solutions over a wide range of surfactant concentrations (from 2mM to 160mM) were prepared and tested only once.

7.3 Theory

7.3.1 Light Scattering

As discussed in Section 7.2.3, the apparent micellar molecular weight can be determined by measuring the Rayleigh ratio of the micellar solution. The apparent micellar molecular weight, M_{app}, can be converted to the actual average micellar molecular weight through the use of the structure factor, which accounts for the effect of intermicellar interactions. The weight-average micellar aggregation number, N_{agg}, can then be obtained from the average micellar molecular weight, as follows,[43, 146]

$$N_{agg} = \frac{M_{app}}{m_s\, S(q \to 0)} \tag{7.4}$$

where m_s is the surfactant molecular weight, $q = (4\pi n_s/\lambda)\sin(\theta/2)$ is the wave vector, where n_s is the refractive index of the solvent and θ is the scattering angle, and $S(q \to 0)$ is the structure factor in the limit of zero scattering angle ($\theta = 0$ or $q \to 0$). Equation (7.4) is valid for micelles which are much smaller than the wavelength of the light scattered. The effective diameter of the micelles studied in this chapter is in the range of 50-300Å, which is well within this regime ($\lambda = 514$nm). Although the measurements were conducted at $\theta = 90°$, because the micelles are much smaller than the wavelength of the light scattered, the structure factor is independent of the scattering angle. Therefore, $S(\theta = 90°) \approx S(\theta = 0°)$

In order to model the effect of intermicellar interactions, the micelles are assumed to be spheres, even though, in some cases, the micelles exhibit growth into elongated structures. This assumption reflects the current lack of an appropriate theory to model the effect of intermicellar interactions for asymmetric particles, such as rods, for which the relative orientation of the interacting particles becomes important.[43] Hence, in the analysis of intermicellar interactions which follows, the elongated mi-

celles are treated as effective spheres having an equivalent volume. Specifically, the radius of these effective spheres is given by $R = [3v_s N_{agg}/(4\pi)]^{1/3}$, where v_s is the volume of a surfactant molecule. One should keep in mind, however, that as the micelles become more elongated, treating them as effective spheres may eventually lead to some quantitative inaccuracy in the treatment of the effect of intermicellar interactions, as well as in the deduced N_{agg} values. The impact of the spherical assumption on the quantitative interpretation of the light scattering results is further discussed in Section 7.4.

In general, for a solution containing spherical micelles which is relatively dilute so that only pairwise intermicellar interactions need to be considered, the structure factor in the limit $q \to 0$ is given by[146, 147, 148]

$$S(q \to 0) = 1 + 32\pi R^3 \rho \int_0^\infty x^2 (g(x) - 1)\, dx \tag{7.5}$$

where ρ is the micelle number density, $g(x)$ is the micelle pair correlation function, and $x = r/2R$ is a dimensionless distance, where r is the distance between the centers of two interacting spherical micelles, and R is the micelle radius. The micelle number density, ρ, is given by

$$\begin{aligned} \rho &= \frac{(c_s - c_1)}{N_{agg}} \approx \frac{c_s}{N_{agg}} \\ &= \frac{3 v_s c_s}{4\pi R^3} \end{aligned} \tag{7.6}$$

where c_s is the concentration (number density) of surfactant molecules, and c_1 is the concentration (number density) of surfactant monomers. Note that for the micellar solutions examined in this chapter, $c_s \approx 3 \times 10^{-5}\text{Å}^{-3} \gg c_1 \approx 6 \times 10^{-7}\text{Å}^{-3}$, and therefore, in Eq. (7.6), the surfactant monomer concentration can be neglected.

Using Eq. (7.6) in Eq. (7.5), one obtains

$$S(0) = 1 + 24 v_s c_s \int_0^\infty x^2 (g(x) - 1)\, dx \tag{7.7}$$

where $S(0)$ is a shorthand notation for $S(q \to 0)$.

Quasielastic (dynamic) light scattering measures the collective micellar diffusion coefficient, D_c, which includes the effect of intermicellar interactions. In other words, when intermicellar interactions are present, the movement of one micelle is affected by the presence of neighboring micelles, which may increase or decrease its overall diffusion. D_c can be related to the individual micellar diffusion coefficient, D_0, as follows[146, 148]

$$D_c = \frac{D_0}{S(0)}[1 + H(0)] \tag{7.8}$$

where $H(0)$ is the perturbation coefficient due to hydrodynamic interactions in the limit of low scattering angle ($q \to 0$).

The hydrodynamic perturbation coefficient, $H(0)$, can be obtained from the hydrodynamic tensor, describing the flow of the solvent around the micelles. As already stressed, the micellar solutions studied here are relatively dilute (the surfactant concentration is approximately $3 \times 10^{-5}\text{Å}^{-3}$), and therefore, the Oseen approximation can be used to estimate $H(0)$. Specifically,[146, 148]

$$H(0) = 16\pi R^3 \rho \int_0^\infty x(g(x) - 1)\, dx \tag{7.9}$$

More sophisticated expressions for $H(0)$ are available, such as those due to Felderhof[148] or Batchelor[43], which account for the flow field at a higher level of detail. For comparison, the Felderhof expression for $H(0)$ was also examined. It was determined that the difference between using Eq. (7.9) and the more complicated Felderhof expression is negligible for the dilute micellar solutions considered here. Using Eq. (7.6) for ρ in Eq. (7.9) yields

$$H(0) = 12 v_s c_s \int_0^\infty x(g(x) - 1)\, dx \tag{7.10}$$

The next step is to identify an appropriate expression for the micelle pair correlation function, $g(x)$, to be used in Eqs. (7.7) and (7.10). The function $g(x)$ can be obtained from the intermicellar interaction potential through an appropriate re-

lationship. Several approximations are available in the literature which establish this relationship, including the MSA[149, 150] and the HNC[146] approximations. However, in view of the dilute nature of the micellar solutions considered here, the relatively simple dilute gas approximation for $g(x)$ is appropriate. It is noteworthy that the dilute gas approximation has the added advantage of being analytical, which greatly reduces computational times. Specifically, the dilute gas expansion for $g(x)$ is given by[146, 148]

$$g(x) = \begin{cases} 0 & , \text{for } x \leq 1 \\ \exp\left(\frac{-V(x)}{k_B T}\right) & , \text{for } x > 1 \end{cases} \tag{7.11}$$

where $V(x)$ is the interaction potential between two spherical micelles of radius R whose centers are separated by a distance r, with $x = r/2R$. Note that the region $r \leq 2R$ (or $x \leq 1$) represents the hard-core interaction region from which the micelles are excluded, and therefore, $g(r) = 0$ in Eq. (7.11). The micelles are in contact at $r = 2R$ (or $x = 1$), and for $r > 2R$ (or $x > 1$), the micelles interact with a potential $V(x)$. Note that, for comparison, the HNC approximation[146] for $g(r)$ was also used to analyze some of the light scattering data, and it was found that the difference between the use of the HNC and the dilute gas approximations was negligible.

Use of Eq. (7.11) in Eqs. (7.7) and (7.10) results in the following expressions for $S(0)$ and $H(0)$

$$S(0) = 1 - v_s c_s \left[8 + 24 \int_1^\infty x^2 \left(1 - e^{-\beta V(x)}\right) dx\right] \tag{7.12}$$

$$H(0) = -v_s c_s \left[6 + 12 \int_1^\infty x \left(1 - e^{-\beta V(x)}\right) dx\right] \tag{7.13}$$

where $\beta = 1/k_B T$. Note that the 8 in Eq. (7.12) and the 6 in Eq. (7.13) result from integrating over the region $0 < x \leq 1$, where $g(x) = 0$.

For the charged dodecyl ethoxy sulfate micelles considered in this study, there are three main types of intermicellar interactions that need to be considered: (i) hard-

core (repulsive), (ii) electrostatic (repulsive), and (iii) van der Waals (attractive). As discussed above, the hard-core interactions were already accounted for in the integration over the region $0 < x \leq 1$. The electrostatic and attractive interactions are modeled using the classical DLVO theory,[67] which provides a well-accepted description of interparticle interactions in the colloidal regime. Specifically, the DLVO interaction potential, $V(x)$, for $x > 1$, is given by[43, 67, 149, 150, 151]

$$V(x) = V_{elec}(x) + V_{att}(x) \tag{7.14}$$

where $V_{elec}(x)$ is a repulsive Coulombic contribution, and $V_{att}(x)$ is an attractive London-van der Waals contribution.

The repulsive Coulombic potential between two charged spheres was calculated in two different limits by Verwey and Overbeek.[67] These limits depend on the ratio of the micelle radius, R, to the Debye screening length, κ^{-1}, a well-known measure of the ion cloud thickness. As discussed in Section 2.3.2, the Debye screening length depends on the solution ionic strength: the higher the ionic strength, the lower the value of κ^{-1}. Specifically,[67, 151]

$$\kappa^{-1} = \left[\frac{4\pi e^2}{\epsilon k_B T} \sum_i c_i z_i^2\right]^{-(1/2)} \tag{7.15}$$

where e is the electronic charge, ϵ is the dielectric constant of the solvent, c_i is the concentration of charged species i, and z_i is the valence of species i. For the systems examined in this chapter, the salt concentration is much greater than the concentration of the charged surfactant monomers. Specifically, the salt concentration, c_{salt}, is 0.1-1.0M, while the monomer concentration, c_1, is less than 0.001M. Hence, the contribution of the charged surfactant monomers to κ^{-1} can be neglected. Accordingly, in Eq. (7.15), $\sum_i c_i z_i^2 \approx 2c_{salt}z^2$, where z is the valence of the salt (assuming a symmetric salt, such as NaCl).

As stated above, κ^{-1} has units of length (see Eq. (7.15)), and can be thought of as a measure of the thickness of the ion cloud surrounding the micelle. When the ionic

strength of the solution is low and κ^{-1} is large, the micelle radius is much smaller than the ion cloud thickness ($R \ll \kappa^{-1}$ or $\kappa R \ll 1$), and the micelles can be treated as interacting point charges.[67, 151] On the other hand, when the ionic strength of the solution is high and κ^{-1} is low, the micelle radius is much larger than the ion cloud thickness ($R \gg \kappa^{-1}$ or $\kappa R \gg 1$), and the spherical shape of the charged surface must be taken into account. This is, in fact, the case for the surfactant systems examined in this chapter (κR ranges from $3 \sim 12$). The electrostatic potential in this regime is given by[67, 151]

$$V_{elec}(x) = \frac{\epsilon R \psi_0^2}{2} \ln\left[1 + e^{-2\kappa R(x-1)}\right] \text{ , for } \kappa R >> 1 \tag{7.16}$$

where ψ_0 is the electrostatic potential at the surface of the micelle, given by[67]

$$\psi_0 = \frac{2k_BT}{e} \sinh^{-1}\left[\frac{z_m e^2}{2\kappa R^2 \epsilon k_B T}\right] \tag{7.17}$$

where z_m is the valence of the micelle. Because only a fraction of the surfactant molecules dissociate, the valence of the micelle is related to the average micelle aggregation number through the fractional charge, α, that is, $z_m = \alpha N_{agg}$.[1]

The attractive London-van der Waals contribution to the DLVO potential for two spheres of equal radius R is given by[43, 67, 151]

$$V_{att}(x) = \frac{-A}{12}\left[\frac{1}{x^2-1} + \frac{1}{x^2} + 2\ln\frac{x^2-1}{x^2}\right] \tag{7.18}$$

where A is the Hamaker constant representing the magnitude of the attractive interactions. Equation (7.18) indicates that as $x = r/2R \to 1$ ($r \to 2R$), V_{att} approaches negative infinity. Physically, this reflects the very large negative (attractive) interaction exhibited by micelles in direct contact with each other due to the relatively short range of the potential. However, mathematically, when V_{att} approaches negative infinity, the integrals in Eqs. (7.12) and (7.13) diverge. In order to carry out the integration, a lower cutoff, $x = 1 + \delta$, must be imposed.[43, 149, 150] This can also

[1]Note that $\alpha = 1 - \alpha_B$, where α_B is the fractional counterion binding discussed in Section 2.4.

be understood physically. In the van der Waals attraction, the surrounding medium (the aqueous solvent) is treated as a continuum. Hence, Eq. (7.18) is not valid for distances which are less than an atomic diameter. The value $\delta = 1$Å, which corresponds approximately to the size of a typical counterion, is used in this analysis. It should be noted that the results of the data analysis are not sensitive to the precise value of δ.

Note that potentials other than the DLVO potential could also be utilized to model intermicellar interactions. In particular, the Yukawa potential has been utilized to model the attractive intermicellar interactions in nonionic micellar solutions.[33, 45, 52, 152] For comparison, this potential was also used to represent the attractive interactions in our case. However, the Yukawa potential contains two unknown parameters (the range and depth of the potential), and it proved difficult to determine a consistent set of two parameters that fit the light scattering data as well as the van der Waals potential, which has only one unknown parameter, the Hamaker constant (see Section 7.4.1 for a description of the fitting procedure). This difficulty may be a manifestation of the fact that the attractive intermicellar interactions in the micellar systems examined here are small and, hence, are not very sensitive to the selection of these parameters.

Equations (7.16) and (7.18) can now be used in Eqs. (7.12) and (7.13) to compute $S(0)$ and $H(0)$. The fractional charge, α, and the Hamaker constant, A, are two unknown parameters, and must be determined by fitting to the light scattering data. The actual fitting procedure is discussed in Section 7.4.1.

The average micelle hydrodynamic radius can be calculated from the individual diffusion coefficient, D_0, using the Stokes-Einstein equation. Specifically,[47, 78, 148]

$$R_h = \frac{k_B T}{6\pi\eta_o D_0} \tag{7.19}$$

where η_o is the viscosity of the solvent, given in Tables 7.1 and 7.2 for the solution conditions studied here.[153]

The alkyl ethoxy sulfate micelles are typically hydrated. Following standard light

scattering procedures for dealing with hydrated micelles,[129, 144] it was assumed that dynamic light scattering is sensitive to the hydrated micelle, while static light scattering is sensitive to the bare micelle (without hydration). The hydration can then be calculated by comparing the bare average micelle radius, calculated using static light scattering, with the average micelle hydrodynamic radius, calculated using dynamic light scattering. Details of this calculation are provided in Section 7.4.1.

7.3.2 Viscosity

The relative viscosity, η_r, is a convenient measureable micellar solution property that can provide useful information about micelle shape and size. Specifically, η_r is defined as the solution viscosity, η, divided by the solvent viscosity, η_0, and depends on the volume fraction of micelles, ϕ, as follows[143, 154, 155, 156, 157]

$$\eta_r = \frac{\eta}{\eta_0} = 1 + \nu\phi + k_1(\nu\phi)^2 + \mathcal{O}(\phi^3) \tag{7.20}$$

where ν, referred to as the shape factor, reflects the shape of the micelles, and k_1 is a coefficient accounting for pairwise hydrodynamic interactions between the micelles. For polydisperse micellar solutions, ν represents the shape of the average micelle. Note that in Eq. (7.20), the micellar volume fraction, ϕ, includes the hydration of the micelle, and is therefore given by $\phi = v_s^{hyd}(c_s - c_1)$, where v_s^{hyd} is the hydrated volume of a surfactant molecule. As discussed above, since $c_s \gg c_1$, it follows that $\phi \approx v_s^{hyd} c_s$.

Physically, one can rationalize Eq. (7.20) as follows.[155, 156] In infinitely dilute colloidal solutions, the flow of the solvent depends only on the shape and size of the individual particles which act completely independently of each other ($\eta_r - 1 = \nu\phi$). As the particle concentration increases, the flow around one particle is affected by the presence of a neighboring particle. These pairwise interactions are accounted for by the second-order term in Eq. (7.20), $k_1(\nu\phi)^2$, where k_1 is a proportionality constant that depends only on the shape (not the size) of the particles. In particular, it has been determined that $k_1 = 2.2$ for spheres,[158] and $k_1 = 0.75$ for elongated

shapes.[2][155, 158] As the particle concentration increases further, physical contact between neighboring particles may occur, which would be accounted for by the third-order term in Eq. (7.20). The particle volume fractions of relevance in the present study are relatively small ($\phi \sim 0.04$), and therefore, the third-order term in Eq. (7.20) is negligible.

When charges are present, as in the case of the charged alkyl ethoxy sulfate micelles considered here, the solution viscosity may be affected by a phenomenon known as the electroviscous effect.[143, 159] It is believed that the electroviscous effect is primarily due to the increase in the effective volume of the micelle as a result of the presence of the electrical double layer around the micelle.[143, 159] Accordingly, more work is required to drive the fluid flow around the charged micelles leading to a viscosity increase. The electroviscous effect can be accounted for using a correction to the second-order term in Eq. (7.20). However, it has been shown[159, 160] that when the salt concentration is greater than or equal to 0.1M, as is the case for all the micellar solutions examined in this chapter, the effective size of the double layer decreases significantly, and electroviscous effects become negligible.

The shape factor, ν, has been calculated for specific shapes based on hydrodynamic considerations. In the simplest case, for a solution consisting of dilute, non-interacting, spherical micelles, $\nu = 2.5$, as derived by Einstein.[143, 154, 161, 158] The second-order term is negligible in this case, and the relative viscosity increases linearly with the micellar volume fraction, with a slope of 2.5, that is,

$$\eta_r = 1 + 2.5\phi = 1 + 2.5 v_s^{hyd} c_s \tag{7.21}$$

In this chapter, viscosity measurements are utilized to investigate the shape and size of alkyl ethoxy sulfate micelles which may form in a variety of shapes and sizes. It is expected that these micelles may grow beyond the limits of the simple Einstein model. Expressions for ν have been derived for several other shapes and are presented

[2] k_1 has not been defined for disc-like shapes. However, when the oblate ellipsoid model was used to model that shape, the resulting micelles had small shape factors, and therefore, the second-order term could be neglected.

in Table 7.3, where f is the micelle axial ratio (the major axis divided by the minor axis), and r_{min} is the micelle minor axis.[143, 155, 156, 157, 161, 158, 162, 163] The micelle minor axis was assumed to correspond to the radius of the smallest spherical micelle, r_{min}, as measured using dynamic light scattering. Specifically, r_{min} = 21Å, 22Å, 24Å, and 25Å for E1S, E2S, E4S, and E6S, respectively.

7.4 Results and Discussion

7.4.1 Light Scattering Data Analysis

The average micelle aggregation number, N_{agg}, and the average micelle hydrodynamic radius, R_H, were extracted from the static and dynamic light scattering data, respectively, by accounting for intermicellar interactions as discussed in Section 7.3.1. The parameters of the DLVO potential, α and A, along with the surfactant molecular hydrated volume, v_s^{hyd}, were determined simultaneously by fitting the light scattering data. Note that only two experimentally measurable properties (M_{app} and D_c) can be fitted for each solution condition (salt concentration or temperature). Hence, if each solution condition were treated individually, only two parameters could be fitted uniquely. Since there are three parameters that must be determined for each surfactant, the same three parameters are fitted over the entire range of solution conditions. That is, it is assumed that α, A, and v_s^{hyd} do not depend on salt concentration or temperature. The validity of this assumption is discussed later. The specific fitting procedure is described in detail below.

For an assumed micelle shape (sphere, prolate ellipsoid, oblate ellipsoid, spherocylinder) corresponding to a given alkyl ethoxy sulfate, the following steps were undertaken:

1. A wide range of possible values was specified for each parameter (α, A, and v_s^{hyd}). Values for each of the parameters were tested within this entire range.

2. For a given solution condition (NaCl concentration or temperature) examined:

Table 7.3: Equations for the average micelle hydrodynamic radius, R_H,[144, 164, 165] and the shape factor, ν,[143, 155, 156, 157, 158, 161, 162, 163] for four micelle shape models. V_{mic}^{hyd} is the total volume of the hydrated micelle, r_{min} is the micelle minor radius, and f is the micelle axial ratio (that is, the major axis divided by the minor axis).

Shape	R_H	ν
Spheres	$R_H = \left(\frac{3V_{mic}^{hyd}}{4\pi}\right)^{1/3}$	$\nu = 2.5$
Prolate Ellipsoid	$R_H = \frac{r_{min} f (1-1/f^2)^{1/2}}{\ln f + \ln[1+(1-1/f^2)^{1/2}]}$ where $f = \left(\frac{3V_{mic}^{hyd}}{4\pi r_{min}^3}\right)$	$\nu = \frac{24}{15} + \frac{f^2}{15}\left[\frac{1}{\ln 2f - 1.5} + \frac{3}{\ln 2f - 0.5}\right]$
Oblate Ellipsoid	$R_H = \frac{r_{min}(f^2-1)^{1/2}}{\arctan[(f^2-1)^{1/2}]}$ where $f = \left(\frac{3V_{mic}^{hyd}}{4\pi r_{min}^3}\right)^{1/2}$	$\nu = \frac{16f}{15\arctan(f)}$
Spherocylinder	$R_H = \frac{r_{min} f}{\ln f + \gamma}$ where $f = \left(\frac{2}{3} + \frac{V_{mic}^{hyd}}{2\pi r_{min}^3}\right)$ $\gamma = 0.32 + \frac{0.4738}{f} + \frac{0.4167}{f^2} - \frac{0.3394}{f^3}$	$\nu = \frac{24}{15} + \frac{\xi^2}{60}\left[\frac{1}{\ln \xi - 1.5} + \frac{3}{\ln \xi - 0.5}\right]$ where $\xi = 3f - 1$

(a) The average micelle aggregation number, N_{agg}, was calculated from the M_{app} value obtained from the static light scattering data using Eq. (7.4), where the structure factor was calculated from Eq. (7.12) using the guessed values of α and A in the interaction potential given by Eqs. (7.14), (7.16), and (7.18). Note that the surfactant molecular volume, v_s, appearing in Eq. (7.12) is the bare surfactant volume, not v_s^{hyd}.

(b) The total volume of the hydrated micelle was then calculated from the average micelle aggregation number deduced in (a), using the guessed value of v_s^{hyd}, that is, $V_{mic}^{hyd} = N_{agg} v_s^{hyd}$. The average micelle hydrodynamic radius, R_H, was then calculated using V_{mic}^{hyd}. (See Table 7.3 for detailed expressions of R_H for each shape tested.[144, 164, 165] Recall that r_{min} = 21Å, 22Å, 24Å, and 25Å for E1S, E2S, E4S, and E6S, respectively.)

(c) The average micellar diffusion coefficient, D_0, was then calculated from the average micelle hydrodynamic radius deduced in (b) using the Stokes-Einstein relation, Eq. (7.19). The solvent viscosities, η_0, at the various NaCl concentrations and temperatures examined are listed in Tables 7.1 and 7.2, respectively.

(d) The hydrodynamic perturbation coefficient, $H(0)$, was calculated from Eq. (7.13) using the guessed values of α and A in the interaction potential given by Eqs. (7.14), (7.16), and (7.18). Note that the surfactant molecular volume, v_s, appearing in Eq. (7.13) is the bare surfactant volume, not v_s^{hyd}.

(e) The collective diffusion coefficient, D_c, was then predicted using Eq. (7.8). The root-mean-squared error (RMS) between the predicted D_c and the D_c obtained from the dynamic light scattering data was then calculated for the given solution condition.

3. For the same surfactant, the RMS values corresponding to each of the solution conditions examined (NaCl concentration or temperature) were calculated as described above, and then added together.

4. By minimizing the total RMS between the predicted and experimental D_c values calculated in 3, the optimal values of α, A, and v_s^{hyd} were determined.

The analysis was repeated for each of the four model shapes: spheres, prolate ellipsoids, oblate ellipsoids, and spherocylinders. For E1S and E2S, the prolate ellipsoid model resulted in the best fit to the data (smallest RMS). For E4S and E6S, the spherical model resulted in the best fit to the data. The optimal parameters deduced for each surfactant are listed in Table 7.4, along with the range of error. The hydration, also shown in Table 7.4, is calculated from the difference between v_s^{hyd} and v_s, where the volume of a water molecule was taken to be approximately 30Å^3. Note that $v_s = v_t + v_{head}$, where v_t was given in Section 2.3, and $v_{head}(\text{in Å}^3) = 120.9 + 63.5j$, where j is the number of ethoxy groups in the head (v_s= 508Å^3, 571Å^3, 698Å^3, and 825Å^3 for E1S, E2S, E4S, and E6S, respectively).[10, 166] The hydration is presented in terms of the number of bound water molecules per EO group. To calculate this number, the total hydration per surfactant molecule was divided by the number of ethoxy groups, after subtracting the hydration due to the sulfate group (10 water molecules[167]).

Table 7.4: Optimal surfactant parameters deduced from the light scattering data using the prolate ellipsoid model for E1S and E2S and the sphere model for E4S and E6S. A is the Hamaker constant representing the magnitude of the intermicellar van der Waals attractions, α is the micelle fractional charge (that is, the fraction of surfactant molecules in the micelle that have dissociated), and v_s^{hyd} is the hydrated surfactant molecular volume. The hydration number is the number of bound water molecules per ethoxy group in the surfactant head.

Surfactant	$A(k_BT)$	α	v_s^{hyd}(Å^3)	Hydration Number
E1S	0±1	0.16 ± 0.04	1450 ± 200	16
E2S	0±1	0.13 ± 0.05	1540 ± 100	8
E4S	1.4±1	0.16 ± 0.05	1860 ± 50	6
E6S	2.0±1	0.19 ± 0.02	2140 ± 200	5

As noted above, it was assumed that α, A, and v_s^{hyd} remain constant over the range of NaCl concentrations and temperatures examined. This assumption can be tested by fixing one parameter, and allowing the other two parameters to vary for

each solution condition. In this manner, the range of error for each fitted parameter was determined. It was found that the range of error for all three parameters was relatively small (see Table 7.4), indicating that assuming that α, A, and v_s^{hyd} do not depend on salt concentration or temperature is a reasonable approximation. Note that the RMS was minimized with respect to each parameter individually, to within a tolerance of 0.1% or less. In addition, a wide range of initial guesses were tested to prove that the optimization procedure was unique.

Recall that the analysis of the intermicellar interactions treats the micelles as effective spheres. Clearly, as the micelles grow and elongate, this approximation will eventually become invalid. In particular, as discussed below in Section 7.4.2, at higher salt concentrations, the light scattering data for E1S and E2S indicated that the micelles were growing. When the fitting procedure described above was applied to this data, it appeared that the hydrated surfactant volume increased with salt concentration to unphysical values. This unlikely variation in the hydration values is due to the approximate treatment of the interactions for these highly elongated micelles. However, this approximation had very little effect on the other two parameters, α and A, which remained approximately constant over the entire salt concentration range examined. Accordingly, in order to avoid inaccuracies in the determination of v_s^{hyd}, only the data from the lower salt concentrations (where the micellar axial ratios were less than 5) were used to calculate v_s^{hyd}. This v_s^{hyd} value was then used to solve for α and A for the entire range of NaCl concentrations examined. As discussed further in Section 7.4.3, the larger heads, E4S and E6S, did not exhibit significant micellar growth, and therefore, the spherical approximation for the intermicellar interactions was applicable over the entire range of salt concentrations and temperatures examined.

The attractive interactions were found to be negligible for the small heads, E1S and E2S, as reflected in the nearly zero values of the Hamaker constants reported in Table 7.4. For E4S and E6S, although the attractions are not negligible, they remain quite small (see Table 7.4). The α values are also relatively small, although they are physically reasonable. It is interesting to note that the α values for all four surfactants

are very close to each other, a property which has been observed in other surfactant families.[168] The hydrated surfactant molecular volume increases with the number of EO groups in the head, as expected. However, the hydration number, the number of water molecules per EO group in the head, decreases with the number of EO groups in the head. The behavior of the hydration numbers will be further discussed below.

In order to gain a better understanding of the meaning of the deduced parameters, they can be compared with similar data from other researchers. Unfortunately, only one other study, a light scattering investigation by Minero et al.[129] was performed on dodecyl ethoxy sulfates at the same conditions examined in the present work. Their light scattering data resulted in larger Hamaker constants and larger fractional charges than those found in the present study. Specifically, they found that $A = 6k_BT$ and $\alpha = 0.30$ for E2S while $A = 1k_BT$ and $\alpha = 0.40$ for E4S (they were unable to fit the data for E1S). However, their study focused only on intermicellar interactions,[129] while both interactions and micellar growth are considered in the present study. If micellar growth is neglected, stronger interactions are required to explain the observed D_c and M_{app} values. For example, when the experimental D_c decreases at higher salt concentrations, they assumed that the observed decrease was due solely to attractive intermicellar interactions rather than to micellar growth,[129] which could only be explained by using relatively high values of A. Consequently, larger values of α were required to balance the large values of A. In the present study, the observed decrease in D_c reflects both micellar growth and intermicellar interactions, and therefore, the deduced A values are smaller. Indeed, when the data of Minero et al. is subjected to the same fitting procedure described above, the deduced A and α values are similar to those found in the present study (within experimental error).

The hydration numbers deduced in the present study (see Table 7.4) are similar to those obtained for some other ionic surfactants. For example, as mentioned above, neutron scattering studies find the hydration of SDS to be approximately 10 water molecules per surfactant molecule,[167] while light scattering studies indicate that dodecyl trimethylammonium bromide has a hydration of 4 to 16 water molecules per surfactant molecule.[169] However, the deduced hydration numbers listed in Ta-

ble 7.4 are larger than those obtained in the light scattering study by Minero et al. The discrepancy cannot be explained by their neglect of micellar growth, nor is it due to the fitting procedure used in this study. Indeed, when the data of Minero et al. is subjected to the same fitting procedure described above, the resulting hydration numbers are very similar to those found in their study. Instead, the difference in hydration must be due to the fact that our samples were obtained from a different source. It has been shown that micellar properties of alkyl ethoxy sulfates are significantly affected by purity, which can be difficult to achieve.[132, 133] Interestingly, the E4S and E6S hydration numbers found in the present study are very similar to the hydration numbers of nonionic alkyl poly(ethlyene oxide) surfactants.[170]

Specific results on micelle shape and size are presented in the following two sections.

7.4.2 E1S and E2S

Using the fitting procedure described above, the light scattering data was used to determine the shape and size of E1S and E2S micelles as a function of NaCl concentration. Figure 7-1 shows the measured average micelle hydrodynamic radius, R_H, of E1S and E2S micelles as a function of NaCl concentration for a fixed surfactant concentration of 50mM at 25°C. Figure 7-2 shows the measured average micelle aggregation number, N_{agg}, for the same experimental conditions. At low salt concentration (0.1M NaCl), the E2S micelles (circles) are small, with an average hydrodynamic radius and an average aggregation number that are consistent with a small spherical micelle. (For comparison, the length of the fully-extended E2S molecule is approximately 30Å. Recall that the R_H values in Figure 7-1 also include the water of hydration.) The E1S micelles (diamonds) are slightly bigger than the E2S micelles at this salt concentration, but are still quite small. As the NaCl concentration increases beyond 0.1M, R_H and N_{agg} of the E1S micelles increase, indicating that the micelles are growing. The E2S micelles remain approximately the same size up to 0.2M NaCl, but beyond this salt concentration, they also exhibit significant increases in R_H and N_{agg}. Note that the results in Figures 7-1 and 7-2 are based on the prolate ellipsoid

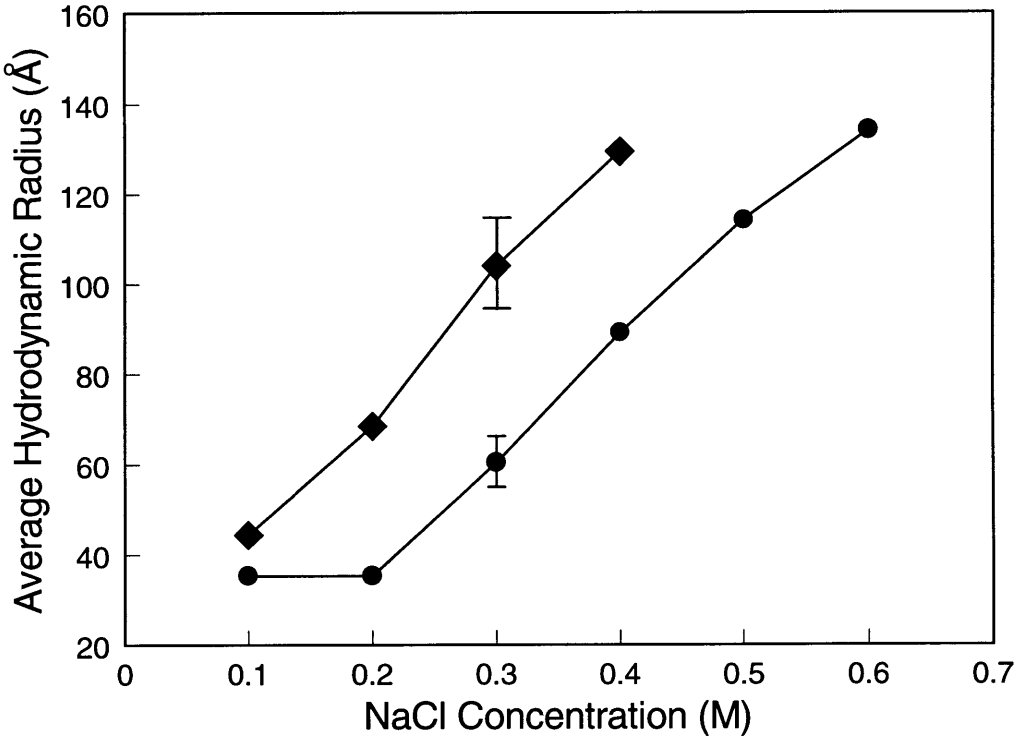

Figure 7-1: Average micelle hydrodynamic radius, R_H, calculated from the dynamic light scattering data as a function of NaCl concentration for E1S micelles (diamonds) and E2S micelles (circles) at a 50mM surfactant concentration and T=25°C. The error in measurement was approximately 10%, as indicated by the representative error bars shown. The lines are drawn to guide the eye.

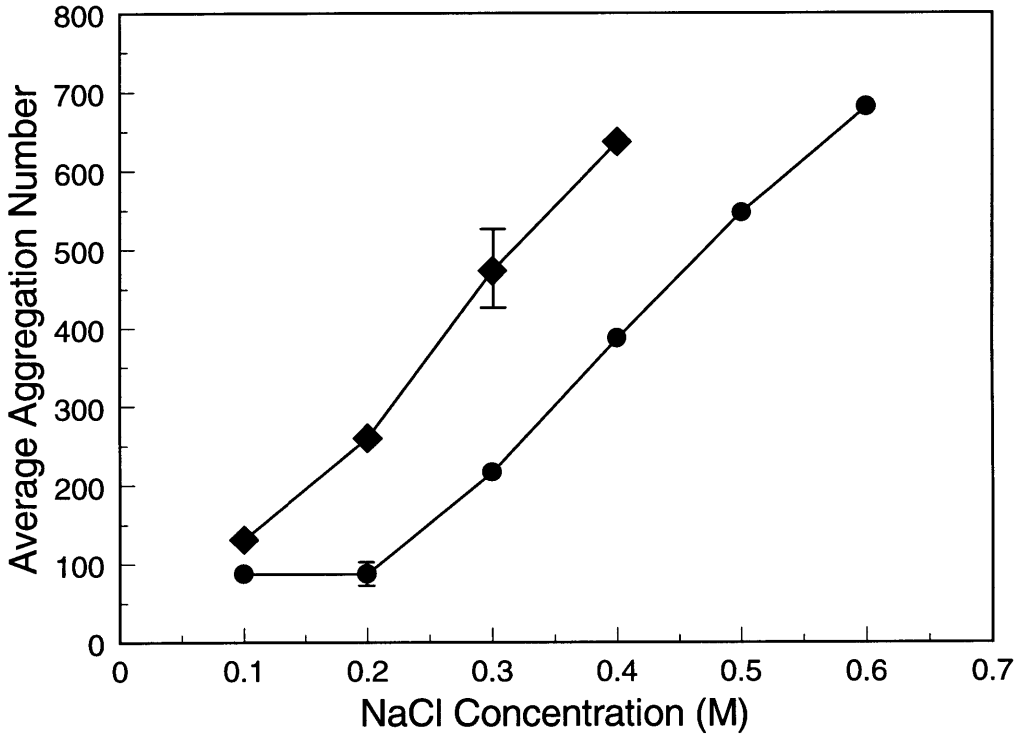

Figure 7-2: Average micelle aggregation number, N_{agg}, calculated from the static light scattering data as a function of NaCl concentration for E1S micelles (diamonds) and E2S micelles (circles) at a 50mM surfactant concentration and T=25°C. The error in measurement was approximately 10%, as indicated by the error bars shown. The lines are drawn to guide the eye.

model which was found to give the best fit to the data (smallest RMS), indicating that the micelles exhibit one-dimensional growth with increasing salt concentration, rather than two-dimensional growth.

For comparison, SDS micelles have been observed to grow at approximately 0.5-0.6M NaCl.[9, 72, 73] In the case of E1S, the charge on the sulfate group is displaced from the micellar core by the EO group, resulting in a lower surface charge density. In addition, the charge may be somewhat shielded by the dipoles of the water of hydration surrounding the EO group. Both of these effects allow the micelle to grow beyond the lower salt concentration of about 0.1M NaCl. For E2S, the charge is displaced even further from the micellar core. However, the presence of the additional EO group induces larger steric head/head interactions, thus delaying the micellar growth to 0.2M NaCl. Note that light scattering measurements could not be conducted on solutions of E1S and E2S at NaCl concentrations greater than 0.4M NaCl and 0.6M NaCl, respectively, because their high viscosity prevented filtration.

To confirm the E1S and E2S micellar growth deduced from the light scattering results, viscosity measurements were conducted on E1S and E2S aqueous solutions at a low (0.1M) and a high (0.4M) NaCl concentration. Note that 0.1M NaCl is the lowest NaCl concentration for which it has been proven that electroviscous effects are negligible,[159, 160] and 0.4M NaCl is the highest salt concentration for which the viscosity of the E1S solution could be measured accurately on our equipment. The viscosity results are presented in Figures 7-3 and 7-4. Figures 7-3(a) and 7-3(b) show the relative viscosity, η_r, as a function of surfactant concentration at 25°C in 0.1M NaCl for E1S (diamonds) and E2S (circles), respectively. Figure 7-4 is a similar plot in 0.4M NaCl. The data at 0.1M NaCl show that, at this low salt concentration, η_r increases linearly with c_s (see lines in Figure 7-3), indicating that the micelles behave like ideal spheres, according to Eq. (7.21). In contrast, at 0.4M NaCl (see Figure 7-4), η_r increases at a greater, nonlinear rate, consistent with the light scattering evidence that the micelles have elongated. In addition, a comparison of the η_r values for E1S and E2S in Figure 7-4 indicates that the E2S micelles exhibit less growth than the E1S micelles.

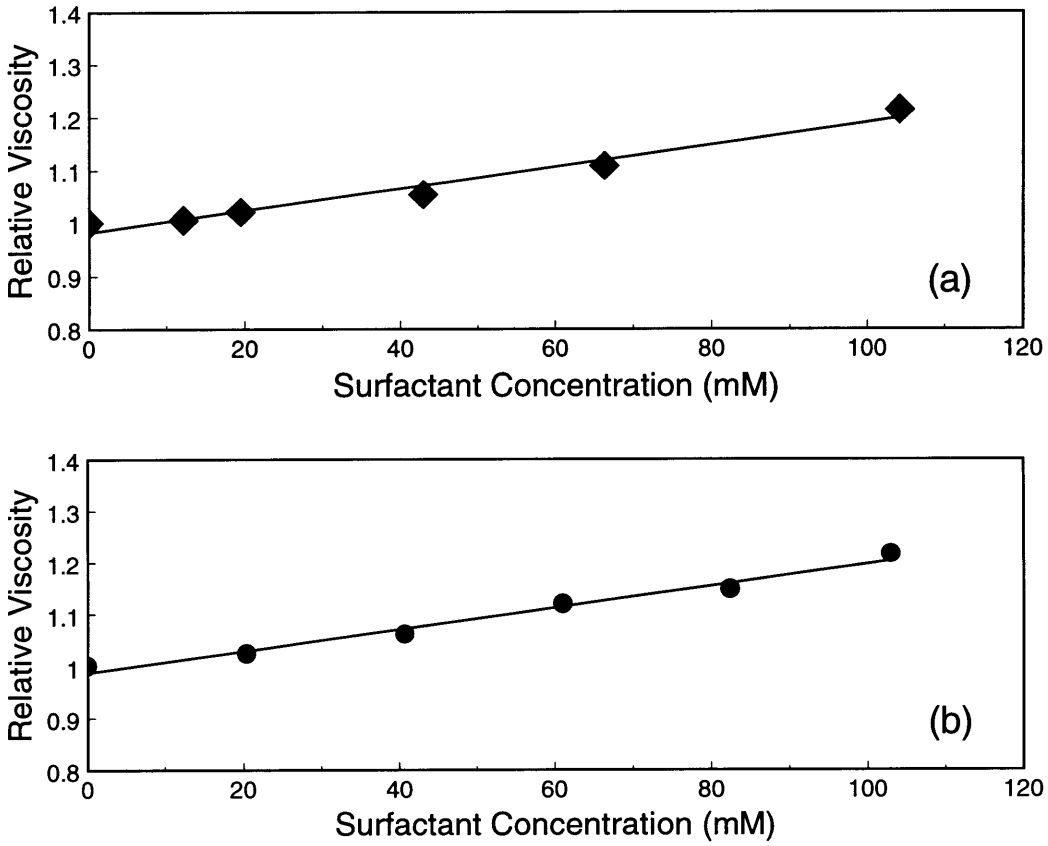

Figure 7-3: Relative viscosity, η_r, of (a) E1S (diamonds) and (b) E2S (circles) aqueous micellar solutions as a function of surfactant concentration, c_s, in 0.1M NaCl at 25°C. The error in measurement was within 2%, and therefore, the error bars are smaller than the size of the symbols. The lines denote the best linear fit through the experimental data.

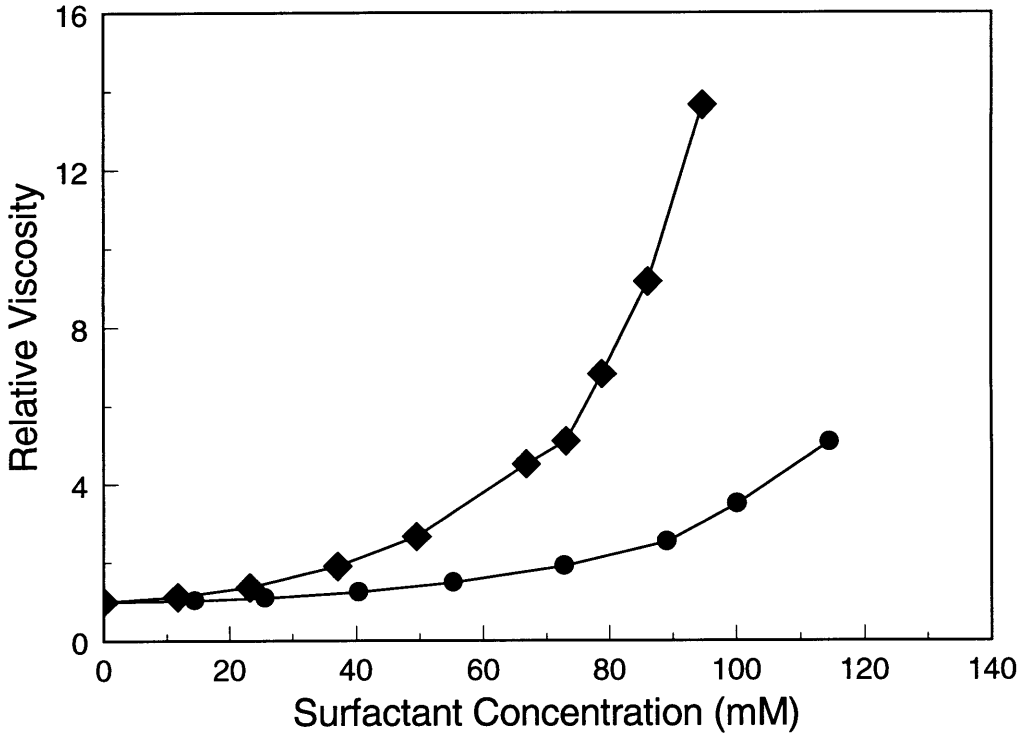

Figure 7-4: Relative viscosity, η_r, of E1S (diamonds) and E2S (circles) aqueous micellar solutions as a function of surfactant concentration, c_s, in 0.4M NaCl at 25°C. The error in measurement was within 2%, and therefore, the error bars are smaller than the size of the symbols. The lines are drawn to guide the eye.

By fitting the 0.1M NaCl η_r data in Figure 7-3 to Eq. (7.21) (solid lines), the hydrodynamic volumes of the E1S and E2S surfactant molecules could be determined. In order to distinguish between the hydrated volume derived from the viscosity data and the v_s^{hyd} derived from the light scattering data (see Table 7.4), the viscosity-deduced hydrated surfactant volume will be denoted as $\hat{v}_s^{hyd}$. For E1S, $\hat{v}_s^{hyd} = 1190\text{Å}^3$, and for E2S, $\hat{v}_s^{hyd} = 1250\text{Å}^3$. These values are slightly lower than the v_s^{hyd} values obtained from the light scattering data (1450Å^3 for E1S and 1540Å^3 for E2S, see Table 7.4). In fact, it is not clear whether these two hydrated volumes, v_s^{hyd} and $\hat{v}_s^{hyd}$, should be equivalent.[143, 163, 171, 172, 173] In many studies, it appears that different experimental methods measure different extents of hydration,[128, 163, 171] with some disagreement over which method should yield larger hydration numbers. From studies on block copolymer micelles[171] and on asphaltene aggregates,[173] it has been observed that neutron and light scattering measurements yield larger hydration numbers than viscosity measurements, in agreement with our results.

To further probe the region of micellar growth, the light scattering and viscosity results were compared as follows. The light scattering data was analyzed as described above for four representative shapes: spheres, prolate ellipsoids, oblate ellipsoids, and spherocylinders. The axial ratio can be calculated from the deduced R_H values using the expressions for R_H given in Table 7.3 for each shape. From the axial ratio, the shape factor for each shape could be obtained, as described in Table 7.3. The relative viscosity can then be calculated using Eq. (7.21) for spherical micelles, and Eq. (7.20) for the other micellar shapes. The $\hat{v}_s^{hyd}$ value obtained from the η_r data at the low salt condition (0.1M NaCl) where the micelles are spherical is used for the hydrated surfactant molecular volume over the entire range of salt concentrations. The resulting *predicted* η_r values are presented in Figure 7-5 for E1S and in Figure 7-6 for E2S as a function of NaCl concentration for each micellar shape examined: prolate ellipsoids (—), spherocylinders ($\cdots$), and oblate ellipsoids ($- - -$). The η_r predictions for the sphere model were very similar to the predictions from the oblate ellipsoid model, and were therefore omitted from these figures for clarity. For comparison, viscosity measurements were conducted on micellar solutions of E1S and E2S under the same

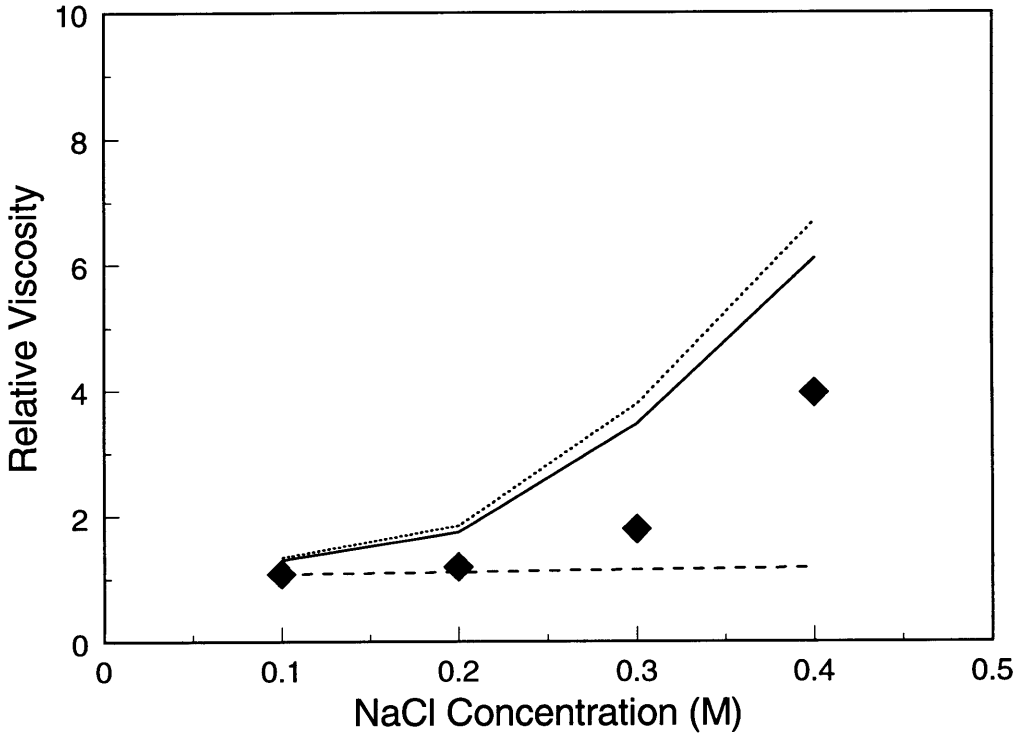

Figure 7-5: Relative viscosity, η_r, of 50mM E1S aqueous micellar solutions as a function of NaCl concentration (diamonds) at 25°C. The lines represent theoretical η_r predictions based on the light scattering data (see text) for prolate ellipsoids (—), spherocylinders ($\cdots$), and oblate ellipsoids (– – –).

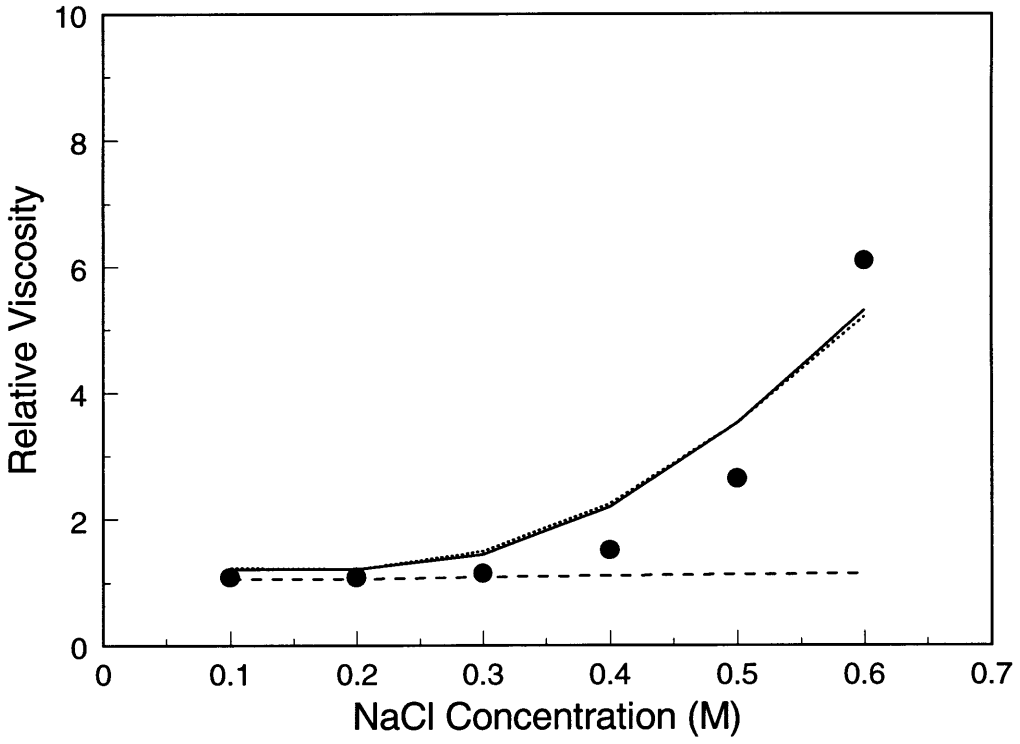

Figure 7-6: Relative viscosity, η_r, of 50mM E2S aqueous micellar solutions as a function of NaCl concentration (circles) at 25°C. The lines represent theoretical η_r predictions based on the light scattering data (see text) for prolate ellipsoids (—), spherocylinders ($\cdots$), and oblate ellipsoids (– – –).

solution conditions (25°C, 50mM surfactant). These are also presented as diamonds in Figure 7-5 for E1S and as circles in Figure 7-6 for E2S.

As the salt concentration increases, both E1S and E2S exhibit a nonlinear increase in η_r, indicating a sphere-to-rod transition, consistent with the light scattering results. For E2S, the η_r predictions show remarkable quantitative agreement with the η_r measurements for the prolate ellipsoid and spherocylindrical models. Although quantitative agreement is not obtained for E1S, it is clear that the upward trend in the η_r measurements (diamonds) is better described as a one-dimensional type of growth (as modeled with a prolate ellipsoid) than a two-dimensional type of growth (as modeled with an oblate ellipsoid). For E2S, it is difficult to distinguish between the prolate ellipsoid model and the spherocylinder model based on the η_r predictions, but it should be noted that the prolate ellipsoid model yields a slightly better fit to the light scattering data (smaller RMS).

The inability of Eq. (7.20) to quantitatively predict η_r values for E1S may be due to the analysis of the intermicellar interactions, which treats elongated micelles as effective spheres. This approximation is clearly inaccurate at the higher salt concentrations where the E1S micelles are elongated. Treating the elongated micelles as effective spheres for the analysis of the intermicellar interactions would slightly increase the R_H values obtained from the light scattering data, which, in turn, would increase the measured axial ratio, thereby increasing the η_r predictions. Because E1S micelles exhibit more growth than E2S micelles, this approximation affects the E1S results more strongly than the E2S results, possibly contributing to the discrepancy in the η_r predictions shown in Figure 7-5.

As mentioned in Section 7.1, the E1S micellar solution was observed to phase separate at room temperature at high ($>$ 0.8M) NaCl concentrations. The cloud-point temperature (the temperature at which the solution phase separates, or becomes turbid) was measured for a range of surfactant concentrations at 0.9M NaCl. The results are presented in Figure 7-7. The scatter in the data is due to the fact that the E1S surfactant molecule began to degrade (hydrolyze) at the high temperature, and therefore, measurements could not be repeated.

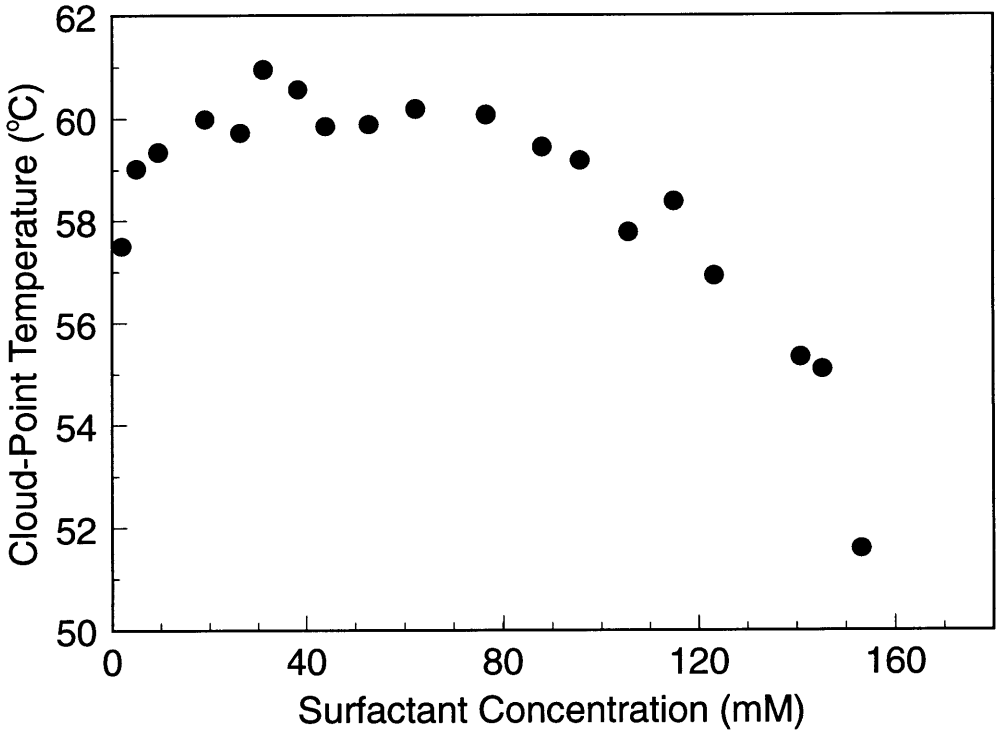

Figure 7-7: Measured cloud-point temperatures as a function of surfactant concentration for aqueous solutions of E1S in 0.9M NaCl.

It is believed that this phase separation is actually a coacervation, whereby the micelle-rich phase consists of a very high concentration of hydrated elongated micelles which are aligned with each other. The driving force for the phase separation is entropic. When the micelles become highly elongated, it is more favorable for them to align with each other, based on excluded-volume considerations.[136, 137, 38] At higher temperatures, it is more favorable for the micelles to be dispersed, and therefore, the solution becomes a single homogeneous phase. This behavior would only occur at high salt concentrations where the E1S micelles are elongated and repulsive electrostatic interactions are screened. Coacervation was not observed for any of the other surfactants at any of the solution conditions examined in this chapter, probably because the micelles did not exhibit the high degree of micellar growth exhibited by the E1S micelles.

7.4.3 E4S and E6S

In order to investigate the effect of NaCl concentration on the shape and size of E4S and E6S micelles, light scattering experiments were conducted at varying NaCl concentrations. Figure 7-8 shows the average micelle hydrodynamic radius, R_H, as a function of added NaCl concentration for solutions of 50 mM E4S (stars) and E6S (squares) at 25°C. It is clear that the E4S and E6S micelles grow very little even at relatively high NaCl concentrations. The small values of the radii (35-40Å) indicate that these micelles are spherical over the entire NaCl concentration range, whereas the E1S and E2S micelles exhibit significant increases in R_H as the NaCl concentration increases (compare Figure 7-8 with Figure 7-1). The steric effects associated with the bulky EO groups dominate the behavior of the E4S and E6S micelles, inhibiting micellar growth even at the high NaCl concentrations.

It is well known in the case of nonionic alkyl ethoxy surfactants that the ethoxy groups dehydrate as the temperature is raised, resulting in micellar growth at high temperatures.[170, 174, 12, 175] To test if this is also the case for the ionic alkyl ethoxy sulfates, light scattering was conducted on E4S and E6S micellar solutions at increasing temperatures. The results are presented in Figure 7-9, where the average

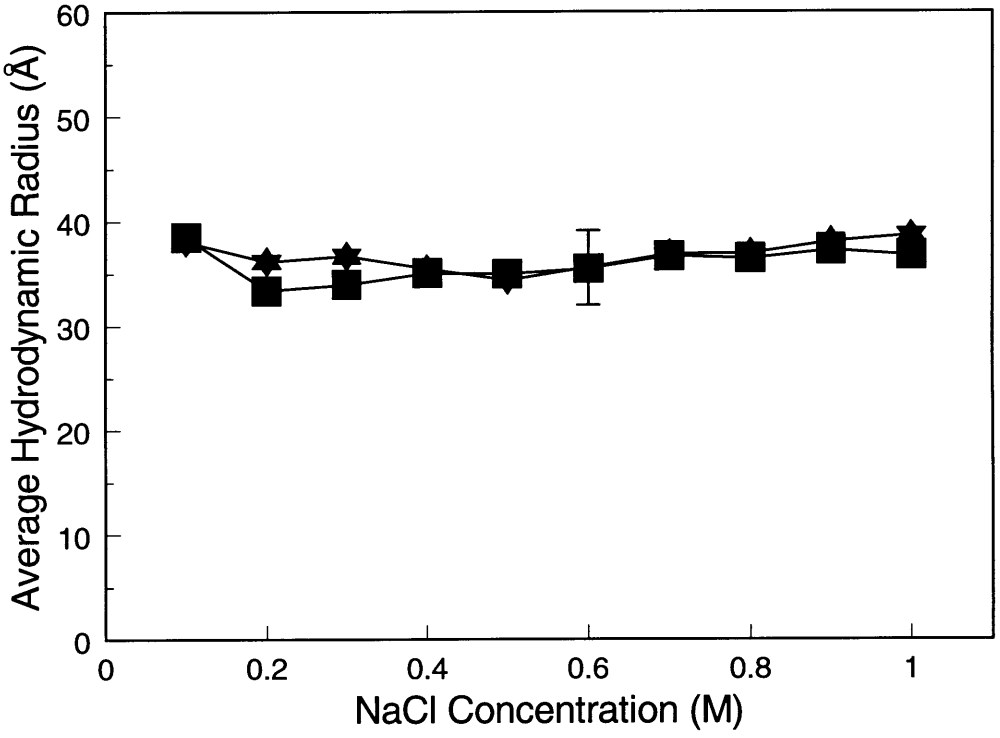

Figure 7-8: Average micelle hydrodynamic radius, R_H, calculated from the light scattering data as a function of NaCl concentration for E4S (stars) and E6S (squares) micelles at a 50mM surfactant concentration and T=25°C. The error in measurement was approximately 10%, as indicated by the representative error bar shown. The lines are drawn to guide the eye.

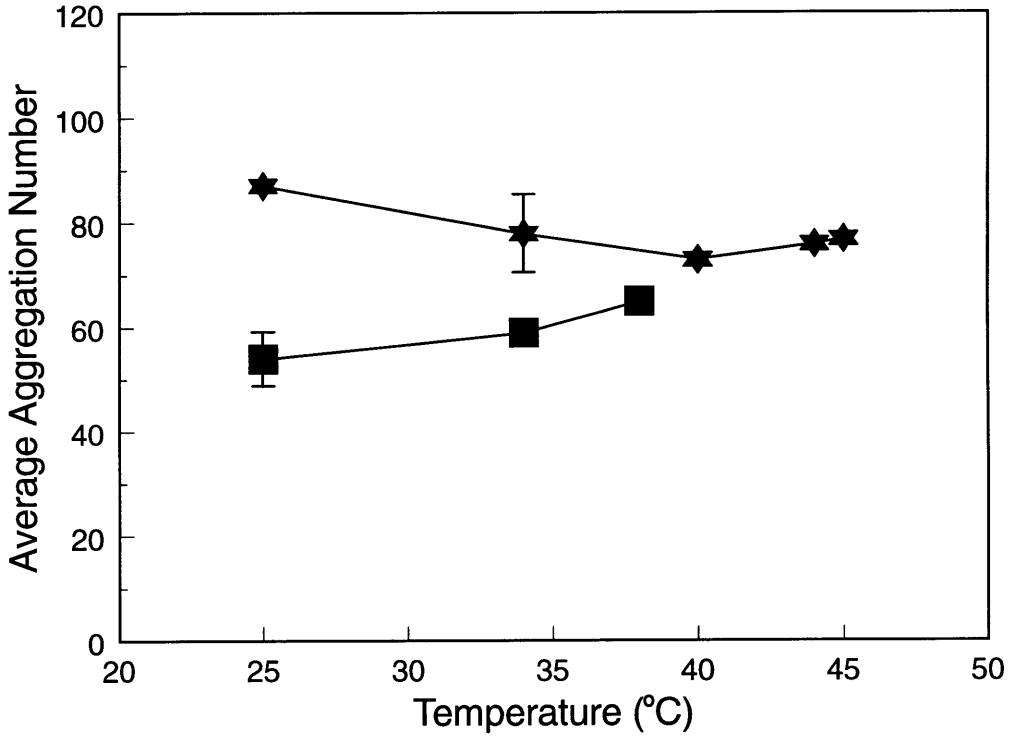

Figure 7-9: Average micelle aggregation number, N_{agg}, calculated from light scattering data as a function of temperature for E4S (stars) and E6S (squares) micelles at a 50mM surfactant concentration in 0.6M NaCl. The error in measurement was approximately 10%, as indicated by the representative error bars shown. The lines are drawn to guide the eye.

micelle aggregation number, N_{agg}, is shown as a function of temperature for 50mM E4S (stars) and E6S (squares) micellar solutions in 0.6M NaCl. The relatively high NaCl concentration was selected to ensure that electrostatic interactions among the surfactant heads would be considerably reduced. It is clear that, even at the higher temperatures, the E4S and E6S micelles remain approximately the same size, within experimental error. The E4S micelles have a slightly higher N_{agg} value (≈ 80) than the E6S micelles (≈ 60). This reflects the fact that the E4S head is smaller than that of E6S, and therefore, it can pack more tightly into a micelle, resulting in higher aggregation numbers. This difference is also reflected in the hydrated surfactant volumes (1860Å^3 for E4S versus 2140Å^3 for E6S, see Table 7.4).

The light scattering results presented in Figures 7-8 and 7-9 were interpreted using the spherical shape model which resulted in the best fit to the data (smallest RMS). In fact, the prolate ellipsoid model resulted in axial ratios that were close to one, indicating that these micelles remain spherical over the range of NaCl concentrations and temperatures examined. Interestingly, it was found that the v_s^{hyd} value did not depend on temperature, indicating that these micelles do not dehydrate as the temperature is increased, in contrast to the nonionic alkyl ethoxy surfactants.[52, 170] The constant v_s^{hyd} value is consistent with the constant micelle size as the temperature increases. In other words, if the EO groups do not dehydrate, there is no incentive for the micelle to elongate. It is possible that a larger temperature range is required to observe dehydration. Indeed, the molecular-thermodynamic theory presented in Chapter 2 predicts that, for example, the volume of the nonionic $C_{12}E_6$ surfactant changes by only 25Å^3 (less than the volume of one water molecule) as the temperature is increased by 20°C.[16]

The highest temperature plotted in Figure 7-9 for E6S is 38°C. Above this temperature, a second peak appeared to develop in the micellar size distribution at very high radii. As the temperature was increased, the second peak shifted to even higher sizes (from 1500Å up to 2000Å). Although this second peak was much smaller than the first peak at 35Å, because it was located at much higher sizes, it skewed the value of the resulting average micelle radius. In quasielastic light scattering, it is possible to

distinguish between the two different length scales and only use the one related to the actual micelle size. However, static light scattering measures the *average* scattered intensity. There is no straightforward way to distinguish between the two length scales in static light scattering. Hence, the analysis was limited to temperatures where only one scattering length scale was detected ($\leq 38°C$).

There are three possible explanations for the second peak. First, the micelles could be "clumping" together, as has been hypothesized for a nonionic alkyl ethoxylate.[176, 177, 178] The second explanation is that a very large aggregate, such as a vesicle, could be forming at high temperatures.[144] The third, and most likely, possibility is that the second peak represents some long-range correlations between the micelles.[12, 52, 152] At high temperatures, it is possible that attractive interactions could develop between neighboring micelles. As the temperature is increased further, the attractions would become longer ranged. This type of behavior is common among the nonionic alkyl ethoxylates, and eventually leads to phase separation.[52, 12] Although phase separation was not detected in the E6S system, it is possible that it occurs in a temperature region that has not yet been examined.

Viscosity measurements were performed in order to confirm the light scattering results and test for the presence of aggregating micelles or vesicles. Figures 7-10(a) and 7-10(b) illustrate the relative viscosity of (a) E4S (stars) and (b) E6S (squares) aqueous micellar solutions as a function of surfactant concentration in 0.6M NaCl at 45°C. The dashed lines (– – –) represent the best linear fit through the data points. The solid lines (—) are viscosity predictions made using Eq. (7.21) with the v_s^{hyd} values determined from the light scattering analysis (see Table 7.4). The excellent fit to Eq. (7.21) indicates that these micelles are small, spherical aggregates with ideal flow behavior. The close resemblance between the η_r predictions (—) and the fit through the experimental data (– – –) is remarkable. By fitting the experimental data (– – –) to Eq. (7.21), a $\hat{v}_s^{hyd}$ value can be obtained from the η_r measurements. This fit results in $\hat{v}_s^{hyd}$ values of 1470Å^3 for E4S and 2040Å^3 for E6S, slightly smaller than the v_s^{hyd} volumes derived from the light scattering data, similar to the results for E1S and E2S.

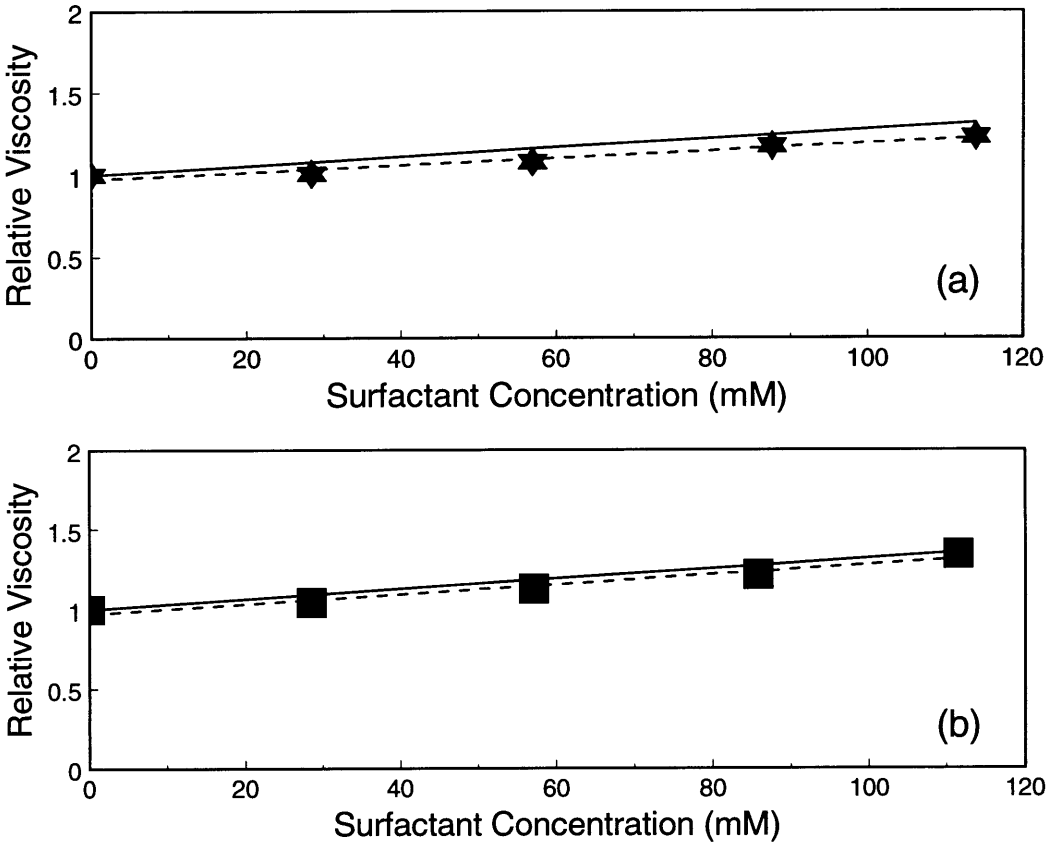

Figure 7-10: Relative viscosity, η_r, of (a) E4S (stars) and (b) E6S (squares) micellar solutions as a function of surfactant concentration in 0.6M NaCl at 45°C. The error in measurement was within 2%, and therefore, the error bars are smaller than the size of the symbols. The solid lines are theoretical viscosity predictions for spherical micelles based on the light scattering data (see text). The dashed lines are linear fits through the experimental data.

7.5 Conclusions

The alkyl ethoxy sulfates with the smaller heads, E1S and E2S, exhibited siginificant micellar growth upon the addition of NaCl, as measured using both light scattering and viscosity. The prolate ellipsoid model gave the best fit to the data, indicating that these micelles exhibit one-dimensional growth with increasing NaCl concentration. In addition, the light scattering data was utilized to *predict* the relative viscosity, which was independently confirmed with actual viscosity measurements. For E2S, quantitative agreement was obtained for the prolate ellipsoid and spherocylindrical models, which is indicative of one-dimensional growth. For E1S, although the predicted η_r values did not agree quantitatively with the experimental values, the viscosity measurements clearly indicated that the micelles exhibit one-dimensional growth, in qualitative agreement with the light scattering results. Interestingly, the micellar growth of E1S eventually led to phase separation at high (> 0.8M) NaCl concentrations.

E2S formed smaller micelles than E1S, indicating that the additional EO group induces more significant steric effects among the surfactant heads. Indeed, the larger heads of E4S and E6S resulted in little or no micellar growth, even at the highest NaCl concentrations (up to 1.0M NaCl), indicating that steric interactions among these bulky heads at the micelle surface have a significant effect on the properties of the micelle. These micelles remained spherical, even at high temperatures (up to 45°C). Unlike the nonionic alkyl ethoxylates,[170, 174, 12, 175] the E4S and E6S surfactants do not appear to dehydrate as the temperature increases, at least over the temperature range examined in this chapter. The charged sulfate group has a high number of water molecules clustered around, as is typical of ionic surfactants.[167, 169] Perhaps, the effect of the sulfate charge extends throughout the entire head region, causing the water of hydration to remain bound, and thus preventing micellar growth, in contrast to the nonionic alkyl ethoxylate case.

In analyzing the intermicellar interactions, the micelles were treated as effective spheres, even under conditions where they were clearly elongated. This approximation

affected not only the deduced R_H and N_{agg} values shown in Figures 7-1 and 7-2, as well as in Figures 7-8 and 7-9, but also the values of the deduced parameters α, A, and v_s^{hyd}. In particular, E1S exhibited a high degree of growth. The inaccurate treatment of the intermicellar interactions for these elongated micelles led to a discrepancy in the η_r predictions (see Figure 7-5). In the future, as techniques for analyzing intermicellar interactions between *elongated* micelles are developed, the light scattering data for E1S should be reexamined.

Additional alkyl ethoxy sulfates should be investigated to further explore the interplay of the electrostatic interactions between the charged sulfate groups and the steric interactions between the hydrated EO groups. It may also be interesting to examine a wider range of solution conditions. In particular, at high temperatures, the E6S micelles exhibited a second peak at large length scales, possible evidence for the presence of long-range attractive interactions. It would be interesting to determine if there are solution conditions, such as higher salt concentrations or higher temperatures, where these attractive interactions could actually lead to phase separation. It may also be possible to see the same behavior in the E4S micelles at higher temperatures. In this case, the micellar solutions would exhibit a lower critical point rather than an upper critical point, as in the coacervation behavior displayed by E1S. This and other suggestions for future research on dodecyl ethoxy sulfates are discussed in the next chapter.

Chapter 8

Conclusions and Future Research Directions

Surfactant solutions display a variety of micelle shapes and sizes, and exhibit a rich phase behavior. Ionic surfactants, in particular, are very commonly used, yet are poorly understood due to the complex electrostatic intramicellar and intermicellar interactions affecting their aqueous solution behavior. This thesis attempted to contribute to a better molecular-level understanding of ionic surfactant solution behavior through both theoretical and experimental investigations, discussed in detail in the previous chapters. In this chapter, the key results of the thesis will be summarized, and possible directions for future research will be discussed.

8.1 Thesis Summary

A molecular-thermodynamic theory of micellization and micellar solution phase behavior had previously been developed by our group for nonionic surfactants. The first major contribution of this thesis was to extend this theory to include ionic surfactants, as discussed in Chapter 2. To calculate the electrostatic contribution to the free energy of micellization, the Poisson-Boltzmann equation was used. Because the Poisson-Boltzmann equation is nonlinear, in order to simplify the calculations and associated computational time, several analytical approximations from the literature

were utilized and compared. To correct for the neglect of the finite size of the ions in the ion cloud, a Stern layer, which is the region immediately surrounding the micelle surface from which the counterions are excluded, was added to the model. Including the Stern layer improved CMC predictions, and provided some counterion specificity (the width of the Stern layer is equal to the radius of the hydrated counterion). However, the Stern layer model severely inhibits growth of ionic micelles in the presence of added salt, contrary to experimental observations. It is believed that this underestimation of micelle size is due to the neglect of electrostatic and excluded-volume intermicellar interactions, which eventually led to the development of a new thermodynamic approach based on rigorous statistical-mechanical principles, as described in Chapters 4 through 6.

In an effort to quantify the actual surface charge of the micelle, the Gibbs adsorption equation was utilized to model the fractional counterion binding. A complete derivation was presented in Section 2.4. Although this theoretical description was found to underestimate the experimentally-measured counterion binding, it correctly predicts the observed experimental trends, as demonstrated through several sample predictions.

In addition to the CMC and the counterion binding predictions presented in Chapter 2, the molecular-thermodynamic theory is capable of predicting a wide range of micellar solution properties for a variety of ionic, nonionic, and zwitterionic surfactants. In an effort to make this theory more accessible to both industrial and academic surfactant researchers, the theory was incorporated into a user-friendly computer program which can make predictions in a matter of seconds. This program, known as program PREDICT, was described in detail in Chapter 3. Examples of many of its predictive capabilities were presented and compared with experimental data.

As mentioned above, the molecular-thermodynamic theory with a Stern layer model underestimates micelle size for ionic surfactants. This underestimation is probably due to the neglect of electrostatic intermicellar interactions, which can have a significant effect on micelle shape and size. In an effort to address intermicellar interactions using a more rigorous, systematic approach, a new statistical-thermodynamic

framework for micellar solutions based on the McMillan-Mayer theory of multicomponent solutions was developed. This theoretical framework was described in detail in Chapter 4. The key result of this framework is an expression for the micellar size distribution. All that is needed to implement the theoretical framework is an appropriate model for the standard-state and EXCESS chemical potentials of the micelles and the monomers.

First, as described in Chapter 5, a model was developed for nonionic surfactant solutions exhibiting attractive and excluded-volume intermicellar interactions, which are, in general, simpler to model than the electrostatic intermicellar interactions. It was found that repulsive intermicellar interactions, such as those of the excluded-volume type, encourage micelle formation and growth. In addition, it was demonstrated that this model could be used to make accurate predictions of several micellar solution properties, such as the CMC, the critical concentration for phase separation, and the osmotic compressibility.

The McMillan-Mayer approach was extended to model the behavior of ionic surfactant solutions in Chapter 6. To model the electrostatic intermicellar interactions, the other charged micelles in solution were included as part of the diffuse ion cloud surrounding the central charged micelle. Two models were used to calculate the electrostatic potential created by the charged micelle and the diffuse ion cloud. First, the Debye-Hückel approximation provided an analytical solution. Because it can be utilized to model both spherical and cylindrical micelles, it could be used to predict micellar growth. Indeed, it was demonstrated that electrostatic intermicellar interactions encourage micellar growth, which is a significant improvement over the predictions of the molecular-thermodynamic theory presented in Chapter 2. However, the Debye-Hückel solution is only an approximation for the electrostatic potential. To improve the accuracy of the calculation of the electrostatic surface potential, a modified Poisson-Boltzmann equation, which includes the effect of the finite size of the ions throughout the ion cloud, was formulated. This description provides a more accurate representation of the electrostatic potential, but it can only be used in the case of spherical micelles. Both models presented in Chapter 6 require some improve-

ments before good quantitative accuracy of the predictions, as compared with the experimental measurements, is obtained. However, they represent a valuable "first step" in the development of a theory for electrostatic intermicellar interactions.

In order to obtain additional data on micellar solution properties, an experimental investigation on dodecyl ethoxy sulfate micelles with 1, 2, 4, or 6 EO groups was conducted. As described in Chapter 7, both static and dynamic light scattering and viscosity techniques were used to measure micelle shape and size at various salt concentrations and temperatures. The DLVO potential was used to quantify the effect of intermicellar interactions on the light scattering data. In addition, quantitative agreement between the light scattering and the viscosity results was attained. It was found that the surfactants with one and two EO groups exhibit one-dimensional growth in the presence of added salt. The added salt screens the electrostatic repulsions among the charged sulfate groups, allowing the micelles to elongate from spheres into cylinders. In contrast, the surfactants with four or six EO groups remain small and spherical over the entire range of salt concentrations and temperatures examined. It is believed that steric interactions among these bulky EO groups prevented micellar growth. This experimental investigation provided valuable insight into the molecular-level interactions which govern the observed equilibrium micelle shapes and sizes.

8.2 Future Research Directions

8.2.1 Theoretical Investigations

Molecular-Thermodynamic Theory

As described in Chapter 2, the molecular-thermodynamic theory of micellization was developed for surfactants consisting of a linear hydrocarbon (or fluorocarbon) tail. Not all surfactants fit into this category. For example, many surfactants have double bonds in their tails, or have branched hydrocarbons as tails. Block copolymer surfactants, particularly those having a poly(propylene oxide) tail and a poly(ethylene

oxide) head, are becoming more common. A new family of surfactants, known as "gemini" surfactants, have two heads and two tails linked together with a hydrocarbon spacer chain.[179, 180] It would be useful to expand the molecular model of micellization to include these novel surfactant structures. In particular, g_{pack}, the free energy associated with packing the surfactant tails in the micellar core, would have to be reevaluated for the novel tail structures. For the gemini surfactants, g_{ster}, the free energy associated with packing the surfactant heads at the micellar surface, would have to be recalculated to account for the connection between the two heads. In addition, if the heads were charged, their effect on g_{elec} would also have to be considered.

In order to model elongated micelles, the free energy of micellization was calculated by linearly interpolating between the free energies of micellization corresponding to spheres and to infinite cylinders. It is unclear whether this is a good approximation if the cylinders are not sufficiently long, particularly with regard to the longer-ranged electrostatic contribution, g_{elec}. Recently, new computational methods for solving the Poisson-Boltzmann equation for ellipsoidal geometries have been developed.[181, 182, 183] Although they can be computationally challenging, it may be worthwhile to explore these new methods to determine if an ellipsoidal shape provides a more accurate representation than the spherocylindrical model for elongated micelles whose size is finite.

The thermodynamic framework presented in Section 2.2 was general, that is, it included micelles of all shapes (S) and sizes (l_c). However, in later calculations, it was assumed that all the micelles exist in the optimal shape, S^*, and micelle core radius, l_c^*. In fact, this is a very good approximation, particularly when the micelles exhibit growth, and the distribution around l_c is very sharply peaked. However, it would be instructive to consider a solution at the transition region where micelles of various shapes and sizes coexist, in which case the entire distribution of l_c and S values should be considered.

Recall that the total free energy of the solution includes a term based on the free energy of mixing the micelles, the monomers, and the water molecules. In the case

of ionic surfactants, the solution also contains counterions, and therefore, the free energy of mixing should also include the mixing of the counterions. This contribution was neglected in the thermodynamic framework presented in Section 2.2. Future researchers may find it worthwhile to modify the thermodynamic framework to include this contribution, keeping in mind that it should be consistent with the description of counterion binding presented in Section 2.4.

In modeling the counterion binding, it was assumed that the counterions do not participate in the micellization process explicitly, but instead are part of a diffuse ion cloud interacting with the micelle being formed. In Appendix C, an alternative approach was presented, whereby a certain fraction of the surfactant molecules in the micelle do not dissociate, and the bound counterions are explicitly included in the micellization description. Theoretical results of this approach are presented in Appendix C, where it was shown that the CMC's predicted using both approaches should be the same. However, more work is required to actually prove that the two approaches are equivalent. Specifically, the model for the calculation of the free energy of micellization when counterions are included explicitly, $\tilde{g}_{mic}$, should be modified to incorporate the effect of the bound counterions, not accounted for in the original calculation of g_{mic}. In particular, the bound counterions will reduce the surface charge density of the micelle, thus significantly decreasing the electrostatic contribution to the free energy of micellization.

McMillan-Mayer Statistical-Thermodynamic Framework

The McMillan-Mayer statistical-thermodynamic framework presented in Chapters 4 through 6 provided a rigorous, systematic investigation of intermicellar interactions, including both excluded-volume and electrostatic interactions, for solutions of single surfactants. However, for many practical purposes, surfactants are used in mixtures, where the composition has been optimized to attain a specific desired property. The molecular-thermodynamic theory of micellization with a Stern layer has already been extended to model binary mixed micelles.[184, 185, 186, 187] The next step is to extend the McMillan-Mayer approach to mixed micelles in order to more accurately

study the effect of intermicellar interactions on the mixed surfactant solution behavior. This is a challenging problem, because there is an additional variable to deal with in the binary mixed micelle case, namely, the solution composition. However, because so many practical applications exploit surfactant mixtures, such a theoretical effort appears worthwhile.

The statistical-thermodynamic framework described in Chapter 4 was developed for micelles which are in their optimal micellar shape, S^*, and optimal micelle core radius, l_c^*. This framework could be generalized to incorporate a micellar solution with a distribution of micelle shapes and sizes, as was done in the case of the molecular-thermodynamic theory described in Section 2.2. Including a range of micelle sizes in the context of the McMillan-Mayer approach is a challenging problem, because both the electrostatic and the excluded-volume EXCESS chemical potentials would also have to be modified to include the full range of micelle core radii. Of course, as discussed above, assuming that all the micelles are at the optimal radius, l_c^*, is typically a very good assumption, and therefore, the inclusion of these additional features may not be as worthwhile.

A key issue that requires improvement relates to the model for the electrostatic intermicellar interactions presented in Chapter 6. The Debye-Hückel model is versatile in that it can model charged cylindrical micelles, and therefore, it can be used to model micellar growth in ionic surfactant systems. However, it is not an accurate representation of the electrostatic potential. The modified Poisson-Boltzmann equation is more accurate, but it cannot yet be utilized to model charged cylindrical micelles. It was demonstrated that including electrostatic intermicellar interactions improves the predictions of micelle size, so it is clear that developing a more accurate model for the electrostatic interactions between charged elongated micelles is worth the additional theoretical and computational effort. An interesting approach is to use the modified Poisson-Boltzmann equation for the case where the central charged micelle is an infinite cylinder, but the micelles in the ion cloud are treated as effective spheres. The EXCESS electrostatic chemical potential of an elongated micelle could then be calculated by interpolating between the chemical potentials corresponding

to an infinite cylinder and a sphere. This is an interesting way to approximate the electrostatic EXCESS chemical potential of a charged spherocylindrical micelle in the presence of other charged micelles. The required theoretical development appears to be relatively straightforward, but the calculations may be time-consuming due to the extra interpolation step. Note that, as discussed above in the context of the molecular-thermodynamic theory, the accuracy of the interpolation should be tested by comparing the predictions with those corresponding to electrostatic models for ellipsoidal micelles.

Another possible approach for calculating the electrostatic potential on the micellar surface is to use a cell model.[24, 25] In a cell model, the solution is divided into cells of equal volume, each containing one micelle and associated counterions and coions. In the context of the cell model, micelles are not included as part of the ion cloud. Instead, intermicellar interactions are included indirectly through the ion distribution. That is, the counterions , coions, and monomers feel the presence of other charged micelles, and therefore, order around the micelle within the cell accordingly. In addition, the size of the cell depends on the micelle concentration, and therefore, as more micelles are created, the potential has less room to decay. Mathematically, this is accounted for through the boundary conditions. At the boundary of the cell, the potential levels off due to the symmetry of the cells, but never actually decays to zero.

In addition to the modified Poisson-Boltzmann equation that was derived in Section 6.4.2, a more well-known modified Poisson Boltzmann equation has been derived which includes liquid-state theory corrections for the ion/ion correlations.[188] This equation can be implemented in the context of the cell model, and is referred to as the MPB equation. The MPB equation is fairly complex mathematically, but it can be applied to spherical, cylindrical, and planar geometries.[189, 190, 191] It would be interesting to implement the MPB equation to determine the effect of a more accurate model of the electrostatic potential on the resulting micellar solution properties.

Finally, as discussed in Appendix G, alternatives to the charging approach are available. A simple liquid-state theory model was presented in Appendix G.1, the

MSA model, which reduced to the Debye-Hückel solution in the limit where the solutes in the ion cloud are point charges. Alternative liquid-state theory approaches are available. For example, Ronis et al. combined[192] the more complex hypernetted-chain approximation (HNC) for the micelle/micelle pair potential with the analytical mean-spherical approximation (MSA) for all other pair potentials (micelle/counterion, micelle/monomer, counterion/coion, etc). In this way, an analytical solution was obtained. Perhaps, some of these principles could be applied to calculate the EXCESS electrostatic chemical potentials.

8.2.2 Experimental Investigations

In addition to the theoretical improvements described above, there are several experimental improvements that could be made as part of future research. The key improvement to be made is to develop a more accurate method for interpreting the light scattering data of charged elongated micelles. As discussed in Chapter 7, in the analysis of the intermicellar interactions, the elongated micelles were treated as effective spheres. This introduced some error in the deduced values of the average hydrodynamic radius and aggregation number for E1S, because the E1S micelles exhibited significant micellar growth. Currently, no model is available to describe electrostatic intermicellar interactions between finite cylindrical or ellipsoidal micelles. As better approaches are developed to model these anisotropic shapes, the light scattering data for E1S should be reexamined.

The micellar growth of the E1S micelles eventually led to phase separation at high salt concentrations. The coexistence curve was measured in 0.9M NaCl. It is postulated that this phase separation corresponds to a coacervation of the micelles. In coacervation, the micelles grow to be very long, and therefore, find it entropically favorable to align, thus forming a separate liquid-crystalline condensed phase. The resulting condensed phase should be examined more closely to determine if it is indeed liquid-crystalline. It would be interesting to measure the coacervation phenomenon at additional salt concentrations, in order to map out the entire cloud-point temperature surface as a function of both surfactant and salt concentration. In addition, more

studies should be conducted to determine if any of the other dodecyl ethoxy sulfates phase separate at solution conditions outside of the range examined in the study presented in Chapter 7. Finally, this coacervation phenomenon is not predicted by any of the theoretical models presented in this thesis. As better models of intermicellar interactions are developed, perhaps eventually, they will be able to predict this complex phenomenon. A systematic investigation of coacervation, linking experimental results with theoretical predictions, may also help in gaining a better understanding of the molecular-level interactions responsible for coacervation.

Recall that a second peak at large length scales was observed for E6S at high temperatures. This phenomenon should be investigated further in order to quantify it more accurately and determine if it is due to intermicellar interactions. Other scattering methods, such as neutron scattering, may help elucidate the nature of the second peak. If it is representative of long-range attractions, perhaps bulk phase separation occurs at some surfactant or salt concentration not investigated in this study. It is also likely that E4S exhibits this secondary peak at high temperatures.

Based on the experimental results presented in Chapter 7, it appears that E1S and E2S behave like typical ionic surfactants. On the other hand, E4S and E6S behave like typical nonionc surfactants, even to the extent of possibly exhibiting strong attractive interactions at high temperatures. Unfortunately, E3S, the surfactant which bridges between these two groups, was unavailable at the time when this investigation was conducted. In the future, if E3S could be synthesized, it would be interesting to study its micellar properties to determine whether its behavior is dominated by electrostatic interactions among the surfactant heads, as in the case of E1S and E2S, or by steric interactions among the surfactant heads, as in the case of E4S and E6S.

Finally, in addition to the experimental investigation presented in this thesis, a parallel study of the shape and size of mixed micelles formed by E6S and $C_{12}E_6$ has been conducted in our group. Indeed, interesting results have been obtained regarding the impact of steric and electrostatic interactions among the heads of the surfactants forming the mixed micelles.[193] It would be interesting to expand the study of mixed micelles to encompass the other alkyl ethoxy sulfates examined in this thesis, namely,

E1S, E2S, and E4S, and quantitatively link these results with those presented in this thesis for the pure surfactant case.

In this thesis, a thorough theoretical and experimental investigation of the micellization and micellar solution behavior of aqueous ionic surfactant solutions was undertaken. It is hoped that the results presented in this thesis not only expand our knowledge of ionic surfactant solution behavior, but also serve as a basis for continuing investigations of these fascinating systems.

Appendix A

Derivation of the Stern Layer Equations

In this appendix, the boundary conditions and relevant equations required for the Stern layer model are derived. Recall that, as illustrated in Figure 2-2, the Stern layer is denoted as region I, and the diffuse ion cloud is denoted as region II.

According to Gauss' Law, the electric field, E, at a distance r outside a charged body of radius R is given by[68]

$$E = \frac{4\pi R^m \sigma}{\epsilon r^m} = \frac{4\pi R^m ez}{\epsilon a r^m} \tag{A.1}$$

where a is the area per charge, $m = S - 1$, and S is a shape factor ($S = 1$ for infinite bilayers, $S = 2$ for infinite cylinders, and $S = 3$ for spheres).

The electrostatic potential, ψ, is related to the electric field as follows

$$E = -\frac{\partial \psi}{\partial r} \tag{A.2}$$

By applying Eqs. (A.1) and (A.2) at the charged surface of the micelle, that is, at $r = R_{ch}$, the boundary condition given in Eq. (2.32) is obtained, that is,

$$\left(\frac{\partial \psi_I}{\partial r}\right)_{r=R_{ch}} = -\frac{4\pi ez}{\epsilon_1 a_{ch}} \tag{A.3}$$

where ϵ_1 is the dielectric constant in region I, and a_{ch} is the area per surfactant molecule at the surface of charge ($r = R_{ch}$). Note that in Eq. (2.32) of the main text it was assumed that the dielectric constant in region I is the same as that in region II. In other words, $\epsilon_1 = \epsilon_2 = \epsilon$.

At the radius of the Stern layer ($r = R_s$), the electrostatic potential, ψ, must be continuous.[68] In other words,

$$\psi_I(R_s) = \psi_{II}(R_s) \tag{A.4}$$

which is Eq. (2.33) of the main text. In addition, the electric field, or the gradient of the potential, in the direction normal to the boundary must be continuous.[68] In other words,

$$\epsilon_1 E_I(R_s) = \epsilon_2 E_{II}(R_s) \tag{A.5}$$

which implies that

$$\epsilon_1 \left(\frac{\partial \psi_I}{\partial r}\right)_{r=R_s} = \epsilon_2 \left(\frac{\partial \psi_{II}}{\partial r}\right)_{r=R_s} \tag{A.6}$$

Equation (A.6) is Eq. (2.34) of the main text, where it was assumed that $\epsilon_1 = \epsilon_2 = \epsilon$. Note that if charges were physically present on the Stern layer surface (at $r = R_s$), the boundary condition given in Eq. (A.6) would have an additional contribution to account for the charge at the Stern layer surface. Specifically,

$$\epsilon_1 \left(\frac{\partial \psi_I}{\partial r}\right)_{r=R_s} = 4\pi\epsilon_2\sigma_s + \epsilon_2 \left(\frac{\partial \psi_{II}}{\partial r}\right)_{r=R_s} \tag{A.7}$$

where σ_s is the surface charge density at the Stern layer surface. In the model presented here, it is assumed that the charges are infinitesimally displaced from the Stern layer surface, so that $\sigma_s = 0$.

By applying Eqs. (A.1) and (A.2) at the radius of the Stern layer, $R = R_s$, the

following equation is obtained

$$\left(\frac{\partial \psi_I}{\partial r}\right)_{r=R_s} = -\frac{4\pi e z}{\epsilon_1 a_{ch}} \left(\frac{R_{ch}}{R_s}\right)^m \tag{A.8}$$

Making use of the continuity of the electric field, Eq. (A.6), the boundary condition given in Eq. (2.41) of the main text is obtained (recall that $R_s = R_{ch}+\delta_i$). Specifically,

$$\left(\frac{\partial \psi_{II}}{\partial r}\right)_{r=R_s} = \frac{\epsilon_1}{\epsilon_2}\left(\frac{\partial \psi_I}{\partial r}\right)_{r=R_s} = -\frac{4\pi e z}{\epsilon_2 a_{ch}(1+\delta_i/R_{ch})^m} \tag{A.9}$$

The final boundary condition is due to electroneutrality in the bulk where the potential decays to zero, namely,

$$\psi_{II}(r \to \infty) = 0 \tag{A.10}$$

$$\left(\frac{\partial \psi_{II}}{\partial r}\right)_{r\to\infty} = 0 \tag{A.11}$$

Now that the boundary conditions have been defined, the Stern layer equations can be derived. First, the Laplace equation, Eq. (2.31) in the main text, is rewritten as follows

$$\nabla^2 \psi_I(r) = \frac{\partial}{\partial r}\left[r^m \frac{\partial \psi_I}{\partial r}\right] = 0 \tag{A.12}$$

Integrating this equation once, and making use of Eq. (A.3), the boundary condition at the surface of charge, results in the following expression

$$r^m \left(\frac{\partial \psi_I}{\partial r}\right) = -\frac{4\pi e z}{\epsilon_1 a_{ch}} R_{ch}^m \tag{A.13}$$

Integrating Eq. (A.13) for each shape separately, one obtains

$$\psi_I(r) = \begin{cases} \frac{4\pi e z R_{ch}^2}{\epsilon_1 a_{ch}}\left[\frac{1}{r}+C\right] & \text{, for spheres} \\ -\frac{4\pi e z R_{ch}}{\epsilon_1 a_{ch}}\left[\ln r + C\right] & \text{, for infinite cylinders} \\ -\frac{4\pi e z}{\epsilon_1 a_{ch}}\left[r + C\right] & \text{, for infinite bilayers} \end{cases} \tag{A.14}$$

where C is an integration constant. The boundary condition at the outer boundary of the Stern layer ($r = R_s$), given in Eq. (A.4), is utilized to solve for C. Hence, the equation for the electrostatic potential in the Stern layer now becomes

$$\psi_I(r) = \begin{cases} \psi_{II}(R_s) + \frac{4\pi e z R_{ch}^2}{\epsilon_1 a_{ch}} \left[\frac{1}{r} - \frac{1}{R_s}\right] & \text{, for spheres} \\ \psi_{II}(R_s) - \frac{4\pi e z R_{ch}}{\epsilon_1 a_{ch}} \left[\ln r - \ln R_s\right] & \text{, for infinite cylinders} \\ \psi_{II}(R_s) - \frac{4\pi e z}{\epsilon_1 a_{ch}} \left[r - R_s\right] & \text{, for infinite bilayers} \end{cases} \tag{A.15}$$

where $\psi_{II}(R_s)$ is the electrostatic potential created by the diffuse ion cloud at the surface of charge, $r = R_s$. This can be calculated by solving the PB equation, Eq. (2.29), in region II, subject to the boundary conditions given in Eqs. (A.9) and (A.10).

Finally, applying Eq. (A.15) at the surface of charge ($r = R_{ch}$) results in the following expression (recall that $R_s = R_{ch} + \delta_i$)

$$\psi_I(R_{ch}) = \begin{cases} \psi_{II}(R_s) + \frac{4\pi e z \delta_i}{\epsilon_1 a_{ch}(1+\delta_i/R_{ch})} & \text{, for spheres} \\ \psi_{II}(R_s) + \frac{4\pi e z R_{ch}}{\epsilon_1 a_{ch}} \ln\left(1 + \delta_i/R_{ch}\right) & \text{, for infinite cylinders} \\ \psi_{II}(R_s) + \frac{4\pi e z \delta_i}{\epsilon_1 a_{ch}} & \text{, for infinite bilayers} \end{cases} \tag{A.16}$$

which is Eq. (2.35) of the main text, where it was assumed that $\epsilon_1 = \epsilon$.

To determine g_{elec}, the surface potential, $\psi_I(R_{ch})$, is integrated according to Eq. (2.28) of the main text (recall that $ez/a_{ch} = \sigma$). Each of the shapes is integrated separately. This yields

Spheres

$$\begin{aligned} \beta g_{elec} &= \frac{a_{ch}}{kT} \int_0^\sigma \psi_{II}(R_s)\, d\sigma + \frac{4\pi\delta_i a_{ch}}{\epsilon_1 kT(1+\delta_i/R_{ch})} \int_0^\sigma \sigma\, d\sigma - \frac{(ze)^2}{2\epsilon_2 r_h k_B T} \\ &= \beta g_{elec,II} + \frac{4\pi\delta_i e^2 z^2}{2\epsilon_1 a_{ch} kT(1+\delta_i/R_{ch})} - \frac{(ze)^2}{2\epsilon_2 r_h k_B T} \end{aligned} \tag{A.17}$$

Infinite Cylinders

$$\begin{aligned}\beta g_{elec} &= \frac{a_{ch}}{kT}\int_0^{\sigma}\psi_{II}(R_s)\,d\sigma + \frac{4\pi R_{ch}a_{ch}}{\epsilon_1 kT}\ln(1+\delta_i/R_{ch})\int_0^{\sigma}\sigma\,d\sigma - \frac{(ze)^2}{2\epsilon_2 r_h k_B T} \\ &= \beta g_{elec,II} + \frac{4\pi R_{ch}e^2z^2}{2\epsilon_1 a_{ch}kT}\ln(1+\delta_i/R_{ch}) - \frac{(ze)^2}{2\epsilon_2 r_h k_B T} \qquad \text{(A.18)}\end{aligned}$$

Infinite Bilayers

$$\begin{aligned}\beta g_{elec} &= \frac{a_{ch}}{kT}\int_0^{\sigma}\psi_{II}(R_s)\,d\sigma + \frac{4\pi\delta_i a_{ch}}{\epsilon_1 kT}\int_0^{\sigma}\sigma\,d\sigma - \frac{(ze)^2}{2\epsilon_2 r_h k_B T} \\ &= \beta g_{elec,II} + \frac{4\pi\delta_i e^2z^2}{2\epsilon_1 a_{ch}kT} - \frac{(ze)^2}{2\epsilon_2 r_h k_B T} \qquad \text{(A.19)}\end{aligned}$$

where $\beta g_{elec,II}$ is obtained by integrating $\psi_{II}(R_s)$ according to Eq. (2.40). Several analytical approximations for $\beta g_{elec,II}$ are given in the main text.

Equations (A.17)-(A.19) can be further simplified in terms of the dimensionless charge density, s, given by

$$s = \frac{4\pi e^2 z^2}{\epsilon_2 \kappa a_{ch} k_B T (1+\delta_i/R_{ch})^m} \qquad \text{(A.20)}$$

which gives Eq. (2.38) of the main text, where $\epsilon_2 = \epsilon$. Note that the surface charge density, $\sigma = ez/a_{ch}$, has units of C/Å^2. By multiplying by the quantity $ez/\epsilon\kappa k_B T$, which has units of Å^2/C, the surface charge density can be made dimensionless. It is further multiplied by $4\pi/(1+\delta_i/R_{ch})^m$ for convenience in order to simplify the expressions for g_{elec}. This yields

$$\beta g_{elec} = \begin{cases} \beta g_{elec,II} + \frac{\kappa s \delta_i}{2}\frac{\epsilon_2}{\epsilon_1}(1+\delta_i/R_{ch}) - \frac{(ze)^2}{2\epsilon_2 r_h k_B T} & \text{, for spheres} \\ \beta g_{elec,II} + \frac{\kappa s R_{ch}}{2}\frac{\epsilon_2}{\epsilon_1}(1+\delta_i/R_{ch})\ln(1+\delta_i/R_{ch}) - \frac{(ze)^2}{2\epsilon_2 r_h k_B T} & \text{, for infinite cylinders} \\ \beta g_{elec,II} + \frac{\kappa s \delta_i}{2}\frac{\epsilon_2}{\epsilon_1} - \frac{(ze)^2}{2\epsilon_2 r_h k_B T} & \text{, for infinite bilayers} \end{cases} \qquad \text{(A.21)}$$

which is Eq. (2.36) along with Eq. (2.37) of the main text, where $\epsilon_1 = \epsilon_2 = \epsilon$.

Appendix B

Numerical Model of Counterion Binding

In addition to the thermodynamic model of counterion binding presented in Section 2.4, it is possible to analyze counterion binding numerically. In this approach, the micelle and its surrounding counterion cloud create an electrostatic potential based on the Poisson-Boltzmann equation, which can be calculated numerically rather than by using an analytical approximation. The counterion profile can then be calculated directly from the electrostatic potential according to the Boltzmann distribution. Specifically,

$$c_i(r) = c_i^\circ \exp\left[\frac{-e\psi(r)z_i}{k_B T}\right] \tag{B.1}$$

where $c_i(r)$ is the concentration of ion i at a distance r from the center of the micelle, c_i° is the bulk concentration of ion i, $\psi(r)$ is the electrostatic potential a distance r from the center of the micelle, z_i is the valence of ion i, e is the electronic charge, k_B is the Boltzmann constant, and T is the absolute temperature. The Poisson-Boltzmann equation was used to solve for $\psi(r)$ in the region immediately surrounding the micelle, with no Stern layer. The purpose of neglecting the Stern layer was to study the way in which the ions distribute based solely on $\psi(r)$ and Eq. (B.1). Then, this ion distribution was used to determine the fraction of ions that are very close to the micelle, in a region which is approximately the size of the Stern layer region.

Sodium dodecyl sulfate (SDS) was studied as a typical example, which forms a spherical micelle with a radius of charge equal to 15.7 Å. A value of $\kappa = 0.029\text{Å}^{-1}$, corresponding to the SDS CMC value of 8mM at 25°C, was used. The ion distribution given by Eq. (B.1) is shown in Figure B-1, where the counterion concentration, c_i, scaled with respect to the bulk concentration,c_i, that is, c_i/c_i°, is plotted as a function of the distance from the surface of charge of the micelle. Very close to the micelle surface, the counterion concentration is higher than 150 times the bulk counterion concentration. Far from the micellar surface, c_i/c_i° approaches unity, indicating that the bulk counterion concentration has been reached.

The same counterion distribution, $c_i(r)$, is illustrated differently in Figure B-2, which shows the cumulative fraction of counterions located around the micelle as a function of distance from the surface of charge. A distance equivalent to the thickness of the Stern layer thickness ($\delta_{Na^+} = 1.85\text{Å}$) is indicated by the dashed line. According to this analysis, only 15% of the counterion cloud is located inside the region equivalent to the Stern layer thickness. The dotted line indicates a distance of one Debye screening length ($\kappa^{-1} \approx 34\text{Å}$). This region includes 65% of the counterions. At large distances, the profile levels off to 100% of the total counterions. It is interesting to note that most experimental techniques measure counterion binding values of 60-80%. According to the numerical analysis presented in Figure B-2, these experimental techniques are measuring counterion binding at a distance equivalent to at least a micelle diameter away from the micellar surface, not at the micellar surface, as is commonly assumed.

In the future, it may be useful to use the numerical analysis presented here to calculate the fractional counterion binding. However, this analysis was found to be computationally challenging and time-consuming. While this approach provides insight into the ion distribution surrounding the micelle, it is too tedious to be useful as a predictive tool. The analytical approach presented in Section 2.4 provides a much faster calculational tool.

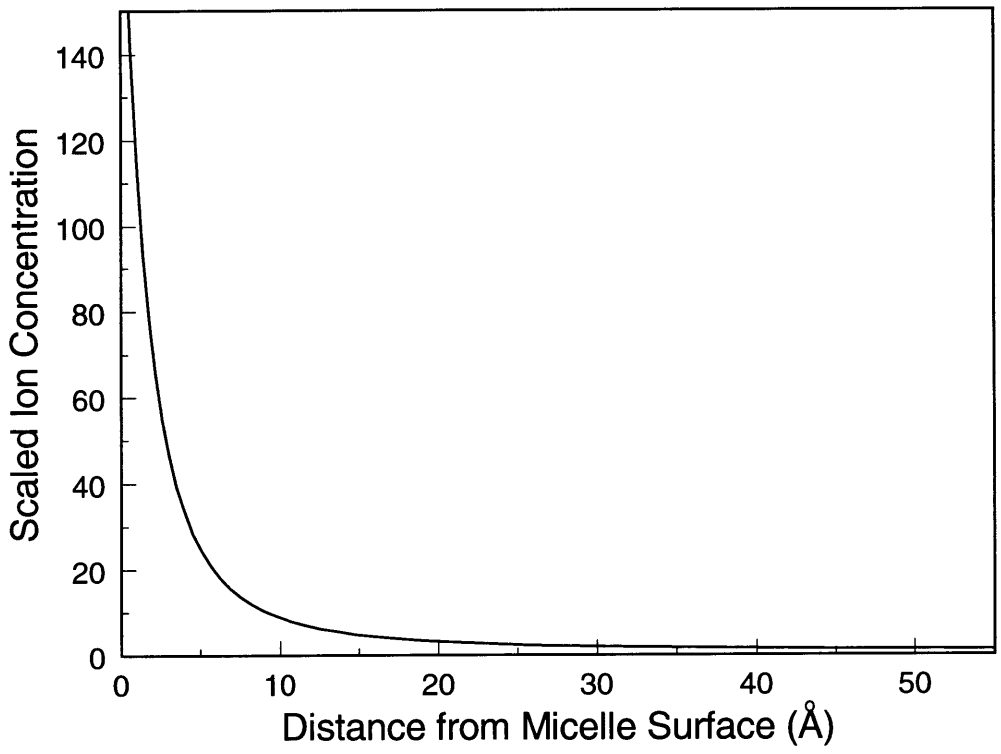

Figure B-1: Scaled ion concentration (c_i/c_i°) as a function of the distance from the surface of charge of a spherical micelle.

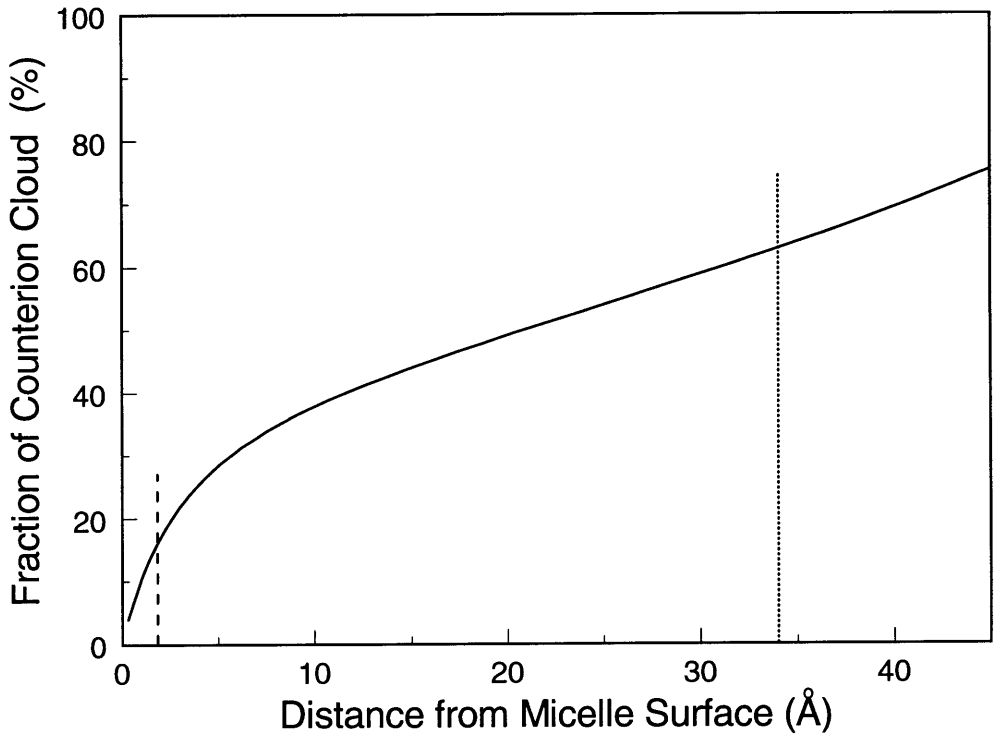

Figure B-2: Fraction of counterions as a function of the distance from the surface of charge of a spherical micelle. The dashed line indicates a distance equivalent to the width of the Stern layer, and the dotted line indicates a distance equivalent to κ^{-1}.

Appendix C

The Role of Counterion Binding in the Micellization Process

As mentioned in Section 2.4, there are two competing viewpoints on the role of counterions in the micellization process. One viewpoint considers the micelle to be formed in the presence of a diffuse ion cloud. The counterions do not participate explicitly in the micellization process except through the interaction of the micelle with the ion cloud in which they are distributed. This is the viewpoint taken in the model presented in Chapter 2.

A competing viewpoint assumes that a certain fraction of the counterions participate explicitly in the micellization process by binding to the micelle surface, and thereby reducing its overall surface charge. This is the viewpoint taken by Zana and others.[81, 84] Both viewpoints are correct, provided that a consistent thermodynamic framework is developed for each. Specifically, if counterions participate in the micellization process, many of the equations derived in Section 2.2 of the main text need to be modified. In this appendix, these modified equations will be derived, and it will be shown that both viewpoints are indeed equivalent.

If the second viewpoint is adopted, the total Gibbs free energy of the micellar solution should be modified to explicitly reflect the presence of the counterions.

Specifically (compare with Eq. (2.1) of the main text),

$$G = \mu_w N_w + \mu_1 N_1 + \mu_{c1} N_{c1} + \sum_{n>1} \tilde{\mu}_n N_n \tag{C.1}$$

where μ_{c1} is the chemical potential of the free counterions, N_{c1} is the number of free counterions, $\tilde{\mu}_n$ is the chemical potential of an n-mer with bound counterions, and all the other variables were defined in Section 2.2. Note that in Eq. (C.1), it was assumed that all the micelles are in their optimal shape, S^*, and optimal core radius, l_c^*, so that the summations over S and l_c are not necessary.

The equilibrium thermodynamic state of the micellar solution corresponds to the minimum of the Gibbs free energy, G. In other words, when the solution is in thermodynamic equilibrium, the following condition is satisfied

$$dG\,|_{T,p,N_s,N_w,N_c} = 0 \tag{C.2}$$

where N_c is the total number of counterions, including those that are free in solution, N_{c1}, and those that are physically bound to the micelles. Using Eq. (C.1) in Eq. (C.2) yields

$$dG\,|_{T,p,N_s,N_w,N_c} = \mu_1 dN_1 + \mu_{c1} dN_{c1} + \sum_{n>1} \tilde{\mu}_n dN_n \tag{C.3}$$

Note that in Eq. (C.3) the variables dN_1, dN_{c1}, and dN_n are not independent due to mass balance constraints on the total number of surfactant molecules and counterions. Specifically, the surfactant mass balance implies that

$$N_s = N_1 + \sum_{n>1} n N_n \tag{C.4}$$

In addition, the counterion mass balance requires that

$$N_c = N_{c1} + \sum_{n>1} n \alpha_B N_n \tag{C.5}$$

where α_B is the fractional counterion binding which is the fraction of surfactant

molecules in the micelle which do not dissociate. Since N_s is constant, and $N_c = N_s$ due to electroneutrality, it follows that

$$dN_1 = -\sum_{n>1} n\, dN_n \tag{C.6}$$

$$dN_{c1} = -\sum_{n>1} n\alpha_B\, dN_n \tag{C.7}$$

Using Eqs. (C.6) and (C.7) in Eq. (C.3) yields

$$dG\,|_{T,p,N_s,N_w,N_c} = \sum_{n>1}\left[\frac{\tilde{\mu}_n}{n} - \mu_1 - \alpha_B\mu_{c1}\right] n\, dN_n = 0 \tag{C.8}$$

which indicates that, at thermodynamic equilibrium, the chemical potentials $\tilde{\mu}_n$, μ_1, and μ_{c1} must satisfy the following constraint

$$n(\mu_1 + \alpha_B\mu_{c1}) = \tilde{\mu}_n \tag{C.9}$$

Equation (C.9) is the equilibrium condition when counterions are included explicitly in the micellization process, and is different from the equilibrium condition for the case when the counterions do not participate explicitly in the micellization process, given in Eq. (2.7) of the main text (again, it is assumed that the micelles are at S^* and l_c^*).

Using expressions for $\tilde{\mu}_n = (\partial G/\partial N_n)_{T,p,N_w,N_{m'},N_{c1}}$, $\tilde{\mu}_1 = (\partial G/\partial N_1)_{T,p,N_w,N_m,N_{c1}}$, and $\tilde{\mu}_{c1} = (\partial G/\partial N_{c1})_{T,p,N_w,N_m}$ derived from G in Eq. (C.1) in the constraint given by Eq. (C.9), the micelle size distribution can be obtained. Specifically (compare with Eq. (2.18) in the main text),

$$\tilde{X}_n = \frac{(X_1 X_{c1}^{\alpha_B} e)^n}{e} \exp\left[-\beta n \tilde{g}_{mic}(n, l_c^*, S^*, \alpha_B)\right] \tag{C.10}$$

where $\tilde{g}_{mic}$ is the free energy of micellization when counterion binding is included and is given by

$$\tilde{g}_{mic} = \frac{\tilde{\mu}_n^\circ}{n} - (\mu_1^\circ + \alpha_B\mu_{c1}^\circ) \tag{C.11}$$

where $\tilde{\mu}_n^\circ$ is the standard-state chemical potential of the n-mer with $n\alpha_B$ bound counterions. Hence, the mole fraction of n-mers depends on (i) the entropic cost of localizing n monomers and $n\alpha_B$ counterions in one location in order to form the micelle, and (ii) the free-energy advantage of forming an n-mer with $n\alpha_B$ bound counterions. Equation (C.11) illustrates the difference between $\tilde{g}_{mic}$ and g_{mic} (where $g_{mic} = \mu_n^\circ/n - \mu_1^\circ$, as described in Section 2.2). That is, the bound counterions must be included in $\tilde{g}_{mic}$. Specifically, the electrostatic contribution, $\tilde{g}_{elec}$, will be significantly lower because a certain fraction, $n\alpha_B$, of the surfactant molecules in the micelle will not be charged. Clearly, when $\alpha_B = 0$, $\tilde{\mu}_n^\circ = \mu_n^\circ$. Therefore, $\tilde{g}_{mic}$ reduces to g_{mic} in the limit of zero counterion binding.

The mole fraction of free counterions, X_{c1}, is equal to the mole fraction of counterions dissociated from the surfactant monomers plus the mole fraction of counterions from the dissociated surfactant molecules in the micelles. That is,

$$X_{c1} = X_1 + (1 - \alpha_B)(X_s - X_1) \tag{C.12}$$

Using Eq. (C.12) in Eq. (C.10), taking the natural log, and retaining only the terms that are of order n, the following expression is obtained for the CMC,

$$CMC \approx \exp\left(\frac{\beta\tilde{g}_{mic} - 1}{1 + \alpha_B}\right) \tag{C.13}$$

The expression for the CMC for the case when counterions participate in the micellization process, Eq. (C.13), is clearly different than that corresponding to the case when counterions do not explicitly participate, as derived in Eq. (2.20). However, recall that $\tilde{g}_{mic}$ will be lower (more negative) than g_{mic} due to the presence of the bound counterions, thus reducing the $\tilde{g}_{elec}$ contribution. Dividing $(\tilde{g}_{mic} - 1)$ by $1 + \alpha_B$ should reduce the exponential term so that it is equivalent to $g_{mic} - 1$. Therefore, the resulting CMC's from both approaches should be equivalent. Indeed, when $\alpha_B = 0$, Eq. (C.13) becomes $CMC \approx (\tilde{g}_{mic} - 1)$, which, because $\tilde{g}_{mic}$ is equal to g_{mic} in the limit of no counterion binding, reduces to Eq. (2.20). It is important to note, however, that including the counterions in the micellization process requires knowledge of an

additional paramter, namely, α_B, which must be determined experimentally.

Appendix D

Excess Gibbs Free Energy and Excess Chemical Potentials

In this appendix, Eq. (4.11) in the main text is derived, along with expressions for the excess chemical potentials (Eqs. (4.12) and (4.13) of the main text). The definition of the excess Gibbs free energy, G^{ex}, is given by

$$G^{ex}(T,p,\{N_\sigma\},N_w) = G(T,p,\{N_\sigma\},N_w) - G^{id}(T,p,\{N_\sigma\},N_w) \qquad \text{(D.1)}$$

The objective is to establish a connection between the Gibbs free energy at pressure p and the McMillan-Mayer free energy at pressure $p+\Pi$. Accordingly, the first step involves transforming $G(T,p,\{N_\sigma\},N_w)$ from pressure p to pressure $p+\Pi$. In view of the fact that

$$\left(\frac{\partial G}{\partial p}\right)_{T,\{N_\sigma\},N_w} = V \qquad \text{(D.2)}$$

where $V(T,p,\{N_\sigma\},N_w)$ is the system volume, integration of Eq. (D.2) from p to $p+\Pi$ yields

$$G(T,p,\{N_\sigma\},N_w) = G(T,p+\Pi,\{N_\sigma\},N_w) - \int_p^{p+\Pi} V(T,p',\{N_\sigma\},N_w)\,dp' \qquad \text{(D.3)}$$

Inserting the expression for G given in Eq. (D.3), along with the expression for G^{id} given in Eq. (4.6), into Eq. (D.1) yields the following expression for G^{ex}

$$\begin{aligned} G^{ex}(T,p,\{N_\sigma\},N_w) &= G(T,p+\Pi,\{N_\sigma\},N_w) - \int_p^{p+\Pi} V(T,p',\{N_\sigma\},N_w)\,dp' \\ &\quad - \left[N_w\mu_w^\circ + \sum_\sigma N_\sigma\mu_\sigma^\circ + k_BT\sum_\sigma N_\sigma(\ln m_\sigma - 1)\right] \end{aligned} \tag{D.4}$$

Next, a Legendre transformation[108] is utilized to transform from the Gibbs free energy, G, to the McMillan-Mayer free energy, F. Specifically, in order to transform from $G(T,p+\Pi,\{N_\sigma\},N_w)$ to $F(T,V^\dagger,\{N_\sigma\},\mu_w^\circ)$, the variables $p+\Pi$ and N_w should be transformed to the variables $V^\dagger$ and μ_w°, respectively (recall that $V^\dagger = V(T,p+\Pi,\{N_\sigma\},N_w)$, as described in Section 4.2). This Legendre transformation yields

$$F(T,V^\dagger,\{N_\sigma\},\mu_w^\circ) = G(T,p+\Pi,\{N_\sigma\},N_w) - (p+\Pi)V^\dagger - N_w\mu_w^\circ \tag{D.5}$$

Utilizing the relation between G and F, established in Eq. (D.5), in Eq. (D.4) yields

$$\begin{aligned} G^{ex}(T,p,\{N_\sigma\},N_w) &= F(T,V^\dagger,\{N_\sigma\},\mu_w^\circ) + (p+\Pi)V^\dagger - \int_p^{p+\Pi} V(T,p',\{N_\sigma\},N_w)\,dp' \\ &\quad - \sum_\sigma N_\sigma\mu_\sigma^\circ - k_BT\sum_\sigma N_\sigma(\ln m_\sigma - 1) \end{aligned} \tag{D.6}$$

Next, the standard-state chemical potentials of the solutes in Eq. (D.6) are transformed from μ_σ° to $\mu_\sigma^\ominus$ with the use of Eq. (4.7). Using this standard state will allow a connection with F^{ID} given in Eq. (4.2). In addition, the resulting expression for G^{ex} is rewritten below utilizing number concentrations, $c_\sigma^\dagger$, rather than molalities, m_σ (recall that $m_\sigma = c_\sigma^\dagger V^\dagger/N_w$). Specifically,

$$\begin{aligned} G^{ex}(T,p,\{N_\sigma\},N_w) &= F(T,V^\dagger,\{N_\sigma\},\mu_w^\circ) + (p+\Pi)V^\dagger \\ &\quad - \int_p^{p+\Pi} V(T,p',\{N_\sigma\},N_w)\,dp' \end{aligned}$$

$$
\begin{aligned}
&-\sum_{\sigma} N_{\sigma}\left[\mu_{\sigma}^{\ominus}+k_{B}T\ln\frac{1}{c_{\sigma}^{\ominus}V_{w}}\right]\\
&-k_{B}T\sum_{\sigma}N_{\sigma}\left[\ln\left(\frac{c_{\sigma}^{\dagger}V^{\dagger}}{N_{w}}\right)-1\right]
\end{aligned}
\tag{D.7}
$$

where $V_w = V(T,p,\{0\},N_w)/N_w$ is the volume per molecule in pure solvent (water).

By rearranging the natural log terms in Eq. (D.7), the following expression for G^{ex} is obtained

$$
\begin{aligned}
G^{ex}(T,p,\{N_\sigma\},N_w) &= F(T,V^{\dagger},\{N_\sigma\},\mu_w^{\circ})+(p+\Pi)V^{\dagger}\\
&\quad-\int_{p}^{p+\Pi}V(T,p',\{N_\sigma\},N_w)\,dp'\\
&\quad-\sum_{\sigma}N_\sigma\mu_\sigma^{\ominus}-k_BT\sum_{\sigma}N_\sigma\left[\ln\left(\frac{c_\sigma^{\dagger}}{c_\sigma^{\ominus}}\right)-1\right]\\
&\quad-Nk_BT\ln\frac{V^{\dagger}}{V_wN_w}
\end{aligned}
\tag{D.8}
$$

where $N=\sum_\sigma N_\sigma$.

Recall that the McMillan-Mayer free energy, F, can be divided into IDEAL and EXCESS contributions (see Eq. (4.3)). Utilizing Eq. (4.2) for F^{ID} in Eq. (4.3), the following expression for F is obtained

$$
F(T,V^{\dagger},\{N_\sigma\},\mu_w^{\circ})=\sum_{\sigma}N_\sigma\mu_\sigma^{\ominus}+k_BT\sum_{\sigma}N_\sigma\left(\ln\frac{c_\sigma^{\dagger}}{c_\sigma^{\ominus}}-1\right)-pV^{\dagger}+F^{EX}(T,V^{\dagger},\{N_\sigma\},\mu_w^{\circ})
\tag{D.9}
$$

Utilizing the expression for F given in Eq. (D.9) in Eq. (D.8), and cancelling the appropriate terms, yields the following expression for G^{ex}

$$
\begin{aligned}
G^{ex}(T,p,\{N_\sigma\},N_w) &= F^{EX}(T,V^{\dagger},\{N_\sigma\},\mu_w^{\circ})+\Pi V^{\dagger}\\
&\quad-\int_{p}^{p+\Pi}V(T,p',\{N_\sigma\},N_w)\,dp'\\
&\quad-Nk_BT\ln\frac{V^{\dagger}}{V_wN_w}
\end{aligned}
\tag{D.10}
$$

Equation (D.10) is the G^{ex} expression given in Eq. (4.11) of the main text. The advantage of utilizing this approach is that the McMillan-Mayer free energy can be

related to a model for solute molecules interacting through vacuum. Equation (D.10) provides the necessary relation to transform the McMillan-Mayer free energy, F^{EX}, to the Gibbs free energy, G^{ex}, for solute molecules interacting through solvent.

The excess contributions to the chemical potentials of the solutes and the solvent can now be obtained directly by differentiation of G^{ex} with respect to N_σ and N_w, respectively. Specifically, for solute σ, one obtains

$$\begin{aligned}\mu_\sigma^{ex} &= \left(\frac{\partial G^{ex}}{\partial N_\sigma}\right)_{T,p,\{N_{\alpha\neq\sigma}\},N_w} \\ &= \left(\frac{\partial F^{EX}}{\partial N_\sigma}\right)_{T,p,\{N_{\alpha\neq\sigma}\},N_w} + \Pi\overline{V}_\sigma^\dagger + V^\dagger\left(\frac{\partial \Pi}{\partial N_\sigma}\right)_{T,p,\{N_{\alpha\neq\sigma}\},N_w} - V^\dagger\left(\frac{\partial \Pi}{\partial N_\sigma}\right)_{T,p,\{N_{\alpha\neq\sigma}\},N_w} \\ &\quad - \int_p^{p+\Pi}\overline{V}_\sigma(p')\,dp' - k_BT\ln\frac{V^\dagger}{V_wN_w} - \frac{Nk_BT}{V^\dagger}\overline{V}_\sigma^\dagger \end{aligned} \tag{D.11}$$

where $\overline{V}_\sigma^\dagger$ is the partial molar volume of solute σ at pressure $p+\Pi$, that is,

$$\overline{V}_\sigma^\dagger = \left(\frac{\partial V^\dagger}{\partial N_\sigma}\right)_{T,p,\{N_{\alpha\neq\sigma}\},N_w} \tag{D.12}$$

and $\overline{V}_\sigma(p')$ is the partial molar volume of solute σ at pressure p'. Note that in taking the derivative of the integral term in Eq. (D.10), the limits of integration must also be differentiated. This yields the additional $-V^\dagger(\partial\Pi/\partial N_\sigma)_{T,p,\{N_{\alpha\neq\sigma}\},N_w}$ term in Eq. (D.11).

Cancelling terms in Eq. (D.11) and rearranging, one obtains the following expression for μ_σ^{ex}

$$\begin{aligned}\mu_\sigma^{ex} &= \left(\frac{\partial F^{EX}}{\partial N_\sigma}\right)_{T,p,\{N_{\alpha\neq\sigma}\},N_w} + \overline{V}_\sigma^\dagger\left[\Pi - \frac{Nk_BT}{V^\dagger}\right] \\ &\quad - \int_p^{p+\Pi}\overline{V}_\sigma(p')\,dp' - k_BT\ln\frac{V^\dagger}{V_wN_w} \end{aligned} \tag{D.13}$$

The osmotic pressure, Π, can be split into IDEAL and EXCESS contributions. Specifically,

$$\begin{aligned}\Pi &= \Pi^{ID} + \Pi^{EX} \\ &= c^{\dagger} k_B T + \Pi^{EX} \end{aligned} \tag{D.14}$$

where $c^{\dagger} = N/V^{\dagger}$ is the total solute concentration.

In addition, the derivative of F^{EX} in Eq. (D.13) can be expressed in terms of its natural variables, $T, V^{\dagger}, \{N_\sigma\}$, and μ_w°. Specifically,

$$\left(\frac{\partial F^{EX}}{\partial N_\sigma}\right)_{T,p,\{N_{\alpha\neq\sigma}\},N_w} = \left(\frac{\partial F^{EX}}{\partial N_\sigma}\right)_{T,V^{\dagger},\{N_{\alpha\neq\sigma}\},\mu_w^\circ} + \left(\frac{\partial F^{EX}}{\partial V^{\dagger}}\right)_{T,\{N_\sigma\},\mu_w^\circ} \left(\frac{\partial V^{\dagger}}{\partial N_\sigma}\right)_{T,p,\{N_{\alpha\neq\sigma}\},N_w} \tag{D.15}$$

In view of the fact that

$$\left(\frac{\partial F^{EX}}{\partial N_\sigma}\right)_{T,V^{\dagger},\{N_{\alpha\neq\sigma}\},\mu_w^\circ} = \mu_\sigma^{EX} \tag{D.16}$$

and

$$\left(\frac{\partial F^{EX}}{\partial V^{\dagger}}\right)_{T,\{N_\sigma\},\mu_w^\circ} = \Pi^{EX} \tag{D.17}$$

Eq. (D.15) can be rewritten as follows

$$\left(\frac{\partial F^{EX}}{\partial N_\sigma}\right)_{T,p,\{N_{\alpha\neq\sigma}\},N_w} = \mu_\sigma^{EX} - \Pi^{EX}\,\overline{V}_\sigma^{\dagger} \tag{D.18}$$

Using Eq. (D.18) for the derivative of F^{EX}, along with Eq. (D.14) for the osmotic pressure, Π, in Eq. (D.13), and cancelling terms, one obtains the following expression for μ_σ^{ex}

$$\mu_\sigma^{ex} = \mu_\sigma^{EX} - \int_p^{p+\Pi} \overline{V}_\sigma(p')\,dp' - k_B T \ln \frac{V^{\dagger}}{V_w N_w} \tag{D.19}$$

Equation (D.19) is the μ_σ^{ex} expression given in Eq. (4.12) of the main text.

For the solvent, the excess chemical potential is also obtained by differentiation

of the G^{ex} expression given in Eq. (D.10). Specifically,

$$\begin{aligned}
\mu_w^{ex} &= \left(\frac{\partial G^{ex}}{\partial N_w}\right)_{T,p,\{N_\sigma\}} \\
&= \left(\frac{\partial F^{EX}}{\partial N_w}\right)_{T,p,\{N_\sigma\}} + \Pi \overline{V}_w^\dagger + V^\dagger \left(\frac{\partial \Pi}{\partial N_w}\right)_{T,p,\{N_\sigma\}} - V^\dagger \left(\frac{\partial \Pi}{\partial N_w}\right)_{T,p,\{N_\sigma\}} \\
&\quad - \int_p^{p+\Pi} \overline{V}_w(p')\, dp' - \frac{N k_B T}{V^\dagger}\left[\overline{V}_w^\dagger - \frac{V^\dagger}{N_w}\right]
\end{aligned} \tag{D.20}$$

where $\overline{V}_w^\dagger$ is the partial molar volume of the solvent at pressure $p + \Pi$, that is,

$$\overline{V}_w^\dagger = \left(\frac{\partial V^\dagger}{\partial N_w}\right)_{T,p,\{N_\sigma\}} \tag{D.21}$$

and $\overline{V}_w(p')$ is the partial molar volume of the solvent at pressure p'.

The derivative of F^{EX} in Eq. (D.20) can be expressed in terms of its natural variables, $T, V^\dagger, \{N_\sigma\}$, and μ_w°. This yields,

$$\begin{aligned}
\left(\frac{\partial F^{EX}}{\partial N_w}\right)_{T,p,\{N_\sigma\}} &= \left(\frac{\partial F^{EX}}{\partial V^\dagger}\right)_{T,\{N_\sigma\},\mu_w^\circ} \left(\frac{\partial V^\dagger}{\partial N_w}\right)_{T,p,\{N_\sigma\}} \\
&= -\Pi^{EX}\, \overline{V}_w^\dagger
\end{aligned} \tag{D.22}$$

Utilizing Eqs. (D.22) and (D.14) in Eq. (D.20), cancelling and rearranging terms, yields the following expression for μ_w^{ex} (recall that $N/N_w = m$)

$$\mu_w^{ex} = k_B T m - \int_p^{p+\Pi} \overline{V}_w(p')\, dp' \tag{D.23}$$

Equation (D.23) is the expression for μ_w^{ex} given in Eq. (4.13) of the main text.

Appendix E

Derivatives of the Monomer and Micelle Concentrations

The derivatives presented in this Appendix apply to the case of micellar solutions consisting of cylindrical micelles which are modeled as rigid spherocylinders. As explained in the main text, this is the optimal micellar shape of experimental interest for the nonionic surfactant systems described in Chapter 5.

The first and second derivatives of the monomer concentration, c_1, and of the zeroth moment, c, with respect to the total surfactant concentration, c_s, can be obtained by utilizing Eqs. (5.31) and (5.32). The resulting derivative expressions are very long and complicated, due to the dependence of the excluded-volume contributions on the size distribution. Specifically, since A_0^{cyl} and A_1^{cyl} depend on c, in order to calculate $(\partial c_1/\partial c_s)$, it is also necessary to determine $(\partial c/\partial c_s)$.

Eq. (5.32) can be rewritten as follows

$$c_1 = c_s - \frac{q^{n_0}}{K(1-q)^2}[n_0(1-q)+q] \tag{E.1}$$

where

$$K = \Omega_w \exp[\beta n_0(g_{sph} - g_{cyl}) + A_0^{cyl}] \tag{E.2}$$

and

$$q = (\Omega_w c_1) \exp[-\beta g_{cyl} + A_1^{cyl}] \tag{E.3}$$

with the excluded-volume parameters, A_0^{cyl} and A_1^{cyl}, given by

$$A_0^{cyl} = a_2 c_s + a_1 c + (a_5 - a_1 - a_2) c_1 \tag{E.4}$$

$$A_1^{cyl} = (a_4 - a_3) c_s + (a_5 - a_2) c + (4a_2 + a_3 - 2a_4 - a_5) c_1 \tag{E.5}$$

where (see Eqs. (5.20) and (5.21))

$$a_1 = \frac{2\pi d^3}{9} \tag{E.6}$$

$$a_2 = \frac{8\Omega_s}{3} \tag{E.7}$$

$$a_3 = \frac{8\Omega_s^2}{\pi d^3} \tag{E.8}$$

$$a_4 = \Omega_s \gamma^2 \tag{E.9}$$

$$a_5 = \Omega_s \gamma^2 n_0^{2/3} \tag{E.10}$$

The first derivative of c_1 in Eq. (E.1) with respect to c_s is given by

$$\left(\frac{\partial c_1}{\partial c_s}\right) = \frac{X_1}{Y_1} \tag{E.11}$$

where

$$\begin{aligned} X_1 = {} & 1 + (2a_2 - a_5) D_1 + (a_3 - a_4) D_2 + a_1 D_3 \\ & + \left(a_2^2 - a_1 a_3 + a_1 a_4 - a_2 a_5\right) \left(D_1^2 - D_2 D_3\right) \end{aligned} \tag{E.12}$$

and

$$\begin{aligned} Y_1 = {} & 1 + 2(a_2 - a_5) D_1 + (3a_2 + a_3 - 2a_4) D_2 + \frac{D_2}{c_1} + a_1 D_3 \\ & - \left(\frac{a_1}{c_1} - a_2^2 + a_1 a_3 + 3a_1 a_2 - 2a_1 a_4 + 2a_2 a_5 - a_5^2\right) \left(D_1^2 - D_2 D_3\right) \end{aligned} \tag{E.13}$$

with D_i ($i = 1$, 2, and 3) given by

$$D_1 = \frac{q^{n_0}}{K(1-q)^2}\left[n_0 + (1-n_0)q\right] \tag{E.14}$$

$$D_2 = \frac{q^{n_0}}{K(1-q)^3}\left[n_0^2 + (1+2n_0-2n_0^2)q + (1-2n_0+n_0^2)q^2\right] \tag{E.15}$$

$$D_3 = \frac{q^{n_0}}{K(1-q)} \tag{E.16}$$

The first derivative of c with respect to c_s is obtained by differentiating Eq. (5.31) with respect to c_s. This yields

$$\left(\frac{\partial c}{\partial c_s}\right) = \frac{X_2}{Y_2} \tag{E.17}$$

where

$$X_2 = \left(\frac{\partial c_1}{\partial c_s}\right)\left(1 + \frac{D_1}{c_1} + (4a_2 + a_3 - 2a_4 - a_5)D_1 + (a_1 + a_2 - a_5)D_3\right) + (a_4 - a_3)D_1 - a_2 D_3 \tag{E.18}$$

and

$$Y_2 = 1 + (a_2 - a_5)D_1 + a_1 D_3 \tag{E.19}$$

A second differentiation of Eqs. (E.11) and (E.17) with respect to c_s yields the corresponding second derivatives. The algebra is tedious, but straightforward. The resulting expression for the second derivative of the monomer concentration is given by

$$\left(\frac{\partial^2 c_1}{\partial c_s^2}\right) = \frac{1}{Y_1}\left(X_1' - \left(\frac{\partial c_1}{\partial c_s}\right)Y_1'\right) \tag{E.20}$$

where

$$X_1' = (2a_2 - a_5)D_1' + (a_3 - a_4)D_2' + a_1 D_3' + (a_2^2 - a_1 a_3 + a_1 a_4 - a_2 a_5)\left(2D_1 D_1' - D_2' D_3 - D_2 D_3'\right) \tag{E.21}$$

and

$$
\begin{aligned}
Y_1' &= 2(a_2 - a_5)D_1' + (3a_2 + a_3 - 2a_4)D_2' + \frac{D_2'}{c_1} - \frac{D_2}{c_1^2}\left(\frac{\partial c_1}{\partial c_s}\right) + a_1 D_3' \\
&\quad - \left(\frac{a_1}{c_1} - a_2^2 + a_1 a_3 + 3a_1 a_2 - 2a_1 a_4 + 2a_2 a_5 - a_5^2\right)\left(2D_1 D_1' - D_2' D_3 - D_2 D_3'\right) \\
&\quad + \left(D_1^2 - D_2 D_3\right)\frac{a_1}{c_1^2}\left(\frac{\partial c_1}{\partial c_s}\right) \qquad \text{(E.22)}
\end{aligned}
$$

In these and the following equations, the $'$ indicates differentiation with respect to c_s. The expression for the second derivative of the micelle concentration is given by

$$
\left(\frac{\partial^2 c}{\partial c_s^2}\right) = \frac{1}{Y_2}\left(X_2' - \left(\frac{\partial c}{\partial c_s}\right) Y_2'\right) \qquad \text{(E.23)}
$$

where

$$
\begin{aligned}
X_2' &= \left(\frac{\partial c_1}{\partial c_s}\right)\left(\frac{D_1'}{c_1} - \frac{D_1}{c_1^2}\left(\frac{\partial c_1}{\partial c_s}\right) + (4a_2 + a_3 - 2a_4 - a_5)D_1' + (a_1 + a_2 - a_5)D_3'\right) \\
&\quad + \left(\frac{\partial^2 c_1}{\partial c_s^2}\right)\left(1 + \frac{D_1}{c_1} + (4a_2 + a_3 - 2a_4 - a_5)D_1 + (a_1 + a_2 - a_5)D_3\right) + (a_4 - a_3)D_1' - a_2 D_3' \qquad \text{(E.24)}
\end{aligned}
$$

and

$$
Y_2' = (a_2 - a_5)D_1' + a_1 D_3' \qquad \text{(E.25)}
$$

The D_i' 's ($i = 1$, 2, and 3) in Eqs. (E.21)-(E.25) are given by

$$
\begin{aligned}
D_1' &= \left(\frac{\partial D_1}{\partial c_s}\right) = \frac{q^{n_0}}{K(1-q)^2}(1 - n_0)\left(\frac{\partial q}{\partial c_s}\right) \\
&\quad + D_1\left\{\left[\frac{n_0}{q} + \frac{2}{(1-q)}\right]\left(\frac{\partial q}{\partial c_s}\right) - \frac{1}{K}\left(\frac{\partial K}{\partial c_s}\right)\right\} \qquad \text{(E.26)} \\
D_2' &= \left(\frac{\partial D_2}{\partial c_s}\right) = \frac{q^{n_0}}{K(1-q)^3}\left\{(1 + 2n_0 - 2n_0^2) + 2(1 - 2n_0 + n_0^2)q\right\}\left(\frac{\partial q}{\partial c_s}\right) \\
&\quad + D_2\left\{\left[\frac{n_0}{q} + \frac{3}{(1-q)}\right]\left(\frac{\partial q}{\partial c_s}\right) - \frac{1}{K}\left(\frac{\partial K}{\partial c_s}\right)\right\} \qquad \text{(E.27)}
\end{aligned}
$$

$$D_3' = \left(\frac{\partial D_3}{\partial c_s}\right) = D_3 \left\{ \left[\frac{n_0}{q} + \frac{1}{(1-q)}\right] \left(\frac{\partial q}{\partial c_s}\right) - \frac{1}{K}\left(\frac{\partial K}{\partial c_s}\right) \right\} \tag{E.28}$$

where

$$\left(\frac{\partial q}{\partial c_s}\right) = q\left[\frac{1}{c_1}\left(\frac{\partial c_1}{\partial c_s}\right) + \left(\frac{\partial A_1^{cyl}}{\partial c_s}\right)\right] \tag{E.29}$$

and

$$\left(\frac{\partial K}{\partial c_s}\right) = K\left(\frac{\partial A_0^{cyl}}{\partial c_s}\right) \tag{E.30}$$

with

$$\left(\frac{\partial A_0^{cyl}}{\partial c_s}\right) = a_2 + a_1\left(\frac{\partial c}{\partial c_s}\right) + (a_5 - a_1 - a_2)\left(\frac{\partial c_1}{\partial c_s}\right) \tag{E.31}$$

$$\left(\frac{\partial A_1^{cyl}}{\partial c_s}\right) = a_4 - a_3 + (a_5 - a_2)\left(\frac{\partial c}{\partial c_s}\right) + (4a_2 + a_3 - 2a_4 - a_5)\left(\frac{\partial c_1}{\partial c_s}\right) \tag{E.32}$$

Appendix F

Hard-Core Contribution to the Excess Chemical Potential

F.1 Nonionic Micellar Solutions

As described in Eq. (5.12) with $n = 1$, the hard-core contribution to the monomer EXCESS chemical potential is given by

$$\beta\mu_1^{EX,HC} = 2B_{11}^{HC}c_1 + 2\sum_{m=n_0}^{\infty} B_{1m}^{HC}c_m \tag{F.1}$$

where B_{11}^{HC} is the hard-core contribution to the second-virial coefficient between two monomers, and B_{1m}^{HC} is the hard-core contribution to the second-virial coefficient between a monomer and an m-mer.

The contribution of the excluded-volume interactions between two monomers to B_{11}^{HC} can be estimated by modeling each monomer as an effective sphere of radius R_1, such that $4\pi R_1^3/3 = \Omega_s$, the volume of a surfactant molecule. In that case, the monomer-monomer excluded volume is given by $8(4\pi R_1^3/3) = 8\Omega_s$. Since B_{11}^{HC} represents the excluded volume *per monomer*, it follows that $B_{11}^{HC} = 8\Omega_s/2 = 4\Omega_s$.

The contribution of the excluded-volume interactions between a spherocylindrical micelle of aggregation number $n \geq n_0$, and a monomer to $B_{n1}^{HC} = B_{1n}^{HC}$ is given

by[111, 103]

$$B_{n1}^{HC} = \frac{2\pi}{3}(R_1 + R)^3 + \frac{\pi}{2}(R_1 + R)^2 L_n \tag{F.2}$$

where L_n is the length of the cylindrical body of a spherocylindrical micelle of aggregation number n, and R is the radius of the two hemispherical endcaps having aggregation number $n_0 = 4\pi(l_c^*)^3/3v_{tail} \approx 4\pi R^3/3\Omega_s$. Note that it has been assumed that the radius of the hemispherical endcaps, R_{sph}, is equal to the cross-sectional radius of the cylindrical body, R_{cyl}. In other words, it is assumed that $R_{sph} = R_{cyl} \equiv R$. For the nonionic surfactants studied in Chapter 5, it is assumed that $R = l_c^*(S = 2) + l_{hg}$, where l_{hg} is the length of the polar head. Note that $l_c^*(S = 2)$ is used rather than $l_c^*(S = 3)$ because the nonionic systems described in Chapter 5 are typically elongated rods, where the majority of the surfactant molecules reside in the cylindrical body of the micelle. For the ionic systems studied in Chapter 6, it was assumed that $l_c^* = l_{max}$, which is a typical conformation for many ionic surfactants. Thus, for the ionic micellar systems, $R = l_{max} + l_{hg}$.

L_n can be calculated by using the total volume of the spherocylindrical n-mer, V_n, which is given by

$$V_n = \pi\left(\frac{d}{2}\right)^2 L_n + \frac{\pi d^3}{6} = n\Omega_s \tag{F.3}$$

where $d = 2R$. Using Eq. (F.3), L_n can be written in terms of the aggregation number, n, as follows

$$L_n = \frac{4n\Omega_s - \frac{2}{3}\pi d^3}{\pi d^2} = \frac{(n - n_0)\Omega_s}{\pi R^2} \tag{F.4}$$

Since $4\pi R^3/3 = \pi d^3/6 = n_0\Omega_s$, Eq.(F.4) indicates that $L_n = 0$ when $n = n_0$. From the definitions of R_1 and R given above, it follows that

$$R_1 = \left(\frac{3\Omega_s}{4\pi}\right)^{1/3} = \frac{R}{n_0^{1/3}} \tag{F.5}$$

Using Eqs. (F.4) and (F.5) in Eq. (F.2), the following expression for B_{n1}^{HC} is obtained

$$B_{n1}^{HC} = \frac{\Omega_s}{2}\left(1+\frac{1}{n_0^{1/3}}\right)^2 (n+n_0^{2/3}) = \frac{\Omega_s\gamma^2}{2}(n+n_0^{2/3}) \text{ , for } \quad n \geq n_0 \tag{F.6}$$

where $\gamma = (1+1/n_0^{1/3})$.

Using B_{n1}^{HC} from Eq. (F.6) along with $B_{11}^{HC} = 4\Omega_s$ in Eq. (F.1) yields

$$\beta\mu_1^{EX,HC} \;=\; 8\Omega_s c_1 + \Omega_s\gamma^2(c_s - c_1) + \Omega_s\gamma^2 n_0^{2/3}(c - c_1) \tag{F.7}$$

where $c_s = c_1 + \sum_{m\geq n_0} m c_m$ and $c = c_1 + \sum_{m\geq n_0} c_m$. Equation (F.7) is the expression for $\beta\mu_1^{EX,HC}$ given in Eq. (5.15) of the main text.

The hard-core contribution to the n-mer EXCESS chemical potential, $\mu_n^{EX,HC}$, was given in Eq. (5.12) in the main text, which is repeated below for completeness

$$\beta\mu_n^{EX,HC} = 2B_{n1}^{HC}c_1 + 2\sum_{m=n_0}^{\infty} B_{nm}^{HC}c_m \tag{F.8}$$

where B_{nm} is the hard-core contribution to the second virial coefficient between an n-mer and an m-mer. B_{nm} was given in Eq. (5.14) of the main text, and is repeated here for completeness

$$B_{nm}^{HC} \;=\; \frac{2\pi d^3}{3} + \frac{\pi d^2}{2}(L_n + L_m) + \frac{\pi}{4}dL_nL_m \tag{F.9}$$

Using Eqs. (F.6) and (F.9) in Eq. (F.8) results in the following expression for $\mu_n^{EX,HC}$

$$\beta\mu_n^{EX,HC} = \Omega_s\gamma^2(n+n_0^{2/3})c_1 + \frac{4\pi d^3}{3}\sum_{m=n_0}^{\infty} c_m + \pi d^2\sum_{m=n_0}^{\infty} c_m(L_n+L_m) + \frac{\pi}{2}d\sum_{m=n_0}^{\infty} c_mL_nL_m \tag{F.10}$$

which gives Eq. (5.16) of the main text.

The expression for L_n in Eq. (F.4) can be utilized in Eq. (F.10) to obtain the

following relation between $\mu_n^{EX,HC}$ and n

$$\beta\mu_n^{EX,HC} = \Omega_s\gamma^2 n_0^{2/3} c_1 + \frac{2\pi d^3}{9}(c-c_1) + \frac{8\Omega_s}{3}(c_s-c_1) + n\left(\Omega_s\gamma^2 c_1 + \frac{8\Omega_s}{3}(c-c_1) + \frac{8\Omega_s^2}{\pi d^3}(c_s-c_1)\right) \tag{F.11}$$

which gives Eq. (5.17) of the main text.

Using Eqs. (F.11) and (F.7), one can compute $\beta(\mu_n^{EX,HC} - n\mu_1^{EX,HC})$ for spherocylindrical micelles. Specifically,

$$\begin{aligned}\beta(\mu_n^{EX,HC} - n\mu_1^{EX,HC}) &= A_0^{cyl} - nA_1^{cyl} \\ &= \Omega_s\gamma^2 n_0^{2/3} c_1 + \frac{2\pi d^3}{9}(c-c_1) + \frac{8\Omega_s}{3}(c_s-c_1) \\ &\quad -n\left[[8-\gamma^2(2+n_0^{2/3})]\Omega_s c_1 + \Omega_s\gamma^2 c_s + \Omega_s\gamma^2 n_0^{2/3} c - \frac{8\Omega_s}{3}(c-c_1) - \frac{8\Omega_s^2}{\pi d^3}(c_s-c_1)\right]\end{aligned} \tag{F.12}$$

Equation (F.12), corresponding to Eq. (5.19) of the main text, permits the identification of A_0^{cyl} and A_1^{cyl}, which are given in Eqs. (5.20) and (5.21) of the main text, respectively.

F.2 Ionic Micellar Solutions

For ionic micellar solutions, there is an additional contribution to the hard-core EXCESS chemical potentials associated with the excluded volume of the counterions and the salt ions. Note that, in principle, nonionic micellar solutions could also contain added salt which would contribute to the excluded volume. However, this is not the case for any of the nonionic systems considered in Chapter 5. In contrast, in some of the ionic systems considered in Chapter 6, salt is present in significant amounts, and therefore, the excluded volume associated with the salt ions and the counterions must be accounted for.

As mentioned in Section 6.2.1, the counterions and coions are assumed to be of the same size, with a radius r_i. Accordingly, the excluded-volume contributions of the counterions and the coions are the same. By adding the additional excluded-volume

contribution of the ions to Eq. (F.1), the hard-core EXCESS chemical potential of the monomers becomes

$$\beta\mu_1^{EX,HC} = 2B_{1i}^{HC}c_i + 2B_{11}^{HC}c_1 + 2\sum_{m=n_0}^{\infty} B_{1m}^{HC}c_m \tag{F.13}$$

where B_{1i}^{HC} is the hard-core contribution to the second-virial coefficient between monomers and ions, and c_i is the total concentration of ions, including counterions and coions, that is, $c_i = c_s + 2c_{salt}$.

Both the monomers and the ions are treated as spheres. As described in Section F.1, the hard-core contribution to the second-virial coefficient between two spheres of radii r_j and r_k is given by $B_{jk} = 2\pi(r_j + r_k)^3/3$. Hence, the hard-core contribution to the second virial coefficient between a spherical ion of radius r_i and a spherical monomer of radius R_1 is given by

$$B_{1i}^{HC} = \frac{2\pi}{3}(R_1 + r_i)^3 \tag{F.14}$$

where $4\pi R_1^3/3 = \Omega_s$, with Ω_s the volume of a surfactant molecule. Similarly, the hard-core contribution to the second-virial coefficient between two ions is given by $B_{ii}^{HC} = (2\pi(2r_i)^3/3) = 4\Omega_i$, where Ω_i is the volume of an ion. Note that B_{ii}^{HC} does not contribute to $\mu_n^{EX,HC}$ or $\mu_1^{EX,HC}$, but it will be useful in deriving the modified Boltzmann distribution presented in Section 6.4.2.

Using Eq. (F.14) for the contribution of the ions in Eq. (F.13), along with the contributions from the micelles and the other monomers given in Eq. (F.7), results in the following expression for $\mu_1^{EX,HC}$

$$\beta\mu_1^{EX,HC} = \frac{4\pi}{3}(R_1 + r_i)^3 c_i + 8\Omega_s c_1 + \Omega_s\gamma^2(c_s - c_1) + \Omega_s\gamma^2 n_0^{2/3}(c - c_1) \tag{F.15}$$

For the hard-core EXCESS chemical potential of the micelles, the excluded-volume

contribution of the ions is given by an additional term in Eq. (F.8). Specifically,

$$\beta\mu_n^{EX,HC} = 2B_{ni}^{HC}c_i + 2B_{n1}^{HC}c_1 + 2\sum_{m=n_0}^{\infty} B_{nm}^{HC}c_m \tag{F.16}$$

where B_{ni}^{HC} is the hard-core contribution to the second-virial coefficient between an n-mer and an ion.

The excluded volume between an ion and a micelle, B_{ni}^{HC}, can be obtained from Eq. (F.2), where the radius of the monomers, R_1, is replaced by the radius of the ions, r_i. In other words,

$$B_{ni}^{HC} = \frac{2\pi}{3}(R+r_i)^3 + \frac{\pi}{2}(R+r_i)^2 L_n \tag{F.17}$$

Using the expression for L_n given in Eq. (F.4), B_{ni}^{HC} in Eq. (F.17) can be simplified as follows

$$B_{ni}^{HC} = (R+r_i)^2\left(\frac{2\pi r_i}{3} + \frac{n\Omega_s}{2R^2}\right) \tag{F.18}$$

Equation (F.18) for the contribution from the ions, combined with the contribution from the monomers and other micelles (given in Eq. (F.11)), results in the following expression for $\mu_n^{EX,HC}$

$$\begin{aligned}\beta\mu_n^{EX,HC} &= (R+r_i)^2\left(\frac{4\pi r_i}{3} + \frac{n\Omega_s}{R^2}\right)c_i + \Omega_s\gamma^2 n_0^{2/3}c_1 + \frac{2\pi d^3}{9}(c-c_1) + \frac{8\Omega_s}{3}(c_s-c_1) \\ &\quad + n\left(\Omega_s\gamma^2 c_1 + \frac{8\Omega_s}{3}(c-c_1) + \frac{8\Omega_s^2}{\pi d^3}(c_s-c_1)\right)\end{aligned} \tag{F.19}$$

Using Eqs. (F.15) and (F.19), one can compute $\beta(\mu_n^{EX,HC} - n\mu_1^{EX,HC})$ for spherocylindrical micelles in the presence of counterions and added salt. Specifically,

$$\beta(\mu_n^{EX,HC} - n\mu_1^{EX,HC}) = A_0^{cyl} - nA_1^{cyl} \tag{F.20}$$

where

$$A_0^{cyl} = \frac{4\pi}{3}r_i(R+r_i)^2 c_i + \Omega_s\gamma^2 n_0^{2/3}c_1 + \frac{2\pi d^3}{9}(c-c_1) + \frac{8\Omega_s}{3}(c_s-c_1) \tag{F.21}$$

and

$$A_1^{cyl} = \frac{4\pi}{3}\left[(R_1+r_i)^3-(R+r_i)^2\frac{R}{n_0}\right]c_i+[8-\gamma^2(2+n_0^{2/3})]\Omega_s c_1 \\ +\Omega_s\gamma^2 c_s+\Omega_s\gamma^2 n_0^{2/3}c-\frac{8\Omega_s}{3}(c-c_1)-\frac{8\Omega_s^2}{\pi d^3}(c_s-c_1) \qquad \text{(F.22)}$$

which correspond to Eqs. (6.29) and (6.30) of the main text.

Appendix G

Alternative Models for the Electrostatic EXCESS Chemical Potentials

G.1 Pairwise Electrostatic Interactions

As mentioned in Section 6.2.3, a charging process is not the only way to calculate the electrostatic EXCESS chemical potentials. In this appendix, a method using pairwise electrostatic interactions will be described. Theoretically, because electrostatic interactions can be very long-ranged, three-body and higher-order interactions may be significant. This issue is further discussed in Appendix G.2. However, incorporating the higher-order terms in the approach described here would make the calculations very complicated. Instead, it will be assumed that the micellar solution is very dilute so that the higher-order terms can be neglected. In the approach described in this appendix, all pairwise electrostatic interactions, including interactions between solutes in the ion cloud, are dealt with explicitly. Liquid-state theory is then used to obtain thermodynamic quantities, including $\mu_j^{EX,elec}$, from the interaction potentials. It will be shown that in the limit $ez\psi/k_BT \ll 1$, the Debye-Hückel expressions for $\mu_n^{EX,elec}$ and $\mu_1^{EX,elec}$ derived in Section 6.3.1 are recovered. It is important to note that the

model described in this appendix is only valid for spherical micelles, and therefore, cannot be used to model micellar growth.

G.1.1 General Theory

The electrostatic interactions between charged bodies i and j a distance r apart can be described using the potential of mean force between the two particles, w_{ij}. For charged particles, the potential of mean force is determined by the electrostatic potential as follows[28]

$$w_{ij}(r) = \begin{cases} ez_j\psi_i(r) & \text{, for } r \geq \sigma_{ij} \\ \infty & \text{, for } r < \sigma_{ij} \end{cases} \tag{G.1}$$

where $\sigma_{ij} = r_i + r_j$ is the closest-contact distance between solutes i and j where r_i and r_j are the radii of solutes i and j,respectively, e is the electronic charge, z_j is the valence of ion j, and $\psi_i(r)$ is the electrostatic potential at a position r from the center of ion i. Note that spherical symmetry is assumed in Eq. (G.1). The pair correlation function between solute i and solute j, g_{ij}, can be obtained from the potential of mean force as follows

$$g_{ij}(r) = \exp[-\beta w_{ij}(r)] = \begin{cases} \exp[-\beta ez_j\psi_i(r)] & \text{, for } r \geq \sigma_{ij} \\ 0 & \text{, for } r < \sigma_{ij} \end{cases} \tag{G.2}$$

Liquid-state theories can be used to calculate thermodynamic quantities from the pair correlation function. For example, the electrostatic EXCESS internal energy per unit volume can be calculated as follows[28, 194, 195]

$$\frac{E^{EX,elec}}{V} = \frac{2\pi e^2}{\epsilon} \sum_j \sum_k \rho_j \rho_k z_j z_k \int_0^\infty dr \, \frac{r^2 g_{jk}(r)}{r} \tag{G.3}$$

where ρ_j and ρ_k are the number densities of solutes j and k, respectively. The EXCESS McMillan-Mayer free energy due to electrostatic interactions can be obtained

by integrating over $E^{EX,elec}$ as follows[28, 194, 195]

$$\frac{F^{EX,elec}}{V} = -T \int \left(\frac{E^{EX,elec}}{V} \right) \frac{dT}{T^2} \tag{G.4}$$

The electrostatic EXCESS chemical potential of species i can now be obtained by differentiating $F^{EX,elec}$ with respect to the number of i molecules, N_i, as follows[28, 194, 195]

$$\mu_i^{EX,elec} = - \left(\frac{\partial F^{EX,elec}}{\partial N_i} \right)_{T,V,\{N_{j \neq i}\}} \tag{G.5}$$

G.1.2 Point Charges

As a first approximation, to simplify the calculations, the exponential term in Eq. (G.2) will be linearized. In other words, $ez_j\psi_i < k_BT$, such that the following approximation can be made

$$g_{ij}(r) = 1 - \frac{ez_j\psi_i(r)}{k_BT} \quad \text{, for } r \geq \sigma_{ij} \tag{G.6}$$

$\psi_i(r)$ can be obtained by solving the Poisson-Boltzmann (PB) equation around solute i. As above, the same linearization approximation is made, and the PB equation simplifies to the Debye-Hückel equation given in Eq. (6.36). The solution to the Debye-Hückel equation for spheres is given by

$$\psi_i(r) = \frac{z_i e}{\epsilon r} \frac{\exp[-\kappa(r - \sigma_{ij})]}{(1 + \kappa\sigma_{ij})} \tag{G.7}$$

where κ is the inverse Debye screening length, described in the main text.

Using Eq. (G.7) in Eq. (G.6), a new expression for the pair correlation function is obtained

$$g_{ij}(r) = 1 - \frac{z_i z_j e^2}{r\epsilon k_BT} \frac{\exp[-\kappa(r - \sigma_{ij})]}{(1 + \kappa\sigma_{ij})} \tag{G.8}$$

In this model, the central micelle (or monomer) has a finite volume with a radius equal to R_{ch} (or r_h for monomers), but all the solutes in the ion cloud are treated

as point charges. In this case, $r_i = R_{ch}$ (or r_h for monomers) and $r_j = 0$ for point charges. Thus, $\sigma_{ij} = R_{ch}$ (or r_h for monomers). Using Eq. (G.8) in Eq. (G.3), the following expression is obtained for the electrostatic EXCESS internal energy, $E^{EX,elec}$

$$\frac{E^{EX,elec}}{V} = \frac{2\pi e^2}{\epsilon}\int_{R_{ch}}^{\infty} dr\, r \sum_i \rho_i z_i \sum_j \rho_j z_j - \frac{2\pi e^2}{\epsilon}\int_{R_{ch}}^{\infty} dr \sum_i \sum_j \rho_i z_i^2 \rho_j z_j^2 \left(\frac{e^2 \exp[-\kappa(r - R_{ch})]}{\epsilon k_B T(1 + \kappa R_{ch})}\right) \tag{G.9}$$

The first integral in Eq. (G.9) equals zero due to electroneutrality. The second integral can be easily completed to obtain[28]

$$\frac{E^{EX,elec}}{V} = -\frac{\kappa^3 k_B T}{8\pi(1 + \kappa R_{ch})} \tag{G.10}$$

The McMillan-Mayer free energy can be calculated by integrating the internal energy according to Eq. (G.4). The integration is straightforward (note that κ also has a temperature dependence), resulting in the following expression[28]

$$\frac{F^{EX,elec}}{V} = \frac{-k_B T}{\pi}\left[\frac{\kappa^2}{8R_{ch}} - \frac{\kappa}{4R_{ch}^2} + \frac{1}{4R_{ch}^3}\ln(1 + \kappa R_{ch})\right] \tag{G.11}$$

Finally, the electrostatic EXCESS chemical potential of an n-mer can be obtained by differentiating Eq. (G.11) according to Eq. (G.5), namely,[28]

$$\mu_n^{EX,elec} = -\frac{V k_B T}{\pi}\left[\frac{\kappa}{4R_{ch}} - \frac{1}{4R_{ch}^2} + \frac{1}{4R_{ch}^2(1 + \kappa R_{ch})}\right]\left(\frac{\partial \kappa}{\partial N_n}\right)_{T,V,\{N_{m\neq n}\},N_{salt},N_w} \tag{G.12}$$

$$= -\frac{(nez)^2 \kappa}{2\epsilon(1 + \kappa R_{ch})} \tag{G.13}$$

Similarly, for a monomer, the electrostatic EXCESS chemical potential is given by

$$\mu_1^{EX,elec} = -\frac{(ez)^2 \kappa}{2\epsilon(1 + \kappa R_{ch})} \tag{G.14}$$

Equations (G.13) and (G.14) can be compared with the electrostatic EXCESS chemical potentials obtained by using the charging process with the Debye-Hückel

approximation given in Eqs. (6.26) and (6.27), and repeated here for completeness

$$\mu_n^{EX,elec} = -BSE + \int_0^{nze} \psi_{mic}(R_{ch})\, dq \quad \text{, for micelles} \tag{G.15}$$

$$\mu_1^{EX,elec} = -\frac{(ze)^2}{2\epsilon r_h} + \int_0^{ze} \psi_{mon}(r_h)\, dq \quad \text{, for monomers} \tag{G.16}$$

where BSE is the Born solvation energy of the micelle, which, for a spherical micelle, is given by

$$BSE = \frac{(nze)^2}{2\epsilon R_{ch}} \tag{G.17}$$

The integral terms were solved in Eqs. (6.44) and (6.50) as follows

$$\int_0^{nze} \psi_{mic}(R_{ch})\, dq = nsk_BT\frac{\kappa R_{ch}}{2(1+\kappa R_{ch})} = \frac{(nez)^2}{2\epsilon R_{ch}(1+\kappa R_{ch})} \quad \text{, for micelles} \tag{G.18}$$

$$\int_0^{ze} \psi_{mon}(r_h)\, dq = \frac{(ez)^2}{2\epsilon r_h(1+\kappa r_h)} \quad \text{, for monomers} \tag{G.19}$$

where s was defined in Eq. (6.46).

Using Eq. (G.19) in Eq. (G.16) for the monomers, the following expression is obtained for the electrostatic EXCESS chemical potential of the monomers

$$\mu_1^{EX,elec} = -\frac{(ez)^2\kappa}{2\epsilon(1+\kappa r_h)} \tag{G.20}$$

Similarly, using Eqs. (G.18) and (G.17) in (G.15), the following expression is obtained for the electrostatic EXCESS chemical potential of the micelles

$$\mu_n^{EX,elec} = -\frac{(nez)^2\kappa}{2\epsilon(1+\kappa R_{ch})} \tag{G.21}$$

Interestingly, Eqs. (G.20) and (G.21) are identical to the electrostatic EXCESS chemical potentials obtained from pairwise interactions (compare with Eqs. (G.14) and (G.13)). The same approximations were made in each approach, that is, the central micelle (or monomer) has a finite volume but the solutes in the ion cloud are point ions. Hence, the same physical model will lead to the same expression for

$\mu_j^{EX,elec}$, although different approaches were used to arrive at that result. In the next section, the implications of using a more accurate model for $g(r)$ will be discussed.

G.1.3 Poisson-Boltzmann Pair Potential

In the previous section, the pair correlation function, g_{ij}, was linearized to obtain expressions for $\mu_n^{EX,elec}$ and $\mu_1^{EX,elec}$. As discussed in Section 6.4.1, this is not a good approximation for the high charge density surrounding a micelle. One alternative is to use the full Poisson-Boltzmann equation for ψ. In this case, the pair correlation function is still given by Eq. (G.2), with Eq. (6.32) to solve for the potential. (Alternatively, one could use Eq. (6.85) to include the effect of finite-sized solutes in the ion cloud.) In dimensionless variables ($y = ez\psi/k_BT$), the pair correlation function, Eq. (G.2), is given by

$$g_{ij}(r) = \exp\left(\frac{-y_i z_j}{z}\right) \tag{G.22}$$

This pair correlation function can then be used in Eqs. (G.3)-(G.5) to obtain $\mu_n^{EX,elec}$ or $\mu_1^{EX,elec}$. However, the exact form of $y(r)$ is not known analytically, and therefore, Eq. (G.3) cannot be integrated directly. Instead, a coupling constant is used. As the coupling constant varies from 0 to 1, it has the effect of placing the micelle in the system. The pair correlation function is multiplied by the coupling constant, λ, to "turn on" the interactions. That is,

$$g_{ij}(r;\lambda) = \lambda \exp\left(\frac{-y_i z_j}{z}\right) \tag{G.23}$$

The EXCESS chemical potential is then given by[195]

$$\mu_j^{EX,elec} = \frac{4\pi e^2 z_j}{\epsilon} \sum_k \rho_k z_k \int_0^1 \int_{\sigma_{ij}}^{\infty} g_{ij}(r;\lambda) r \, dr \, d\lambda \tag{G.24}$$

where $j = n$ for micelles and $j = 1$ for monomers. Using a coupling constant is essentially the same as the charging approach described in Section 6.2.3, and will result in the same expressions for $\mu_n^{EX,elec}$ and $\mu_1^{EX,elec}$. No additional accuracy is

gained by using pairwise interactions. In other words, the accuracy of the electrostatic EXCESS chemical potentials is determined by the model used for the calculation of ψ, and not by the method used to calculate $\mu_j^{EX,elec}$ from ψ.

G.2 Virial Equation - Mayer Cluster Integrals

As described in Section 6.2.3, another alternative method for calculating the EXCESS properties of the system is to use the viral equation of state. The virial equation of state is given by

$$\beta\Pi = c + \sum_j \sum_k B_{jk}^{(2)} c_j c_k + \sum_j \sum_k \sum_l B_{jkl}^{(3)} c_j c_k c_l + \cdots \tag{G.25}$$

where Π is the osmotic pressure, and c is the total concentration of solutes. The summations are over all the solutes including micelles, monomers, counterions and coions. $B_{jk}^{(2)}$ is the second-virial coefficient between solute j and solute k, and $B_{jkl}^{(3)}$ is the third-virial coefficient between solutes j, k, and l. Typically, micellar solutions are dilute so that three-body interactions are negligible. In this case, the virial equation of state can be truncated at quadratic order. The second-virial coefficient can be calculated from the potential of mean force as follows[195, 196]

$$B_{jk}^{(2)} = -2\pi \int_0^\infty \left[e^{-\beta w_{jk}(r)} - 1\right] r^2 \, dr \tag{G.26}$$

where $w_{jk}(r)$ is the potential of mean force between solutes j and k located a distance r from each other.

For electrostatic interactions, the potential of mean force can be modeled in terms of a Coulombic interaction, as follows[196, 197]

$$u_{jk}(r) = \begin{cases} \infty & \text{, for } r \leq \sigma_{jk} \\ \frac{z_j z_k e^2}{\epsilon r} & \text{, for } r > \sigma_{jk} \end{cases} \tag{G.27}$$

where $\sigma_{jk} = r_j + r_k$ is the closest-contact distance between ions j and k, where r_j and

r_k are the radii of ions j and k. This potential is commonly known as the primitive model. The primitive model is generally a good description for dilute solutions of electrolytes, where it is not necessary to evaluate very short-range potentials.[195, 151]

When the potential of mean force given in Eq. (G.27) is used in Eq. (G.26) to determine the second-virial coefficient for electrostatic interactions, the integral diverges. Physically, the divergence is due to the fact that the Coulombic interaction is infinitely long-ranged, and therefore, the many-body interactions cannot be decomposed into a series of two-body, three-body, *etc.* interactions. In other words, higher-order terms cannot be neglected. However, the divergence in the integral does not lead to a divergence in the osmotic pressure because summing over all the ions in solution will cause the integral to go to zero due to electroneutrality.

In view of the above, it is clear that a traditional virial representation cannot be used to express EXCESS properties due to electrostatics. Instead, an alternative approach based on an expansion in cluster integrals was derived by Mayer.[196] It was determined that all the infinite contributions of each of the virial coefficients can be summed in such a way that they mutually cancel, and thus a finite result is obtained. The Coulombic potential was recast with an exponential decay as follows[196]

$$w_{jk}(r) = \frac{z_j z_k e^2}{\epsilon r} e^{-\kappa r} + w_{jk}^{(s)} \tag{G.28}$$

where $w_{jk}^{(s)}$ is the short-range (hard-core) potential, and $e^{-\kappa r}$ is a convergence factor to assure that all the integrals converge. In the dilute limit, $\kappa \to 0$, and the integrals become relatively straightforward. In this limit, the Debye-Hückel result is obtained by summing only the integrals which are lowest order in concentration, also known as the cyclic graphs. In using only the cyclic graphs, short-range interactions are neglected, that is, the ions are treated as point ions. The resulting equation of state is given by[196]

$$\beta\Pi = c - \frac{\kappa^3}{24\pi} \tag{G.29}$$

The corresponding electrostatic EXCESS chemical potential is given by[196]

$$\mu_i^{EX,elec} = -\frac{(ez_i)^2\kappa}{2\epsilon} \tag{G.30}$$

Note that, in the limit where the central micelle (or monomer) is also a point ion ($R_{ch} = r_h = 0$), the EXCESS chemical potentials derived in Appendix G.1, Eqs. (G.21) and (G.20), would reduce to Eq. (G.30). In other words, in the Debye-Hückel limit for point ions, no matter what approach is used, the same EXCESS chemical potential will be recovered. However, it would be a strong approximation to treat the central micelle as a point ion.

Mayer demonstrated that the finite size of the ions could be accounted for by including all the cluster graphs (higher-order in concentration).[196, 198] However, the resulting equations are only tractable for a solution consisting of ions of the same size. Clearly, this is not the case for a micellar solution where the radius of a micelle may be 20 times that of a counterion. It may be possible to extend this approach to asymmeteric ions, but it would require extensive statistical-mechanical calculations, and is probably not worth the computational effort.

Bibliography

[1] S.J. Ainsworth. Personal care products. *C&EN*, 72:38, 1994.

[2] For an introduction to the field of micellar solutions see Mittal, K.L., Ed.*Micellization, Solubilization, and Microemulsions*; Plenum: New York, 1977; Vols. 1 and 2; and Gelbart, W. M.; Ben-Shaul, A; Roux, D., Eds. *Micelles, Membranes, Microemulsions, and Monolayers*; Springer: Berlin, 1994.

[3] C. Tanford. *The Hydrophobic Effect.* John Wiley and Sons, Inc., 1980.

[4] Y. Chevalier and T. Zemb. The structure of micelles and microemulsions. *Rep. Prog. Phys.*, 53:279, 1990.

[5] J. Israelachvili. *Intermolecular and Surface Forces.* Academic Press, second edition, 1992.

[6] D. Blankschtein, G. Thurston, and G. Benedek. Phenomenological theory of equilibrium thermodynamic properties and phase separation of micellar solutions. *J. Chem. Phys.*, 85:7268, 1986.

[7] J. N. Israelachvili, D. J. Mitchell, and B. W. Ninham. Theory of self-assembly of hydrocarbon amphiphiles into micelles and bilayers. *J. Chem. Soc., Faraday Trans. II*, 72:1525, 1976.

[8] R. Nagarajan and E. Ruckenstein. Aggregation of amphiphiles as micelles or vesicles in aqueous media. *J. Coll. Int. Sci.*, 71:580, 1979.

[9] P. J. Missel, N. A. Mazer, G. B. Benedek, C. Y. Young, and M. C. Carey. Thermodynamic analysis of the growth of sodium dodecyl sulfate micelles. *J. Phys. Chem.*, 84:1044, 1980.

[10] T. R. Carale and D. Blankschtein. Theoretical and experimental determinations of the crossover from dilute to semidilute regimes of micellar solutions. *J. Phys. Chem.*, 96:459, 1992.

[11] D. Blankschtein, G. M. Thurston, and G. B. Benedek. Theory of phase separation in micellar solutions. *Phys. Rev. Lett.*, 54:955, 1985.

[12] M. Corti, C. Minero, and V. Degiorgio. Cloud point transition in nonionic micellar solutions. *J. Phys. Chem.*, 88:309, 1984.

[13] R. R. Balmbra, J. S. Clunie, J. M. Corkill, and J. F. Goodman. Effect of temperature on the micelle size of a homogeneous non-ionic detergent. *Trans. Faraday Soc.*, 58:1661, 1962.

[14] H. Fujimatsu, S. Ogasawara, and S. Kuroiwa. Lower critical solution temperature (LCST) and theta temperature of aqueous solutions of nonionic surface active agents of various polyoxyethylene chain lengths. *Coll. Polym. Sci.*, 266:594, 1988.

[15] J. C. Lang and R. D. Morgan. Nonionic surfactant mixtures. I. Phase equilibria in $C_{10}E_4$-H_2O and closed-loop coexistence. *J. Chem. Phys.*, 73:5849, 1980.

[16] S. Puvvada and D. Blankschtein. Molecular-thermodynamic approach to predict micellization, phase behavior and phase separation of micellar solutions. I. Application to nonionic surfactants. *J. Chem. Phys.*, 92:3710, 1990.

[17] N. Zoeller and D. Blankschtein. Development of user-friendly computer programs to predict solution properties of single and mixed surfactant systems. *Ind. Eng. Chem. Res.*, 34:4150, 1995.

[18] N. Zoeller, A. Shiloach, and D. Blankschtein. Predicting surfactant solution behavior. *CHEMTECH*, 26(3):24, 1996.

[19] R. Nagarajan and E. Ruckenstein. Theory of surfactant self-assembly: A predictive molecular thermodynamic approach. *Langmuir*, 7:2934, 1991.

[20] J. C. Eriksson and S. Ljunggren. Molecular calculations for interacting surfactant monolayers. *Progr. Colloid Polym. Sci.*, 76:188, 1988.

[21] D. F. Evans and B. W. Ninham. Ion binding and the hydrophobic effect. *J. Phys. Chem.*, 87:5025, 1983.

[22] D. F. Evans, D. J. Mitchell, and B. W. Ninham. Ion binding and dressed micelles. *J. Phys. Chem.*, 88:6344, 1984.

[23] J. B. Hayter. A self-consistent theory of dressed micelles. *Langmuir*, 8:2873, 1992.

[24] H. Wennerstrom and B. Jonsson. Amphiphile-water systems and electrostatic interactions. *Physics Abstracts*, 6:1033, 1988.

[25] I. Johnson, G. Olofsson, and B. Jonsson. Micelle formation of ionic amphiphiles. *J. Chem. Soc., Farady Trans. I*, 83:3331, 1987.

[26] D. Stigter. Micelle formation by ionic surfactants. III. Model of stern layer, ion distribution, and potential fluctuations. *J. Phys. Chem.*, 79:1008, 1975.

[27] D. Stigter. Micelle formation by ionic surfactants. IV. Electrostatic and hydrophobic free energy from Stern-Gouy ionic double layer. *J. Phys. Chem.*, 79:1015, 1975.

[28] L. Blum. Primitive electrolytes in the mean spherical approximation. In *Theoretical Chemistry: Advances and Perspectives, Vol. 5*, page 1. Academic Press, 1980.

[29] C. W. Outhwaite. Equilibrium theory of electrolyte solutions. In *Statistical Mechanics, Vol. II*, chapter 3, page 188. The Chemical Society, London, 1975.

[30] P. Linse. Accurate solution of a highly asymmetric electrolyte: Molecular dynamics simulation and integral equation. *J. Chem. Phys.*, 93:1376, 1990.

[31] L. Belloni. A hypernetted chain study of highly asymmetrical polyelectrolytes. *Chemical Physics*, 99:43, 1985.

[32] J. B. Hayter and J. Penfold. An analytic structure factor for macroion solutions. *Mol. Phys.*, 42:109, 1981.

[33] L. Reatto and M. Tau. A statistical model for non-ionic micellar solutions and their phase diagrams. *Chem. Phys. Lett.*, 108:292, 1984.

[34] M. Tau and L. Reatto. Phase diagram and correlations of fluids with very steep attractive forces. *J. Chem. Phys.*, 83:1921, 1985.

[35] C. Leng. Interacting C_nE_m non-ionic micellar systems. *J. Chem. Soc. Faraday Trans. 2*, 84:145, 1985.

[36] H. Evans, D. J. Tildesley, and C. A. Leng. Theories of cloud-curve phase separation in non-ionic alkyl polyoxyethylene micellar solutions. *J. Chem. Soc. Faraday Trans. 2*, 83:1525, 1987.

[37] T. Odijk. Effect of micellar flexibility on the isotropic-nematic phase transition in solutions of linear aggregates. *J. Physique*, 48:125, 1987.

[38] A. Ben-Shaul W. M. Gelbart, W. E. McMullen. Nematic stability and the alignment-induced growth of anisotropic micelles. *J. Physique*, 46:1137, 1985.

[39] R. Nagarajan. Modelling solution entropy in the theory of micellization. *Colloids Surfaces A: Physicochem. Eng. Aspects*, 71:39, 1993.

[40] J. N. Israelachvili and D. Sornette. The interdependence of intra-aggregate and inter-aggregate forces. *J. Physique*, 46:2125, 1985.

[41] S. Ljunggren and J. C. Eriksson. Shape fluctuations of spherical micelles. *J. Chem. Soc. Faraday Trans. 2*, 80:489, 1984.

[42] M. Bergström. Derivation of size distributions of surfactant micelles taking into account shape, composition, and chain packing density fluctuations. *J. Coll. Int. Sci.*, 181:208, 1996.

[43] M. Corti and V. Degiorgio. Quasi-elastic light scattering study of intermicellar interactions in aqueous sodium dodecyl sulfate solutions. *J. Phys. Chem.*, 85:711, 1981.

[44] W. M. Gelbart, A. Ben-Shaul, W. E. McMullen, and A. Masters. Micellar growth due to interaggregate interactions. *J. Phys. Chem.*, 88:861, 1984.

[45] P. U. Kenkare, C. K. Hall, and P. K. Kilpatrick. The effects of salts on the lower consolute boundary of a nonionic micellar solution. *J. Coll. Int. Sci.*, 184:456, 1996.

[46] R. Dorshow, J. Briggs, C. A. Bunton, and D. F. Nicoli. Dynamic light scattering from cetyltrimethylammonium bromide micelles: intermicellar interactions at low ionic strengths. *J. Phys. Chem.*, 86:2388, 1982.

[47] R. Dorshow, C. A. Bunton, and D. F. Nicoli. Comparative study of intermicellar interactions using dynamic light scattering. *J. Phys. Chem.*, 87:1409, 1983.

[48] J. Appell and G. Porte. An investigation on the micellar shape using angular dissymmetry of light scattered by solutions of cetylpyridinium bromide. *J. Coll. Int. Sci.*, 81:85, 1981.

[49] G. Porte and J. Appell. Growth and size distributions of cetylpyridinium bromide micelles in high ionic strength solutions. *J. Phys. Chem.*, 85:2511, 1981.

[50] T. Kato, S. Anzai, S. Takano, and T. Seimiya. Intermicellar interactions and micelle size distribution in aqueous solutions of polyoxyethylene surfactants. *J. Chem. Soc. Faraday Trans. 1*, 85:2499, 1989.

[51] E. Sheu, C.-F. Wu, and S.-H. Chen. Effects of ion sizes on the aggregation and surface charge of ionic micelles in 1:1 electrolyte solutions. *J. Phys. Chem.*, 90:4179, 1986.

[52] M. Zulauf, K. Weckström, J. B. Hayter, V. Degiorgio, and M. Corti. Neutron scattering study of micelle structure in isotropic aqueous solutions of poly(oxyethylene) amphiphiles. *J. Phys. Chem.*, 89:3411, 1985.

[53] J. S. Huang, S. A. Safran, M. W. Kim, G. S. Grest, M. Kotlarchyk, and N. Quirke. Attractive interactions in micelles and microemulsions. *Phys. Rev. Lett.*, 53:592, 1984.

[54] M. P. Taylor, A. E. Berger, and J. Herzfeld. Theory of liquid crystalline phases in amphiphilic systems. *Mol. Cryst. Liq. Cryst.*, 157:489, 1988.

[55] S. A. Safran, P. A. Pincus, M. E. Cates, and F. C. MacKintosh. Growth of charged micelles. *J. Phys. France*, 51:503, 1990.

[56] G. Briganti, S. Puvvada, and D. Blankschtein. Effect of urea on micellar properties of aqueous solutions of nonionic surfactants. *J. Phys. Chem.*, 95:8989, 1991.

[57] J. O'M. Bockris and A. K. N. Reddy. *Modern Electrochemistry*, volume 1. Plenum Press, 1970.

[58] D. J. Mitchell and B. W. Ninham. Curvature elasticity of charged membranes. *Langmuir*, 5:1121, 1989.

[59] L. R. White. Approximate analytic solution of the Poisson-Boltzmann equation for a spherical colloidal particle. *J. Chem. Soc., Faraday Trans. II*, 73:577, 1977.

[60] H. Ohshima, T. W. Healy, and L. R. White. Accurate analytic expressions for the surface charge density/surface potential relationship and double-layer potential distribution for a spherical colloidal particle. *J. Coll. Int. Sci.*, 90:17, 1982.

[61] Y. Nikas, S. Puvvada, and D. Blankschtein. Surface tensions of aqueous nonionic surfactant mixtures. *Langmuir*, 8:2680, 1992.

[62] K. E. Forsten, R. E. Kozack, D. A. Lauffenburger, and S. Subramanian. Numerical solution of the nonlinear Poisson-Boltzmann equation for a membrane-electrolyte system. *J. Phys. Chem.*, 98:5580, 1994.

[63] A. B. Schmidt and E. Ruckenstein. Symmetrized Poisson-Boltzmann equation for mixtures containing colloidal particles and an electrolyte. *J. Coll. Int. Sci.*, 150:169, 1992.

[64] P. J. Missel, N. A. Mazer, M. C. Carey, and G. B. Benedek. Influence of alkali-metal counterion identitiy on the sphere-to-rod transition in alkyl sulfate micelles. *J. Phys. Chem.*, 93:8354, 1989.

[65] Y.-S. Chao, E. Y. Sheu, and S.-H. Chen. Experimental test of a theory of dressed micelles: The case of the monovalent counterion. *J. Phys. Chem.*, 89:4862, 1985.

[66] A. Naor, S. Puvvada, and D. Blankschtein. An analytical expression for the free energy of micellization. *J. Phys. Chem.*, 96:7830, 1992.

[67] E. J. W. Verwey and J. Th. G. Overbeek. *Theory of the Stability of Lyophobic Colloids.* Elsevier Publishing Co., New York, 1948.

[68] J. D. Jackson. *Classical Electrodynamics.* John Wiley and Sons, Inc., second edition, 1975.

[69] M. J. Rosen. *Surfactants and Interfacial Phenomena.* John Wiley and Sons, Inc., first edition, 1978.

[70] K. J. Mysels and L. H. Princen. Light scattering by some lauryl sulfate solutions. *J. Phys. Chem.*, 63:1696, 1959.

[71] R. A. Robinson and R. H. Stokes. *Electrolyte Solutions.* Academic Press, New York, 1959.

[72] J. R. Mishic and M. R. Fisch. The size and flexibility of grown sodium dodecyl sulfate micelles in aqueous sodium chloride solutions. *J. Chem. Phys.*, 92:3222, 1990.

[73] S. Hayashi and S. Ikeda. Micelle size and shape of sodium dodecyl sulfate in concentrated NaCl solutions. *J. Phys. Chem.*, 84:744, 1980.

[74] R. J. Hunter. *Foundations of Colloid Science, Vol. I.* Oxford University Press, New York, 1987.

[75] S. H. Chen. Small angle neutron scattering studies of the structure and interaction in micellar and microemulsion systems. *Ann. Rev. Phys. Chem.*, 37:351, 1986.

[76] P. Karpe and E. Ruckenstein. The enzymatic superactivity in reverse micelles: Role of the dielectric constant. *J. Colloid Int. Sci.*, 141:534, 1991.

[77] E. B. Leodidis. *Solubilization of Ions and Amino Acids in AOT Reversed Micellar Solutions.* PhD thesis, Massachusetts Institute of Technology, 1990.

[78] V. Athanassakis, J. R. Moffatt, C. A. Bunton, R. B. Dorshow, G. Savelli, and D. F. Nicoli. Fractional ionization of cetyltrimethylammonium hydroxide micelles determined by dynamic light scattering. *Chem. Phys. Lett.*, 115:467, 1985.

[79] D. G. Hall. Thermodynamic and kinetic aspects of micellisation in solutions of ionic surfactants. *Colloids and Surfaces*, 4:367, 1982.

[80] D. G. Hall. The effect of electrolyte on ionic surfactant adsorption. *Colloids Surfaces A: Physiochem. Eng. Aspects*, 90:285, 1994.

[81] E. Ruckenstein and J. A. Beunen. A model for counterion binding to ionic micellar aggregates. *J. Coll. Int. Sci.*, 96:469, 1983.

[82] E. Ruckenstein and J. A. Beunen. Effect of counterion binding on micellization. *Langmuir*, 4:77, 1988.

[83] P. Mukerjee, K. J. Mysels, and P. Kapauan. Counterion specificity in the formation of ionic micelles – size, hydration, and hydrophobic bonding effects. *J. Phys. Chem.*, 71:4166, 1967.

[84] R. Zana. Critical micellization concentration of surfactants in aqueous solution and free energy of micellization. *Langmuir*, 12:1208, 1996.

[85] R. Defay and I. Prigogine. *Surface Tension and Adsorption.* John Wiley and Sons, Inc., New York, 1966.

[86] K. Shinoda and H. Nakayama. Separate determinations of the surface excesses of surface-active ions and of gegenions at the air-solution interface. *J. Colloid Sci.*, 18:705, 1963.

[87] D. G. Hall, B. A. Pethica, and K. Shinoda. The interpretation of surface tension data for solutions of ionic surfactants in the presence of electrolyte. *Bull. Chem. Soc. Jpn.*, 48:324, 1975.

[88] D.K. Chattoraj and K.S. Birdi. *Adsorption and the Gibbs Surface Excess.* Plenum Press, New York, 1984.

[89] A. Heindl and H.-H. Kohler. Rod formation of ionic surfactants: A thermodynamic model. *Langmuir*, 12:2464, 1996.

[90] P. Mukherjee and K. J. Mysels. *Critical Micelle Concentration of Aqueous Surfactant Systems.* Number 36 in Natl. Stand. Ref. Data Ser. - Natl. Bur. Stand. U. S. Dept. of Commerce, Washington, D. C., 1971.

[91] P. Becher. Micelle formation in aqueous and nonaqueous solutions. In M. J. Shick, editor, *Nonionic Surfactants*, page 478. Arnold, London, 1967.

[92] K. Meguro, Y. Takasawa, N. Kawahashi, Y. Tabata, and M. Ueno. Micellar properties of a series of octaethylene glycol-n-alkyl ether with homogeneous ethylene oxide chain and their temperature dependence. *J. Coll. Int. Sci.*, 83:50, 1981.

[93] C. Sarmoria, S. Puvvada, and D. Blankschtein. Prediction of critical micelle concentrations of nonideal binary surfactant mixtures. *Langmuir*, 8:2690, 1992.

[94] K. L. Stellner and J. F. Scamehorn. Surfactant precipitation in aqueous solutions containing mixtures of anionic and nonionic surfactants. *J. Am. Oil Chem. Soc.*, 63:566, 1986.

[95] W. Brown, Z. Pu, and R. Rymden. Size and shape of nonionic amphiphile micelles: NMR self-diffusion and static and quasi-elastic light-scattering measurements on $C_{12}E_5$, $C_{12}E_7$, and $C_{12}E_8$ in aqueous solution. *J. Phys. Chem.*, 91:3565, 1987.

[96] R. Zana and C. Weill. Effect of temperature on the aggregation behavior of nonionic surfactants in aqueous solutions. *J. Phys. Lett. (Paris)*, 46:L–953, 1985.

[97] B. A. Mulley and A. D. Metcalf. Nonionic surface-active agents Part IV. The critical micelle concentration of some polyoxyethylene glycol monohexyl ethers in binary and ternary systems. *J. Colloid Sci.*, 17:523, 1962.

[98] R. Strey and A. Pakusch. Critical fluctuations, micelle kinetics and phase diagram of water-nonionic surfactant, H_2O-$C_{12}E_6$. In K. L. Mittal and P. Bothorel, editors, *Surfactants in Solution*, page 465. Plenum, New York, 1986.

[99] F. Jost, H. Leiter, and L. Schwuger. Synergisms in binary surfactant mixtures. *Coll. Polym. Sci.*, 266:554, 1988.

[100] M. T. Garcia, J. Sanchez Leal, and I. Ribosa. Effect of various parameters on sodium dodecyl sulfate (SDS) flux through a collagen membrane. *J. Am. Oil Chem. Soc.*, 69:20, 1992.

[101] L. D. Rhein, F. A. Simion, R. L. Hill, R. H. Cagan, J. Mattai, and H. I Maibach. Human cutaneous response to a mixed surfactant system: Role of solution phenomena in controlling surfactant irritation. *Dermatologica*, 180:18, 1990.

[102] H. A. Himpler. Properties and performance characteristics of linear, branched and aryl nonionic surfactants. *INFORM*, 6:22, 1995.

[103] L. Lue and D. Blankschtein. A liquid-state theory approach to modeling solute partitioning in phase-separated solutions. *Ind. Eng. Chem. Res.*, 35:3032, 1996.

[104] W. G. McMillan and J. E. Mayer. The statistical thermodynamics of multicomponent systems. *J. Chem. Phys.*, 13:276–305, 1945.

[105] G. A. Mansoori, N. F. Carnahan, K. E. Starling, and Jr. T. W. Leland. Equilibrium thermodynamic properties of the mixture of hard spheres. *J. Chem. Phys.*, 54:1523, 1971.

[106] G. C. Maitland, M. Rigby, E. B. Smith, and W. A. Wakeham. *Intermolecular Forces: Their Origin and Determination.* Clarendon Press, 1981.

[107] H. L. Friedman. Lewis-Randall to McMillan-Mayer conversion for the thermodynamic excess functions of solutions. Part I. Partial free energy coefficients. *J. Sol. Chem.*, 1:387–411, 1972.

[108] J. W. Tester and M. Modell. *Thermodynamics and Its Applications.* Prentice-Hall, third edition, 1996.

[109] P. W. Atkins. *Physical Chemistry.* Freeman, third edition, 1986.

[110] A. Ben-Shaul and W. M. Gelbart. Effect of interaggregate forces on the size distribution of micelles. *J. Phys. Chem.*, 86:316, 1982.

[111] L. Onsager. The effects of shape on the interactions of colloidal particles. *Ann. N. Y. Acad. Sci.*, 51:627, 1949.

[112] B. Barboy and W. M. Gelbart. Series representation of the equation of state for hard particle fluids. *J. Chem. Phys.*, 71:3053, 1979.

[113] M. Corti and V. Degiorgio. Micellar properties and critical fluctuations in aqueous solution of nonionic amphiphiles. *J. Phys. Chem.*, 85:1442, 1981.

[114] T. Boublik. Hard convex body equation of state. *J. Chem. Phys.*, 63:4084, 1975.

[115] T. Boublik, C. Vega, and M. Diaz-Pena. Equation of state of chain molecules. *J. Chem. Phys.*, 93:730, 1990.

[116] C. A. Coulson. *Electricity.* Oliver and Boyd, 1958.

[117] E. Ruckenstein and D. Schiby. Effect of the excluded volume of the hydrated ions on double layer forces. *Lanmuir*, 1:612–615, 1985.

[118] M. J. Sparnaay. Ion-size corrections of the Poisson-Boltzmann equation. *J. Electroanal. Chem.*, 37:65–70, 1972.

[119] W. H. Press, B. P. Flannery, S. A. Teukolsky, and W. T. Vetterling. *Numerical Recipes.* Cambridge University Press, 1986.

[120] X. Domingo. Alcohol and alcohol ether sulfates. In H. W. Stache, editor, *Anionic Surfactants: Organic Chemistry*, chapter 5, page 223. Marcel Dekker, Inc., New York, 1996.

[121] M. J. Schwuger. Interfacial and performance properties of sulfated polyoxyethylenated alcohols. In M. J. Rosen, editor, *Structure/Performance Relationships in Surfactants*, number 253 in ACS Symposium Series, chapter 1, page 3. American Chemical Society, Washington, D. C., 1984.

[122] C. Gamboa, H. Rios, and L. Sepulveda. Effect of the nature of counterions on the sphere-to-rod transition in cetyltrimethylammonium micelles. *J. Phys. Chem.*, 93:5540, 1989.

[123] S. Ikeda, S. Ozeki, and M.-A. Tsunoda. Micelle molecular weight of dodecyldimethylammonium chloride in aqueous solutions, and the transition of micelle shape in concentrated NaCl solutions. *J. Coll. Int. Sci.*, 73:27–37, 1980.

[124] Z. Lin, J. J. Cai, L. E. Scriven, and H. T. Davis. Spherical-to-wormlike micelle transition in CTAB solutions. *J. Phys. Chem.*, 98:5984, 1994.

[125] M. Dahanayake, A. W. Cohen, and M. J. Rosen. Relationship of structure to properties of surfactants. 13. Surface and thermodynamic properties of some oxyethylenated sulfates and sulfonates. *J. Phys. Chem.*, 90:2413, 1986.

[126] K. Shinoda and T. Hirai. Ionic surfactants applicable in the presence of multivalent cations: physicochemical properties. *J. Phys. Chem.*, 81:1842, 1977.

[127] K. Shinoda, N. Yamaguchi, and A. Carlsson. Physical meaning of the Krafft point: Observation of melting phenomenon of hydrated solid surfactant at the Krafft point. *J. Phys. Chem.*, 93:7216, 1989.

[128] F. Tokiwa and K. Ohki. Micellar properties of a series of sodium dodecylpolyoxyethylene sulfates from hydrodynamic data. *J. Phys. Chem.*, 71:1343, 1967.

[129] C. Minero, E. Pramauro, E. Pelizzetti, V. Degiorgio, and M. Corti. Micellar properties of sodium dodecylpoly(oxyethylene) sulfates. *J. Phys. Chem.*, 90:1620, 1986.

[130] R. Alargova, J. Petkov, D. Petsev, I. B. Ivanov, G. Broze, and A. Mehreteab. Light scattering study of sodium dodecyl polyoxyethylene-2-sulfate micelles in the presence of multivalent counterions. *Langmuir*, 11:1530, 1995.

[131] R. G. Alargova, K. D. Danov, J. T. Petkov, P. A. Kralchevsky, G. Broze, and A. Mehreteab. Sphere-to-rod transition in the shape of anionic surfactant micelles determined by surface tension measurements. *Langmuir*, 13:5544, 1997.

[132] M. F. Cox. Effect of alkyl carbon chain length and ethylene oxide content on the performance of linear alcohol ether sulfates. *J. Am. Oil Chem. Soc.*, 66:1637, 1989.

[133] D. L. Smith. Comparison of salt thickening of conventional and peaked alcohol ether sulfates. *J. Am. Oil Chem. Soc.*, 68:629, 1991.

[134] K. Kubota, N. Kuwahara, and H. Sato. Critical behavior of a cationic surfactant in an aqueous solution. *J. Chem. Phys.*, 100:4543, 1994.

[135] J. Appell and G. Porte. Cloud points in ionic surfactant solutions. *J. Physique*, 44:L–689, 1983.

[136] I. Cohen and T. Vassiliades. Critical phenomena in aqueous solutions of long chain quaternary ammonium salts. II. Specificity and light scattering properties. *J. Phys. Chem.*, 65:1774, 1961.

[137] I. Michaeli, J. Th. G. Overbeek, and M. J. Voorn. Phase separation of polyelectrolyte solutions. *J. Polym. Sci.*, 23:443, 1957.

[138] R. S. Stock and W. H. Ray. Interpretation of photon correlation spectroscopy data: A comparison of analysis methods. *J. Polym. Sci.*, 23:1393, 1985.

[139] P. Schurtenberger and C. Cavaco. Polymer-like lecithin reverse micelles. 1. A light scattering study. *Langmuir*, 10:100, 1994.

[140] R. A. Chamberlin. *Light Scattering Studies on Lecithin Micellar Solutions.* PhD thesis, Massachusetts Institute of Technology, 1991.

[141] T. M. Bender, R. J. Lewis, and R. Pecora. Absolute Rayleigh ratios of four solvents at 488 nm. *Macromolecules*, 19:244, 1986.

[142] J. A. Finnigan and D. J. Jacob. Light scattering from benzene, toluene, carbon disulphide and carbon tetrachloride. *Chem. Phys. Lett.*, 6:141, 1970.

[143] P. C. Hiemenz and R. Rajagopalan. *Principles of Colloid and Surface Chemistry.* Marcel Dekker, Inc., New York, third edition, 1997.

[144] H. G. Thomas, A. Lomakin, D. Blankschtein, and G. B. Benedek. Growth of mixed nonionic micelles. *Langmuir*, 13:209, 1997.

[145] ASTM Method D445-88.

[146] F. Ortega, R. Bacaloglu, D. C. McKenzie, C. A. Bunton, and D. F. Nicoli. Static and dynamic light scattering study of strongly interacting micelles: Hypernetted chain vs dilute gas approximation. *J. Phys. Chem.*, 94:501, 1990.

[147] S.-H. Chen. Determination of intra- and inter-particle structures of ionic micelles by small-angle neutron scattering. In V. Degiorgio and M. Corti, editors, *Physics of Amphiphiles: Micelles, Vesicles, and Microemulsions*, page 281. North-Holland, Amsterdam, 1985.

[148] P. N. Pusey and R. J. A. Tough. Particle interactions. In R. Pecora, editor, *Dynamic Light Scattering*, chapter 4, page 85. Plenum Press, New York, 1985.

[149] D. Bendedouch and S.-H. Chen. Structure and interparticle interactions of bovine serum albumin in solution studied by small-angle neutron scattering. *J. Phys. Chem.*, 87:1473, 1983.

[150] D. Bendedouch and S.-H. Chen. Effect of an attractive potential on the interparticle structure of ionic micelles at high salt concentration. *J. Phys. Chem.*, 88:648, 1984.

[151] K. S. Schmitz. *Macroions in Solution and Colloidal Suspension.* VCH Publishers, New York, 1983.

[152] J. B. Hayter and M. Zulauf. Attractive interactions in critical scattering from non-ionic micelles. *Coll. Polym. Sci.*, 260:1023, 1982.

[153] R. C. Weast. *CRC Handbook of Chemistry and Physics.* CRC Press, Boca Raton, FL, 1986.

[154] M. Huggins. The viscosity of dilute solutions of long-chain molecules. IV. Dependence on concentration. *J. Am. Chem. Soc.*, 64:2716, 1942.

[155] R. R. Matheson. Viscosity of solutions of rigid rodlike macromolecules. *Macromolecules*, 13:643, 1980.

[156] R. Nagarajan. Are large micelles rigid or flexible? A reinterpretation of viscosity data for micellar solutions. *J. Coll. Int. Sci.*, 90:477, 1982.

[157] R. Nagarajan, K. M. Shah, and S. Hammond. Viscometric detection of sphere to cylinder transition and polydispersity in aqueous micellar solutions. *Colloid Surf. A*, 4:147, 1982.

[158] R. Simha. Effect of concentration on the viscosity of dilute solutions. *J. Res. Natl. Bur. Stand.*, 42:409, 1949.

[159] R. A. Parker and S. J. Wasik. Electroviscous effect in dilute aqueous solutions of detergents. *J. Phys. Chem.*, 62:967, 1958.

[160] R. J. Hunter. *Zeta Potential in Colloid Science.* Academic Press, Inc., San Diego, CA, 1981.

[161] R. Simha. The influence of Brownian movement on the viscosity of solutions. *J. Phys. Chem.*, 44:25, 1940.

[162] H.-H. Kohler and J. Strnad. Evaluation of viscosity measurements of dilute solutions of ionic surfactants forming rod-shaped micelles. *J. Phys. Chem.*, 94:7628, 1990.

[163] C. Tanford. *Physical Chemistry of Macromolecules.* John Wiley and Sons, Inc., 1961.

[164] F. Perrin. Mouvement brownien d'un ellipsoide (II). Rotation libre et dépolarisation des fluorescences. translation et diffusion de molécules ellipsoidales. *J. Phys. Radium*, 7:1, 1936.

[165] T.-L. Lin, Y. Hu, and W.-J. Liu. Thermodynamic theory and dynamic light scattering studies of mixed short-chain lecithin micelles. *Langmuir*, 13:1422, 1997.

[166] A. Wells. *Structural Inorganic Chemistry.* Oxford University Press, second edition, 1984.

[167] S.-H. Chen. Small angle neutron scattering studies of the structure and interaction in micellar and microemulsion systems. In H. L. Strauss, editor, *Annual Review of Physical Chemistry*, page 351. Annual Reviews, Inc., Palo Alto, CA, 1986.

[168] D. F. Nicoli and R. B. Dorshow. The role of intermicellar interactions in interpretations of micellar diffusion coefficients. In V. Degiorgio and M. Corti, editors, *Physics of Amphiphiles: Micelles, Vesicles, and Microemulsions*, page 429. North-Holland, Amsterdam, 1985.

[169] M. Pisarcik, F. Devinsky, and E. Svajdlenka. Spherical dodecyltrimethylammonium bromide micelles in the limit region of transition to rod-like micelles. A light scattering study. *Colloid Surf. A*, 119:115, 1995.

[170] G. Briganti and A. Bonincontro. Interfacial conformation and composition of $C_{12}E_6$ micelle in water inferred by dielectric spectroscopy. *J. Non-Cryst. Solids*, 172-174:1173, 1994.

[171] A. Poppe, L. Willner, J. Allgaier, J. Stellbrink, and D. Richter. Structural investigation of micelles formed by an amphiphilic PEP-PEO block copolymer in water. *Macromolecules*, 30:7462, 1997.

[172] D. Biddle, C. Walldal, and S. Wall. Characterisation of colloidal silica particles with respect to size and shape by means of viscosity and dynamic light scattering measurements. *Colloid Surf. A*, 118:89, 1996.

[173] D. Fenistein, L. Barre, D. Broseta, D. Espinat, A. Livet, J.-N. Roux, and M. Scarsella. Viscosimetric and neutron scattering study of asphaltene aggregates in mixed toluene/heptane solvents. *Langmuir*, 14:1013, 1998.

[174] T. Kato, M. Kanada, and T. Seimiya. Measurements of light scattering intensities on extremely dilute solutions of nonionic surfactant. *Langmuir*, 11:1867, 1995.

[175] R. R. Balmbra, J. S. Clunie, J. M. Corkill, and J. F. Goodman. Variations in the micelle size of non-ionic detergents. *Trans. Faraday Soc.*, 60:979, 1964.

[176] C. Stubenrauch, M. Nyden, G. Findenegg, and B. Lindmann. NMR self-diffusion study of aqueous solutions of tetraoxyethylene *n*-octyl ether (C_8E_4). *J. Phys. Chem.*, 100:17028, 1996.

[177] H. Strunk, P. Lang, and G. H. Findenegg. Clustering of micelles in aqueous solutions of tetraoxyethylene *n*-octyl ether (C_8E_4) as monitored by static and dynamic light scattering. *J. Phys. Chem.*, 98:11557, 1994.

[178] P. Lang and O. Glatter. Small-angle x-ray scattering from aqueous solutions of tetraoxyethylene *n*-octyl ether. *Langmuir*, 12:1193, 1996.

[179] L. D. Song and M. J. Rosen. Surface properties, micellization, and premicellar aggregation of gemini surfactants with rigid and flexible spacers. *Langmuir*, 12:1149, 1996.

[180] R. Zana. Gemini (dimeric) surfactants. *Curr. Opin. in Coll. Int. Sci.*, 1:566, 1996.

[181] P. Belouschek, D. Lorenz, and Z. Adamczyk. Calculation of electrostatic interaction forces between ellipsoidal particles. *Colloid Polym. Sci.*, 269:528, 1991.

[182] B. J. Yoon and S. Kim. Electrophoresis of spheroidal particles. *J. Coll. Int. Sci.*, 128:275, 1989.

[183] J.-P. Hsu and B.-T. Liu. Exact solution to the linearized Poisson-Boltzmann equation for spheroidal surfaces. *J. Coll. Int. Sci.*, 175:785, 1996.

[184] S. Puvvada and D. Blankschtein. Thermodynamic description of micellization, phase behavior, and phase separation of aqueous solutions of surfactant mixtures. *J. Phys. Chem.*, 96:5567, 1992.

[185] S. Puvvada and D. Blankschtein. Theoretical and experimental investigations of micellar properties of aqueous solutions containing binary mixtures of nonionic surfactants. *J. Phys. Chem.*, 96:5579, 1992.

[186] A. Shiloach and D. Blankschtein. Prediction of critical micelle concentrations and synergism of binary surfactant mixtures containing zwitterionic surfactants. *Langmuir*, 13:3968, 1997.

[187] A. Shiloach and D. Blankschtein. Predicting micellar solution properties of binary surfactant mixtures. *Langmuir*, 14:1618, 1998.

[188] L.B. Bhuiyan, C.W. Outhwaite, M. Molero, and E. Gonzalez-Tovar. The primitive model of ionic fluids near its critical point in the Poisson-Boltzmann and modified Poisson-Boltzmann theories. *J. Chem. Phys.*, 100:8301, 1994.

[189] D. Bratko T. Das, L.B. Bhuiyan, and C.W. Outhwaite. Modified Poisson-Boltzmann theory applied to linear polyelectrolyte solutions. *J. Phys. Chem.*, 99:410, 1995.

[190] C.W. Outhwaite and L.B. Bhuiyan. A modified Poisson-Boltzmann analysis of the electric double layer around an isolated spherical macroion. *Mol. Phys.*, 74:367, 1991.

[191] D. Bratko and V. Vlachy. Distribution of counterions in the double layer around a cylindrical polyion. *Chem. Phys. Lett.*, 90:434, 1982.

[192] S. Khan, T. L. Morton, and D. Ronis. Static correlations in macro-ionic suspensions: Analytic and numerical results in a hypernetted-chain–mean-spherical approximation. *Phys. Rev. A*, 35:4295, 1987.

[193] A. Shiloach. *Theoretical Predictions and Experimental Measurements of Micellar Solution Properties of Surfactant Mixtures.* PhD thesis, Massachusetts Institute of Technology, 1998.

[194] L. Blum. Mean spherical model for asymmetric electrolytes I. Method of solution. *Mol. Phys.*, 30:1529–1535, 1975.

[195] D. A. McQuarrie. *Statistical Mechanics.* Harper Collins, 1976.

[196] J. E. Mayer. The theory of ionic solutions. *J. Chem. Phys.*, 18:1426–1436, 1950.

[197] L. Belloni. Electrostatic interactions in colloidal solutions: Comparison between primitive and one-component models. *J. Chem. Phys.*, 85:519–526, 1986.

[198] J. C. Poirier. Thermodynamic functions from Mayer's theory of ionic solutions I. Equations for thermodynamic functions. *J. Chem. Phys.*, 21:965–972, 1953.